A STUDY ON COSMOLOGICAL MODELS IN GENERAL RELATIVITY AND MODIFIED GRAVITY THEORIES

A thesis submitted to

DELHI TECHNOLOGICAL UNIVERSITY

in partial fulfillment of the requirements for the award of the degree of

DOCTOR OF PHILOSOPHY

in

MATHEMATICS

By

SIMRAN KAUR

Under the Supervision of

Prof. Chandra Prakash Singh

DEPARTMENT OF APPLIED MATHEMATICS
DELHI TECHNOLOGICAL UNIVERSITY
(Formerly Delhi College of Engineering)
BAWANA ROAD, NEW DELHI-110 042, INDIA.

November, 2022 **Enroll. No. : 2K18/PHD/AM/02**

DECLARATION

I, the undersigned, hereby declare that the research work reported in this thesis entitled "**A Study on Cosmological Models in General Relativity and Modified Gravity Theories**" for the award of the degree of *Doctor of Philosophy in Mathematics* has been carried out by me under the supervision of *Prof. Chandra Prakash Singh*, Department of Applied Mathematics, Delhi Technological University, Delhi, India.

The research work embodied in this thesis, except where otherwise indicated, is my original research. This thesis has not been submitted by me earlier in part or full to any other University or Institute for the award of any degree or diploma. This thesis does not contain other person's data, graphs, or other information unless specifically acknowledged.

Date : **(Simran Kaur)**

Enroll. No. : 2K18/PHD/AM/02

CERTIFICATE

On the basis of a declaration submitted by **Ms. Simran Kaur**, Ph.D. scholar, I hereby certify that the thesis titled **"A Study on Cosmological Models in General Relativity and Modified Gravity Theories"** submitted to the Department of Applied Mathematics, Delhi Technological University, Delhi, India for the award of the degree of *Doctor of Philosophy in Mathematics*, is a record of bonafide research work carried out by her under my supervision.

I have read this thesis and, in my opinion, it is fully adequate in scope and quality as a thesis for the degree of Doctor of Philosophy.

To the best of my knowledge, the work reported in this thesis is original and has not been submitted to any other Institution or University in any form for the award of any Degree or Diploma.

(Dr. Chandra Prakash Singh)
Supervisor and Professor
Associate Head
Department of Applied Mathematics
Delhi Technological University
New Delhi, India.

(Dr. S. Sivaprasad Kumar)
Professor and Head
Department of Applied Mathematics
Delhi Technological University
New Delhi, India.

ACKNOWLEDGEMENTS

I express my deep sense of gratitude to my supervisor Prof. Chandra Prakash Singh, Associate Head, Department of Applied Mathematics, Delhi Technological University (DTU), New Delhi, India who expertly guided me throughout my Ph.D. in all the time of research and writing of this thesis. His unwavering enthusiasm for research kept me constantly engaged with my research. I extend my warmest thanks to him for his continuous support, patience, motivation, enthusiasm, and immense knowledge. It is indeed a great privilege and honor for me to work under his supervision.

I am extremely thankful to Dr. S. Sivaprasad Kumar, Professor and Head, Department of Applied Mathematics, DTU, New Delhi, India for providing me a constant support and the necessary facilities in the Department.

I also wish to extend my gratitude to SRC members: Prof. Shri Ram, Ex. Head, Department of Mathematics, Indian Institute of Technology, Banaras Hindu University, Varanasi, Prof. J.K. Singh, Head, Department of Mathematics, Netaji Subhas University of Technology, New Delhi and Dr. M. Jayasimhadri, Department of Applied Physics, DTU for their valuable guidance from the beginning of my Ph.D. research work.

I am grateful to the DRC Chairman and all faculty members of the Department of Applied Mathematics, DTU for their constant support and encouragement.

My acknowledgements would not be complete without thanking the academic and technical support of the Delhi Technological University, Delhi, and its staff, particularly the Academic-PG section. The library facilities of the University have been indispensable. I also extend my thanks to everyone in the Department of Applied Mathematics for their support and assistance.

Above ground, I am indebted to my family for their love, prayers and sacrifices for educating me and preparing me for my future.

My appreciation also extends to Dr. Milan Srivastava, Dr. Ajay Kumar and Ms. Vinita Khatri for valuable discussions on the subject matter and helping me develop my ideas. I also place on record, my sense of gratitude to one and all who helped me directly or indirectly in this journey.

I would like to acknowledge the Council of Scientific and Industrial Research (CSIR), Government of India, for providing fellowship (JRF and SRF) that made my Ph.D. work possible.

I am extremely thankful to the Cosmology and Astrophysics community whose research works have helped me a lot to complete my Ph.D. work.

Finally, I thank GOD, the Almighty, for letting me through all the difficulties and for showering his blessings throughout my research work to complete the research successfully.

Date : **(SIMRAN KAUR)**

Place : DTU, Delhi, India.

Dedicated

to

My Family

Contents

Preface

Cosmology is a branch of science which deals with the study of the origin of the universe, its evolution and its eventual fate. The modern cosmology is based on the Big Bang theory, where the universe is considered as emerged out of the Big Bang, which occurred about 13.7 billion years ago. The cosmology assumes the homogeneous (no change during linear motion) and isotropic (no change during angular motion) universe, which is justified on the scales of larger than 100 Mpc. These properties lead us to make an assumption about the model of the universe, called the Cosmological Principle. This principle is the basis of the Big Bang cosmology. For the evolution of the universe, various models have been proposed by scientists from time to time. Since the development of general relativity, cosmology has changed our perception of the laws of the universe remarkably. *The First Three Minutes* written by Steven Weinberg and *A Brief History of Time* by Stephen Hawking are the famous books which create the interest in this subject.

The rapid development in observational cosmology witnesses that the universe is expanding with an accelerated rate. Several theories have been proposed to explain the accelerated phenomena for past two decades. It has been observed that a large part of the universe has One a mysterious component with negative pressure, so-called *dark energy* (DE). The most natural and successful candidate of DE is the cosmological constant which was introduced by Albert Einstein to obtain a static universe. Some other DE candidates like scalar fields, Chaplygin gas, holographic dark energy, Ricci dark energy, etc. have been proposed to explain the accelerated expansion of the universe. Recently, it has been studied that the bulk viscosity and matter creation are another alternative candidates to explain the present acceleration of the universe.

The motive of this thesis's work is to explore the effects of bulk viscosity and matter creation in explaining the dark energy phenomena within the framework of a spatially homogeneous and isotropic flat Friedmann-Lemaître-Robertson-Walker metric in

general relativity and its modified theories. We extract the useful information about the bulk viscosity and matter creation by using observational data to fit the model according to the accepted model. Chapter 1 is introductory in nature. Chapters 2 – 6 are based on the research work published in the form of research papers in reputed refereed journals. The last chapter contains the conclusion and future scope of the thesis work. Each chapter begins with a brief outline of the work carried out in that chapter.

Date : **(SIMRAN KAUR)**

Place : DTU, New Delhi, India.

List of Figures

List of Tables

Chapter 1

Introduction

The introduction gives an overview of the basic principles of cosmology, general theory of relativity, Einstein's field equations, energy-momentum tensor, dark energy and dark matter which govern the evolution of the universe. Bulk viscosity and matter creation cosmology are discussed. Some scalar-tensor theories, preferably the Brans-Dicke theory and dynamical dark energy models, like holographic dark energy are studied. The various cosmological parameters in describing the dynamical behaviour of cosmological models are discussed. Recent observational data from Type Ia supernova (cJLA and Pantheon samples), observational Hubble data (using Cosmic Chronometers, Differential Age Technique, BAO etc.), baryon acoustic oscillations, cosmic microwave background data and Strong Lensing System are discussed. This chapter contains two parts, one devoted to the theoretical aspects and second part concentrating on observational aspects of cosmology which finally ends with the motivation and plan of the work carried out in thesis.

I. Introduction

Cosmology is the study of physical and kinematical nature of the universe, when considered as a whole i.e. to study about the origin and large-scale structures of the universe, such as the distribution of galaxies and their motions and density of dust through intergalactic space. The geometry (shape) and size, the age, the mass density and total mass content, the phase of its present dynamical behaviour with time are some of the basic requirement in formulating a comprehensive theory of cosmology. The study of large-scale structure of universe began just after the discovery of general theory of relativity. The study of cosmology depends crucially on general theory of relativity, which was introduced by Albert Einstein in 1915 and published in 1916 [1]. Modern cosmology within the framework of general relativity has entered into data driven era. Remarkable findings through the latest observational data depicts that universe is expanding with an accelerating rate which might be due to the existence of mysterious components of universe : dark matter and dark energy. Following sections brings out the brief introduction of elementary topics of cosmology which would help us to understand the observational evidences of present-day universe.

1.1 General Relativity and Cosmology

Albert Einstein, in 1905, proposed the special theory of relativity which only accounts for inertial systems. According to this theory, all systems of co-ordinates are equally suitable for description of physical phenomena. In 1915, Einstein extended his special theory of relativity for non-inertial frame and presented a general theory of relativity (GTR). In GTR, the gravity is not an ordinary force but rather a property of space-time geometry. Due to the presence of gravity, GTR is valid in every coordinate system in the curved space-time. This theory is a classical field theory of gravitation because it does not contain quantum effects. GTR provides the natural conceptual framework for cosmology. GTR depends on two fundamental principles: the principle of general covariance and the principle of equivalence.

1. **Principle of general covariance**: It states that the laws of physics can be expressed in a form which is independent of the coordinate systems, i.e., under the general coordinate transformations all physics equations must be covariant.

This can be done by expressing the laws of nature in the form of tensor equations because a tensor equation has exactly the same form in all co-ordinate systems.

2. **Principle of Equivalence**: The cornerstone of Einstein's theory is the principle of equivalence between gravity and acceleration which says that uniform gravitational fields are equivalent to frames that accelerate uniformly relative to inertial frames.

1.2 The Cosmological Principle

The study of cosmology is based on a basic hypothesis called the cosmological principle (CP). According to the cosmological principle (CP), the universe looks the same from all positions in space at any given cosmic time, and that all directions in space at any point are equivalent. Thus, on the large scale of hundreds of megaparsecs (Mpc), the universe possesses two important properties at each epoch, namely, homogeneity and isotropy. Homogeneity means the universe looks the same at each point, i.e., there is no special places in the universe. Isotropy means the universe looks the same in all directions, i.e., there is no special directions in the universe.

1.3 The metric of space-time

General relativity gives an excellent description of gravitational physics. An important idea is the metric of space-time, that describes the physical distance between points. The metric of space-time is important both for correctly interpreting the geometry of the universe and to fully understand the ideas of luminosity and distances in cosmology. In general relativity, the distribution of mass and energy determines the geometry of space-time. Einstein's theory shows that, in the presence of a gravitational field, space becomes curved and its geometry is then Riemannian.

The space-time in general relativity is a combination of three dimensional space and time coordinates. Therefore, the space-time is a four-dimensional geometry in Riemannian space in which the points are labelled by a general coordinate system $(x^0,\, x^1,\, x^2,\, x^3)$, often written as x^μ $(\mu = 0,\, 1,\, 2,\, 3)$. As per the principle of general covariance physics equations must be expressed in tensorial form as tensor equation has exactly the same form in all coordinate systems. The second rank covariant ten-

sor $g_{\mu\nu}$ (number of indices gives the rank of the tensor), known as the metric tensor or fundamental tensor, gives all the information of gravitational field. This tensor determines the space-time interval ds^2 between infinitesimally separated events x^μ and $x^\mu + dx^\mu$ as follows:

$$ds^2 = g_{\mu\nu} dx^\mu dx^\nu. \tag{1.3.1}$$

As (1.3.1) is defined in Riemannian space, it is independent of the coordinate system. Therefore, ds^2 is an invariant. The contravariant tensor corresponding to $g_{\mu\nu}$ is denoted by $g^{\mu\nu}$ where $g_{\mu\nu}g^{\nu\sigma} = \delta^\sigma_\mu$, where $\delta_{\sigma\mu}$ is kronecker delta, defined as $\delta^\sigma_\mu = 1$ if $\sigma = \mu$, and zero otherwise. The indices can be raised or lowered by using the metric tensor as $A^\mu = g^{\mu\nu}A_\nu$ or $A_\mu = g_{\mu\nu}A^\nu$.

The ordinary (or partial) differentiation to Riemannian space is carried out by covariant differentiation which is defined as

$$A_{\mu;\nu} = \frac{\partial A_\mu}{\partial x^\nu} - \Gamma^\sigma_{\mu\nu} A_\sigma, \tag{1.3.2}$$

$$A^\mu{}_{;\nu} = \frac{\partial A^\mu}{\partial x^\nu} + \Gamma^\mu_{\nu\sigma} A^\sigma, \tag{1.3.3}$$

where $\Gamma^\mu_{\nu\sigma}$ is called Christoffel sysmbols, which is defined as

$$\Gamma^\mu_{\nu\sigma} = \frac{1}{2} g^{\mu h}(g_{h\nu,\sigma} + g_{h\sigma,\nu} - g_{\nu\sigma,h}), \tag{1.3.4}$$

where a comma denotes partial derivative with respect to the corresponding variable. It should be noted that $g_{\mu\nu;\lambda} = 0$.

The mixed Riemannian- Christoffel tensor is given by

$$R^\lambda_{\mu\nu\sigma} = \frac{\partial}{\partial x^\nu}\Gamma^\lambda_{\mu\sigma} - \frac{\partial}{\partial x^\sigma}\Gamma^\lambda_{\mu\nu} + \Gamma^\alpha_{\mu\sigma}\Gamma^\lambda_{\alpha\nu} - \Gamma^\alpha_{\mu\nu}\Gamma^\lambda_{\alpha\sigma}. \tag{1.3.5}$$

The contraction of Riemannian-Christoffel tensor with respect to σ gives the second rank tensor called the Ricci tensor which is defined as

$$R_{\mu\nu} = R^\lambda_{\mu\nu\lambda} = \frac{\partial}{\partial x^\nu}\Gamma^\lambda_{\mu\lambda} - \frac{\partial}{\partial x^\lambda}\Gamma^\lambda_{\mu\nu} + \Gamma^\alpha_{\mu\lambda}\Gamma^\lambda_{\alpha\nu} - \Gamma^\alpha_{\mu\nu}\Gamma^\lambda_{\alpha\lambda}. \tag{1.3.6}$$

Ricci tensor is symmetric tensor, i.e., $R_{\mu\nu} = R_{\nu\mu}$. If the Ricci tensor is further contracted, we get an invariant R, called the scalar curvature or Ricci scalar and is defined by

$$R = g^{\mu\nu} R_{\mu\nu}. \tag{1.3.7}$$

In general, the metric $g_{\mu\nu}$ in equation(1.3.1) is function of the coordinates. However, it can be simplified by assuming the cosmological principle which says that at a given time, the universe is isotropic and homogeneous. A spatially isotropic and homogeneous universe in spherical polar coordinates (r,θ,ϕ) can be described by [2]

$$ds^2 = -c^2dt^2 + a^2(t)\left[\frac{dr^2}{1-kr^2} + r^2(d\theta^2 + sin^2\theta d\phi^2)\right], \tag{1.3.8}$$

The above line element (1.3.8) is known as the **Friedmann-Lemaître-Robertson-Walker (FLRW) metric** [3,4]. In Eq.(1.3.8), k is an undetermined constant which measures the curvature of space. Without loss of generality, we can scale the coordinate r in such a way as to make k takes one of the three values $+1$, 0, -1. This corresponds to the three possible spatial geometries spherical, flat or hyperbolic respectively. Also, $a(t)$ is the scale factor of the universe which describes the expansion or contraction of the universe.[1]

1.4 Einstein's law of gravitation

A cosmological model represents the universe at a particular scale and is defined by specifying:

- the **space-time geometry** which is determined by the metric tensor $g_{\mu\nu}$.
- the **matter content in the universe** which is represented by the energy momentum tensor $T_{\mu\nu}$, i.e., equations governing the behaviour of each matter component and the interaction terms between them, ranging from early enough times to present day.
- the **interaction of geometry and matter**.

According to Newtonian theory of gravitation, the field equations in the presence of matter are given by

$$\nabla^2\phi = 4\pi G\rho, \tag{1.4.1}$$

where ϕ is the gravitational potential, ρ is the density of matter and G is the Newtonian gravitational constant.

In non-relativistic limit, the metric $g_{\mu\nu}$ plays the role of gravitational potential, we

[1] We consider the speed of light $c = 1$ and 'space-like convention' (-, +, +, +) for the metric (1.3.8) throughout the thesis.

must replace ϕ by $g_{\mu\nu}$ in the relativistic theory of gravitation. Hence, left hand side of (1.4.1) must be expressed in terms of the second order derivatives of $g_{\mu\nu}$.

As the density ρ is of second rank energy-momentum tensor, therefore, right hand side must be expressed in terms of material energy tensor $T_{\mu\nu}$ in such a way that its divergence vanishes.

Therefore, the most appropriate field equations in general relativity are the Einstein field equations which are given by

$$G_{\mu\nu} = 8\pi G\, T_{\mu\nu}, \tag{1.4.2}$$

where $G_{\mu\nu} = R_{\mu\nu} - \frac{1}{2}g_{\mu\nu}R$ is the Einstein tensor which plays a very important role in general relativity and $T_{\mu\nu}$ is the energy-momentum tensor of the source producing gravitational field. Einstein's field equations tell us that how the presence of matter curves space-time, therefore, we need to define the matter under consideration. In this regard, we consider the perfect fluid which has no viscosity or heat flow. The energy-momentum tensor for the perfect fluid is given by

$$T_{\mu\nu} = (\rho + p)u_\mu\, u_\nu + p\, g_{\mu\nu}, \tag{1.4.3}$$

where p represents the pressure, ρ represents the energy density and $u^\mu = \frac{dx^\mu}{ds}$ is the four-velocity of matter. The four-velocity vector u^μ can be considered as a contravariant vector field whose components are functions of the space-time point x^μ $(\mu = 0,\, 1,\, 2,\, 3)$. In normalized form, we have $g_{\mu\nu}u^\mu u^\nu = -1$.

According to definition of divergence of a tensor, the divergence of Einstein's tensor is identically zero, that is,

$$G^\mu_{\nu;\mu} = \left(R^\mu_\nu - \frac{1}{2}g^\mu_\nu R\right)_{;\mu} = 0, \tag{1.4.4}$$

which implies from (1.4.2) that

$$T^\mu_{\nu;\mu} = 0, \tag{1.4.5}$$

where the semicolon is a covariant derivative. This is known as the conservation equation for energy-momentum tensor. Writing out the covariant derivative, it gives

$$T^\mu_{\nu,\mu} + \Gamma^\mu_{\alpha\mu}T^\alpha_\nu - \Gamma^\alpha_{\nu\mu}T^\mu_\alpha = 0, \tag{1.4.6}$$

where a comma denotes an ordinary derivative. Although this gives four equations, only the time component gives a non-trivial equation which is given by

$$\dot{\rho} + 3\frac{\dot{a}}{a}(\rho + p) = 0, \tag{1.4.7}$$

where a dot denotes derivative with respect to the cosmic time t. This is also known as the **Matter conservation equation**. It is noted that there are two terms which contribute the change in density. The first term within the bracket corresponds to dilution in the density as the volume increases whereas the second term corresponds to the loss of energy due to the work done by pressure as the volume increases. Thus, the energy lost from the fluid through work done transfers into gravitational potential energy, i.e., the energy is always conserved.

1.5 Friedmann Universe

Our aim now is to substitute the FLRW space-time metric (1.3.8) into Einstein's field equations (1.4.2) for energy-momentum tensor of perfect fluid (1.4.3) to obtain predictions for the dynamical evolution of the universe. The field equations (1.4.2) give 10 equations, but in view of the homogeneity and isotropic assumptions there are only two independent equations for a perfect fluid in co-moving coordinates as below.

$$\frac{\dot{a}^2}{a^2} = \frac{8\pi G}{3}\rho - \frac{k}{a^2}, \tag{1.5.1}$$

$$\frac{2\ddot{a}}{a} + \frac{\dot{a}^2}{a^2} = -8\pi G p - \frac{k}{a^2}, \tag{1.5.2}$$

where a dot represents the derivative with respect to the cosmic time t. The first equation (1.5.1) is known as the **Friedmann equation** [2]. This is the most important equation in cosmology which describes the expansion of the universe. Cosmologists try to solve this equation under different assumptions depending on the material content in the universe.

Using the Friedmann equation (1.5.1), we may rewrite the second equation (1.5.2) as

$$\frac{\ddot{a}}{a} = -\frac{4\pi G}{3}(\rho + 3p), \tag{1.5.3}$$

which is an important equation known as the **acceleration equation**. This equation does not feature the curvature parameter k. This equation has a vital role in explaining

the evolution of universe. The universe decelerates for $\rho + 3p > 0$, while accelerates for $\rho + 3p < 0$.

In cosmology, we have a unique pressure associated with each density, i.e., $p = p(\rho)$. This relationship is known as the **equation of state**. Once the equation of state is specified, the Friedmann equation (1.5.1) and conservation equation (1.4.7) can describe the evolution of the universe. The perfect fluid relevant to cosmology follows the simple equation of state

$$p = w\rho, \tag{1.5.4}$$

where w is known as equation of state parameter. Using (1.5.4) in the conservation equation (1.4.7) we obtain

$$\frac{\dot{\rho}}{\rho} = -3(1+w)\frac{\dot{a}}{a}. \tag{1.5.5}$$

If ω is constant, this can be integrated to get

$$\rho \propto a^{-3(1+w)}. \tag{1.5.6}$$

The cosmological fluid is assumed to consist of three non-interacting components- pressureless matter ($w = 0$), radiation ($w = 1/3$) and vacuum ($w = -1$).

The **pressureless matter** means non-relativistic matter which exerts negligible pressure ($p = 0$). In this case, from equations (1.5.1) and (1.4.7) for $k = 0$, we find that the energy density and the scale factor vary as $\rho \propto a^{-3}$ and $a \propto t^{2/3}$, respectively. Thus, the density decreases in proportion to the volume of the universe.

In case of **radiation**, it obeys $p = \rho/3$. Consequently equations (1.5.1) and (1.4.7) give $\rho \propto a^{-4}$ and $a \propto t^{1/2}$. This suggests that the universe expands more slowly if radiation dominates.

In **vacuum**, the equation of state gives $p = -\rho$. Using this in field equations we find that the energy density is constant and the scale factor varies in exponential form. A negative pressure is something like a tension in a rubber band which expands the volume instead of compressing it.

1.6 The Cosmological constant

From the acceleration equation (1.5.3), we see that if we want a static solution, i.e., one in which $\ddot{a} = 0$, we must have $\rho + 3p = 0$ which is nonphysical condition. This is

because assumption of zero pressure gives zero energy density.

While formulating general relativity, Einstein believed that the universe was static although his theory did not permit it. Therefore, in order to make a static universe, he modified his field equations by adding the so-called *Cosmological Constant* to his equation (1.4.2), which is as follows:

$$R_{\mu\nu} - \frac{1}{2} g_{\mu\nu} R + \Lambda g_{\mu\nu} = 8\pi G\, T_{\mu\nu}, \tag{1.6.1}$$

where Λ is the cosmological constant has units $[time]^{-2}$ or sometimes it is $[length]^{-2}$. Equations (1.5.1) and (1.5.2) for perfect fluid (1.4.3) are then modified as follows:

$$\frac{\dot{a}^2}{a^2} = \frac{8\pi G}{3}\rho - \frac{k}{a^2} + \frac{\Lambda}{3}, \tag{1.6.2}$$

$$\frac{2\ddot{a}}{a} + \frac{\dot{a}^2}{a^2} = -8\pi G p - \frac{k}{a^2} + \Lambda. \tag{1.6.3}$$

In principle, Λ can be positive or negative. Now, if we assume the universe to be static with $a(t) = a_0$, a constant, and, say zero pressure, we get

$$\rho = \frac{\Lambda}{8\pi G},\ k = \Lambda a_0^2. \tag{1.6.4}$$

Thus, a positive Λ represents a repulsive force, so that the attractive force due to the matter is balanced by this repulsive force in the Einstein's static universe. In the dynamical models when the galaxies are very far apart after a period of expansion, the attractive force of matter becomes weak and ultimately the repulsive force due to the cosmological constant dominates. The dynamic solutions with the cosmological constant were first studied by Georges Lemaître [5]. Nowadays, the $\Lambda-$term is most often considered in context of the universe with flat Euclidean geometry, $k = 0$. The acceleration equation (1.5.3) is now modified as

$$\frac{\ddot{a}}{a} = -\frac{4\pi G}{3}(\rho + 3p) + \frac{\Lambda}{3}. \tag{1.6.5}$$

We can observe from (1.6.5) that a positive Λ gives a positive contribution to $\ddot{a}$, and therefore, acts as a repulsive force. We can say that for sufficiently large Λ, it can overcome the gravitational attraction caused by the first term and leads to an acceleration.

In recent years, there are some other motivations for introducing a cosmological

constant and such a term arises in many different contexts. Introducing the cosmological constant as a fluid with energy-momentum tensor $\tilde{T}_{\mu\nu}$

$$\tilde{T}_{\mu\nu} = (\rho_\Lambda + p_\Lambda)u_\mu u_\nu + p_\Lambda g_{\mu\nu} = \frac{\Lambda}{8\pi G} g_{\mu\nu}, \tag{1.6.6}$$

so that the energy density ρ_Λ and pressure p_Λ of this fluid due to cosmological constant are given by

$$\rho_\Lambda = \frac{\Lambda}{8\pi G}, \qquad p_\Lambda = -\frac{\Lambda}{8\pi G}. \tag{1.6.7}$$

The above equations bring the Friedmann equation into the form

$$\left(\frac{\dot{a}}{a}\right)^2 = \frac{8\pi G}{3}(\rho + \rho_\Lambda) - \frac{k}{a^2} \tag{1.6.8}$$

and the conservation equation is given by

$$\dot{\rho} + \dot{\rho_\Lambda} + 3\frac{\dot{a}}{a}(\rho + \rho_\Lambda + p + p_\Lambda) = 0. \tag{1.6.9}$$

Now, using (1.4.7) into above equation, we get

$$\dot{\rho_\Lambda} + 3\frac{\dot{a}}{a}(\rho_\Lambda + p_\Lambda) = 0. \tag{1.6.10}$$

Since ρ_Λ is constant by definition, we must have

$$p_\Lambda = -\rho_\Lambda. \tag{1.6.11}$$

Thus, the cosmological constant has a negative effective pressure. Therefore, when the universe expands, the work is done on the cosmological constant fluid which allows its energy density to remain constant even though the volume of the universe increases. The cosmological constant term is sometimes considered as the energy density of 'empty' space, i.e., vacuum energy density. In the latest cosmological discussion, Λ plays a crucial role causing an accelerating universe and is said to constitute the so-called '*dark energy*'.

1.7 Observational Parameters

The whole of the observational cosmology, in fact, depends on some of the vital parameters, such as the Hubble parameter, the deceleration parameter, density parameter, etc. which describe the physical and dynamical behavior of the universe. Let us discuss about these parameters one by one:

1.7.1 Hubble Parameter

The Friedmann equation (1.5.1) or (1.6.2) is considered to explain Hubble's discovery which was made by Edwin Hubble in 1929 [6]. During the observation of moving galaxies, Hubble observed that the almost all the galaxies are receding from us. The further away from us a galaxy is, the faster it is receding. He observed that the velocity of recession of a galaxy was proportional to the distance from us. That is, if $\vec{v}$ is velocity of recession of galaxy and $\vec{r}$ is the distance from us, then $\vec{v} = H_0 \vec{r}$ which is a linear relation between velocity and distance. This is known as **Hubble's law**. The proportionality constant H_0 is known as **Hubble's constant** which means that, at a given cosmic time, H_0 is independent of the separation distance and the recessional velocity.

Let the velocity of recession is given by $\vec{v} = d\vec{r}/dt$ and is in the same direction as $\vec{r}$. Thus, we have

$$\vec{v} = \frac{|\dot{\vec{r}}|}{|\vec{r}|}\vec{r} = \frac{\dot{a}}{a}\vec{r}, \tag{1.7.1}$$

where $\vec{r} = a\vec{x}$ and assume that the comoving position $\vec{x}$ is a constant. Thus, the proportionality constant is defined as

$$H = \frac{\dot{a}}{a}. \tag{1.7.2}$$

Although this is constant in space due to the cosmological principle, it is treated as a function of time and is known as '*Hubble parameter*'. This parameter tells us the expansion rate of the universe. The value of H measured today is denoted by H_0 in unit $Km\,sec^{-1}\,Mpc^{-1}$, which is known as 'Hubble constant'. The inverse of the Hubble's constant at present epoch, the Hubble time, has the value of $t_H \equiv H_0^{-1} = 13.6$ Gyr, which gives the age of the universe from the 'big bang'.

We can write the Friedmann equation $(1.6.8)$ as the evolution equation for $H(t)$ as

$$H^2 = \frac{8\pi G}{3}(\rho + \rho_\Lambda) - \frac{k}{a^2}. \tag{1.7.3}$$

It has been observed that the galaxies have a set of absorption and emission lines in their spectra. If the galaxy recedes, the spectra lines move towards the red end of the spectrum. This effect is known as redshift which is denoted by z, and is defined as

$$1 + z = \frac{\lambda_{obs}}{\lambda_{em}}, \tag{1.7.4}$$

where λ_{obs} and λ_{em} are the wavelengths at the point of observation (us) and emission (galaxy) respectively. On the other hand, the wavelength λ and the scale factor a is proportional to each other, i.e., $\lambda \propto a$, which gives

$$1 + z = \frac{a(t_{obs})}{a(t_{em})}, \tag{1.7.5}$$

which is normally used to light received by us at the present time.

1.7.2 Critical density

The strength of the gravitational attraction is determined by the density of the universe. The critical density, denoted by ρ_c is a special value of density which is required to make the geometry of the universe flat, $k = 0$, assuming $\Lambda = 0$ regardless of its actual value. Thus, on putting $k = 0$ in the Friedmann equation $(1.6.8)$, the critical density is defined as

$$\rho_c = \frac{3H^2}{8\pi G}. \tag{1.7.6}$$

It is to be noted that the critical density changes with time. Using the present value of Hubble parameter H_0, we may calculate the present value of the critical density. Observations show that the actual density of our universe is very close to the critical density, and this is achieved if we take $k = 0$ (the universe is flat).

1.7.3 Density parameter

The density parameter is a very useful tool for specifying the density of the universe. The critical density as discussed above is not necessarily the true density of the universe because the universe may not be flat. However, it describes a natural scale for

the density of the universe. Hence, it is often useful to quote the value of density of the universe with respect to the critical density. This dimensionless quantity is known as the density parameter Ω and is defined by

$$\Omega = \frac{\rho}{\rho_c}. \tag{1.7.7}$$

Using (1.7.7) into (1.7.3) and simplifying, we get

$$\Omega - 1 = \frac{k}{a^2 H^2}. \tag{1.7.8}$$

It should be noted that a, H and Ω all evolve with time. Their values at any particular epoch t have to be related by (1.7.8). Their values at present epoch are denoted by a_0, H_0 and Ω_0. The above equation implies that Ω defines the geometry of the universe, i.e., a closed, flat or open universe, as the sign of k will determine if density parameter is greater than, equal to or less than unity. Current research shows that Ω is very close to unity which implies that the universe is (nearly) flat.

It is important to note that the ρ used in the calculation of Ω is the total mass/energy density of the universe. It is the sum of matter content (baryonic + cold matter) and dark energy suggested by recent observations whose densities can be denoted by ρ_m and ρ_Λ respectively. Hence total density is given by $\rho = \rho_m + \rho_\Lambda$ and therefore

$$\Omega = \Omega_m + \Omega_\Lambda \tag{1.7.9}$$

where $\Omega_m = \rho_m/\rho_c$ represents the density parameter of matter content (baryonic + dark) and $\Omega_\Lambda = \rho_\Lambda/\rho_c$ is the density parameter for dark energy. The density parameter associated with the curvature term is given by $\Omega_k = -k/a^2H^2$. Thus, the Friedmann equation (1.7.3) in terms of the density parameters can be written as

$$\Omega_m + \Omega_\Lambda + \Omega_k = 1. \tag{1.7.10}$$

The observational data obtained from Tyep Ia supernovae, cosmic microwave background (CMB) and studies of the evolution of galaxy clusters all suggest that our universe at present has $\Omega_\Lambda = 0.7$, $\Omega_m = 0.3$ and $\Omega_k = 0$. This means that we live in a flat universe, dominated by a positive cosmological constant. The studies of formation of elements in the early universe say that the density of baryonic matter (normal matter made of protons, neutrons and electrons) has $\Omega_b = 0.04$. Thus, most of the matter

in the universe is non-baryonic which does not emit radiation. It can be detected only through its gravitational effects. This matter is known as 'dark matter'. Therefore, Ω_m can split into its components: $\Omega_m = \Omega_b + \Omega_c$, where $\Omega_b = 0.04$ and $\Omega_c = 0.26$.

1.7.4 Deceleration parameter

The deceleration parameter is an important cosmological quantity which measures the rate of change of expansion. It is defined as

$$q = -\frac{a\ddot{a}}{\dot{a}^2} = -\frac{\dot{H}}{H^2} - 1\,, \tag{1.7.11}$$

It is an indicator of deceleration/acceleration phase of the evolution of universe. The positive value of q denotes the decelerated phase of the universe and the negative value denotes the accelerated phase of the universe. The transition from decelerating $(q > 0)$ to the accelerating $(q < 0)$ phase occurs at redshift z_{tr} when the deceleration parameter vanishes, i.e., $q(z_{tr}) = 0$. Hence, it is an important tool to check the phase transition of universe. The universe has gone through two phase transitions, one from early time inflation to decelerated expansion and then decelerated expansion to late-time accelerated expansion. In the late 1990s, the first convincing measurements of deceleration parameter were made by two research groups studying distant supernovae of a class known as type Ia, which are believed to be good standard candles and got the result that $q < 0$ i.e. the universe is accelerating at present.

1.8 Dark matter and Dark energy

Dark matter(DM) is a hypothetical form of matter thought to account for approximately 26.8% of the matter content in the universe. The existence and properties of DM are derived mainly from its gravitational effects observed on the visible matter, radiation, and the large-scale structure of the universe. It neither emits nor absorbs any kind of electromagnetic radiation. The first person to interpret the evidence of dark matter was Dutch astronomer Jan Oort in 1932. Later on, study of motion of galaxies gave the evidence about the dark matter.

Dark energy(DE) is the mysterious component of the universe that contains about 68.3% of the energy density today making the universe nearly flat and is responsible for accelerating the universe. Two teams of astronomers: the High-Z supernovae

search team in 1998 led by Adam Riess [7] and the Supernovae Cosmological Project in 1998 led by Saul Perlmutter, [8] used supernovae explosions of Type Ia as standard candles at redshifts-z: $0.4 - 0.7$ and confirmed that the expansion of the universe has not been slowing down due to gravity, rather it has been accelerating. The phase transition of universe from decelerating to accelerating was also confirmed by various observations like Wilkinson Microwave Anisotropy Probe (WMAP) [9, 10], Sloan Digital Sky Survey (SDSS) [11], Planck collaboration [12, 13], Cosmic Microwave Background (CMB) [14], the Baryon Acoustic Oscillations (BAO) [15] etc. The most accepted hypothesis to explain the accelerated expansion of universe is the presence of a mysterious energy called "dark energy" which makes up 68.3% of the total mass-energy density of the universe. It is a hypothetical form of energy that exerts a negative, repulsive pressure, behaving like the opposite of gravity.

However, both dark energy and dark matter are simply names describing unknown entities. The various theoretical models for dark energy are being investigated since last two decades.

1.9 The Lambda-CDM model

During the past two decades, cosmology has seen a set of major achievements. We have developed a standard model to describe the origin and future evolution of the universe. Many of the basic cosmological parameters have been deduced in several independent ways which describe the consistent set of results. Several results show that our universe is infinite and spatially flat having matter/energy density equal to the critical density, $\Omega_0 = 1$. Yet observationally, including both the baryonic and dark matter, we can only find less than a third of this value after neglecting the contribution of radiation part at present epoch: $\Omega_m = \Omega_b + \Omega_c \simeq 0.30$. Thus, it appears that there is some missing energy in a flat universe. A possible resolution of this problem of flat universe would be to assume the presence of dark energy.

The simplest candidate of dark energy is the Einstein's cosmological constant, with $w = -1$. Such a cosmological constant assumed to be present even after inflation. The constant dark energy density ρ_Λ is about three-quarters of the critical density to provide the required missing energy. Such matter density is made up mostly of cold dark matter. This standard model is often called the Lambda-Cold dark matter

(ΛCDM) model. In this model, the universe contains three major components: 1) a cosmological constant Λ which is associated to the dark energy (vacuum energy), 2) Cold dark matter- dark matter which moves slowly as compared to the speed of light and has weak interaction with ordinary matter and electromagnetic radiation, and 3) ordinary matter.

The ΛCDM model is the simplest model which describes the properties of existence and structure of the cosmic microwave background, the large scale structure in the distribution of galaxies and the accelerating expansion of the universe. This model assumes that the general relativity is the correct theory on the cosmological scales. The cosmological constant Λ is currently associated with vacuum energy or dark energy in empty space. This vacuum energy explains the accelerating expansion of the space against the attractive effects of gravitational field. As we know that the $\Lambda-$term has negative pressure $p_\Lambda = -\rho_\Lambda$ which is responsible for the accelerating universe. Such model often has an equation of state parameter $w \neq w_\Lambda = -1$.

Since the densities of various matter scale as different powers of the scale factor, for example, $\rho \propto a^{-3}$ for matter-dominated phase, $\rho \propto a^{-4}$ for radiation-dominated phase and $\rho \propto a^{-3(1+w)}$ for different dark energy, therefore, the Friedmann equation can be rewritten in terms of various density parameters as

$$H(a) = H_0\sqrt{(\Omega_c + \Omega_b)\, a^{-3} + \Omega_{rad}\, a^{-4} + \Omega_k\, a^{-2} + \Omega_\Lambda\, a^{-3(1+w)}}, \tag{1.9.1}$$

or equivalently,

$$H(z) = H_0\sqrt{(\Omega_c + \Omega_b)\, (1+z)^3 + \Omega_{rad}\, (1+z)^4 + \Omega_k\, (1+z)^2 + \Omega_\Lambda\, (1+z)^{3(1+w)}}, \tag{1.9.2}$$

where w is the equation of state parameter.

In ΛCDM model, it is assumed that the density parameter for curvature, $\Omega_k = 0$ and $w = -1$, then the equation (1.9.2) reduces to

$$H(z) = H_0\sqrt{\Omega_m\, (1+z)^3 + \Omega_{rad}\, (1+z)^4 + \Omega_\Lambda}, \tag{1.9.3}$$

where $\Omega_c + \Omega_b = \Omega_m$. The observations show that the radiation density is very small today, $\Omega_{rad} \sim 10^{-4}$, therefore, finally, we get the expression for $H(z)$ as

$$H(z) = H_0\sqrt{\Omega_m\, (1+z)^3 + \Omega_\Lambda}. \tag{1.9.4}$$

Although, the ΛCDM model is the best known model till date to explain the accelerating phenomena of present-day universe, it suffers from some problems. From theoretical point of view, fine tuning and cosmic coincidence are the shortcomings of the model [16–19]. There is a large discrepancy between the theoretical and observed values of cosmological constant Λ which differs by at least 120 orders of magnitude [20,21] and thus the problem is known as fine-tuning problem. Second problem is associated with the coincidence between the observed vacuum energy density Ω_Λ and the matter density Ω_m. Up to date we still know little about realistic nature of the dark energy to resolve problems arising from the standard ΛCDM model.

1.10 Alternative models

Since the last two decades theorists have been trying to explain the observable behaviour of universe in two ways: one by introducing some unknown kind of matter in the framework of Einstein gravity which does the modification in the matter part of EFEs and known as the dark energy models and other is to modify the geometric part of the Einstein's equation, known as the modified theories of gravity models. In what follows, we explain the evolution of universe with both the cases.

1.10.1 Dynamical dark energy models

The dynamical dark energy models have been proposed to solve the theoretical problems connected with the standard model of cosmology. Many dynamic dark energy equation of state have been built to describe the late time acceleration. For a given equation of state parameter, the dynamics of the expansion are determined. Unlike the ΛCDM model with $w = -1$, the equation of state dynamically changes with time for dynamical dark energy. The concept of quintessence [22–31] arose after the 1998 discovery of cosmic acceleration which used a *scalar particle field* [32–40]. The quintessence model gives the solution to the fine-tuning problem and the coincidence problem. Some other candidates of dynamical DE have also been proposed in literature such as phantom field (with negative kinetic energy) [41–47], the quintom (a combination of quintessence and phantom scalar fields) [48–50], tachyonic field [51, 52], k-essence [53–55], Chaplygin gas [56, 57], etc. Considering such forms of DE candidates as a responsible agent to explain the evolution of the universe has become a common way. Using significant properties of quantum mechanics, various other dark

energy models have been proposed. Out of which we have worked on *holographic dark energy* (HDE) models in this thesis to explain the evolution of universe. Let us discuss briefly the theory of HDE.

Holographic Dark Energy

Cosmologists are still working on the origin and types of dark energy. A theoretical attempt of applying Holographic Principle to dark energy emerged the concept of holographic dark energy. This was basically done to align the vacuum energy density with the holographic principle [58–60] of quantum gravity. Holographic principle (HP) states that the entropy of any system is not related to its volume but to its surface area. According to the principle, the maximum entropy limit set by the system should not be greater than the entropy of black hole of same size. Susskind [59] further discussed this principle in the context of string theory. Holographic dark energy (HDE) is originated from the HP in which ultra-violet (UV) cut-off of DE is associated with an infrared (IR) cut-off. It is significant to note that the UV cut-off is related to vacuum energy, while the IR cut-off is related to the large-scale structure of universe. Hence, HDE is worth studying being an interesting and simple idea to explain the accelerated expansion of the universe.

HDE originates from the quantum zero-point energy predicted by an effective quantum field theory with a proper UV/IR connection. Cohen et al. [61] proposed that for a system with size L and vacuum energy density ρ_Λ which is related to UV cut-off must be $L^3\rho_\Lambda \leq LM_p^2$, $M_p \sim \frac{1}{\sqrt{8\pi G}}$ is the reduced Planck mass and L is the IR cut-off. A natural candidate for IR cut-off, free from causality, is the Hubble horizon i.e., L as Hubble scale, $L = H^{-1}c$ [62]. Li [63] considered the largest possible L to saturate this inequality and therefore the energy density related to HDE is given by

$$\rho_\Lambda = 3b^2 M_p^2 L^{-2}, \tag{1.10.1}$$

where b is a numerical constant and coefficient 3 is for mathematical convenience.

The HDE model is an attempt to investigate the nature of dark energy in fundamental theory originating from some considerations of the features of quantum gravity theory [64]. Several [65–73] authors have investigated holographic dark energy model with different matter content. Myung [74–76] in his various papers reviewed the origin of HDE and also investigated how it is different than other dynamical models like Chaplygin gas, and tachyon model with a constant potential.

As mentioned IR cut-off is related to the universe's large-scale structure so we have various choices for IR cut-off for a given holographic dark energy model, for example, Hubble horizon, event horizon, Granda-Oliveros cut-off, particle horizon, or Ricci scalar.

Hsu [62] showed that the HDE model with Hubble horizon does not exhibit the accelerated expansion of the universe. However, the HDE model with event horizon, i.e., $L = a(t)\int_t^\infty dt'/a(t')$ provides the sufficiently negative EoS to obtain the accelerated expansion of the universe [77]. It has been found that the HDE using event horizon is also not compatible with the age of some old high redshift objects [78]. Later on, Pavón and Zimdahl [79] showed that the interacting HDE model with the Hubble horizon, $L = H^{-1}$ might give a suitable EoS for DE. It was also observed that there might be a constant ratio of the energy densities of HDE and DM irrespective of the type of interaction.

Granda-Oliveros [80] proposed an IR cut-off for the HDE, which is a combination of the square of Hubble scale and the time derivative of Hubble scale. They defined the holographic energy density as $\rho_d = 3(n_1H^2 + n_2\dot{H})$, where n_1 and n_2 are constants. This IR cut-off avoids the problem of causality and solves the coincidence problem. Many authors [81–90] have used this cut-off to explain the evolution of universe. Nojiri and Odintsov [91] showed that a unified model of the universe may be achieved in a generalized HDE model and coincidence problem may be resolved. Thus, HDE models having the advantage over other DE models may be able to solve the cosmic coincidence problem. Hence for different choices of the IR cut-off, various HDE, have been considered in Refs. [90, 92–99]. The HDE model with suitable choice of IR cut-off favors the current cosmic observational data [100–103].

1.10.2 Modified Theory of gravity

The modified theories of gravity are the extension of general theory of relativity, to incorporate it in a larger, more unified theory. A large number of models with modification to Einstein's gravity can explain the dark energy phenomena. Notable examples are Eddington's theory of connections [104], Weyl's scale independent theory [105] and higher dimensional theories of Kaluza and Klein [106, 107]. The idea of constructing a quantum field theory of gravity arose with rise of super gravity and string theories [108, 109]. These thoeries influenced the later scientists and opened the many possible ways of modifying gravity. The theories like the scalar-tensor theo-

ries [110, 111] are well known examples of extra fields included in the field equations. One of the most simple and well studied scalar-tensor theory is Brans-Dicke Theory.

Brans-Dicke Theory

In 1961, Brans and Dicke [112] proposed a theoretical framework to explain the gravitation known as Jordan-Brans-Dicke or simply the Brans-Dicke(BD) theory. This theory is an attempt to properly incorporate both the Mach's principle [113] and the Dirac's Large Number Hypothesis [114] in which the gravitational constant G is allowed to vary with space-time. The Brans Dicke theory offers alternative predictions of the solar system tests of gravity which escalated the experimental techniques and to make accurate measurements for distinguishing between the predictions of this theory and general relativity, and explain the accelerated expansion of universe [115]. It describes the gravitation through spacetime metric $g_{\mu\nu}$ and a massless scalar field ϕ. This was the first theory of gravity which described the dynamics of gravity by a scalar field and a metric tensor represented the spacetime dynamics. In Jordan frame, the action for the BD theory with matter fields is given by [116]

$$S = \int d^4x\sqrt{-g}\left[\frac{1}{16\pi}\left(\phi R - \frac{\omega}{\phi}\nabla_\alpha\phi\nabla^\alpha\phi\right) + \mathscr{L}_m\right], \tag{1.10.2}$$

where R is the Ricci scalar, ϕ is the BD scalar field and ω is known as the BD coupling parameter. ω measures how strongly ϕ couples with matter and $\mathscr{L}_m$ represents the matter Lagrangian density excluding the scalar field. By the appropriate scaling we can show that BD theory approaches to GTR as $\omega \to \infty$.

The dark energy models emerging from the BD theory can still be significantly different from standard cosmology sufficiently early in the universe. This theory is widely used to study the inflationary epoch of the universe [117–119] but the inflationary regime can be different because of the additional term in the action. Theorists have explored a variation in the Brans-Dicke theme by adding higher-order couplings of the scalar field with gravity. Banerjee and Beesham [120] presented a second order thermodynamic viscous model in the framework of BD theory. They found the exact solutions of the FRW model by assuming the power-law form of BD scalar field. Ram and Singh [121, 122] have studied the flat FRW model with variable EoS parameter using the power law form of BD scalar field.

In 1998, Liddle et al. [123] have discussed the BD theory to describe the transition between the radiation era and the matter dominated era. The BD theory has also

been investigated to describe the emergent universe [124]. Singh [125] studied the early time cosmology with particle creation in BD theory to analyze its thermodynamical effect in open thermodynamical systems. The various aspects of black hole have been investigated in BD theory in Refs. [126–130]. The BD theory, due to its association with string theory and higher dimensional theories [131–133], has got much interest to explain the accelerated expansion .

The variation of action (1.10.2) with respect to the metric tensor and scalar field yield

$$G_{\mu\nu} = R_{\mu\nu} - \frac{1}{2}g_{\mu\nu}R = \frac{8\pi}{\phi}T_{\mu\nu} + 8\pi T^{BD}_{\mu\nu}, \tag{1.10.3}$$

and

$$\nabla_\alpha \nabla^\alpha \phi = \frac{8\pi}{(2\omega+3)}T^\lambda_\lambda. \tag{1.10.4}$$

where $T^{BD}_{\mu\nu}$ is the energy-momentum tensor for the BD scalar which is defined as

$$T^{BD}_{\mu\nu} = \frac{1}{8\pi}\Big[\frac{\omega}{\phi^2}\left(\nabla_\mu\phi\nabla_\nu\phi - \frac{1}{2}g_{\mu\nu}\nabla_\alpha\phi\nabla^\alpha\phi\right) + \frac{1}{\phi}\left(\nabla_\mu\nabla_\nu\phi - g_{\mu\nu}\nabla_\alpha\nabla^\alpha\phi\right)\Big]. \tag{1.10.5}$$

The BD theory is an alternative to the general relativity and finds wide interests in the modern cosmology, it is worthy to study the dark energy models in this framework.

1.11 Viscous and matter creation cosmology

In what follows, we discuss the role of viscous fluid and matter creation in cosmology in describing the evolution of the universe.

1.11.1 Viscous cosmology

Inflation is a crucial part of universe as it has solved many problems in cosmological history. One needs to consider a suitable mechanism to obtain the inflationary phase which is either a scalar field in the framework of GR or a degree of freedom arising from gravitational modification. In literature, so far cosmological fluid (non viscous) has been considered as an ideal fluid. It is worth finding out how the cosmological solutions of GR behave after introducing viscosity term. Viscosity is a concept in fluid mechanics and is related to an exotic fluid with few thermodynamical features like bulk and/or shear viscosities. In view of the spatial isotropy of the universe which is commonly accepted, one usually omits the shear viscosity. This is further motivated by the

Planck observations [13] and WMAP [14], and is supported by theoretical calculations which show that isotropization is quickly established in a large class of homogeneous and anisotropic universes.

The bulk viscosity arises due to the decay of dark matter particles into relativistic products. Bulk viscosity helps in reducing the equilibrium pressure in an expanding Universe. Thus, for large bulk viscous coefficient it is possible for negative pressure term to dominate and an accelerating cosmology to ensue. The pressure provided by bulk viscous coefficient dominantly surpasses the remaining pressure contributions from other cosmic energy-matters. Therefore, it is necessary to clearly define the bulk viscosity for the system of interest.

The interest in viscous cosmology has increased a lot in recent years. Many theorists have explored how several parts of cosmological theory become affected when a bulk viscosity is brought into formalism. The bulk viscosity arises anytime a fluid expands (or contracts) too fast and ceases to be in thermodynamic equilibrium. Hence, the bulk viscosity is a measure of effective pressure needed to restore the system to its thermal equilibrium.

There are two types of dissipative model based on relativistic theory of non-equilibrium thermodynamics. The first order type was developed by C. Eckart [134]. There is a linear relation between the Hubble parameter H and the bulk viscous pressure Π which results from the first order deviations of the equilibrium states i.e. $\Pi = -3\zeta H$ where ζ is the bulk viscous coefficient. To avoid violating the causality principle, higher order deviations from the equilibrium states have been taken into considerations, mostly the second order derivations of the thermodynamics quantities. Full causality theory of a relativistic second order theory was developed by Israel and Stewart [135] which has been studied in the evolution of universe. The full Israel-Stewart transport equation is given by [136]. In this theory, the transport equation for bulk viscous pressure Π is given by

$$\Pi + \tau\dot{\Pi} = -3\zeta H - \frac{\tau\Pi}{2}\left(3H + \frac{\dot{\Pi}}{\Pi} - \frac{\dot{T}}{T} - \frac{\dot{\zeta}}{\zeta}\right). \tag{1.11.1}$$

When relaxation time $\tau = 0$, the second-order theory reduces to the Eckart first-order theory. The existence of bulk viscosity leads to a modification of the perfect fluid energy-momentum tensor

$$T_{\mu\nu} = (\rho + p)u_\mu u_\nu + g_{\mu\nu}p + \Delta T_{\mu\nu}. \tag{1.11.2}$$

The dissipative contribution $\Delta T_{\mu\nu}$ which guarantees translation and rotational invariance for a fluid in motion is given by

$$\Delta T_{\mu\nu} = -3\zeta\frac{\dot{a}}{a}\left(g_{\mu\nu}+u_\mu u_\nu\right) \tag{1.11.3}$$

where ζ is the bulk viscous coefficient. Thus, the total energy-momentum tensor is

$$T_{\mu\nu} = \left(\rho + p - 3\zeta\frac{\dot{a}}{a}\right)u_\mu u_\nu + g_{\mu\nu}\left(p - 3\zeta\frac{\dot{a}}{a}\right). \tag{1.11.4}$$

According to the Eckart's theory, if cosmic fluid has viscosity and p is the thermodynamic pressure of matter content then the effective pressure is given by

$$\tilde{p} = p + \Pi, \tag{1.11.5}$$

where $\Pi = -3\zeta H$, is the dissipative pressure where ζ is the coefficient of bulk viscosity. Hence the energy-momentum tensor (1.4.3) with viscous fluid transforms to

$$T_{\mu\nu} = (\rho + \tilde{p})u_\mu\, u_\nu + \tilde{p}\, g_{\mu\nu}. \tag{1.11.6}$$

Some anisotropic models with viscous term have also been studied to observe the effect of viscous term [137–140]. Many authors [141–169] have studied the dark energy models with bulk viscosity in the cosmic medium. All these cited works show that, for an appropriate viscosity coefficient, an accelerated cosmology may be obtained without the requirement of a cosmological constant. In this thesis, we probe the viscous counterparts in various cosmological models depending on the form of bulk viscosity as well as on the equation of state.

1.11.2 Matter creation cosmology

It is well known that the key ingredient required for accelerating universe is a sufficient negative pressure. This happens naturally in various ways when physical systems depart from the thermodynamic equilibrium. The matter creation is one of the example which is induced by the time-varying gravitational field during expansion of the universe. The negative pressure generated by the matter creation can be derived through relativistic non-equilibrium thermodynamics.

To understand the observed large scale structure of universe we need a mecha-

nism for the existence of the irreversible processes prevalent at all levels of physical description and we believe that this irreversibility comes from the dissymmetrical relation between space-time and matter. This can be done by reinterpreting the matter-energy stress tensor in Einstein's equations. This creation of particles is due to an irreversible energy flow from the gravitational field to the created matter constituents. This consequent from consideration of the thermodynamics of open systems within the framework of cosmology. It is appeared that the second law of thermodynamics requires that space-time transforms into matter while the inverse transformation is forbidden.

Prigogine et al. [170, 171] dealt with the matter creation problem using the thermodynamical theory of irreversible processes, in the framework of the standard hot big bang cosmology. They came up with an interesting type of cosmological history including large scale entropy production assuming the cosmological thermodynamics of open systems and the creation of particles can occur only as an irreversible process at the cost of the gravitational field. This phenomenon within the context of GTR has been studied by many authors in detail [172–178]. Matter creation has ability to generate an effective negative pressure and therefore can play the role of a dark energy component. Several authors [179–187] reconsidered the idea of irreversible matter development.

On a phenomenological level, the matter creation has been defined in the literature in terms of a bulk viscous stress [188, 189]. However, Prigogine et al. [170, 171] made the differences between the bulk viscosity and matter creation processes and showed that they result in different histories of universe evolution. The equivalence between bulk viscosity and matter creation has been discussed by Triginer and Pav*ó*n [190], and Brevik and Stokkan [191]. It has been found that matter creation and bulk viscosity have different thermodynamic feature of the universe while the dynamics of both ideas could be similar. The observational consequence of matter creation in the early universe has been discussed by Singh and Beesham [192].

In the gravitationally induced matter creation mechanism, the number of fluid particles is not conserved, i.e., $N^{\mu}_{;\mu} \neq 0$. In this case, the continuity equation for the particle number density takes the form [173]

$$N^{\mu}_{;\mu} \equiv \dot{n} + 3nH = n\Gamma, \tag{1.11.7}$$

where $N^\mu = n\,u^\mu$ is the particle flux vector, N is the total number of particles in a co-moving volume V, $n = N/V$ is the particle density and Γ is the rate of matter creation from the gravitational field with dimension $time^{-1}$. In theoretical physics, $\Gamma > 0$ represents the source (matter creation), $\Gamma < 0$ represents the sink (matter annihilation), and when there is no matter creation then $\Gamma = 0$. In the process of adiabatic particle creation, the particles and entropy are generated but the entropy per particle does not vary. The particle creation pressure, under such 'adiabatic condition', can be given as [176, 179, 190, 193]:

$$p_c = -\left(\frac{\rho + p}{3H}\right)\Gamma, \tag{1.11.8}$$

where p_c is the pressure due to the matter creation. Now, the dynamics of the universe can be explained if we know the particle creation rate. The nature of Γ is still not known as the associated quantum field theory (QFT) is yet to be developed. In theory, different forms of Γ, e.g., $\Gamma = constant$ [194], $\Gamma \propto H$ [195], $\Gamma \propto H^2$ [175, 196], and a linear combination [197], have been already taken to explain the early and present-day acceleration of the universe. However, the models with linear and quadratic forms of Γ do not show transition redshift, i.e., they are not compatible with the current cosmology. Therefore, a natural extension is to consider the linear combinations of H, $H^2 \ldots$, and the derivative of the Hubble parameter. At last, we can check the viability of such models with observational data.

Due to the addition of matter creation, energy momentum tensor changes as per the second law of thermodynamics. Therefore, the energy- momentum tensor of perfect fluid $(1.4.3)$ empowered with the mechanism of matter creation is given as

$$T_{\mu\nu} = (\rho + p + p_c)u_\mu\, u_\nu + (p + p_c)\, g_{\mu\nu}. \tag{1.11.9}$$

The entropy flux vector has the form $\mathbb{S}^\mu = n\sigma u^\mu \equiv su^\mu$, with $\sigma = \mathbb{S}/N$ is the basic entropy per particle and $\mathbb{S} = sa^3$ being the entropy in a comoving amount. The second law of thermodynamics imposes a relationship

$$\mathbb{S}^\mu_{;\mu} = n\dot{\sigma} + \sigma n\Gamma \geq 0. \tag{1.11.10}$$

The divergence of $\mathbb{S}^\mu$ is reduced to $\mathbb{S}^\mu_{;\mu} = \sigma n\Gamma$ if the creation process is such that the specific entropy per particle is constant. However, matter creation and bulk viscosity are two distinct processes, the viscous term's specific entropy rate per particle is

calculated as [190]

$$\dot{\sigma} = \frac{\zeta \theta^2}{n\mathbb{T}}, \tag{1.11.11}$$

where $\mathbb{T}$ is the temperature. It is clear that the existence of Γ has no bearing on the production of entropy per particle, which is completely dependent on the nature of bulk viscosity. As stated previously, if $\zeta = 0$, the entropy per particle is constant.

1.12 Geometrical diagnostic parameters

The study of cosmological parameters like the Hubble parameter H, deceleration parameter q and equation of state parameter ω help us to study the behaviour of universe through different cosmological models. These parameters are defined by taking the first and second order derivatives of the scale factor. To get the more precision about the universe through cosmological models that matches the observational data as well, some other parameters are defined by involving the higher order derivatives of the scale factor. In what follows, we discuss such diagnostic parameters which have been used in this thesis to analyse cosmological phenomena.

1.12.1 Statefinder Parameter

Sahni et al [198] and Alam et al [199] introduced a new pair of diagnostic, known as statefinder parameter, denoted by $\{r,s\}$ to distinguish the different dark energy models with ΛCDM model. This pair is defined as

$$r = \frac{\dddot{a}}{aH^3} = \frac{\ddot{H}}{H^3} - 3q - 2 \quad \text{and} \quad s = \frac{r-1}{3(q-1/2)}. \tag{1.12.1}$$

The statefinder pair is geometrical in nature as it is derived from the space-time metric directly. Depending on the values of pair $\{r,s\}$ in $s-r$ plane, we can classify the dark energy into three categories:

- $r > 1,\ s < 0$, Chaplygin gas model;
- $r < 1,\ s > 0$, quintessence model;
- $r = 1,\ s = 0$, the standard ΛCDM model.

One can plot the trajectories in $s-r$ and $q-r$ planes to discriminate various dark energy models.

1.12.2 Om diagnostic

As a complementary to $\{r,s\}$, Sahni et al [200] proposed another new diagnostic called $Om(z)$ parameter. It is defined as

$$Om(z) = \frac{\frac{H^2(z)}{H_0^2} - 1}{(1+z)^3 - 1}. \tag{1.12.2}$$

The slope of the trajectory in $Om - z$ plane is used to classify into different categories:

- a negative slope means a quintessence type DE;
- a positive slope means a phantom-like DE;
- a horizontal line means a ΛCDM model.

Many authors [201–203] have studied the dark energy models based on *Om(z)* diagnostic.

1.12.3 Cosmographic Parameters

Apart from the above mentioned two geometric parameters, a comparison of DE models can also be carried out by cosmography. A Taylor series expansion of the scale factor at present time is used to define the cosmographic parameter (CP), which involve the higher order derivatives of the scale factor. The usual CP are the *jerk(j)*, *snap(s)*, *lerk (m)* and m which are respectively defined as [204, 205]

$$j = \frac{1}{aH^3}\frac{d^3a}{dt^3}\ ,\ s = \frac{1}{aH^4}\frac{d^4a}{dt^4}\ ,\ l = \frac{1}{aH^5}\frac{d^5a}{dt^5}\ ,\ m = \frac{1}{aH^6}\frac{d^6a}{dt^6}. \tag{1.12.3}$$

The above cosmographic parameters in terms of redshift are defined as

$$j = -q + (1+z)\frac{dq}{dz} + 2q(1+q), \tag{1.12.4}$$

$$\mathbf{s} = j - 3j(1+q) - (1+z)\frac{dj}{dz}, \tag{1.12.5}$$

$$l = \mathbf{s} - 4\mathbf{s}(1+q) - (1+z)\frac{d\mathbf{s}}{dz}, \tag{1.12.6}$$

$$m = l - 5l(1+q) - (1+z)\frac{dl}{dz}. \tag{1.12.7}$$

Here, r and j are same; but the s parameter defined in (1.12.3) is not same with one defined in (1.12.1). The jerk parameter informs about inflection points in the expansion history of the Universe. However, there is no such physical significance of snap and m parameters but being important part of the Taylor series of the Hubble parameter in cosmography, they give us the information about the models. The study of the above parameters for any dark energy model along with the Hubble parameter H and deceleration parameter q is known as the cosmography of the model. Using the equation (1.12.3) it can be deduced that the cosmography of any cosmological model will be true whenever the Hubble parameter is fourth-order differentiable.

1.13 Model Selection Criterion

A chi-squared statistic is a very popular method that measures how a model compares to actual observed data. The reduced chi-squared, denoted by χ^2_{red}, method is used for model assessment, model comparison, convergence diagnostic, and error estimation in astronomy. If ν is the degree of freedom, the reduced χ^2 is then defined as

$$\chi^2_{red} = \frac{\chi^2_{min}}{\nu}. \tag{1.13.1}$$

If $\mathbb{N}$ is the number of data points and d is the free parameters, then degree of freedom is defined as the difference between total number of data points and the number of free parameters i.e., $\nu = \mathbb{N} - d$. If a model is fitted to data and the resulting χ^2_{red} is larger than one, it is considered a "bad" fit, whereas if χ^2_{red} is less than one, it is considered an over-fit. The model with the minimum reduced chi-squared is usually the preferred one.

Statistical analysis takes the number of parameters required into account to decide which model is "better", and how well the models complement the data. **Akaike Information Criterion** (AIC) [206] and the **Bayesian or Schwarz Information Criterion** (BIC) [207] are used to evaluate the goodness of our model in comparison to a given reference model. The AIC parameter is defined as follows [206]

$$AIC = -2\, ln\mathscr{L}_{max} + 2d, \tag{1.13.2}$$

where $\mathscr{L}_{max} = e^{-\chi^2_{tot}/2}$ is the maximum likelihood obtained for the cosmological model. Minimizing the Akaike information criterion allows selection between models with dif-

fering number of parameters. The "preferred model" for this criterion is the one with the smaller value of AIC. We calculate $\Delta AIC_{kl} = AIC_k - AIC_l$ to compare the model k with the model l, which may be interpreted as "evidence in favor" of the model k over the model l. We have "strong evidence in favor" of model k for $0 \leq \Delta AIC_{kl} < 2$, "average evidence in favor" of model k for $2 < \Delta AIC_{kl} < 4$, "less evidence in favor" of model k for $4 < AIC_{kl} \leq 7$, and "no evidence in favor" of model k for $\Delta AIC_{kl} > 10$ [208].

The BIC, on the other hand, is defined as [207]

$$BIC = -2\, ln\mathscr{L}_{max} + d\, ln\mathbb{N}, \tag{1.13.3}$$

Similar to ΔAIC_{kl}, $\Delta BIC_{ij} = BIC_i - BIC_j$ may be interpreted as "evidence favor" the model i compared to the model j. For $0 \leq \Delta BIC_{ij} < 2$, there is "not enough evidence against" the model i, for $2 \leq \Delta BIC_{ij} < 6$, there is "evidence against" the model i and for $6 \leq \Delta BIC_{ij} < 10$, there is "strong evidence against" model i [208].

II. Observational Cosmology

1.14 Observational Analysis

Now that we have precision cosmological data, it has become significant to compare cosmological models with data. Once we have decided our cosmological model we use our observations to measure the value of its parameters and to learn about our universe and its material composition. Usually a compilation of several different type of data, analysed simultaneously, is used.

1.14.1 Methodology

This section introduces the statistical methods used to perform the data analysis. Cosmologists use the Bayesian statistics to tackle the data analysis. A software package *COSMOMC* is used which carries out an Monte Carlo Markov Chain (MCMC) analysis using a CAMB program to carry out the theoretical calculations. COSMOMC is a publicaly available code [2]. There have been many cosmological probes till date that can be used to perform the data analysis. There is an efficient way of exploring parameter space (set of model free parameters) using MCMC method. An MCMC

[2] Go to http://cosmologist.info for more information

sampler provides an efficient way to generate a list of samples. Foreman-Mackey et al [209] introduced a Python implementation of the ensemble sampler for MCMC, the 'EMCEE'. We have adopted this for analysing the cosmological models in this thesis. In this approach, the algorithm drifts towards the highest likelihood regions, where the fit to the data is best. For this, parameter space is explored by 'jumping' randomly from one set of parameter values to the next, with a rule for whether the jump is accepted or rejected depending on how the likelihood of the new point compares to the old. We are fortunate to have access to a software package EMCEE which carries out the MCMC analysis and many datasets have been incorporated into it making it relatively easier for cosmologists to carry out analysis of new cosmological models and to discover the effect of emerging data.

1.14.2 Observational Data

We list herewith some of the observations in this thesis which are important in the context of late time acceleration. These are the observations of Type Ia supernova, strong lensing system, observational measurement of Hubble parameter, the baryon acoustic oscillation, and the cosmic microwave background radiation, etc.

Type Ia supernova: cJLA

Type Ia supernova type Ia (SNe) are the result of the explosion of a carbon-oxygen white dwarf in a binary system. They are the brightest of all supernovae and are characterized by a silicon absorption feature in their maximum light spectra. Type Ia are also known as thermonuclear supernovae. This type of explosion does not take place when the core of a massive star collapses. They instead occur in binary system, where one of two stars must be a white dwarf. The other star is often a low mass star like our sun or can be a red giant star. If the white dwarf grows to over 1.4 solar mass, at this point electrons are no longer strong enough to prevent the star from collapsing and star explodes as Type Ia SNe.

SNe are one of the brightest event in the universe. One would expect these supernovae to be regular candles, with the same luminosity every time, because explosion always takes place when white dwarf reaches a set mass. SNe is one of the best probes for confirming the redshift-distance relation under this hypothesis, as they give a clear measurement of the luminosity distance independent of redshift determination. As a result, SNe are considered the best distance indicators available to astronomer-

s. We use standard candles, like SNe to measure distances in space. They were the objects observed when dark energy was discovered in 1998. These observations have helped prove that the universe is expanding and accelerating.

In this thesis, we use samples from the compressed Joint Light-curve Analysis (cJLA) compilation, which consists of 31 binned data points within the range $0.01 < z < 1.3$ [210]. The distances of a supernova at different redshift z are measured in the form of distance modulus $\mu_b(z)$ which is same as the difference between the apparent magnitude m_b and the absolute magnitude M_b of the B-band (wavelength band of the blue line) of the observed spectrum of the supernova.

$$\mu_b(z) = m_b - M_b = 5\, log\left(\frac{d_L(z)}{10Mpc}\right) + M, \tag{1.14.1}$$

where M is the normalization parameter, d_L is the luminosity distance defined as

$$d_L = c(1+z)\int_0^z \frac{dz'}{H(z',\Theta)}, \tag{1.14.2}$$

where c is the speed of light and Θ is the set of model parameters.

We use the chi-square, χ^2-statistics in order to estimate the free parameters of the cosmological models. The likelihood is evaluated :

$$\chi^2_{SNe} = x^T C_b^{-1} x, \tag{1.14.3}$$

where $x = \mu_b - M - 5\, log_{10} d_L$ and C_b is the covariance matrix of μ_b [Table F.2 in [210]].

Type Ia supernova: Pantheon data

We also use the another latest compilation of SNe (Pantheon sample), consisting 40 binned data points in the redshift range $0.014 \leq z \leq 1.62$ or 1048 data points in the redshift range of $z \in [0.014, 2.3]$ from SNLS, SDSS, Pan-STARRS1, HST survey [211].

The χ^2 function for SNe is defined as

$$\chi^2_{Pan} = \mu C^{-1} \mu^T, \tag{1.14.4}$$

where $\mu = \mu_i^{obs} - \mu^{th}$ and C is the covariance matrix of μ^{obs} given in [212]. The observed distance modulus is given in [210] . Also, the theoretical distance modulus is given by

$$\mu^{th} = 5\, log_{10}[d_L(z)/10pc] + M, \tag{1.14.5}$$

where M is the nuisance parameter, c is the speed of light and the dimensionless luminosity distance $d_L(z)$ is defined as [211]

$$d_L(z) = (1+z)\int_0^z \frac{dz'}{H(z',\Theta)} \tag{1.14.6}$$

where Θ represents the model parameters.

Observational Hubble Data

The other important part of fitting parameters is to determine the Hubble parameter using observational data. Lately, the measurement of Hubble parameter $H(z)$ has received much attention from the researchers because of its model-independent nature. The observational Hubble data (OHD) is based on differential ages of the galaxies [213]. OHD presents the Hubble parameter estimated at different redshift z. We have used 43 data points of the Hubble parameter in the redshift range $0 < z < 2.5$ [214] in our statistical analysis.

The χ^2 function is defined as

$$\chi^2_{OHD} = \sum_{i=1}^{n} \frac{[H(z_i) - H_{obs}(z_i,\Theta)]^2}{\sigma_i^2}, \tag{1.14.7}$$

where $H(z_i)$ and $H_{obs}(z_i,\Theta)$ denotes the theoretical and observed values of Hubble parameter, respectively. σ_i denotes the standard deviation in the observed value.

OHD(CC + Galaxy distribution)

We use Hubble data $H(z)$ to study the cosmic expansion history which includes 36 measurements in which 31 measurements are determined from the cosmic chronometric technique (CC) [215], 3 correlated measurements from the radial BAO signal in the galaxy distribution [216], and 2 measurements determined from the BAO signal in Lyman forest distribution alone [217, 218].

The expression for χ^2 function for $H(z)$ is

$$\chi^2_{H(z)36} = \chi^2_{CC+Ly\alpha} + \chi^2_{gal}. \tag{1.14.8}$$

where

$$\chi^2_{CC+Ly\alpha} = \sum_{i=1}^{33} \frac{[H^{obs}(z_i) - H^{th}(z_i)]^2}{\sigma_i^2}, \tag{1.14.9}$$

Here, $H^{th}(z_i)$ and $H^{obs}(z_i)$ represent the theoretical and observed values at redshift z_i, respectively and σ_i^2 the standard deviation of each $H^{obs}(z_i)$,

and

$$\chi^2_{gal} = A^T \mathbf{C}^{-1} A, \tag{1.14.10}$$

C is the covariance matrix of 3 galaxy distribution measurements, given in Ref. [216] and

$$A = \begin{bmatrix} H_{obs}(0.38) - H_{th}(0.38) \\ H_{obs}(0.51) - H_{th}(0.51) \\ H_{obs}(0.61) - H_{th}(0.61) \end{bmatrix}$$

Hz(DA+BAO)

Here we use the updated collection of 57 $H(z)$ data points in the range $z \in [0.07, 2.36]$ that consists of 31 points measured from differential age(DA) technique and 26 data points received through BAO and other methods. The minimized chi squared function for determining the best fit values of model is

$$\chi^2_{H(z)}(\theta) = \sum_{i=1}^{57} \frac{[H(z_i) - H_{obs}(z_i, \Theta)]^2}{\sigma_i^2} \tag{1.14.11}$$

where $H(z_i)$ are theoretical values of Hubble parameter and $H_{obs}(z_i, \Theta)$ are the observed values of Hubble parameter. The standard deviation measurement uncertainty in $H_{obs}(z_i, \Theta)$ is represented by σ_i [219]. The corresponding data has been shown in Table 1.1.

Baryon Acoustic Oscillations and Cosmic Microwave Background

Baryon acoustic oscillations (BAO) are a pattern of wrinkles in the density distribution of the clusters of galaxies spread across the universe. They provide an independent way to measure the expansion rate of the universe and how the rate has changed throughout the cosmic history. Until recombination, the acoustic oscillations in the baryon-photon fluid imprint a fixed comoving length scale in the statistics of galaxies distribution, which is given by the comoving sound horizon at recombination,

$$r_s(z_*) = \int_{z_*}^{\infty} \frac{c_s(z)}{H(z)} dz, \tag{1.14.12}$$

in which c_s is the sound speed and z_* denotes the photons decoupling redshift and holds the value $z_* = 1090$ as per the Planck 2015 results [13]. The peak positions in

Table 1.1: H(z) datasets consisting of 57 points

DA Method (31 points)

z	$H(z)$	$\sigma_h(z)$	$Ref.$	z	$H(z)$	$\sigma_h(z)$	$Ref.$
0.070	69	19.6	[222]	0.4783	80	99	[231]
0.90	69	12	[220]	0.480	97	62	[222]
0.120	68.6	26.2	[222]	0.593	104	13	[215]
0.170	83	8	[220]	0.6797	92	8	[215]
0.1791	75	4	[215]	0.7812	105	12	[215]
0.1993	75	5	[215]	0.8754	125	17	[215]
0.200	72.9	29.6	[227]	0.880	90	40	[222]
0.270	77	14	[220]	0.900	117	23	[220]
0.280	88.8	36.6	[227]	1.037	154	20	[215]
0.3519	83	14	[215]	1.300	168	17	[220]
0.3802	83	13.5	[231]	1.363	160	33.6	[230]
0.400	95	17	[220]	1.430	177	18	[220]
0.4004	77	10.2	[231]	1.530	140	14	[220]
0.4247	87.1	11.2	[231]	1.750	202	40	[220]
0.4497	92.8	12.9	[231]	1.965	186.5	50.4	[230]
0.470	89	34	[232]				

BAO and other method (26 points)

z	$H(z)$	$\sigma_h(z)$	$Ref.$	z	$H(z)$	$\sigma_h(z)$	$Ref.$
0.24	79.69	2.99	[221]	0.52	94.35	2.64	[234]
0.30	81.7	6.22	[228]	0.56	93.34	2.3	[234]
0.31	78.18	4.74	[234]	0.57	87.6	7.8	[226]
0.34	83.8	3.66	[221]	0.57	96.8	3.4	[229]
0.35	82.7	9.1	[224]	0.59	98.48	3.18	[234]
0.36	79.94	3.38	[234]	0.60	87.9	6.1	[223]
0.38	81.5	1.9	[216]	0.61	97.3	2.1	[216]
0.40	82.04	2.03	[234]	0.64	98.82	2.98	[234]
0.43	86.45	3.97	[221]	0.73	97.3	7.0	[223]
0.44	82.6	7.8	[223]	2.30	224	8.6	[225]
0.44	84.81	1.83	[234]	2.33	224	8	[233]
0.48	87.79	2.03	[234]	2.34	222	8.5	[217]
0.51	90.4	1.9	[216]	2.36	226	9.3	[218]

the CMB anisotropy power spectrum is determined using this scale. After recombination the baryons decouple from the photons. Their perturbations evolve under the influence of only gravity, which is dominated by dark matter due to its high density. Eventually, baryon and dark matter both perturbations adopt the same power spectrum, with the acoustic oscillations function diluted in comparison to the CMB. We adjust the size of the scale to find the history of expansion of universe.

In this thesis, we assume the combined BAO and CMB data from different observational missions [235]. We have taken the data from BAO distances measurements from SDSS(R) [236], the 6dF Galaxy survey [237], BOSS CMASS [229] and three parallel measurements from WiggleZ survey [238]. We combine these results with the Planck 2015 [13].

The angular diameter, $d_A(z,\Theta)$, in context of BAO, is given as

$$d_A(z_*,\Theta) = c\int_0^{z_*} \frac{dz'}{H(z',\Theta)}, \tag{1.14.13}$$

where $D_v(z,\Theta)$ represents the dilation scale which is given by $D_v(z,\Theta) = \left(\frac{d_A^2(z,\Theta)cz}{H(z,\Theta)}\right)^{1/3}$.

The distant redshift d_z is given by

$$d_z = \frac{r_s(z_*)}{D_v(z,\Theta)}, \tag{1.14.14}$$

where $r_s(z_*)$ is the co-moving sound horizon at the time when photons decouple [235].

The χ^2 function for BAO/CMB can be written as [235]

$$\chi^2_{BAO} = A^T C^{-1} A \tag{1.14.15}$$

where A is the matrix

$$A = \begin{bmatrix} \frac{d_A(z_*,\Theta)}{D_v(0.106,\Theta)} - 30.84 \\ \frac{d_A(z_*,\Theta)}{D_v(0.35,\Theta)} - 10.33 \\ \frac{d_A(z_*,\Theta)}{D_v(0.57,\Theta)} - 6.72 \\ \frac{d_A(z_*,\Theta)}{D_v(0.44,\Theta)} - 8.41 \\ \frac{d_A(z_*,\Theta)}{D_v(0.6,\Theta)} - 6.66 \\ \frac{d_A(z_*,\Theta)}{D_v(0.73,\Theta)} - 5.43 \end{bmatrix}$$

and the inverse of the covariance matrix C^{-1} [235] is given by

$$C^{-1} = \begin{bmatrix} 0.52552 & -0.03548 & -0.07733 & -0.00167 & -0.00532 & -0.00590 \\ -0.03548 & 24.97066 & -1.25461 & -0.02704 & -0.08633 & -0.09579 \\ -0.07733 & -1.25461 & 82.92948 & -0.05895 & -0.18819 & -0.20881 \\ -0.00167 & -0.02704 & -0.05895 & 2.91150 & -2.98873 & 1.43206 \\ -0.00532 & -0.08633 & -0.18819 & -2.98873 & 15.96834 & -7.70636 \\ -0.00590 & -0.09579 & -0.20881 & 1.43206 & -7.70636 & 15.28135 \end{bmatrix}$$

We have taken the correlation coefficient from Ref. [9].

Strong Lensing System

We gather a new data from Strong Lensing System (SLS) to constrain the model parameters. Due to the presence of gravity, light rays passing near matter get bent in accordance with the General theory of Relativity and this bending of light gives rise to multiple images of source. This phenomenon is known as strong gravitational lensing [239]. For elliptical galaxies acting as lenses, Image separation depends on the mass of the lens and also on the angular diameter distance between the lens and the source and also between the observer and the lens.

When a lens is described under the assumption of Singular Isothermal Sphere(SIS), the Einstein radius is defined as

$$\theta_e = 4\pi \frac{\sigma_{SIS} D_{ls}}{c^2 D_s} \tag{1.14.16}$$

where D_{ls} is the angular diameter distances between the lensing galaxy and the source and D_s is the angular diameter distances between the observer and the source, σ_{SIS} is velocity dispersion of lensing galaxy and c is the speed of light.
Since the angular diameter distance D, in terms of redshift can be defined as

$$D(z) = \frac{c}{H_0(1+z)} \int_0^z \frac{dz'}{E(z')} \tag{1.14.17}$$

where H_0 is the Hubble constant. The main advantage of this system is that H_0 is being eliminated in defining the theoretical distance ratio as $D^{th} = \frac{D_{ls}}{D_s}$ to obtain

$$D^{th}(z_l, z_s, \Theta) = \frac{\int_{z_l}^{z^s} \frac{dz'}{E(z')}}{\int_0^{z_s} \frac{dz'}{E(z')}} \tag{1.14.18}$$

where Θ is the set of free model parameters, z_l and z_s are the redshifts to the lens and source respectively and its observable counterpart can be obtained as

$$D^{obs} = \frac{c^2\theta_e}{4\pi\sigma^2} \tag{1.14.19}$$

where σ is the measured velocity dispersion of the lens. We can constrain the cosmological parameters by minimizing the χ^2 function given by [240]

$$\chi^2_{SLS} = \sum_{i=1}^{N_{SL}} \frac{\{D^{th}(z_l, z_s, \Theta) - D^{obs}(\theta_e, \sigma^2)\}^2}{(\delta D^{obs})^2} \tag{1.14.20}$$

where the sum is over all the (N_{SL}) lens systems and δD^{obs} is the uncertainty of each D^{obs} measurement which can be computed employing the standard way of error propagation as

$$\delta D^{obs} = D^{obs}\sqrt{\left(\frac{\delta\theta_e}{\theta_e}\right)^2 + 4\left(\frac{\delta\sigma}{\sigma}\right)^2} \tag{1.14.21}$$

where $\delta\theta_e$ and $\delta\sigma$ are the error reported for the Einstein radius and velocity dispersion respectively.

Local Hubble constant

In addition, we take the recently measured local Hubble constant H_0 as $H_0 = 73.5 \pm 1.4$ $Km\,sec^{-1}\,Mpc^{-1}$ by SH0ES as mentioned in [241].

1.15 Motivation

Cosmological observations carried out by many researchers [7–15] show that the universe recently went under transition from a decelerating to an accelerating expansion. The reason behind this cosmic acceleration is still a mystery and constitutes a challenging problem of modern cosmology.

In relativistic cosmology, an accelerating universe is obtained by considering the existence of a DE component (an exotic fluid endowed with negative pressure). Several theorists have proposed many cosmological models to investigate the behavior of the dark energy. The two most accepted DE models are that of a *cosmological constant* (ΛCDM) or a non-zero vacuum energy density and a slowly varying rolling scalar field (quintessence models). The ΛCDM model faces a number of difficulties. For example,

the data requires a fine-tuned value for the energy density of the vacuum ($\Omega \approx 0.26$). It's critical to find and investigate a number of physical processes that could explain the universe's late-time acceleration. The inconsistency between the local H_0 reported as $H_0 = 74.03 \pm 1.42 \quad Km\, sec^{-1}\, Mpc^{-1}$ and its estimation through the Planck CMB with $H_0 = 67.36 \pm 0.54 \quad Km\, sec^{-1}\, Mpc^{-1}$, certainly emerges as the greatest challenge of the modern cosmology. These issues open alternative approaches beyond the ΛCDM model, such as considering either modifications of GR or new description for DE or different theories of DM. Some approaches in order to investigate the DE are: the dynamical DE, phantom DE, quintessence, chaplygin gas, holographic DE, etc.

As universe continues to expand over time, the negative pressure associated with the cosmological constant (the form of DE in ΛCDM) dominates over opposing gravitational forces, and the expansion of the universe accelerates. Among several models, the thermodynamics approach has been widely investigated. In this regard, bulk viscosity and matter creation cosmology may be the possible candidates for the accelerating universe. Dark energy models with bulk viscosity and matter creation have obtained good results by a description based on fluids, modified GR and a scalar fluid framework. Bulk viscosity and matter creation play an important role in the universe dynamics at the background level because it satisfy cosmological principle. These quantities depend on time and can be written in terms of the Hubble parameter. These quantities also satisfy the transportation equation and therefore can be extended to more general forms that contain derivatives of the Hubble parameter and energy density, $\zeta = \zeta(z, \rho, H, \dot{H})$ and $\Gamma = \Gamma(z, \rho, H, \dot{H})$.

In this thesis work, I investigate a spatially homogeneous and isotropic flat FLRW model with bulk viscosity and matter creation in general relativity and scalar-tensor theory by assuming the different forms of bulk viscous coefficient, ζ and particle creation rate, Γ to observe the effects of these thermodynamical quantities in explaining the DE phenomena.

The thesis entitled **"A Study on Cosmological Models in General Relativity and Modified Gravity Theories"** consists of seven chapters. The bibiliography and the list of publications are given at the end of the thesis.

Chapter 1 titled *"Introduction"* lays out the basic concept of general theory of relativity and cosmology. It deals with the concept of space and time, cosmological principle, Einstein field equations, Friedmann equation, various cosmological param-

eters, the ΛCDM model, the alternative theory. It gives a brief overview for explaining the decelerated-accelerated expansion of the universe. The thermodynamics of dissipative processes of bulk viscosity and matter creation have been discussed. A brief studies on holographic dark energy and Brans-Dicke theory have been carried out. Some of the latest observational data such as Type Ia supernova (SNe), Strong Lensing System (SLS) Observational Hubble parameter data (OHD), Baryon acoustic oscillations (BAO), and cosmic microwave background (CMB) data are discussed. The motivation of the work in this thesis has been discussed at the end. Thus, the current chapter establishes a context and explains the purpose of the thesis work.

Chapter 2 titled *"Probing bulk viscous matter dominated model in Brans-Dicke theory"* explores a matter dominated model with bulk viscosity in BD theory. We solve the field equations by assuming the constant bulk viscous coefficient and BD scalar field proportional to some power of the scale factor to explain the accelerated expansion of universe. The statistical analysis of model is carried out to obtain the best fit values of model parameters. Using the best fit values of model parameters we calculate and plot the deceleration parameter with redshift to show the phase transition of universe. We also discuss age of the universe, statefinder and $Om(z)$ parameter to compare our model with standard ΛCDM model. We also apply the model selection criteria, namely, AIC and BIC to discriminate the viscous model based on the penalization associated to the number of parameters.

Chapter 3 titled *"Viscous cosmology in holographic dark energy with Granda-Oliveros cut-off"* proposes a holographic dark energy (HDE) model with bulk viscosity, whose IR cut-off is set by Granda Oliveros (GO). HDE model with bulk viscosity exhibits the solution that unify the early and late-time acceleration. We assume the most generalized form of bulk viscous coefficient $\zeta = \zeta_0 + \zeta_1 H + \zeta_2 \left(\frac{\dot{H}}{H} + H\right)$, where ζ_0, ζ_1 and ζ_2 are all constants. The model is tested with the latest observational data from Strong lensing System (SLS), measurements of Hz(DA+BAO), SNe(Pantheon) and local H_0. With two different combination of these datasets we constrain our model parameters with the MCMC method to achieve the best fit values of the free parameters. The HDE model with bulk viscosity shows the phase transition from decelerated epoch to accelerated epoch. We also discuss the model through diagnostic parameters and compare our model with standard ΛCDM model.

Chapter 4 titled *" Matter creation cosmology in Brans-Dicke theory: Observational tests and thermodynamical analysis"* outlines a matter dominated model with gravitationally induced matter creation in the framework of BD theory. We assume the particle creation rate as $\Gamma = 3\gamma H_0 + 3\beta H$, where β and γ are the constants, and the BD scalar field proportional to some power of scale factor. We perform the statistical analysis for our model using the four combination of latest observational data of SNe, OHD, and combined data of BAO and CMB. We employ the publicly available EMCEE codes for the implementation of the MCMC method and obtain the best-fit values for the model parameters. We present the evolution of various cosmological parameters using best-fit values of model parameters and study the geometrical diagnostics parameters analytically and graphically. Further we test the thermodynamic viabilities of the matter creation model.

Chapter 5 titled *" Constraints on Holographic dark energy model with matter creation in Brans-Dicke theory and thermodynamical analysis"* examines the HDE model with adiabatic matter creation in context of BD theory to show the evolution of universe. We solve the field equations with and without particle creation rate Γ. The models are tested with the latest observational data from SNe (pantheon sample), measurements of OHD and local H_0 data. By using MCMC method, we obtain the best fit values of the parameters for different models. HDE model without matter creation does not achieve the phase transition when Hubble horizon is taken as an IR cut-off but HDE model with matter creation with same IR cut-off as Hubble horizon shows the phase transition and leads to a solution that unify the early and late-time acceleration. Using AIC and BIC, and geometrical diagnostic parameters, we compare the models with ΛCDM model and discuss the viability of the model. A detailed thermodynamic analysis is also carried out.

Chapter 6 titled *" Evolution of Holographic dark energy model with adiabatic matter creation"* explores HDE with adiabatic matter creation process to explain the observed accelerated expansion of the universe. The field equations are solved analytically with a more generalized form of matter creation rate. The viability of such model is checked by using the recent data of Type Ia supernovae Pantheon sample, Hubble function $H(z)$ data, joined data of BAO/CMB and latest local H_0 by SH0ES.

The last chapter titled *"Conclusion and Future Scope"* provides the conclusion of

the thesis work and future research plan.

Finally, the thesis concludes with a bibliography and a list of the author's publications.

****

Chapter 2

Probing Bulk Viscous matter-Dominated model in Brans-Dicke Theory

---

In this chapter [1]*, we study a matter-dominated model with bulk viscosity in the framework of Brans-Dicke theory. We assume the bulk viscous coefficient as constant and Brans-Dicke scalar field as the power of the scale factor to obtain the exact solution of the field equations. The model parameters are constrained using the latest available astronomical data. The best-fit values of model parameters show that the viscous model shows the phase transition from decelerated epoch to accelerated epoch. The viscous model also alleviates the age problem. We plot the evolution of cosmological parameters to analyse the physical behavior of the viscous model. Geometrical analysis of the model is carried out to compare the model with the standard dark energy model,* ΛCDM *model. We further apply Akaike information criterion* (AIC) *and Bayesian information criterion* (BIC) *to distinguish the viscous model with the reference model,* ΛCDM*.*

---

[1]This chapter is based on a published research paper "Probing Bulk Viscous matter-Dominated model in Brans-Dicke Theory, *Astrophysics and Space Science* **365**, 2 (2020)".

2.1 Introduction

Cosmologists have presented various models to explain the observable acceleration, one of them is the assumption of the existence of mysterious component called *dark energy* (DE). It is assumed that DE has negative pressure which provides the dynamical mechanism for the accelerated expansion of the Universe. In recent years it has also been attempted in modelling the missing energy of the universe and to explain its late time accelerated expansion in view of scalar tensor theories. The scalar-tensor theories of gravity are amongst the most established and well studied alternative theories of gravity that exist in the literature. The interest in scalar-tensor theories of gravity arises from inflationary cosmology, supergravity and superstring theory. The pioneering study on scalar-tensor theories was carried out by Brans and Dicke in 1961 [112], known as Brans-Dicke (BD) theory. The scalar field in BD theory has a very active role for the description of the early era as well as the present phase of the evolution of the Universe. The BD theory provides useful clues to the solutions for some of the outstanding problems in cosmology and could generate sufficient acceleration in the matter dominated Universe.

The idea of viscous dark energy models in cosmology has been presented in different ways to understand the evolution of the universe. Ren and Meng [147] have investigated the universe evolution through a cosmological model with bulk viscosity. Tawfik and Harko [242] have discussed phase transition of the viscous early universe. Singh and Kumar [159] and, Kumar and Singh [161] have explored different aspects of viscosity in $f(R,T)$ gravity taking Hubble horizon as IR cut-off. Viscous cosmology with inhomogeneous equation of state have also been proposed and studied in Refs. [143, 145].

The possibility of distinguishing between cosmological constant and dark energy models is one of the most intriguing questions concerning the late time accelerating expansion in the universe. A reliable diagnostic measure should be introduced using the model independent properties. Using diagnostic analysis, we study some kinematic properties of the dark energy model with bulk viscosity.

The purpose of this chapter is to explore the role of bulk viscosity in BD theory. Such a viscous term acts as a negative pressure. It is well known that bulk viscosity can generate early and late time accelerated expansion. But, such possibility has been investigated only in the context of the primordial universe, concerning also the search

of non-singular models [141, 243]. Indeed, it has been shown in Ref. [244] that for the right viscosity coefficient, we do not need a cosmological constant to explain the accelerating cosmology. We consider a simple bulk viscosity model, in the context of the Eckart formalism [134]. Inspite of the problems of this theory, it has been used to model bulk viscous model as responsible for the observed acceleration of the Universe assuming that the approximation of vanishing relaxation time is valid [245]. Avelino and Nucamendi [246, 247] have studied and constrained a matter-dominated model with bulk viscosity using observational data and found that the model is viable just if the bulk viscosity is triggered in recent times in case bulk viscous coefficient is proportional to the Hubble parameter. However, the model is ruled out by the observations when bulk viscous coefficient is taken to be constant. In this chapter, we extend this work to matter-dominated model with constant bulk viscous coefficient in BD Theory.

Chapter 2 is organized as follows: In section 2.2, we consider the matter-dominated bulk viscous model in the framework of Friedmann-Lemaître-Roberston-Walker (FLRW) line element in BD theory. The solutions of field equations are presented in section 2.3 and discuss the evolution of the scale factor and deceleration parameter. In section 2.4 we discuss two diagnostic parameters, namely statefinder parameter and *Om* parameter to discriminate our model with ΛCDM model. Section 2.5 uses the observational data of Type Ia SNe, Observational Hubble data and Baryon Acoustic Oscillation data to constrain our viscous model parameters. we analyze the constrain of model parameters in the solutions and accordingly discuss the evolution of our model in section 2.6. Section 2.7 deals the information criteria to select the model. Finally, in section 2.8 we conclude the outcomes of our work.

2.2 Viscous model in Brans-Dicke theory

In the context of the Brans-Dicke theory (1961), the action in the presence of matter with Lagrangian $\mathscr{L}_m$ in Jordan frame is given by equation $(1.10.2)$ [116]. The gravitational field equations derived from variation of action $(1.10.2)$ with respect to the metric given in equation $(1.10.3)$. We have assumed the matter content of the universe to be composed of a fluid represented by the energy-momentum tensor

$$T_{\mu\nu} = \left(\rho_m + \tilde{P}\right) u_\mu u_\nu + \tilde{P}\, g_{\mu\nu} \tag{2.2.1}$$

where ρ_m and $\tilde{P}$ represents the energy density and effective pressure of the fluid, respectively, and u_μ is the four velocity of the fluid, i.e., $u_\mu u^\nu = -1$.

The wave equation that follows from equation $(1.10.2)$, by varying the action with respect to the scalar field ϕ, is given in $(1.10.4)$.

We consider a homogenous and isotropic flat Friedmann-Lemaître-Robertson-Walker (FLRW) line-element which is given by $(1.3.8)$. In such a universe, the dissipative effects arise due to the presence of bulk viscosity ζ in cosmic fluids.

The first approach to study the relativistic bulk viscosity process in thermodynamics systems is based on the Eckart theory [134]. It is known that this theory is unstable and non-causal against perturbations around the thermodynamical equilibrium state [248], i.e., it describes that all the equilibrium states are unstable and the signals can propagate through the fluids faster than the speed of light, i.e., with superluminal velocities. These problems could be traced back to their restriction to the first -order deviations from equilibrium. In order to solve these problems, Israel and Stewart [135] proposed a second-order full causal theory in relativistic framework. Despite of instability and non-causality, Eckart theory is still suitable for cosmological investigations while dealing with the accelerating universe with bulk viscous fluids. This is due to the fact that this theory is a good approximation to the IS theory in the limit when the relaxation time vanishes in late time. Another reason is that Eckart theory is less complicated than the IS theory, it has been widely used by many authors to characterize the bulk viscous fluid in describing the late time acceleration when the relaxation time goes to zero. Considering Eckart's theory as a first order limit of Israel-Stewart scenario with zero relaxation time, one can re-express the effective pressure $\tilde{P}$ at the thermodynamical equilibrium as

$$\tilde{P} = p_m + \Pi = p_m - 3\zeta H, \tag{2.2.2}$$

where $\Pi = -3\zeta H$ is the bulk viscous pressure, ζ is the bulk viscous coefficient, ρ_m and p_m are the energy density are pressure of the fluid respectively.

The energy-momentum tensor with viscous fluid is given by equation $(1.11.6)$ where $\tilde{P} = p_m - 3\zeta H$. The dynamics of a FLRW universe in BD theory in the presence of bulk viscosity is governed by the following two equations:

$$H^2 + H\frac{\dot{\phi}}{\phi} - \frac{\omega}{6}\frac{\dot{\phi}^2}{\phi^2} = \frac{8\pi}{3\phi}\rho_m, \tag{2.2.3}$$

$$2\frac{\ddot{a}}{a}+H^2+\frac{\omega}{2}\frac{\dot{\phi}^2}{\phi^2}+2H\frac{\dot{\phi}}{\phi}+\frac{\ddot{\phi}}{\phi}=-\frac{8\pi}{\phi}\tilde{P} \tag{2.2.4}$$

The scalar field evolution equation (1.10.4) is written as

$$\ddot{\phi}+3H\dot{\phi}=\frac{8\pi}{2\omega+3}(\rho_m-3\tilde{P}). \tag{2.2.5}$$

The wave equation (2.2.5) combines with (2.2.3) and (2.2.4) leads to the energy conservation equation

$$\dot{\rho_m}+3(\rho_m+\tilde{P})H=0. \tag{2.2.6}$$

One interesting thing about BD theory in the Jordan frame is that the conservation equation holds separately for the matter and scalar field or in a slightly different way, the Bianchi identity along with the wave equation (1.10.4) gives the matter conservation equation.

Let us consider that the bulk viscous fluid is the non relativistic matter with $p_m=0$. Therefore, the effective pressure is only due to the negative viscous matter, i.e. $\tilde{P}=-3\zeta H$. For the explicit form of ζ, we can principally solve the matter density ρ_m with respect to cosmic time t. The conservation equation (2.2.6) now becomes

$$\dot{\rho_m}+3(\rho_m-3\zeta H)H=0, \tag{2.2.7}$$

which in terms of scale factor can be written as

$$a\frac{d\rho_m}{da}=3(3\zeta H-\rho_m). \tag{2.2.8}$$

Equation (2.2.8) is valid for any parametrization of ζ. However, in this chapter, we consider the simplest parametrization of the bulk viscous coefficient as

$$\zeta=const.=\zeta_0 \tag{2.2.9}$$

We assume the bulk viscous coefficient to be positive, i.e., $\zeta_0>0$ to preserve the validity of second law of thermodynamics.

The general analytical solutions to the system (2.2.3)-(2.2.5) are not known. However, physical sense guides us into searching for possible solutions in which the BD scalar field ϕ evolves very slowly. We assume that BD scalar field can be described as a power-law of the scale factor, namely $\phi=\phi_0\,a^\alpha=\frac{1}{G}a^\alpha$, where ϕ_0 and α are constant [249,250], and here we set the present scale factor $a_0=1$ which implies $\phi_0=1/G$. A

case of particular interest is that when α is small whereas ω is high so that the product $\alpha\omega$ results of order unity [249]. This is interesting because local experiments set a very high lower bound on ω. This choice with small α can lead to consistent results which may justify this specific choice among other possible choices [249]. We note that in Ref. [251] this kind of power-law solution is used to show that BD cosmology with a cosmological term can mimic the running vacuum model, which is very convenient in order to improve the fitting of the cosmological data [252]. With this power-law assumption,

$$\phi = \phi_0\, a^{\varepsilon} \tag{2.2.10}$$

where ϕ_0 and ε are constants. Equation (2.2.3) can be rewritten as

$$H^2 = \frac{16\pi}{(6+6\varepsilon-\omega\varepsilon^2)\phi_0}\frac{\rho_m}{a^{\varepsilon}}. \tag{2.2.11}$$

It is to be noted that the solar system experiments Cassini predict a very stringent high bound result on ω as $|\omega| > 40000$ [115, 253] but the cosmological observations put comparatively lower bounds on ω [254].

Substituting (2.2.11) into (2.2.8) we obtain

$$a\frac{d\rho_m}{da} + 3\rho_m - \kappa\frac{\rho_m^{1/2}}{a^{\varepsilon/2}} = 0, \tag{2.2.12}$$

where $\kappa = 9\left(\frac{16\pi}{(6+6\varepsilon-\omega\varepsilon^2)\phi_0}\right)^{1/2}\zeta_0$.

On solving (2.2.12), we get the evolution for energy density as

$$\rho_m = \left[\frac{\kappa}{(3-\varepsilon)}a^{-\varepsilon/2} + \left(\rho_{m0}^{1/2} - \frac{\kappa}{(3-\varepsilon)}\right)a^{-3/2}\right]^2 \tag{2.2.13}$$

where ρ_{m0} is the present value of energy density. We assume that the value of scale factor at present is $a_0 = 1$. Now, by considering that $a = (1+z)^{-1}$, the energy density in (2.2.13) can be rewritten as

$$\rho_m = \left[\frac{\kappa}{(3-\varepsilon)}(1+z)^{\varepsilon/2} + \left(\rho_{m0}^{1/2} - \frac{\kappa}{(3-\varepsilon)}\right)(1+z)^{3/2}\right]^2 \tag{2.2.14}$$

Inserting (2.2.14) into (2.2.11), we obtain

$$H(z) = H_0(1+z)^{-\varepsilon/2}\left[\frac{\bar{\zeta}_0(1+z)^{\varepsilon/2}}{(3-\varepsilon)} + \left(\Omega_{m0}^{1/2} - \frac{\bar{\zeta}_0}{(3-\varepsilon)}\right)(1+z)^{3/2}\right] \tag{2.2.15}$$

where H_0 is the present Hubble constant, $\kappa = \bar{\zeta}_0/H_0$ is the dimensionless bulk viscous coefficient and $\Omega_{m0} = \rho_{m0}/\rho^0_{crit}$, where $\rho^0_{crit} = 3\phi_0\, H_0^2/8\pi$ is the present critical density. Taking $\Omega_{m0} = 1$ at present as bulk viscous matter is the only component, Eq. (2.2.15) finally becomes

$$H(z) = \frac{H_0}{(3-\varepsilon)}(1+z)^{-\varepsilon/2}\left[\bar{\zeta}_0(1+z)^{\varepsilon/2} + \left(3-\varepsilon-\bar{\zeta}_0\right)(1+z)^{3/2}\right] \tag{2.2.16}$$

It should be noticed that for $\varepsilon = 0$, the above expression reduces to the solution derived in Ref. [245].

2.3 Solution of viscous model

Equation (2.2.16) has the solution

$$\int_1^a \frac{\acute{a}^{\frac{3}{2}-\frac{\varepsilon}{2}}\, d\acute{a}}{\acute{a}\left[\bar{\zeta}_0\acute{a}^{\frac{3}{2}-\frac{\varepsilon}{2}} + \left(3-\varepsilon-\bar{\zeta}_0\right)\right]} = \frac{H_0}{(3-\varepsilon)}\int_{t_0}^t d\acute{t} \tag{2.3.1}$$

where t is the cosmic time and t_0 is the present cosmic time. In the absence of bulk viscous term, $\bar{\zeta}_0 = 0$, equation (2.3.1) gives the scale factor for matter-dominated universe in BD theory as

$$a(t) = \left(\frac{3-\varepsilon}{2}H_0(t-t_0)+1\right)^{2/(3-\varepsilon)}, \quad (3-\varepsilon) \neq 0, \tag{2.3.2}$$

which is power-law of expansion. The model decelerates for $0 \leq \varepsilon < 1$ and accelerates for $\varepsilon \geq 1$.

For $\bar{\zeta}_0 \neq 0$, Equation (2.3.1) gives

$$a = \left[\frac{(3-\varepsilon)\exp\left(\frac{\bar{\zeta}_0 H_0}{2}(t-t_0)\right) - (3-\varepsilon-\bar{\zeta}_0)}{\bar{\zeta}_0}\right]^{2/(3-\varepsilon)}, \tag{2.3.3}$$

where $\bar{\zeta}_0 \neq 0$ and $(3-\varepsilon) \neq 0$.

The transition from one phase to another phase can also be obtained by defining the deceleration parameter q, as in (1.7.11). Using (2.3.3) in (1.7.11), the value of q for the viscous model takes the following form

$$q(t) = -\frac{1}{2}\left[2 - (3-\varepsilon-\bar{\zeta}_0)e^{-\frac{\bar{\zeta}_0 H_0}{2}(t-t_0)}\right]. \tag{2.3.4}$$

In terms of redshift, q is given by

$$q(z,\bar{\zeta}_0) = -1 + \frac{1}{2}\frac{(3-\varepsilon-\bar{\zeta}_0)(3-\varepsilon)}{\bar{\zeta}_0\,(1+z)^{-\frac{(3-\varepsilon)}{2}} + (3-\varepsilon-\bar{\zeta}_0)} \tag{2.3.5}$$

We find that the value of q is time-dependent and hence the model shows the transition. We see that $q = (1-\varepsilon)/2$ in the absence of bulk viscous term, i.e., for $\bar{\zeta}_0 = 0$. Thus, for $0 \leq \varepsilon < 1$, the model decelerates and accelerates for $\varepsilon \geq 1$.

The solution of BD scalar field is given by

$$\phi = \phi_0 \left[\frac{(3-\varepsilon)\exp\left(\frac{\bar{\zeta}_0 H_0}{2}(t-t_0)\right) - (3-\varepsilon-\bar{\zeta}_0)}{\bar{\zeta}_0}\right]^{(2\varepsilon)/(3-\varepsilon)}. \tag{2.3.6}$$

Now, we will discuss the solutions for three different values of $\bar{\zeta}_0$ which are as follows:

Case(i): $0 < \bar{\zeta}_0 < (3-\varepsilon)$

In this case, we observe that as $t \to \infty$, the scale factor $a \sim \exp\left(\frac{\bar{\zeta}_0 H_0}{(3-\varepsilon)}(t-t_0)\right)$ i.e., to have the form like de Sitter universe. It is obvious that for any value of $\bar{\zeta}_0$ in $0 < \bar{\zeta}_0 < (3-\varepsilon)$, the model predicts a Big-bang in past during time $t_B = t_0 + \frac{2}{\bar{\zeta}_0 H_0} ln\left(1 - \frac{\bar{\zeta}_0}{(3-\varepsilon)}\right)$. The elapsed time between Big-bang time t_B until today t_0, the age of the Universe, is given by $|t_B - t_0| = \frac{2}{\bar{\zeta}_0 H_0} ln\left(1 - \frac{\bar{\zeta}_0}{(3-\varepsilon)}\right)$. Thus, there is decelerating epoch followed by a transition from deceleration to acceleration epoch in late time. To compute the value of scale factor where transition happens, we have from (2.2.16)

$$\frac{d\dot{a}}{da} = \frac{H_0}{(3-\varepsilon)}\left[\bar{\zeta}_0 + \frac{(\varepsilon-1)(3-\varepsilon-\bar{\zeta}_0)}{2}\, a^{\frac{\varepsilon-3}{2}}\right]. \tag{2.3.7}$$

Equating (2.3.7) to zero, we get

$$a_{tr} = \left[\frac{(1-\varepsilon)(3-\varepsilon-\bar{\zeta}_0)}{2\bar{\zeta}_0}\right]^{2/(3-\varepsilon)}, \tag{2.3.8}$$

where the subscript “tr" denotes the transition.

We plot the evolution of $a(t)$ as a function of t in Fig.2.1 for different values of ε and $\bar{\zeta}_0$ in $0 \leq \bar{\zeta}_0 \leq (3-\varepsilon)$. It is observed that phase transition from decelerated to accelerated phase occurs in future ($a_{tr} > 1$) for the value of $\bar{\zeta}_0$ in interval $0 < \bar{\zeta}_0 < (1-\varepsilon)$. When $\bar{\zeta}_0 = (1-\varepsilon)$, we get $a_{tr} = 1$, i.e., the transition takes place today whereas the

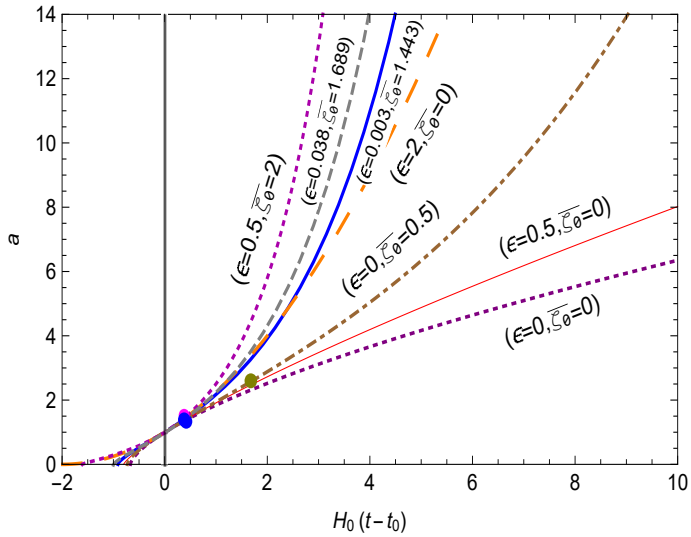

Figure 2.1: $a(t)$ as a function of t for different values of ε and $\bar{\zeta}_0$ in the range of $0 \leq \bar{\zeta}_0 \leq (\varepsilon - 3)$. The grey dotted line represents the evolution coming from $SNe + OHD$ and the blue solid line corresponds trajectory coming from $SNe + OHD + BAO$ data set analysis (see, section 2.6). The dots show the transition point.

transition occurs in past $(0 < a_{tr} < 1)$ for the values of $\bar{\zeta}_0$ in $(1-\varepsilon) < \bar{\zeta}_0 < (3-\varepsilon)$. We observe that as the value of $\bar{\zeta}_0$ increases, the transition from deceleration to acceleration occurs in the past. In the limiting case when $\bar{\zeta}_0$ approaches to $(3-\varepsilon)$, $a_{tr} \to 0$, i.e., the transition takes place very close to Big-bang.

In this case, the deceleration parameter decreases from $q(1) = -1 + \frac{1}{2}(3 - \varepsilon - \bar{\zeta}_0)$ to $q(\infty) = -1$ which shows the transition from positive to negative. When $\bar{\zeta}_0 = (1-\varepsilon)$, $q = 0$, i.e., the transition from decelerated to accelerated phase takes place today.

Case(ii): $\bar{\zeta}_0 = (3-\varepsilon)$

In this case, equation (2.3.3) gives $a(t) = \exp(H_0(t-t_0))$ and $q = -1$ that corresponds to the de Sitter universe. The model has singularity at infinite past, i.e., as $(t-t_0) \to -\infty$, $a \to 0$ and as $(t-t_0) \to \infty$, $a \to \infty$. The matter density is constant, $\rho_m = \frac{(6+6\varepsilon-\omega\varepsilon^2)\phi_0 H_0^2}{16\pi(3-\varepsilon)}$. In Fig. 2.2, the dotted line $\varepsilon = 0.5$ and $\bar{\zeta}_0 = 2.5$ corresponds to $\bar{\zeta}_0 = (3-\varepsilon)$ (the de Sitter universe).

Case(iii): $\bar{\zeta}_0 > (3-\varepsilon)$

In this case, we observe that the viscous model always accelerates. There is not any deceleration-acceleration transition. The deceleration parameter always gives negative value. In this case, the model starts with minimum scale factor (Einstein static universe) and behaves as a de Sitter universe in future. The evolution of the

scale factor is presented in Fig. 2.2 for different values of ε and $\bar{\zeta}_0$ in $\bar{\zeta}_0 \geq (3-\varepsilon)$.

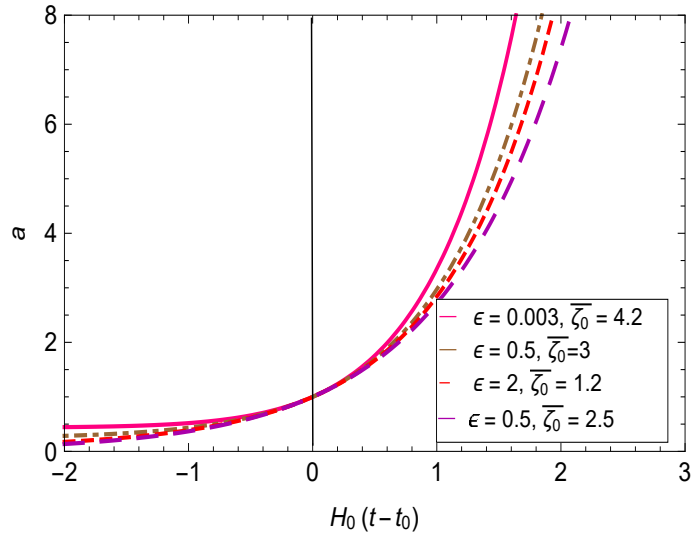

Figure 2.2: Plot of the scale factor as function of time for different values of $\bar{\zeta}_0$ in the range of $\bar{\zeta}_0 \geq (\varepsilon - 3)$

2.4 Diagnostic analysis

One of the most intriguing questions concerning the late time accelerating expansion in the universe is that, the possibility of distinguishing between cosmological constant and dark energy models. High sensitivity as well as model independent properties should be considered for introducing a reliable diagnostic measure. Using diagnostic analysis, we are able to study some kinematic properties of the viscous dark energy model. In this context, Sahni et al. (2003) [198,199] introduced a new geometrical diagnostic pair $\{r,s\}$, known as statefinder parameters, which is constructed from the scale factor and its derivatives up to the third order. The statefinder pair $\{r,s\}$ is geometrical in the nature as it is constructed from the space-time metric directly. Therefore, the statefinder parameters are more universal parameters to study the DE models than any other physical parameters. In a flat ΛCDM model, the statefinder pair has a fixed point value $\{r,s\} = \{1,0\}$ where as it is $\{r,s\} = \{1,1\}$ for SCDM model. One can plot the trajectories in $r-s$ and $r-q$ planes to discriminate various DE models. We will discuss the statefinder diagnostic for viscous model and obtain the fixed point values of statefinder pair under suitable constraints.

As a complementary to $\{r,s\}$, Sahni et al.(2008) [200] proposed another new diagnostic called, *Om(z)*. This diagnostic helps to distinguish the present matter density Ω_{om} in different models more effectively. The *O*m(z) diagnostic is indeed a geomet-

rical diagnostic which combines Hubble parameter and redshift. It can differentiate dark energy model from ΛCDM. For ΛCDM model *Om(z)* $= \Omega_{0m}$ while for other dark energy models, *Om(z)* depends on redshift. Phantom like dark energy corresponds to the positive slope of *Om(z)* whereas the negative slope means dark energy behaves like quintessence.

In this section, we discuss about the statefinder parameter $\{r,s\}$, which discriminates the proposed model with ΛCDM model. The diagnostic statefinder parameter $\{r,s\}$ is defined in $(1.12.1)$ and for this viscous BD model, the statefinder parameters are given by

$$\begin{aligned} r &= \frac{1}{4}e^{-\bar{\zeta}_0 H_0(t-t_0)}\left[(3-\varepsilon)e^{\frac{\bar{\zeta}_0 H_0}{2}(t-t_0)}-(3-\varepsilon-\bar{\zeta}_0)\right]^2+ \\ &\quad \frac{3}{4}(\varepsilon-1)e^{-\frac{\bar{\zeta}_0 H_0}{2}(t-t_0)}\left[(3-\varepsilon)e^{\frac{\bar{\zeta}_0 H_0}{2}(t-t_0)}-(3-\varepsilon-\bar{\zeta}_0)\right]+\frac{1}{2}(\varepsilon-1)(\varepsilon-2) \end{aligned} \quad (2.4.1)$$

and

$$s=\frac{(r-1)}{3\left[-\frac{3}{2}+\frac{(3-\varepsilon-\bar{\zeta}_0)}{2}e^{-\frac{\bar{\zeta}_0 H_0}{2}(t-t_0)}\right]} \quad (2.4.2)$$

We observe that as $(t-t_0)\to\infty$, the statefinder pair $\{r,s\}\to\{\frac{(\varepsilon-1)(\varepsilon-2)}{2},\frac{2-(\varepsilon-1)(\varepsilon-2)}{9}\}$, which deviates from the ΛCDM model. However, it corresponds to the ΛCDM model for $\varepsilon=0$.

Now, we discus another diagnostic parameter, known as *Om(z)*, which is defined as in $(1.12.2)$. Using $(2.2.16)$ into $(1.12.2)$, we get

$$Om(z)=\frac{\left[\bar{\zeta}_0+(3-\varepsilon-\bar{\zeta}_0)(1+z)^{\frac{(3-\varepsilon)}{2}}\right]-(3-\varepsilon)^2}{(3-\varepsilon)^2[(1+z)^3-1]}. \quad (2.4.3)$$

In the case of $z=-1$, *Om(z)* $=1-\frac{\bar{\zeta}_0}{(3-\varepsilon)^2}$, which is constant, which deviates from the ΛCDM model. However, in the absence of bulk viscosity we get *Om(z)* $=1$. We will discuss in details the trajectories of $\{r,s\}$ and *Om(z)* in section 2.6.

2.5 Observations and Methodology

It is very interesting to study the effects of viscous model at cosmological scales on the evolution of universe. To study quantitatively the effects of bulk viscosity, we perform the global constraints on viscous model using the latest cosmological obser-

vations which are exhibited as follows:

- **SNe(cJLA data):**
  SNe is a powerful probe of cosmology. Betoule et al. [210] reported the results of 'Joint light-curve Analysis' (JLA) dataset of 31 check point (30 bins) covering the redshift range, $z = [0.01, 1.3]$.

- **OHD:** We use the OHD data of 43 measurement points collected in Ref. [214] in the redshift range $0 < z < 2.5$.

- **BAO:**
  BAO are excellent geometrical probes. We include the sample of BAO distances measurements from from SDSS(R) [236], the 6dF Galaxy survey [237], BOSS CMASS [229] and three parallel measurements from WiggleZ survey [238].

The data description of SNe, OHD and BAO data are given in Section (1.14). Using the above cosmological observations, we adopt the Markov Chain Monte Carlo (MCMC) method to find the best-fit value of model parameters of viscous model. The χ^2 for each data, namely, χ^2_{SNe}, χ^2_{OHD} and χ^2_{BAO} are given in equations $(1.14.3)$, $(1.14.7)$ and $(1.14.15)$ respectively.

2.6 Results and Analysis

We implement the constraint on viscous model using two different combination $SNe + OHD$ and $SNe + OHD + BAO$. We use the MCMC method to obtain the best -fit parameters and the corresponding χ^2_{min}. The results of the estimation of the model parameters of the viscous BD model from the observational data sets, namely (i) $SNe + OHD$ and (ii) $SNe + OHD + BAO$, are presented in Table 2.1. The contour plots of parameters with $1\sigma(68.3\%)$ and $2\sigma(95.4\%)$ confidence level for $SNe + OHD$ and $SNe + OHD + BAO$ are shown in Figs. 2.3 and 2.4, respectively.

The evolution of the scale factor is shown in Figs. 2.1 and 2.2. for different values of model free parameters. Using the best fitting data of parameters listed in Table 2.1, we plot the trajectories of the scale factor. In Fig. 2.1, the trajectories are shown for $0 < \bar{\zeta}_0 < (3 - \varepsilon)$. The grey dotted line and the solid blue line represent the evolution of the scale factor for best fitting data of parameters obtained from $SNe + OHD$ and

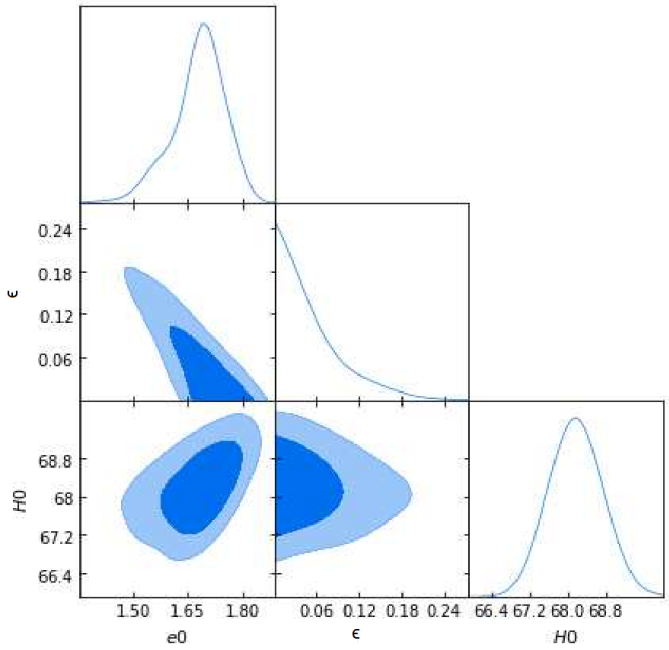

Figure 2.3: The contour maps of $\bar{\zeta}_0$, ε, H_0 at $1\sigma(68.3\%)$ and $2\sigma(95.4\%)$ confidence level using $SNe+OHD$. In Fig. $e0$ means $\bar{\zeta}_0$

Table 2.1: The results of statistical analysis for the viscous BD model parameters.

Parameters	SNe+OHD	SNe+OHD+BAO
$\bar{\zeta}_0$	$1.689^{+0.062}_{-0.087}$	$1.443^{+0.027}_{-0.030}$
ε	$0.038^{+0.064}_{-0.025}$	$0.003^{+0.005}_{-0.002}$
H_0	$68.187^{0.566}_{-0.601}$	$65.324^{+0.487}_{-0.391}$
$\chi^2_{d.o.f.}$	0.493	0.931

$SNe+OHD+BAO$, respectively. The trajectories show that the viscous universe decelerates in early time and accelerates in late time. Figure 2.2 shows the trajectories for $\bar{\zeta}_0 \geq (3-\varepsilon)$. The transition scale factor a_{tr} for best fitting data, where the transition from decelerated phase to accelerated phase takes place, for both the datasets is listed in Table 2.2.

We plot the deceleration parameter versus redshift in Fig. 2.5 for best-fit values of model parameters. Both the trajectories show that model transits from decelerated phase (negative redshift) to accelerated (positive redshift) phase. In Fig. 2.5, red dotted line represents trajectory obtained by $SNe+OHD$ where as the blue solid line represents the trajectory from $SNe+OHD+BAO$. From (2.3.5) we can obtain the val-

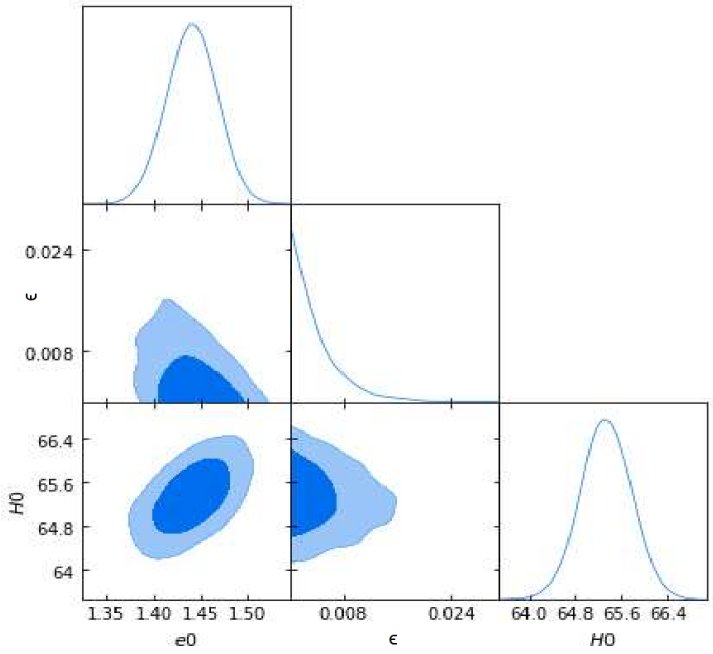

Figure 2.4: The contour maps of $\bar{\zeta}_0$, ε, H_0 at $1\sigma(68.3\%)$ and $2\sigma(95.4\%)$ confidence level using $SNe+OHD+BAO$. In Fig. $e0$ means $\bar{\zeta}_0$

Table 2.2: The transition scale factor and redshift, and present values of $q(z)$ and w_{eff} using best-fit results of model parameters

Data	a_{tr}	z_{tr}	q_0	w_{eff}
SNe+OHD	0.504	0.984	-0.363	-0.575
SNe+OHD+BAO	0.660	0.515	-0.223	-0.482

ue of q_0 as $q(z=0,\bar{\zeta}_0)=(1-\varepsilon-\bar{\zeta}_0)/2$. Using the best-fit values of parameters from Table 2.1, the present value of deceleration parameter is listed in Table 2.2. This is comparatively higher from the observational results on the present value of q, which is around -0.64 [255, 256]. The transition redshift, at which q enters the negative value region, corresponding to an accelerating epochs are also listed in Table 2.2. An analysis of the ΛCDM model with combined $SNe+CMB$ data gives the transition redshift as $z_{tr}=0.45-0.73$ [257].

Using (2.4.1) and (2.4.2), the trajectories of $\{r,s\}$ in $s-r$ plane for different values of ε and $\bar{\zeta}_0$ are shown in Fig. 2.6. It is found that in $0\leq\bar{\zeta}_0\leq(3-\varepsilon)$, the trajectories start from quintessence region ($r<1$, $s>0$) in early time and tend to ΛCDM in late time. However, for the values in $\bar{\zeta}_0\geq(3-\varepsilon)$, the trajectories start from chaplygin gas region ($r>1$, $s<0$). It reveals that the (r,s) trajectory for best fitted parameters are lying in the region of quintessence. In all cases we find that the viscous model tends to

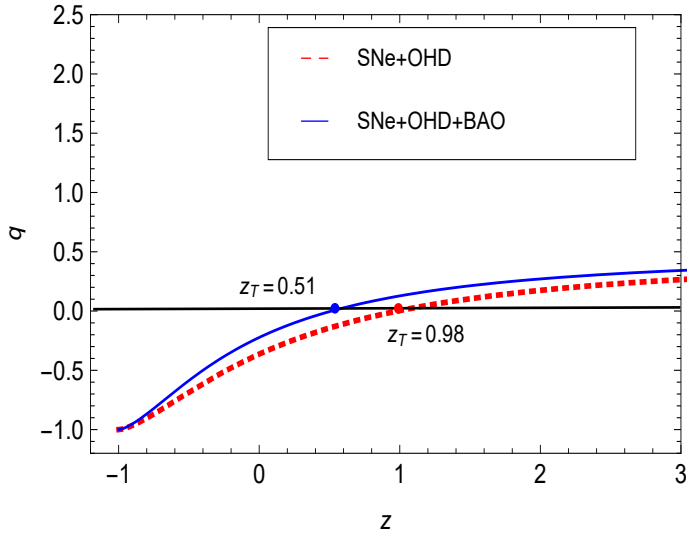

Figure 2.5: Plot of the deceleration parameter q with redshift z for best-fit values of model parameters obtained from two sets of joint analysis of observational data

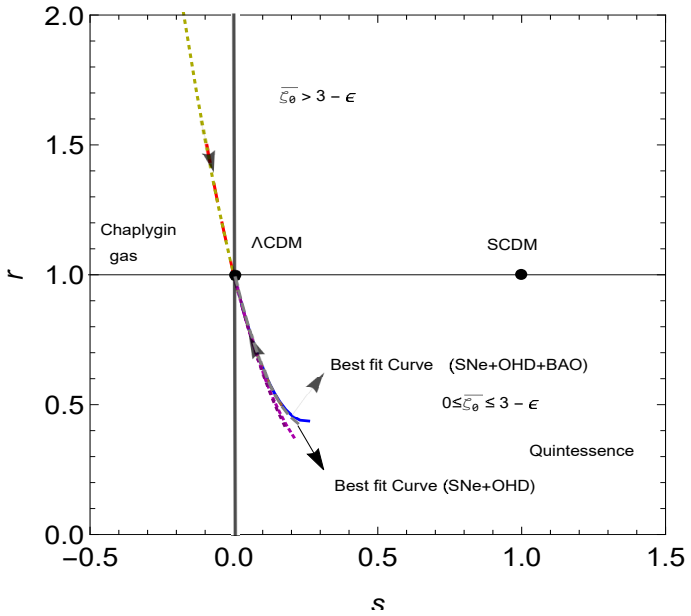

Figure 2.6: The trajectory of $\{r,s\}$ in $s-r$ plane for the best-fit values and other different values of model parameters. The arrow shows the direction of the evolution of the trajectory.

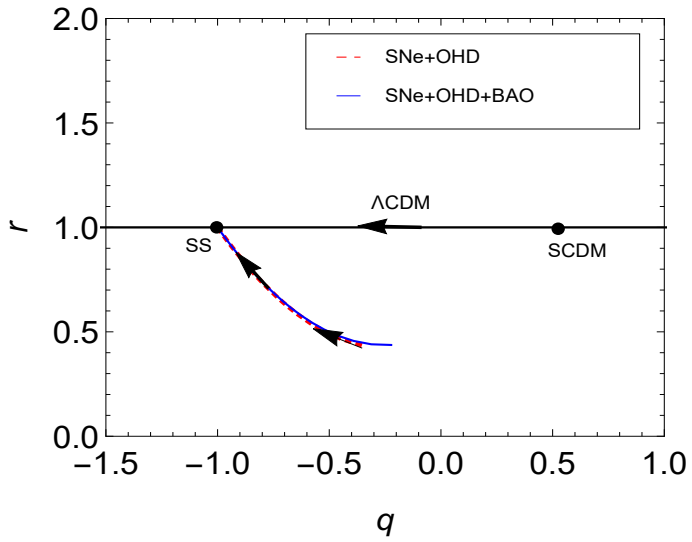

Figure 2.7: The trajectory of $\{r,q\}$ in $q-r$ plane for the best-fit values of model parameters obtained from two sets of joint analysis of observational data. The arrow shows the direction of the evolution of the trajectory.

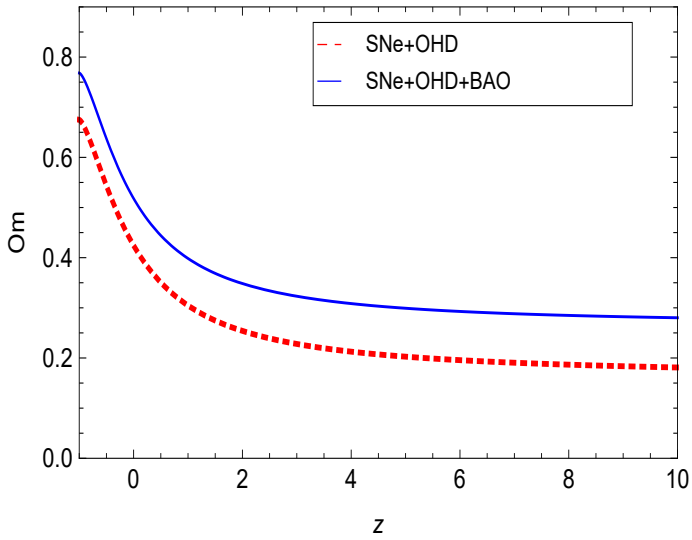

Figure 2.8: The trajectory of $Om(z)$ for the best-fit values of model parameters obtained from two sets of joint analysis of observational data.

ΛCDM model in late time. So the present model resembles the ΛCDM model in future. The present position of the universe dominated by the viscous matter corresponds to $\{r_0, s_0\} = \{0.43706, 0.2595\}$. Thus, the viscous model is distinguishably different from the ΛCDM model.

The $r-q$ relation for the model is shown in Fig. 2.7. The $SCDM$ model corresponds to $\{r,q\} = \{1, 0.5\}$ and steady state (SS) model corresponds to fixed points and $\{r,q\} = \{1,-1\}$. The horizontal line at $r = 1$ corresponds to the time evolution of ΛCDM model. The viscous model approaches to the standard model like ΛCDM and quintessence model [198] in late time.

Using best fit values as given in Table 2.1 into equation (2.4.3), the trajectory of *Om* with redshift z is shown in Fig. 2.8. The trajectories reveal that the viscous model shows deviation from the horizontal line which belongs to ΛCDM model. Moreover, the negative slope of the trajectories indicate that our model has a quintessence behavior.

Next, we find the effective equation of state (EoS) parameter to observe the accelerated expansion of the universe. It is to be noted that an accelerated expansion is possible only if the effective EoS parameter $w_{eff} < -1/3$, or $3w+1 < 0$. The EoS parameter can be obtained using the standard relation [258] as

$$w_{eff} = -1 - \frac{1}{3}\frac{2a}{h}\frac{dh}{da}, \tag{2.6.1}$$

where $h = H/H_0$ is the dimensionless Hubble parameter. Using equation (2.2.16) into equation (2.6.1), we get

$$w_{eff} = -1 + \frac{1}{3}\frac{(3-\varepsilon-\bar{\zeta}_0)(1+z)^{\frac{(3-\varepsilon)}{2}}}{h} \tag{2.6.2}$$

As $z \to -1$, $(a \to \infty)$, we get $w_{eff} \to -1$, which can also be observed from Fig. 2.9. It means that the model tends to de Sitter in future time. Viscous model is free from big-rip singularity as EoS does not cross the phantom divide line $w \leq -1$.

The current value ($h = 1$) of w_{eff} is found to be

$$w_{eff}(z=0) = -1 + \frac{(3-\varepsilon-\bar{\zeta}_0)}{3}. \tag{2.6.3}$$

This shows that $w_{eff}(z=0)$ makes transition from positive values to negative values for $\bar{\zeta}_0 \geq (1-\varepsilon)$. It can also be understood by the present values of $q_0(z=0)$, where

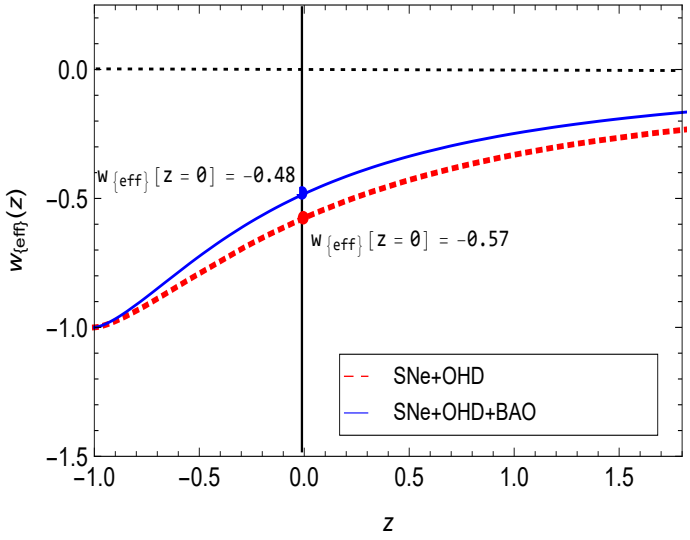

Figure 2.9: Plot of effective equation of state parameter w_{eff} versus redshift z for best-fit values of model parameters obtained from two sets of joint analysis of observational data. The dot denotes the present value of w_{eff} which is within the quintessence region

q makes the transition for $\bar{\zeta}_0 \geq (1-\varepsilon)$, which is discussed in section (2.3). As stated above, $w_{eff} < -1/3$ is the condition for accelerating universe. From eq. (2.6.3), it is obvious that $w_{eff}(z=0) < -1/3$ only for $\bar{\zeta}_0 \geq (1-\varepsilon)$, i.e., $(1-\varepsilon) \leq \bar{\zeta}_0 \leq (3-\varepsilon)$. The present value of the EoS parameter using the best-fitted values of model parameters obtained from both joint data, is listed in Table 2.2. These values are comparatively higher than that predicted by the joint analysis of $WMAP+BAO+H_0+SNe$ data, which is around -0.93 [14]. The evolution of effective EoS with redshift for the best estimated values of model parameters is given in Fig. 2.9. The trajectories show that the viscous BD model favors the quintessence type of DE.

In Fig. 2.10, we compare our viscous model with the standard ΛCDM model with the error bar plots of Hubble dataset. We conclude that the fitting achieved from our statistical analysis is compatible with the Hubble observational data.

Let us calculate the age of the universe. The age of the universe is the time elapsed since the Big Bang. As ΛCDM model is well understood theoretically and strongly supported by recent high precision astronomical observations such as WMAP. So today age of universe is carried out in context of ΛCDM model.

The age of our universe at redshift z is given by $t(z) = T(z)/H_0$, where

$$T(z) = \int_z^\infty \frac{dz'}{(1+z')(H(z)/H_0)} \tag{2.6.4}$$

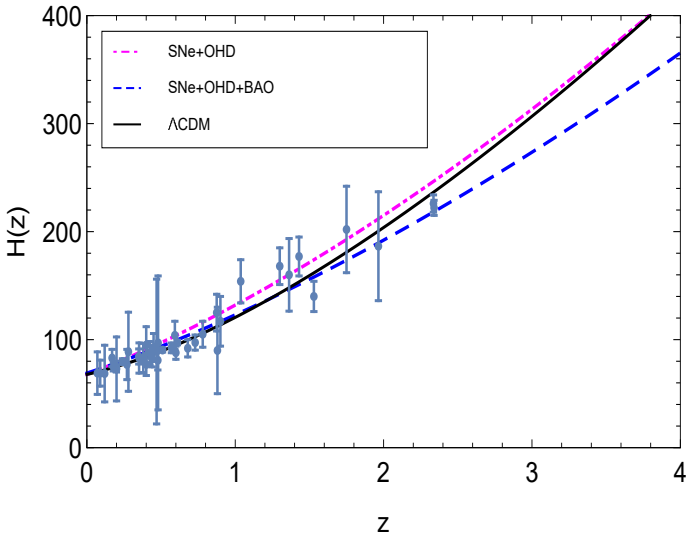

Figure 2.10: Plot of Hubble evolution of the ΛCDM model and the best-fit values of model parameters obtained from two sets of joint analysis of observational data with error bar plots from Hubble data

is the dimensionless age parameter. For the ΛCDM model, in which the density parameter, $\Omega_{m0} \approx 0.27$, the age parameter is [152]

$$T(z) = \int_z^{\infty} \frac{dz'}{(1+z')[\Omega_{m0}(1+z)^3 + (1-\Omega_{m0})]^{1/2}} \tag{2.6.5}$$

It is to be noted that the present age of the universe for a flat CDM model dominated by matter ($\Omega_{m0} = 1,\ t_0 = 2/(3H_0)$) gives $t_0 \approx 8 - 10\ Gyr$, which does not satisfy the stellar age bound: $t_0 > 11 - 12\ Gyr$, as the age of the universe should be longer than any objects in the universe. Therefore, this model suffers the age problem. However, for ΛCDM model, it easily satisfies the constraint $t_0 > 11 - 12\ Gyr$. It seems that the problem is caused by the fact that matter is diluted too fast. Feng and Li [152] claimed that once the viscosity is taken into account, this age problem is alleviated. In our viscous model, Fig. 2.11 shows that the trajectory for the Viscous model deviates a little from that of ΛCDM. It indicates that the viscosity could really resolve the age problem. Addition of viscosity makes the matter dilution little bit slower, changes the energy conservation equation and then the age problem is resolved.

2.7 Model selection

Based on the statistical analysis, we use Akaike Information Criterion (AIC) and the Bayesian Information Criterion (BIC) to check which model is better. The AIC and BIC have been discussed in section 1.13.

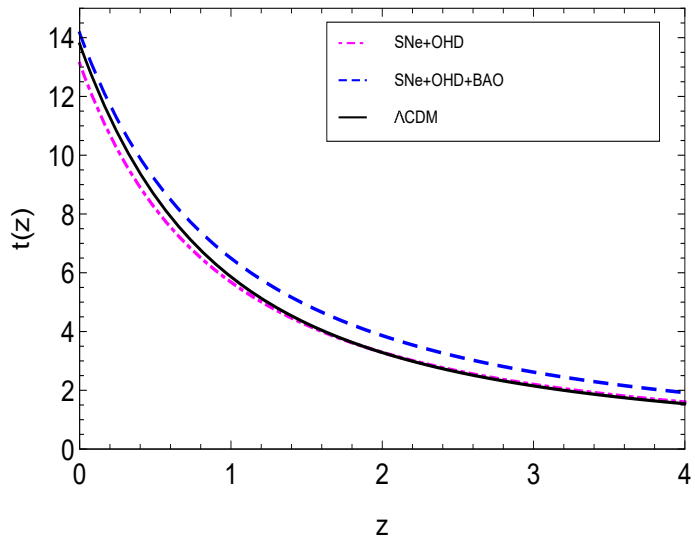

Figure 2.11: The age of universe of viscous model for best-fit values of model parameters obtained from two sets of joint analysis of observational data and ΛCDM model.

Table 2.3: Summary of the *AIC* and *BIC* for ΛCDM model and viscous BD model

Model	Data set	χ^2_{min}	AIC	BIC
ΛCDM				
	SNe+OHD	27.89	31.89	36.49
	SNe+OHD+BAO	30.45	34.45	39.21
Viscous BD				
	SNe+OHD	34.81	38.81	43.41
	SNe+OHD+BAO	72.67	76.67	81.43

Using equations (1.13.2) and (1.13.3), it is obvious that a model giving a small AIC and a small BIC is favoured by the observations. It requires a 'reference model' for comparison, and ΛCDM could be the best reference model and we choose that for the purpose. Table 2.3 presents the results of AIC and BIC of ΛCDM model and viscous BD model.

In our analysis ΛCDM is the model with lower AIC and BIC parameters when we use data from the joint analysis of $SNe+OHD$ and $SNe+OHD+BAO$, respectively. From Table 2.3, considering ΛCDM as the referring model, we find $\Delta AIC = 6.92$ corresponds to $SNe+OHD$ and $\Delta AIC = 42.22$ corresponds to $SNe+OHD+BAO$. This indicates that the viscous BD model with joint analysis of SNe and OHD is in the region of "less evidence in favor" where as viscous model using joint analysis of SNe, OHD and BAO is in "no evidence in favour". Regarding BIC, we find $\Delta BIC = 6.92$ corresponds to $SNe+OHD$ and $\Delta BIC = 42.22$ corresponds to $SNe+OHD+BAO$. This shows that the model has "strong evidence against". We notice a tension between AIC and BIC results, while AIC indicates there is "less evidence in favor" with $SNe+OHD$, BIC indicates that there is "strong evidence against" for the same model. This is due to the fact that BIC strongly penalizes model. We can say that the viscous BD model obtained from joint analysis of SNe and OHD is marginally better than other results.

2.8 Conclusion

In this chapter, we have discussed a bulk viscous matter-dominated universe with constant bulk viscous coefficient, $\zeta = \zeta_0$ in BD theory. We have solved the evolution equations to obtain the scale factor and other cosmological parameters. We have identified three possible conditions for bulk viscous coefficient, $0 \leq \bar{\zeta}_0 < (3-\varepsilon)$, $\bar{\zeta}_0 = (3-\varepsilon)$ and $\bar{\zeta}_0 > (3-\varepsilon)$. Depending on these conditions, we have analyzed the different possible evolutions predicted by the viscous model. We have observed that the viscous model depicts a universe with a Big-bang in the past and then transition from decelerating epoch to an accelerating epoch in late times for the values of $\bar{\zeta}_0$ in the range $0 < \bar{\zeta}_0 \leq (3-\varepsilon)$. For $\bar{\zeta}_0 = (3-\varepsilon)$, the model corresponds to the de Sitter and it always predicts accelerated expansion for $\bar{\zeta}_0 > (3-\varepsilon)$. We have calculated the value of the scale factor where the transition happens. We have found that the transition from decelerated phase to accelerated one occurs in future in $0 < \bar{\zeta} < (1-\varepsilon)$. When $\bar{\zeta}_0 = (1-\varepsilon)$, the transition from decelerated to accelerated epoch takes place

today. The transition between the deceleration-acceleration epoch takes place in past in $(1-\varepsilon) < \bar{\zeta}_0 \leq (3-\varepsilon)$. In limiting case, when $\bar{\zeta}_0$ approaches to $(3-\varepsilon)$, the transition takes place very close to Big-bang. The evolutions of the scale factor are plotted in Figs. 2.1 and 2.2 for different values of $\bar{\zeta}_0$ and ε.

We have constrained the present viscous model using two sets of combined observational data coming from $SNe+OHD$ and $SNe+OHD+BAO$. The value of bulk viscous coefficient is positive which satisfies the second law of thermodynamics. We have shown the contour maps of parameters H_0, ε and $\bar{\zeta}_0$ with $1\sigma(68.3\%)$ and $2\sigma(95.4\%)$ confidence level in Figs. 2.3 and 2.4.

We have studied the evolution of the deceleration parameter which is found to be time-dependent. We have calculated the present value of $q_0 = (1-\varepsilon-\bar{\zeta}_0)/2$. The present universe enters into accelerating phase at an early stage, corresponds to $q_0 < 0$ for $\bar{\zeta}_0 > (1-\varepsilon)$. It enters into accelerating epoch in future time if $0 < \bar{\zeta}_0 < (1-\varepsilon)$, and the accelerating phase occurs at present time if $\bar{\zeta}_0 = (1-\varepsilon)$, i.e., $q_0 = 0$. The variations of q with z are shown in Fig. 2.5 for two set of joint analysis of model parameters. It is found that for the best estimates, the universe enters into accelerating phase in recent past at a redshift $z_{tr} = 0.984$ using joint observational data set of SNe and OHD where as it is $z_{tr} = 0.515$ using $SNe+OHD+BAO$.

We have analyzed the statefinder and *Om* diagnostic parameters to discriminate our model from the other existing models especially from ΛCDM model. In Fig. 2.6, the trajectory of $\{r,s\}$ in $s-r$ plane for best fitted value of model parameters has been plotted. It reveals that the trajectory starts from quintessence region and tends to ΛCDM model in late times. The present value of $\{r,s\}$ in the $s-r$ plane corresponds to $\{r_0,s_0\} = \{0.43706, 0.2595\}$ using joint data of SNe,OHD and BAO which shows that the viscous model is distinguishably different from the ΛCDM model. However, as $a \to \infty$, $\{r,s\} \to \{1,0\}$ corresponds to ΛCDM point. In Fig. 2.8, negative slope of *Om(z)* trajectories also reveal that our model has quintessence behavior.

We have discussed the effective EoS parameter for the best estimates of the viscous model. It is observed that $\omega_{eff} \to -1$ as $z \to -1$, which shows that the viscous model behaves like de Sitter in future. The model has no big rip singularity as ω_{eff} does not cross the phantom divide line as shown in Fig. 2.9. The present value of ω_{eff} is around $\omega_{eff} \simeq -0.575$ through $SNe+OHD$ and $\omega_{eff} \simeq -0.482$ through $SNe+OHD+BAO$ for the best-fit values of parameters.

We have compared our model with the ΛCDM model with the error bar of Hubble dataset as shown in Fig. 2.10. It is found that the fitting achieved through our statistical

analysis is compatible with the observational data used. We have also calculated the age of the universe and plotted $t(z)$ versus z in Fig. 2.11. It is found that the trajectories of viscous model deviate very slightly from that of ΛCDM model in $t_0 > 13-14\,Gyr$. Thus, the viscous model in BD theory alleviates the age problem.

Lastly, we have performed the information criterion of AIC and BIC to discriminate our model with ΛCDM model. The analyses based on the AIC indicates that there is less support for the viscous model when compared to the ΛCDM model, while those based on the BIC indicates that there is strong evidence against it in favor of the ΛCDM model.

****

Chapter 3

Viscous cosmology in holographic dark energy with Granda-Oliveros cut-off

---

In this chapter [1], we study the the effect of bulk viscosity on the holographic dark energy (HDE) with Granda Oliveros IR cut-off. We focus on a generalized form of bulk viscous coefficient which describes successfully the present-day evolution of the universe. We observe that the model with bulk viscosity provides an elegant description of the early and late-time evolution of the universe. We constrain the model through the combined observational data of Strong Lensing System (SLS), measurements of Hubble parameter consisting, sample of Type Ia SNe Pantheon sample and local H_0 measured by SH0ES. Using best-fit values obtained from two different combinations of data, we show that HDE model with bulk viscosity exhibits the phase transition from decelerated epoch to accelerated epoch. A comparison of the model with standard ΛCDM model is discussed with the statefinder and cosmographic parameters.

---

[1] This chapter is based on a research paper "Viscous cosmology in holographic dark energy with Granda-Oliveros cut-off, *Communication in Theoretical Physics*, **Accepted** (2022)".

3.1 Introduction

Modern cosmology has plunged into data driven era. According to various independent observational evidences [7, 8, 255, 256, 259–263], the universe is under an accelerated expansion which gives rise to the concept of dark energy (DE). It has been observed that the universe contains 70% dark energy components and rest 30% includes baryons and cold dark matter. In order to give a reasonable explanation to DE, a large number of attempts have been done. These attempts include the modified gravity and DE models. It has been found that these models fit the observational data, but they also have their own demerits. Therefore, the study is still continued to explain the cosmic acceleration.

In recent years, it has been proposed that the DE is a dynamically evolving component. Several dynamical models of DE have been proposed. One of such dynamical model is the holographic dark energy (HDE) which is based on the holographic principle (HP) [58, 59]. The HP gives a connection between the short distance (UV) cut-off and long distance (IR) cut-off as described in subsection: 1.10.1. The HDE energy density depends on the choice of the IR cut-off which represents the large length scale of the universe. Hsu [62] considered the Hubble Horizon as an IR cut-off and observed that the HDE model could not drive the observable late-time expansion of the universe. Granda and Oliveros [80] proposed a new IR cut-off which is a combination of Hubble parameter and its time derivative to solve the causality problem. This cut-off has been studied by many authors [81–90, 264, 265] to explain the present-day evolution of the Universe.

In case of homogenous and isotropic Universe, assuming the cosmological principle, the dissipative process within a thermodynamical approach can be modeled as a bulk viscosity. The bulk viscous pressure is characterized by the bulk viscous coefficients ζ. There are various parametrization of ζ available in literature. The simplest parametrization of the bulk viscous coefficient is considered to be constant, i.e., $\zeta = \zeta_0$. The other parametrization has been considered as $\zeta = \zeta_1 H$, where ζ_1 is a constant and H is the Hubble parameter and a linear combination form $\zeta = \zeta_0 + \zeta_1 H$. Many authors [93, 147, 148, 266–275] have discussed viscous cosmology to show the late-time evolution of the universe by assuming these parameterized form of the bulk viscous coefficient. Some authors [166, 277–280] have studied the viscous cosmological model with bulk viscous coefficient depending on both expansion and acceleration

rates, i.e., $\zeta = \zeta_0 + \zeta_1 H + \zeta_2 \ddot{a}/\dot{a}$, where ζ_2 is a constant, a denotes the scale factor and dot represents the differentiation with respect to cosmic time.

It has already been found that a non-viscous HDE model with Granda-Oliveros IR cut-off does not show the observable evolution of universe [90]. In this chapter, we examine the viscous effect in a dynamical HDE model with new IR cut-off suggested by Granda and Oliveros [80] to achieve the present-day evolution of the universe. In this dynamical HDE model we consider that our universe is filled with dark matter jointly with bulk viscosity and HDE dark energy. We study the evolution of the universe by considering a more generalized form of bulk viscous coefficient as proposed in paper [277–279]. We constrain the model to get the best fit values of model parameters by using different observational data like, Type Ia SNe (Pantheon), Hubble data, strong lensing data and local Hubble value of SH0ES. We distinguish the viscous model with standard ΛCDM model by studying the statefinder parameters and cosmographic parameters.

This chapter is divided into the following sections: section 3.2 presents the basic equations of HDE model with bulk viscosity and the solutions for Hubble parameter, along with some other main cosmological parameters. In section 3.3, we estimate the best fit values of parameters using the latest observational data. We use the best-fit values to discuss the evolution of the different cosmological parameters in section 3.5. A discussion on statefinder parameters and cosmographic parameters is presented in section 3.6. In section 3.7 we conclude our results.

3.2 Bulk viscous HDE Model

We consider the line element for an isotropic and homogeneous flat Friedmann-Lemaitre-Robertson-Walker (FLRW) metric is given in $(1.3.8)$. In a homogeneous and isotropic universe, the only dissipative process allowed is the bulk viscosity. It is well known that bulk viscosity plays an important role in the universe dynamics at the background level because it satisfies the cosmological principle. The viscous process fundamentally change the equation of motion of relativistic fluids through the addition of new terms of hydrodynamic in energy-momentum tensor.

It has been observed that the HDE model with Granda-Oliveros as the IR cut-off can not exhibit the phase transition [90]. However, the observations indicate a transition phase from deceleration to acceleration during the evolution of the Universe. The

recent works on bulk viscosity [166, 277–280] show that this dissipative fluid plays an important role in describing the late-time evolution. Therefore, it will be worthy to discuss the HDE model with bulk viscosity by using Granda-Oliveros IR cut-off to explain phase transition.

In dissipative cosmology with bulk viscosity, the Einstein's field equations are given by $R_{\mu\nu} - \frac{1}{2}g_{\mu\nu}R = T^{eff}_{\mu\nu}$, where $T^{eff}_{\mu\nu}$ is the effective energy-momentum tensor of the cosmic fluids including the bulk viscosity. This tensor is written as $T^{eff}_{\mu\nu} = (\rho + P)u_\mu u_\nu + Pg_{\mu\nu}$, where $\rho = \rho_m + \rho_h$ is the total energy density of matter and HDE, and with P as the effective fluid pressure which may be defined as $P = p_m + \Pi + p_h$. Here p_m, Π and p_h represent the dark matter pressure, bulk viscous pressure and HDE pressure, respectively. In Eckart formalism, the bulk viscous pressure Π is considered as $\Pi = -3\zeta H$, where ζ is the bulk viscous coefficient.

Let us consider the FLRW Universe dominated by pressureless dark matter with viscous term and the energy of the HDE. The non-vanishing equations of Einstein's field equations are

$$3H^2 = \rho_m + \rho_h \tag{3.2.1}$$

and

$$(\dot{\rho_m} + \dot{\rho_h}) + 3(\rho_m + \rho_h + p_h - 3\zeta H)H = 0, \tag{3.2.2}$$

Assuming that there is no interaction between the dark matter with bulk viscosity and HDE, the conservation equation (3.2.2), therefore, conserves separately, which are given by

$$\dot{\rho}_m + 3H(\rho_m - 3H\zeta) = 0 \tag{3.2.3}$$

and

$$\dot{\rho}_h + 3H(1 + w_h)\rho_h = 0, \tag{3.2.4}$$

where $p_h = w_h\rho_h$ is the equation of state for HDE. Here, w_h is the equation of state (EoS) parameter for HDE. An overdot denotes derivative with respect to cosmic time t.

In HDE model the UV cut-off is related to the vacuum energy, and IR cut-off is related to the large scale of the universe, for example Hubble horizon, future event horizon or particle horizon. Taking L as the size of the current universe, for instance, the Hubble scale, the resulting energy density is comparable to the present-day DE. Hsu [62] studied HDE model with Hubble horizon as IR cut-off and found that the evolution of DE is the same as that of the dark matter (dust matter). Therefore, it cannot drive the

the universe to accelerated expansion. The same appears if one chooses the particle horizon of the universe as the length scale L. However, Li [63] studied HDE model with event horizon as IR cut-off and found that the holographic DE not only gives the observation value of DE in the Universe, but also can drive the Universe to an accelerated expansion phase. In that case, however, an obvious drawback concerning causality appears in this proposal. Event horizon is a global concept of spacetime; existence of event horizon of the universe depends on future evolution of the universe; and event horizon exists only for universe with forever accelerated expansion. Granda-Oliveros [80] proposed a new IR cut-off for HDE, which is a combination of Hubble parameter and its time derivative. This model depends on local quantities and avoids the problem of causality which appears using the event horizon area as the IR cut-off. The new IR cut-off for HDE defined by Granda and Oliveros [80], which is given by

$$\rho_h = 3(n_1 H^2 + n_2 \dot{H}) \tag{3.2.5}$$

where n_1 and n_2 are the dimensionless parameters to be computed by the current observational data. Granda and Oliveros argued that since the underlying origin of the holographic DE is still unknown, the inclusion of the time derivative of the Hubble parameter may be expected as this term appears in the curvature scalar, and has the correct dimension. This kind of density may appear as the simplest case of more general $f(H,\dot{H})$ holographic density in the FLRW background. Comparing (3.2.5) with the HDE density $\rho_h = 3b^2 M_P^2 L^{-2}$ shows that the corresponding IR cut-off for the model (3.2.5) is

$$L = H^{-1}\left(1 + \frac{n_2}{n_1}\frac{\dot{H}}{H^2}\right)^{-1/2} \tag{3.2.6}$$

which depends on local quantities and avoids the causality problem.

Using the above mentioned energy density for HDE, equations (3.2.1), (3.2.3) and (3.2.4) give the evolution equation for Hubble function as

$$\dot{H} + \frac{3(1+n_1 w_h)}{(2+3n_2 w_h)} H^2 = \frac{3\zeta H}{2+3n_2 w_h} \tag{3.2.7}$$

Using $x = \ln a$, the above equation can be transformed into

$$h' + \frac{3(1+n_1 w_h)}{(2+3n_2 w_h)} h = \frac{3\zeta}{(2+3n_2 w_h)H_0} \tag{3.2.8}$$

where $h = H/H_0$ is the dimensionless Hubble parameter and $h' = dh/dx$ i.e. prime indicates the derivative with respect to $\ln a$. The above evolution equation can analytically be solved provided to assume a specific form of bulk viscous coefficient ζ.

In an expanding Universe, the bulk viscous coefficient may depend on both the velocity and acceleration. The most reasonable form can be a linear combination of three terms: the first term is a constant ζ_0, the second term is proportional to the Hubble parameter, which features the dependence of the bulk viscosity on velocity, and the third is proportional to $\ddot{a}/\dot{a}$, featuring the effect of acceleration on the bulk viscosity. Thus, we consider the parameterized bulk viscous coefficient as a combination of three terms which is given by [278]

$$\zeta = \zeta_0 + \zeta_1 \frac{\dot{a}}{a} + \zeta_2 \frac{\ddot{a}}{\dot{a}}, \tag{3.2.9}$$

In terms of the Hubble parameter, this can be written as

$$\zeta = \zeta_0 + \zeta_1 H + \zeta_2 \left(\frac{\dot{H}}{H} + H \right), \tag{3.2.10}$$

where ζ_0, ζ_1 and ζ_2 are constants. Defining the dimensionless bulk viscous parameters $\xi_0 = \zeta_0/H_0$, $\xi_1 = \zeta_1 + \zeta_2$, $\xi_2 = \zeta_2$ and $\xi = \zeta/H_0$, Eq. (3.2.10) reduces to

$$\xi = \xi_0 + \xi_1 h + \xi_2 h'. \tag{3.2.11}$$

Using (3.2.11) into (3.2.8), we finally get the evolution equation as

$$h' + \frac{3(1 + n_1 w_h - \xi_1)}{(2 + 3n_2 w_h - 3\xi_2)} h = \frac{3\xi_0}{2 + 3n_2 w_h - 3\xi_2}. \tag{3.2.12}$$

Integrating the above equation to get the solution of dimensionless Hubble parameter as

$$h = \frac{\xi_0}{1 + n_1 w_h - \xi_1} + \left(1 - \frac{\xi_0}{1 + n_1 w_h - \xi_1} \right) a^{-\frac{3(1+n_1 w_h - \xi_1)}{(2+3n_2 w_h - 3\xi_2)}}, \tag{3.2.13}$$

which can further be simplified by considering a normalized relation between the scale factor and redshift, $a = (1+z)^{-1}$ to get the solution for Hubble parameter as

$$H = H_0 \left[\frac{\xi_0}{1 + n_1 w_h - \xi_1} + \left(1 - \frac{\xi_0}{1 + n_1 w_h - \xi_1} \right) (1+z)^{\frac{3(1+n_1 w_h - \xi_1)}{(2+3n_2 w_h - 3\xi_2)}} \right]. \tag{3.2.14}$$

It should be noted that for ξ_0, ξ_1 and ξ_2 equal to zero, the Hubble parameter gives $H = H_0(1+z)^{3(1+n_1 w_h)/(2+3n_2 w_h)}$, which corresponds to the power-law solution of HDE

Universe. Further, $n_1 = 0$ and $n_2 = 0$ reduces the model to the matter-dominated Universe $H = H_0(1+z)^{3/2}$ whose solution give the power-law expansion of the Universe. However, Eq. (3.2.14) gives the solution of scale factor which has power-law form in early times and exponential expansion in late-time evolution of the Universe. Therefore, we obtain a solution which shows a phase transition from deceleration epoch to acceleration epoch during the evolution. The transition from decelerated to accelerated phase can be further explained by finding the deceleration parameter using Eq. (3.2.13) and (1.7.11), we get

$$q = -1 + \frac{3(1+n_1 w_h - \xi_1)}{2+3n_2 w_h - 3\xi_2} \frac{\left(1 - \frac{\xi_0}{1+n_1 w_h - \xi_1}\right)(1+z)^{\frac{3(1+n_1 w_h - \xi_1)}{2+3n_2 w_h - 3\xi_2}}}{\left[\frac{\xi_0}{1+n_1 w_h - \xi_1} + \left(1 - \frac{\xi_0}{1+n_1 w_h - \xi_1}\right)(1+z)^{\frac{3(1+n_1 w_h - \xi_1)}{(2+3n_2 w_h - 3\xi_2)}}\right]} \tag{3.2.15}$$

which depends on cosmic time and hence shows the phase transition. We observe that $q(z)$ approaches to -1 in the late-time (negative redshift). The transition redshift z_{tr} can be obtained by substituting $q = 0$ in above equation, which is obtained as

$$z_{tr} = -1 + \left[1 + \frac{(1+n_1 w_h - \xi_1)(1+3(n_1 - n_2)w_h - 3(\xi_0 + \xi_1 - \xi_2))}{\xi_0(2+3n_2 w_h - 3\xi_2)}\right]^{-\frac{2+3n_2 w_h - 3\xi_2}{3(1+n_1 w_h - \xi_1)}}. \tag{3.2.16}$$

From (3.2.15), the present value of $q(z)$ corresponds to $z = 0$ is

$$q_0 = -1 + \frac{3(1+n_1 w_h - \xi_1 - \xi_0)}{2+3n_2 w_h - 3\xi_2}. \tag{3.2.17}$$

Let us derive effective equation of state (EoS) parameter to discuss the evolution of the Universe using the standard relation (2.6.1). For this viscous HDE model we get

$$w_{eff} = -1 + \frac{2(1+n_1 w_h - \xi_1 - \xi_0)}{2+3n_2 w_h - 3\xi_2} \frac{(1+z)^{\frac{3(1+n_1 w_h - \xi_1)}{2+3n_2 w_h - 3\xi_2}}}{h}. \tag{3.2.18}$$

The present value of w_{eff} at $z = 0$ for our model is

$$w_{eff}(z=0) = -1 + \frac{2(1+n_1 w_h - \xi_1 - \xi_0)}{2+3n_2 w_h - 3\xi_2}. \tag{3.2.19}$$

3.3 Data Samples

In this section, following the derivation of $H(z)$ obtained in $(3.2.14)$, we constrain the space parameters $(H_0, \xi_0, \xi_1, \xi_2, n_1, n_2, w_h)$ of viscous HDE model using the two different combinations $DS1$ and $DS2$ of the following datasets:

- **Strong lensing system:**
  We gather a new data from Strong Lensing System (SLS) to constrain the model parameters. We constrain the model parameters for 204 SLS in the redshift $0.063 < z_l < 0.950$ for lens and $0.196 < z_s < 3.595$ for the source is given by [240].

- **Hubble data:**
  We use the updated collection of 57 Hubble $H(z)$ data points between the redshift range $0.07 \leq z \leq 2.36$ that consists of 31 points collected from differential age(DA) technique and 26 data points received through line-of-sight BAO and other methods.

- **SNe(Pantheon data):**
  We use the latest compilation of SNe (Pantheon sample), consisting 1048 data points from SNLS, SDSS, Pan-STARRS1, HST survey in the redshift range of $0.014 \leq z \leq 2.3$ [211].

- **Local Hubble constant:** We also take the recently measured local Hubble constant H_0 as $H_0 = 73.5 \pm 1.4\ km\ s^{-1} Mpc^{-1}$ by SH0ES as mentioned in [241].

The detail of SLS, $H(z)$ and SNe(Pantheon data) are provided in subsection 1.14.2 of Section 1.14.

3.4 Methodology

The minimized χ^2 function, for two combinations of our analysis, is given as, $\chi^2_{DS1} = \chi^2_{pan} + \chi^2_{H(z)} + \chi^2_{SLS} + \chi^2_{H_0}$ and DS2 for which the minimized χ^2 is given as $\chi^2_{DS2} = \chi^2_{pan} + \chi^2_{H(z)} + \chi^2_{SLS}$ where χ^2_{pan}, $\chi^2_{H(z)}$, χ^2_{SLS} and $\chi^2_{H_0}$ are defined in equations $(1.14.4)$, $(1.14.11)$ and $(1.14.20)$ respectively.

We perform fitting to determine the best fit values of model parameters using the MCMC method. The best fit values obtained for both the combinations of DS1 and DS2

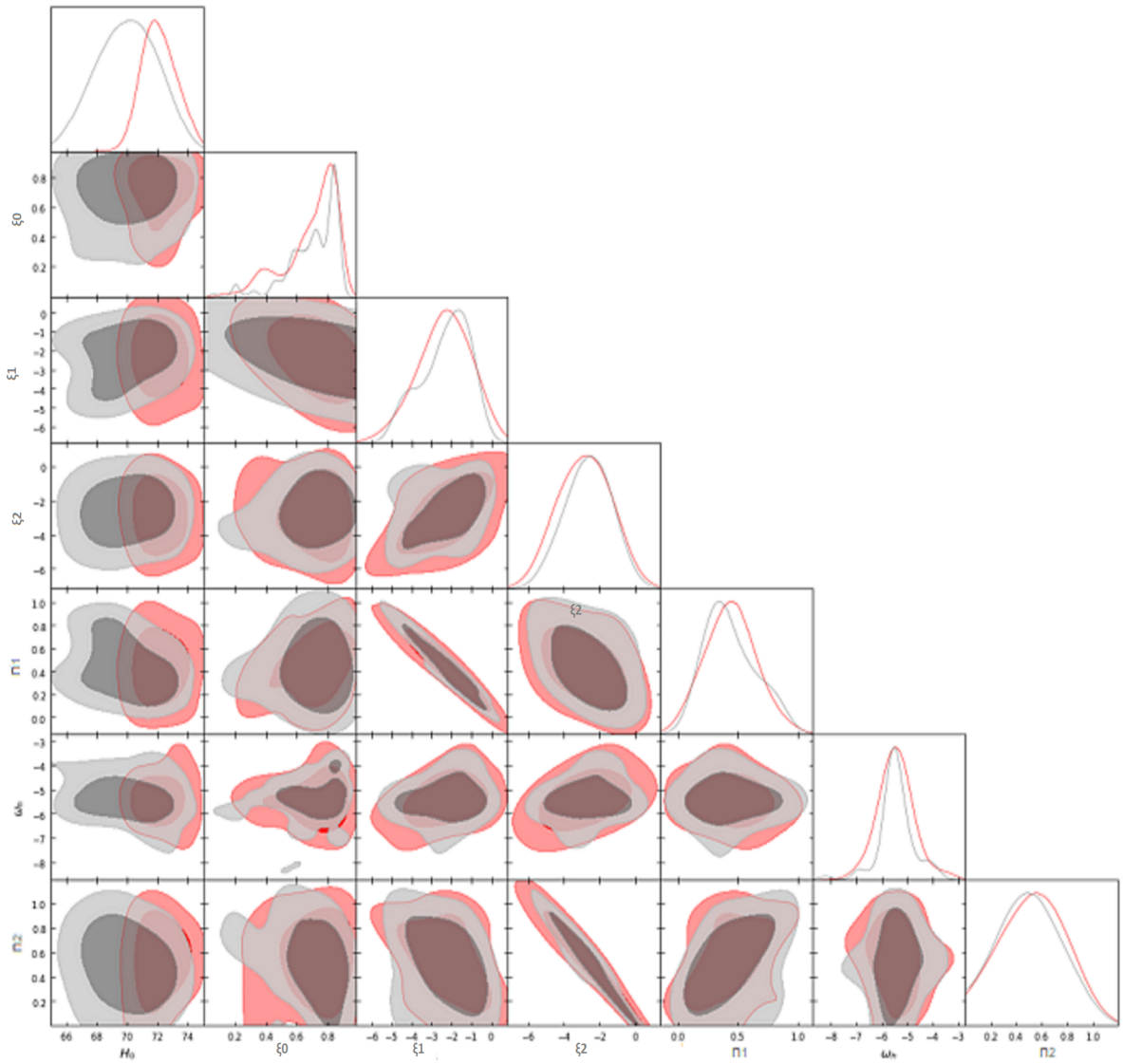

Figure 3.1: The likelihood contours at 68.3% CL and 95.4% CL for viscous HDE model correspond to DS1(red color) and DS2 (grey color) datasets

Table 3.1: The best-fit values of free parameters of HDE and ΛCDM models with errors from DS1 and DS2 datasets

	$DS1$		$DS2$	
$Model$	HDE	ΛCDM	HDE	ΛCDM
H_0	$71.567^{+1.448}_{-0.848}$	$70.061^{+0.775}_{-0.852}$	$69.197^{+1.563}_{-1.924}$	$68.944^{+0.738}_{-0.530}$
ξ_0	$0.758^{+0.097}_{-0.221}$	–	$0.652^{+0.146}_{-0.220}$	–
ξ_1	$-2.690^{+1.335}_{-1.650}$	–	$-2.458^{+1.327}_{-2.056}$	–
ξ_2	$-2.835^{+1.410}_{-1.608}$	–	$-2.940^{+1.447}_{-1.906}$	–
α	$0.460^{+0.261}_{-0.275}$	–	$0.462^{+0.294}_{-0.266}$	–
w_h	$-5.556^{+0.917}_{-0.782}$	–	$-5.576^{+0.336}_{-0.525}$	–
β	$0.517^{+0.294}_{-0.238}$	–	$0.565^{+0.301}_{-0.263}$	–
Ω_m	$0.308^{+0.121}_{-0.093}$	$0.286^{+0.004}_{-0.007}$	$0.26^{+0.122}_{-0.103}$	$0.288^{+0.004}_{-0.006}$
Ω_Λ	$0.668^{+0.112}_{-0.103}$	$0.711^{+0.010}_{-0.006}$	$0.73^{+0.122}_{-0.123}$	$0.707^{+0.009}_{-0.005}$
χ^2_{min}	525.033	537.330	525.473	530.538

through statistical analysis for viscous HDE and ΛCDM models are provided in Table 3.1. The space parameters $(H_0, \xi_0, \xi_1, \xi_2, n_1, w_h, n_2)$ with $1\sigma(68.3\%)$ and $2\sigma(95.4)\%$ confidence level for both the data sets DS1 and DS2 are represented in Fig. 3.1. The data set DS1 fitted is shown by the red contours while the greyish contours are derived from DS2 data set. The best-fit values of space parameters of viscous HDE and of ΛCDM models obtained by both the combinations are provided in Table 3.1. In the following section, we present and discuss the results obtained from the above mentioned datasets.

3.5 Result and discussion

We estimate the best-fit values of model parameters from two different joint combinations DS1 and DS2 datasets. Using the best-fit values we study few observational parameters namely Hubble constant, deceleration parameter, equation of state pa-

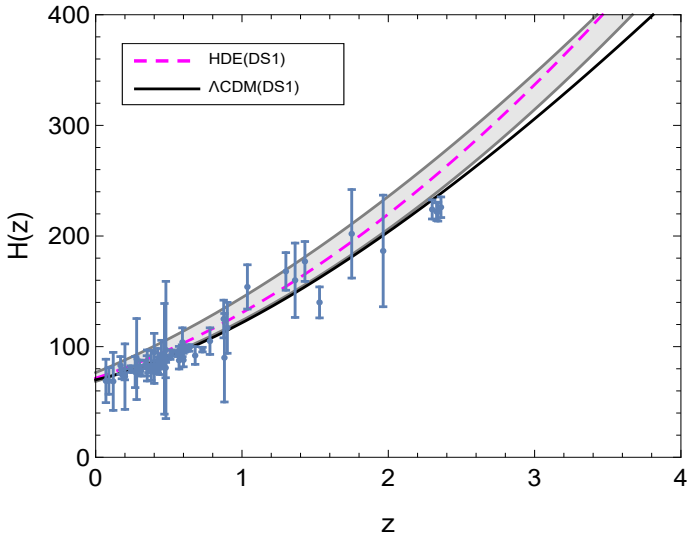

Figure 3.2: Plot of the Hubble function as a function of redshift for HDE model with bulk viscosity for DS1 dataset over H(z) points and its comparison with ΛCDM model (solid black line). The 57 $H(z)$ data points are also shown with error bars in blue dots. The band corresponds to the error at the 95.4% confidence level.

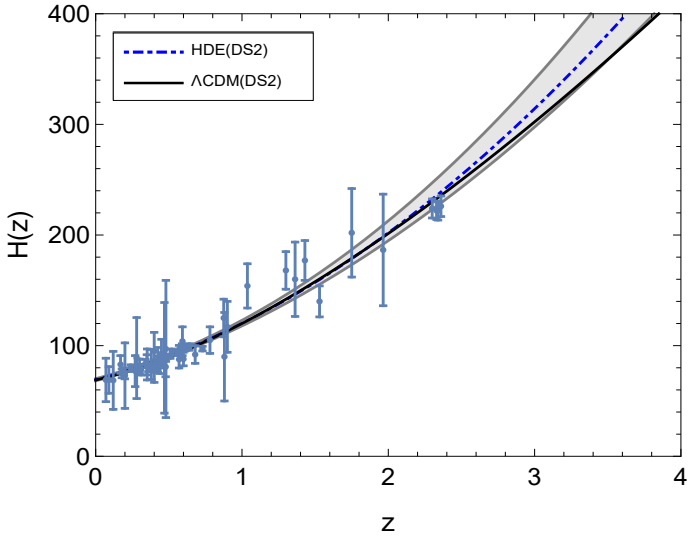

Figure 3.3: Plot of the Hubble function as a function of redshift for viscous HDE model with bulk viscosity for DS2 dataset over H(z) points and its comparison with ΛCDM model (solid black line). The 57 $H(z)$ data points are also shown with error bars in blue dots. The band corresponds to the error at the 95.4% confidence level.

rameter and age of Universe to describe the global dynamics of the Universe.

Figs. 3.2 and 3.3 presents the evolution of the Hubble parameter $H(z)$ as a function of the redshift using the best-fit values of free parameters constrained from both the datasets DS1 and DS2. We have also traced the trajectory of ΛCDM model to compare the evolution of viscous HDE models. The bars stand for the observational data of $H(z)$ as mentioned in Ref. [219] as well as given in Table 1.1. It is observed that the fit obtained from DS2 is consistent with observational $H(z)$ data points.

The present values of Hubble constant are $H_0 = 71.567^{+1.448}_{-0.848}$ and $H_0 = 69.197^{+1.563}_{-1.924}$, respectively. The first value of H_0 is slightly lower than the value obtained by SH0ES project $H_0 = 73.5 \pm 1.4\ km\ s^{-1}Mpc^{-1}$ [241] where as the second result of H_0 is slightly higher than Planck result [281], where $H_0 = 67.7 \pm 0.46\ km\ s^{-1}Mpc^{-1}$.

The respective χ^2 with DS1 and DS2 data sets are 525.033 and 525.473. The reduced χ^2 statistics is very beneficial in goodness of fit testing. It is defined as $\chi^2_{red} = \chi^2_{min}/\nu$, where ν is known as degree of freedom (dof) and is defined as the difference between the total number of combined data points used and the number of estimated free model parameters. We have the number of data points for DS1 as $N = 1310$ (1048 data of SNe, 57 data of H(z), 204 data of SLS and 01 data of local H_0) and for DS2 it is $N = 1309$ (1048 data of SNe, 57 data of H(z) and 204 data of SLS). The viscous HDE has seven free parameters where as the ΛCDM has 3. Thus, the $\chi^2_{\rm red}$ for ΛCDM comes out to be $\chi^2_{\rm red} = 0.411$ and $\chi^2_{\rm red} = 0.406$ where as for viscous HDE model, these are $\chi^2_{\rm red} = 0.402$ and $\chi^2_{\rm red} = 0.403$, respectively, which is less than unity with each dataset, showing that both the models fit well and data sets are compatible with the considered model.

Table 3.2 presents the values of transition redshift, present value of q and $\omega_{\rm eff}$ of viscous HDE and ΛCDM models. Fig. 3.4 shows the evolution of the deceleration parameter defined in equation $(3.2.15)$ for best-fit values of free parameters with the joint datasets. The deceleration parameter shows the transition from $q > 0$ to $q < 0$ with respect to $DS1$ and $DS2$ data. In this cosmological scenario, the signature flipping occurs at the transition redshift $z_{tr} = 0.666^{+0.426}_{-0.310}$ and $z_{tr} = 0.777^{+0.234}_{-0.130}$ corresponding to DS1 and DS2 datasets, which are very close to ΛCDM model's transition values. These results are also consistent with the results reported in Ref. [282]. Thus, the Universe has an transition from early decelerated era to current observable accelerated era. The present value of $q(z)$ is found to be about $q_0 = -0.535^{+0.016}_{-0.016}$ and $q_0 = -0.536^{+0.016}_{-0.016}$, respectively, which are comparable with $q_0 = -0.55 \pm 0.01$ of the Planck spacecraft data [281]. It is to be noted that Capozziello et al [283] have ob-

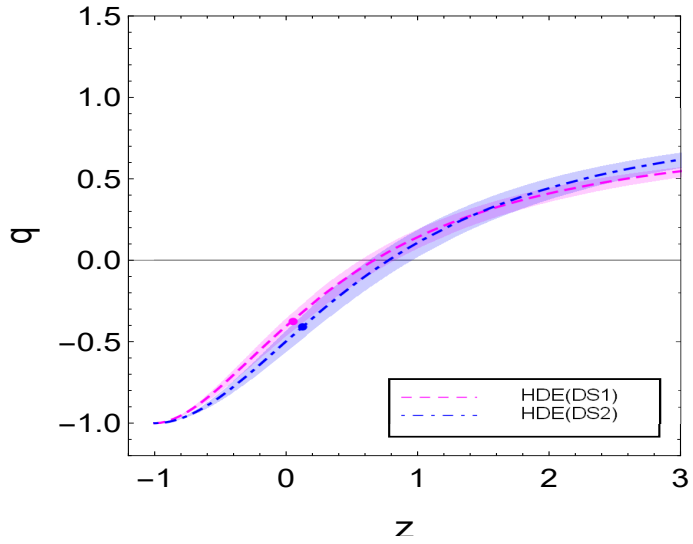

Figure 3.4: Plot of deceleration parameter q versus redshift z for best-fit values of free parameters obtained from DS1 and DS2 data sets. The current value q_0 is shown by a dot on the trajectory. The band corresponds to the error at the 95.4% confidence level.

Table 3.2: Values of z_{tr}, q_0, $w_{eff}(z=0)$ and t_0 (Gyr) for different combinations of data sets.

	$DS1$		$DS2$	
$Model$	HDE	ΛCDM	HDE	ΛCDM
$z_{\rm tr}$	$0.666^{+0.426}_{-0.310}$	$0.707^{+0.223}_{-0.205}$	$0.777^{+0.234}_{-0.130}$	$0.699^{+0.143}_{-0.125}$
q_0	$-0.535^{+0.016}_{-0.016}$	$-0.568^{+0.013}_{-0.012}$	$-0.536^{+0.016}_{-0.016}$	$-0.563^{+0.012}_{-0.012}$
$w_{\rm eff}(z=0)$	$-0.690^{+0.010}_{-0.010}$	$-0.615^{+0.006}_{-0.006}$	$-0.691^{+0.011}_{-0.011}$	$-0.611^{+0.068}_{-0.068}$

tained $q_0 = -0.56 \pm 0.04$.

Next we analyze the cosmic expansion using the effective equation of state parameter w_{eff}. We have plotted the trajectory of w_{eff} versus redshift z in Fig. 3.5, using the best-fit values of free parameters of both the combinations of datasets. The present values of effective EoS parameter are $w_{eff}(z=0) = -0.690^{+0.010}_{-0.010}$ and $w_{eff}(z=0) = -0.691^{+0.010}_{-0.010}$ for both the combination of data sets which are also listed in Table 3.2. These values are comparatively larger than $w_0 = -0.93$ which was predicted by joint analysis of $WMAP + BAO + H(z) + SNe$. The model behaves like quintessence DE. Note that $w_{eff} \to -1$ in future time of evolution which implies that the viscous holographic dark energy model approaches to de Sitter model in late time . Finally, we estimate the age of the Universe as $t_0 \approx 13.26\ Gyr$ and $t_0 \approx 13.56\ Gyr$, respectively, which are comparable to the value reported in Ref. [281] with $t_0 = 13.79 \pm 0.02\ Gyr$.

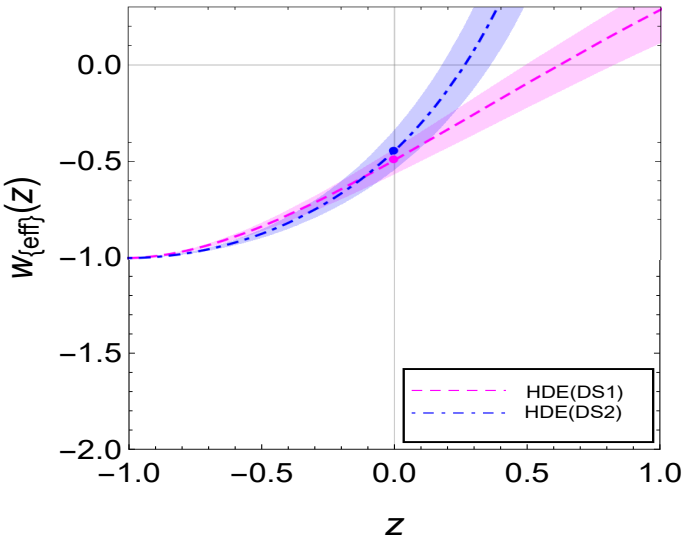

Figure 3.5: Plot of Effective equation of state parameter w_{eff} versus redshift z for best-fit values of free parameters obtained from DS1 and DS2 data sets. The current $w_{eff}(z=0)$ is shown by a dot on the trajectory. The band corresponds to the error at the 95.4% confidence level.

3.6 Diagnostic and cosmographic parameters

In this section, we discuss diagnostic parameters, like statefinder parameters and cosmography parameters, like jerk, snap, lerk and m parameters to discriminate the proposed viscous HDE model with dark energy model, like ΛCDM model.

Substituting the values of scale factor and its derivatives from (3.2.14) in (1.12.1), we get

$$r = \frac{9(1+n_1w_h-\xi_0-{\xi_1}^2)}{2+3n_2w_h-3{\xi_2}^2}e^{-\frac{6\xi_0(t-t_0)}{2+3n_2w_h-3\xi_2}} - 9\frac{(1+n_1w_h-\xi_0-\xi_1)(1-n_1w_h+3n_2w_h+\xi_1-3\xi_2)}{2+3n_2w_h-3{\xi_2}^2}e^{-\frac{3\xi_0(t-t_0)}{2+3n_2w_h-3\xi_2}} + (2+3n_2w_h-3\xi_2), \tag{3.6.1}$$

and

$$s = \frac{1}{(2+3n_2w_h-3\xi_2)\{2(1+n_1w_h-\xi_0-\xi_1)-e^{-\frac{3\xi_0(t-t_0)}{2+3n_2w_h-3\xi_2}}(2+3n_2w_h-2\xi_2)\}} \times \left[2e^{-\frac{6\xi_0(t-t_0)}{2+3n_2w_h-3\xi_2}}(1+n_1w_h-\xi_0-\xi_1)\{1+n_1w_h-\xi_0-\xi_1-e^{-\frac{6\xi_0(t-t_0)}{2+3n_2w_h-3\xi_2}}(1+\xi_1-3\xi_2-n_1w_h+3n_2w_h)\}\right]. \tag{3.6.2}$$

Figure 3.6 shows the $s-r$ plane trajectories of viscous holographic dark energy model for best fit values of parameters achieved through DS1 and DS2 data. It can be observed that the $\{r, s\}$ evolutions start from a region of chaplygin gas where $r>1$, $s<0$ and tends to $\{r, s\}\to\{1, 0\}$ in future, a value of ΛCDM model. The present values of statefinder parameters are $\{r_0=0.6415, s_0=0.132\}$ and $\{r_0=0.716, s_0=0.094\}$

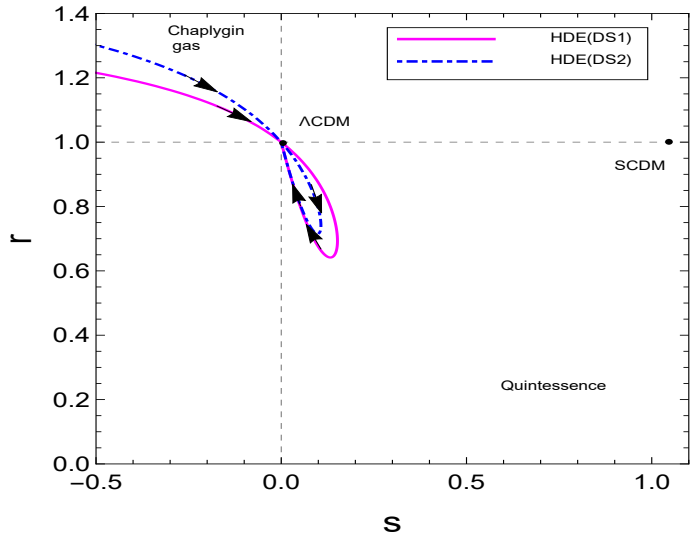

Figure 3.6: The evolution of $\{r,s\}$ in $s-r$ plane corresponding to best fit values of free parameters obtained from DS1 and DS2. The direction of the evolution is shown by the arrows on each trajectory.

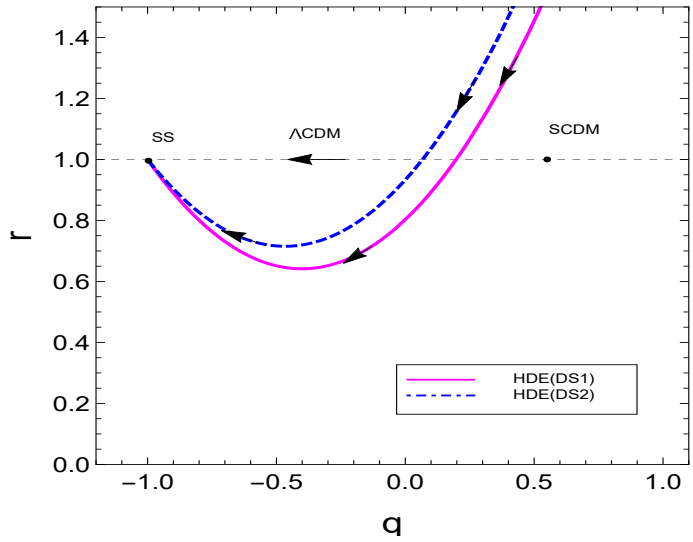

Figure 3.7: The evolution of $\{r,q\}$ in $q-r$ plane corresponding to best fit values of free parameters obtained from DS1 and DS2.

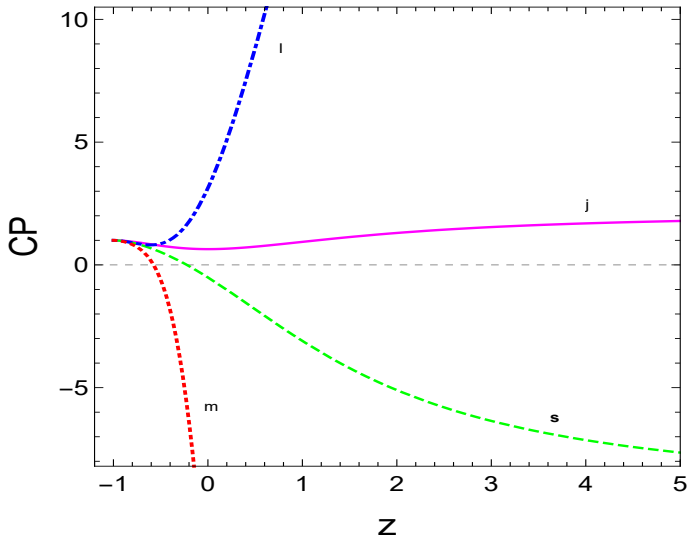

Figure 3.8: The evolutions of $jerk, lerk, snap$ and m parameters corresponding to best fit values of model parameters obtained from DS1 and DS2. The direction of the evolution of each trajectory is shown by the arrow.

for DS1 and DS2, respectively which show a deviation from ΛCDM model. An alternate way to check the differences between the models is through the $\{q,\ r\}$ trajectory. In Fig. 3.7 we plot such $q-r$ trajectory for both data sets. The arrow represents the direction of the evolution of the model. The trajectories evolute from deceleration phase to accelerated epoch. We find that $\{q,\ r\}$ converges to steady state (SS) model $\{-1,\ 1\}$ in the future $(z \to -1)$ with both data sets.

In addition to the above, we calculate the high order cosmography parameters $(jerk, snap, lerk, m)$ for best fit values of parameters of viscous HDE model using (1.12.3). Using the best fit values of model parameters, the evolution of these CP for our model has been shown graphically against redshift, for DS1, and the same can be plotted for the data set DS2. It can be checked through the graph that all the cosmological parameters j, $\mathbf{s}$, l and $m \to 1$ as $z \to -1$, i.e., our model is in good agreement with the observations of standard ΛCDM model in late time evolution. We find that $jerk$ and $lerk$ parameters have the trajectories in the same direction while $\mathbf{s}$ and m have the same evolution but different than j and l and both transit from initial negative values to later positive ones. A positive $jerk$ and $lerk$ implies that Universe has gone under transition from deceleration to acceleration. The current values of these parameters are found to be $\{j_0 = 0.6415,\ \mathbf{s}_0 = -0.5082,\ l_0 = 3.1301$ and $m_0 = -14.614\}$ and $\{j_0 = 0.716,\ \mathbf{s}_0 = -0.323,\ l_0 = 2.852$ and $m_0 = -12.490\}$ for DS1 and DS2 respectively. Thus, we report a deviation from the standard ΛCDM model in cosmography parameters due to the contributions of bulk viscosity.

3.7 Conclusion

In this chapter, we have studied the effect of bulk viscosity in HDE model with Granda-Oliveros as an IR cut-off in the framework of FLRW space-time. The viscous term has a negative pressure, therefore, it has been studied to observe the early and late-time accelerated expansion of the universe. It is well known that the HDE model with Granda-Oliveros IR cut-off does not show the phase transition which contradicts with the present observable universe. Instead of assuming the other cut-off, we have included viscous term in HDE model with the same IR cut-off to observe the phase transition. We have assumed a more general form of bulk viscous coefficient ξ in terms of H and $\dot{H}$ to demonstrate how does the bulk viscosity explain the accelerating Universe. We have obtained the solution of different cosmological parameters such as Hubble parameter, deceleration parameter and equation of state parameter.

We have constrained the space parameters of the viscous HDE model using the latest observational data of Strong Lensing system containing 204 data points, $H(z)$ data comprising 57 points, SNe (pantheon data) of 1048 points and local H_0. We have performed two joint analysis namely DS1 and DS2 comprising $SLS+SNe+H(z)+H_0$ and $SLS+SNe+H(z)$, respectively to find the best-fit values of parameters. We have also assumed ΛCDM model as concordance model to compare the results of viscous HDE model. The best-fit values for both the models are listed in Table 2. Using the the best -fit values we have investigated the effects of bulk viscosity on the evolution of the universe by plotting the trajectory of different cosmological parameters. We have found that the viscous HDE model fits well to both data sets. We have found good agreement to data sets according to the $\chi^2_{\rm red}$ value. We have also obtained the evolutions of cosmographic parameters and statefinder parameters. In the following, we summarize the main results.

We have plotted and analyzed the trajectory of each of the main observable cosmological parameters such as $H(z)$, $q(z)$ and $\omega_{\rm eff}(z)$ using the best-fit values of model parameters. In Figs. 3.2 and 3.3, the Hubble function obtained analytically has been confronted by error bars of Hubble data with best-fit values and compared with ΛCDM. We have found that the model predicts a better fit along with ΛCDM model. From Figs. 3.4 and 3.5, the evolution of the deceleration and EoS parameters show that the mod-

el transits from deceleration phase to the accelerated phase. In late-time, we have found that the parameters tend to -1. The present value of deceleration and EoS parameters are very near to the values of ΛCDM model as mentioned in Table 3.2. The ages of the Universe predicted by the viscous HDE model from two data sets are slightly lower than the value of ΛCDM model. We have also studied the diagnostic parameters namely statefinder and cosmographic parameters for viscous HDE model and compared with the ΛCDM model. Using the best-fit values, we have plotted the evolutions of $\{r,s\}$, $\{r,q\}$ in $(s-r)$ and $(q-r)$ planes, respectively in Figs. 3.6 and 3.7 and discussed the behavior accordingly. In Fig. 3.8, we have plotted the evolution of cosmographic parameters which explain the dynamics of the model. It has been observed that these parameters tend to 1 as z tends to -1, that is, the viscous HDE model is in good agreement with the observation of concordance model in late-time evolution.

The presence of bulk viscosity in dark energy models is an interesting and significant approach to show the phase transition of universe. The present model gives a good alternative to explain the accelerating phenomena of the universe.

****

Chapter 4

Matter creation cosmology in Brans-Dicke theory: observational test and thermodynamic analysis

---

In this chapter [1]*, a matter-dominated model with gravitationally induced matter creation is proposed in the framework of BD theory. We obtain the main cosmological functions like scale factor of the universe, the Hubble expansion rate and deceleration parameter analytically. We explore the viability of the model to explain the current observable expansion of the universe. In this scenario the present cosmic acceleration is supposed to drive only by the creation of negative pressure associated with the matter component. The evolution of such model is tested by statistical analysis of latest* SNe*,* OHD *and* BAO *probes. We analyse the model through the trajectories of deceleration parameter, statefinder diagnostic and compared the model with standard* ΛCDM *model.*

---

[1]This chapter is based on a published research paper "Matter creation cosmology in Brans-Dicke theory: observational tests and thermodynamic analysis, *Physical Review D* **100**, 084057 (2019)".

4.1 Introduction

In the past several years, after the discovery of the accelerating universe the matter creation has been reconsidered to explain it and got some unexpected results. In general relativistic cosmology, the presence of a negative pressure is the key ingredient to accelerate the expansion. Cosmological models dominated by pressureless fluid like a cold dark matter (CDM) component expands in a decelerating way. Matter creation is considered in the context of the thermodynamics of open systems. A detailed study of the thermodynamics of the matter creation with changing specific entropy has been discussed in Ref. [173, 174] as described in chapter 1.

The irreversible creation process, in comparison to the standard equilibrium equations, is described by two new ingredients: a negative pressure term in the energy-momentum tensor and a balance equation for the particle number density. Second law of thermodynamics relates these quantities in a very definite way. Several interesting features of cosmological models with matter creation have been investigated by many authors [181–183,196,284]. This field is very appealing for several important observations carried out in the last ten years. It has been pointed out that models with particle creation can mimic ΛCDM cosmology [182, 194, 197, 244, 285–287]. Further, Nunes and Pavón [288] have shown that the matter creation models can explain the phantom behavior of the universe without invoking any phantom fields. Particle creation models in modified theories of gravity have attracted several authors at recent time [89, 90, 177].

There have been attempts in modelling the missing energy of the universe and to explain its late time accelerated expansion in purview of the scalar tensor theories where the scalar field is non-minimally coupled to gravity sector. The study of matter creation processes in the context of the cosmological models has recently attracted a lot of interest in cosmology. In this chapter, we study the role of irreversible processes, corresponding to the creation of matter out of gravitational energy in BD theory. The aim of this work is to build a cosmological model based on matter creation in the framework of BD theory. In a flat FLRW geometry, we consider a general creation rate to demonstrate how matter creation explains the accelerating universe. We obtain the analytical solutions of the Hubble function and the scale factor of the FLRW universe. We also constrain the model using the latest compilation of Type Ia SNe data, O-HD data and BAO data. We examine the models using two independent diagnoses,

namely the statefinder parameter and *Om* from observational constraints. Further, we test the thermodynamic viabilities of the matter creation model.

The chapter is arranged as follows: In section 4.2, we present the model field equations for matter creation in a flat FLRW space-time in BD theory. We obtain the analytical solutions of Hubble parameter, scale factor and the deceleration parameter in section 4.3. In section 4.4, we test the cosmological model with matter creation in BD theory with the recent observational data and derive the constraints on the model parameters. The results obtained by observational data are also given in section 4.5. In section 4.6, we study the evolution of the universe with the best fitted values of parameters. Diagnostic analysis has been done in section 4.7. We present the thermodynamic analysis of the model in Section 4.8. At the end, in section 4.9 we discuss our findings.

4.2 Model and Field equations

Let us consider that the universe is filled with two fluid components: dark matter and matter creation. Thus, the energy-momentum tensor for perfect fluid modifies to $T_{\mu\nu} = T^{(m)}_{\mu\nu} + T^{(c)}_{\mu\nu}$, where $T^{(m)}_{\mu\nu}$ is the energy-momentum tensor for the perfect fluid, i.e.,

$$T^{(m)}_{\mu\nu} = (\rho_m + p_m)u_\mu u_\nu + p_m\, g_{\mu\nu}, \tag{4.2.1}$$

and $T^{(c)}_{\mu\nu}$ is the energy-momentum tensor which corresponds to the matter creation, i.e.,

$$T^{(c)}_{\mu\nu} = p_c(g_{\mu\nu} + u_\mu u_\nu). \tag{4.2.2}$$

Thus the modified EMT is given by

$$T_{\mu\nu} = (\rho_m + p_m + p_c)u_\mu u_\nu + (p_m + p_c)\, g_{\mu\nu} \tag{4.2.3}$$

where ρ_m, p_m and p_c are the energy density, kinetic pressure and creation pressure, respectively.

In a spatially homogeneous and isotropic flat FLRW cosmology (1.3.8) filled with dark matter and matter creation (4.2.3), the gravitational equations in BD theory can be written as

$$H^2 + H\frac{\dot{\phi}}{\phi} - \frac{\omega}{6}\frac{\dot{\phi}^2}{\phi^2} = \frac{\rho_m}{3\phi}, \tag{4.2.4}$$

The scalar field evolution equation is

$$\ddot{\phi} + 3H\dot{\phi} = \frac{\rho_m - 3(p_m + p_c)}{(2\omega + 3)}. \tag{4.2.5}$$

Here, we note that the case of $\omega = -3/2$ is not allowed. The energy conservation equation $T^{\mu\nu}_{;\nu} = 0$ leads to

$$\dot{\rho_m} + 3H(\rho_m + p_m + p_c) = 0. \tag{4.2.6}$$

A self gravitating simple fluid endowed only with gravitational matter creation is characterized by an energy-momentum tensor $T_{\mu\nu}$, a particle current N^μ and an entropy current S^μ. In homogenous and isotropic case, these quantities sastisfy the following relations:

$$T^{\mu\nu}_{;\nu} = 0, \quad N^{\mu}_{;\mu} = n\Gamma, \quad \text{where } N^\alpha = n\,u^\mu, \quad S^\mu = n\sigma u^\mu. \tag{4.2.7}$$

It is to be noted that the creation pressure p_c is defined in terms of the creation rate Γ and other physical quantities describing the fluid. In adiabatic particle creation (meaning particles are created but the specific entropy per particle remains constant), the creation pressure is given by

$$p_c = -\left(\frac{\rho_m + p_m}{3H}\right)\Gamma, \tag{4.2.8}$$

We assume the non-relativistic matter with $(p_m = 0)$, and therefore above equation reduces to

$$p_c = -\frac{\rho_m}{3H}\Gamma \tag{4.2.9}$$

Using second law of thermodynamics, we have the constraint

$$dS = \frac{s}{n}d(nV) \geq 0, \tag{4.2.10}$$

where $s = S/V$ is the entropy density, n is the particle number density, $V = a^3$ denotes the volume.

4.3 Solution of field equations

Equation (4.2.9) shows how matter creation rate, Γ, modifies the evolution of the scale factor and density of fluid. The evolution of matter dominated model can be

determined by assuming a suitable form of the creation rate. Although there is no precise functional form of Γ, still various phenomenological parametrization have been proposed in literature. The simplest choices of Γ is $\Gamma \propto H$, however, this model is not consistent with Type Ia SNe. The other forms of Γ are $\Gamma = H_0$ [194], $\Gamma \propto H^2$ [196] and $\Gamma \propto H^{-1}$ [197]. Steigman et al. [182] proposed a linear combination in the terms of Hubble parameter as

$$\Gamma = 3\gamma H_0 + 3\beta H, \tag{4.3.1}$$

where γ and β are constants contained in the interval $[0,1]$, and H_0 is the present value of H.

With the power law assumption $\phi = \phi_0\, a(t)^{\varepsilon}$ [249,250], equation (4.2.4) can be rewritten as

$$\left(1+\varepsilon-\frac{\varepsilon^2\omega}{6}\right)H^2 = \frac{\rho}{3\phi_0 a^{\varepsilon}}. \tag{4.3.2}$$

From the above Eq.(4.3.2), we get

$$2\frac{\dot{H}}{H} = \frac{\dot{\rho}}{\rho} - \varepsilon H. \tag{4.3.3}$$

Now, equation (4.2.6) gives

$$\frac{\dot{\rho}}{\rho} = -3\left(1-\frac{\Gamma}{3H}\right)H. \tag{4.3.4}$$

Using equations (4.3.4) and (4.3.1) into (4.3.4), we get

$$\frac{\dot{h}}{h} + \frac{(\varepsilon+3(1-\beta))}{2}H_0 h - \frac{3}{2}\gamma H_0 = 0. \tag{4.3.5}$$

where $h = H/H_0$ is the dimensionless Hubble parameter. Using $\frac{d}{dt} = \frac{\dot{a}}{a}\frac{d}{d\,lna}$, the above equation can be written as

$$h' + \frac{(\varepsilon+3(1-\beta))}{2}h = \frac{3}{2}\gamma. \tag{4.3.6}$$

where prime denotes the derivative with respect to conformal time lna.

Integration of equation (4.3.6), we obtain

$$h(a) = \left[\frac{3\gamma}{\varepsilon+3(1-\beta)} + \left(1-\frac{3\gamma}{\varepsilon+3(1-\beta)}\right)\left(\frac{a_0}{a}\right)^{\frac{\varepsilon+3(1-\beta)}{2}}\right] \tag{4.3.7}$$

From equation (4.3.7), we obtain the solution of scale factor $a(t)$ as function of time,

$$a(t) = a_0 \left[1 + \frac{\varepsilon + 3(1-\beta)}{3\gamma}\left(e^{\frac{3\gamma}{2}H_0(t-t_0)} - 1\right)\right]^{\frac{2}{\varepsilon+3(1-\beta)}}, \tag{4.3.8}$$

where a_0 is the present value of the scale factor at cosmic time $t = t_0$ and in thereafter we take $a_0 = 1$, and $\varepsilon + 3(1-\beta) \neq 0$, $\gamma \neq 0$. As $(t - t_0) \to 0$, the scale factor $a(t) \to \left[1 + \frac{\varepsilon+3(1-\beta)}{2}H_0(t-t_0)\right]^{\frac{2}{\varepsilon+3(1-\beta)}}$ which corresponds to early deceleration and as $(t - t_0) \to \infty$, the scale factor $a(t) \propto e^{\frac{3\gamma}{2}H_0(t-t_0)}$, corresponds like that of the de Sitter universe.

The Hubble parameter in terms of cosmic time t reads

$$H = \frac{H_0\, e^{\frac{3\gamma}{2}H_0(t-t_0)}}{\left[1 + \frac{\varepsilon+3(1-\beta)}{3\gamma}\left(e^{\frac{3\gamma}{2}H_0(t-t_0)} - 1\right)\right]} \tag{4.3.9}$$

In terms of redshift, it is given by

$$H(z) = H_0\left[\frac{3\gamma}{\varepsilon+3(1-\beta)} + \left(1 - \frac{3\gamma}{\varepsilon+3(1-\beta)}\right)(1+z)^{\frac{\varepsilon+3(1-\beta)}{2}}\right] \tag{4.3.10}$$

Using $a(t) = 0$ in (4.3.8), the cosmic time t_{BB} when Big-bang happens, is given by

$$t_{BB} = t_0 + \frac{2}{3\gamma H_0}\, ln\left(1 - \frac{3\gamma}{\varepsilon+3(1-\beta)}\right) \tag{4.3.11}$$

The energy density ρ_m in terms of z is given by

$$\rho_m = \rho_{m0}(1+z)^{-\varepsilon}\left[\frac{3\gamma}{\varepsilon+3(1-\beta)} + \left(1 - \frac{3\gamma}{\varepsilon+3(1-\beta)}\right)(1+z)^{\frac{\varepsilon+3(1-\beta)}{2}}\right]^2 \tag{4.3.12}$$

where ρ_{m0} is constant quantity. The scalar field ϕ has the solution

$$\phi = \phi_0\left[1 + \frac{\varepsilon+3(1-\beta)}{3\gamma}\left(e^{\frac{3\gamma}{2}H_0(t-t_0)} - 1\right)\right]^{\frac{2\varepsilon}{\varepsilon+3(1-\beta)}}, \tag{4.3.13}$$

which shows that BD scalar field increases exponentially with time.

Let us discuss the matter creation model in the sense of irreversible process. Adiabatic gravitational matter creation means that the total entropy S increase, but the specific entropy (per particle), $\sigma = S/N$ remains constant ($\dot{\sigma} = 0$), which implies that

$$\frac{\dot{S}}{S} = \frac{\dot{N}}{N}. \tag{4.3.14}$$

Now, from $N = nV$ where $V = a^3$, we have

$$\frac{\dot{N}}{N} = \frac{\dot{n}}{n} + \frac{3\dot{a}}{a}. \tag{4.3.15}$$

Inserting equations (1.11.7) and (4.3.1) into (4.3.16), a straightforward integration yields

$$N(t) = N_0\, a^{3\beta}\, e^{3\gamma H_0(t-t_0)}, \tag{4.3.16}$$

where N_0 is the present number of particles. The number of particle is increasing function of time. Using (4.3.16) into (4.3.14) and integrating, we get

$$S(t) = S_0\, a^{3\beta}\, e^{3\gamma H_0(t-t_0)}, \tag{4.3.17}$$

where S_0 is the present entropy.

The solution for particle number density is given by

$$n = n_0\, a^{-3(1-\beta)}\, e^{3\gamma H_0(t-t_0)}, \tag{4.3.18}$$

which shows that the particle number density first decreases and then increases exponentially with cosmic time t.

The exact solutions coming out from (4.2.4) and (4.2.6) are consistent solutions if these satisfy the wave equation (4.2.5). From (4.2.5), the conditions of consistency are

$$(2w+3)(\varepsilon - 3(1-\beta)+2)\varepsilon - (6+6\varepsilon-\varepsilon^2 w)(1+3\beta) = 0, \tag{4.3.19}$$

and

$$3\varepsilon(2w+3) - (6+6\varepsilon-\varepsilon^2 w) = 0. \tag{4.3.20}$$

It is straightforward to calculate the deceleration parameter which determines the transition from one phase to another. For this model, using (1.7.11), it is calculated as

$$q(t) = -1 - \left(\frac{3\gamma - 3(1-\beta) - \varepsilon}{2}\right) e^{-\frac{3\gamma}{2}H_0(t-t_0)}. \tag{4.3.21}$$

The deceleration parameter in terms of the redshift is written as

$$q(z) = \frac{1}{2}\left[\frac{-6\gamma + (1-3\beta+\varepsilon)(\varepsilon+3(1-\beta)-3\gamma)(1+z)^{\frac{\varepsilon+3(1-\beta)}{2}}}{(\varepsilon+3(1-\beta)-3\gamma)(1+z)^{\frac{\varepsilon+3(1-\beta)}{2}} + 3\gamma}\right]. \tag{4.3.22}$$

When $\varepsilon+3(1-\beta)=3\gamma$, we have $q=-1$ that belongs to the de Sitter universe. From the above expression, the present-day value of q is given by,

$$q_0=\frac{1}{2}\left[\frac{-6\gamma+(1-3\beta+\varepsilon)(\varepsilon+3(1-\beta)-3\gamma)}{\varepsilon+3(1-\beta)}\right]. \tag{4.3.23}$$

For $\varepsilon=0$, equation (4.3.22) reduces to result of Ref. [181] in general relativity. For $\beta=0$, we find

$$q(z)=\frac{1}{2}\left[\frac{-6\gamma+(1+\varepsilon)(3+\varepsilon-3\gamma)(1+z)^{\frac{(\varepsilon+3)}{2}}}{(3+\varepsilon-3\gamma)(1+z)^{\frac{(\varepsilon+3)}{2}}+3\gamma}\right] \tag{4.3.24}$$

Equation (4.3.24) shows that the creation of matter is negligible at high redshifts while due to matter creation at redshifts of the order of a few, a transition from a decelerating to an accelerating phase occurs. For $\gamma=0$, from (4.3.22) we get

$$q=\frac{1+\varepsilon-3\beta}{2} \tag{4.3.25}$$

Equation (4.3.25) shows that $\beta=(1+\varepsilon)/3$ is a critical value for which $q=0$. For $\beta<(1+\varepsilon)/3$, the possible value of $q(z)$ are always constant and positives while for $\beta>(1+\varepsilon)/3$, it remains constant and negative in the course of expansion. There is no transition from deceleration to acceleration phase.

The transition redshift z_{tr} can be obtained by taking $q=0$ in equation (4.3.22), which implies that

$$z_{tr}=\left[\frac{6\gamma}{(1+\varepsilon-3\beta)(\varepsilon+3(1-\beta)-3\gamma)}\right]^{\frac{2}{(\varepsilon+3(1-\beta))}}-1, \tag{4.3.26}$$

Note that the case $\gamma=0$ gives $z_{tr}=-1$, which shows that the transition would be in infinite future. This gives contradiction with SNe data. Equation (4.3.26) equivalently can be written as,

$$\gamma=\frac{1}{3}\frac{(1+\varepsilon-3\beta)(\varepsilon+3(1-\beta))(1+z_{tr})^{\frac{(\varepsilon+3(1-\beta))}{2}}}{2+(1+\varepsilon-3\beta)(1+z_{tr})^{\frac{(\varepsilon+3(1-\beta))}{2}}}. \tag{4.3.27}$$

which for $\beta=0$, becomes

$$\gamma=\frac{1}{3}\frac{(1+\varepsilon)(\varepsilon+3)(1+z_{tr})^{\frac{(\varepsilon+3)}{2}}}{2+(1+\varepsilon)(1+z_{tr})^{\frac{(\varepsilon+3)}{2}}}. \tag{4.3.28}$$

4.4 Observational datasets

In this section, we use Hubble parameter $(4.3.10)$ to perform the four different statistical analysis involving the latest observational data, namely :

- **SNe(cJLA data):** We use the results of 'Joint light-curve Analysis' (cJLA) dataset of 31 check point (30 bins) by Betoule et al. [210], in the redshift range, $z = [0.01, 1.3]$.
- **OHD:** We use the OHD data of 43 measurement points collected in Ref. [214] in the redshift range $0 < z < 2.5$.
- **BAO:** The sample of BAO distances measurements from BOSS CMASS [229],SDSS(R) [236], the 6dF Galaxy survey [237] and three parallel measurements from WiggleZ survey [238] are used in analysis.

The χ^2 for the above mentioned datsets are χ^2_{SNe}, χ^2_{OHD} and χ^2_{BAO} in section 1.14 respectively. We obtain the best fit of the model parameters, namely, ε, β and γ. The goodness-of-fit of the model is obtained by the χ^2-minimization and likelihoods by using Markov Chain Monte Carlo (MCMC) method [209]. In this study we have taken the value of the Hubble constant, $H_0 = 67.8\ Km\ sec^{-1}\ Mpc^{-1}$ [13].

4.5 Results

In our analysis, we perform a global fitting to determine the model parameters using the MCMC method. Table 4.1 summarizes the best-fit values of model parameters obtained by statistical analysis carried out using different sets of observational data. The results of SNe and $SNe + BAO$ are little different from which of $SNe + OHD$ and $SNe + OHD + BAO$.

In statistical analysis, we find the best-fit values of model parameters satisfying the constraints $0 < \varepsilon < 3$, $0 < \beta < 1$, $0 < \gamma < 1$ and $1 < (\beta + \gamma) < 2$. Figs. 4.1-4.4 show confidence contours on parameters and the marginalized likelihood function of model obtained from the joint analysis with different data sets. The best-fit values of model parameters are given in Table 4.1.

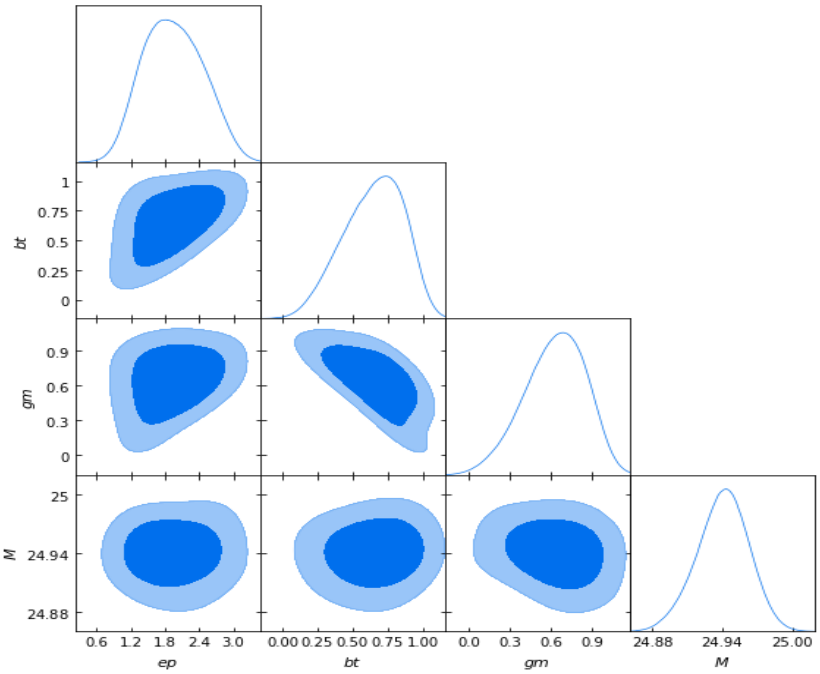

Figure 4.1: The likelihood contours at 68.3% CL and 95.4% CL using data from *SNe* with marginalized probability for the parameters. In Fig. the words *ep*, *bt* and *gm* denote ε, β and γ parameters, respectively.

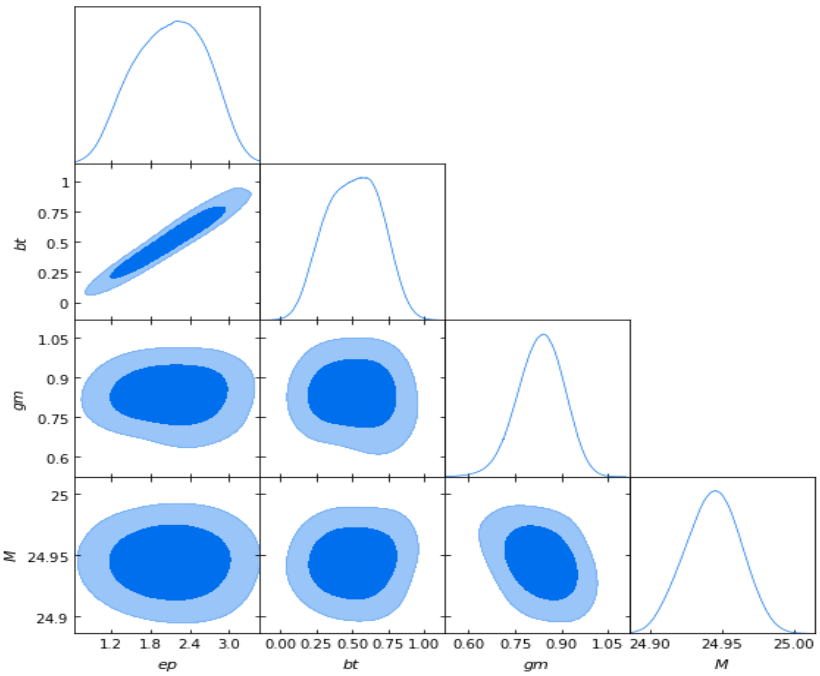

Figure 4.2: The likelihood contours at 68.3% CL and 95.4% CL based on joint analysis of *SNe* + *OHD*. In Fig. the words *ep*, *bt* and *gm* denote ε, β and γ parameters, respectively.

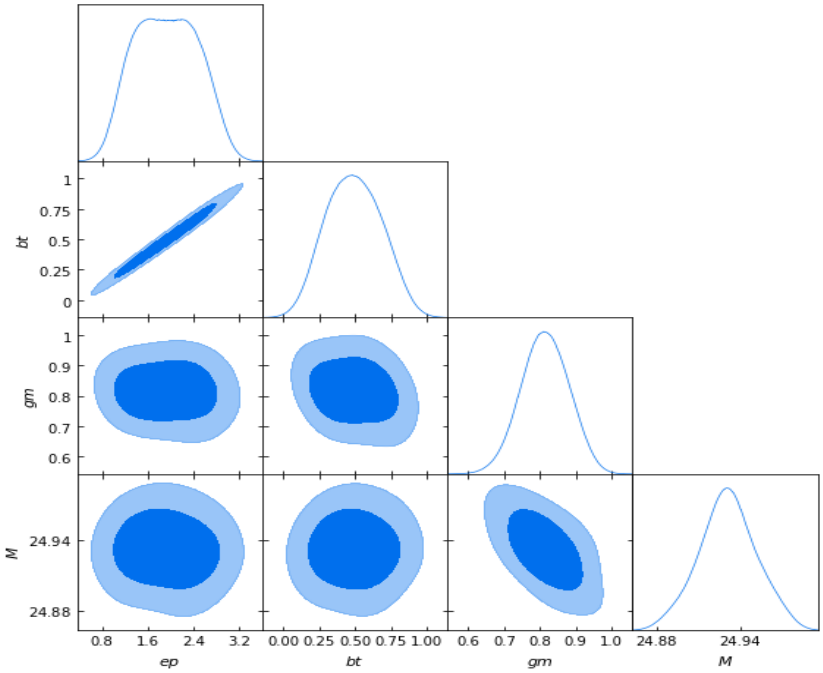

Figure 4.3: The likelihood contours at 68.3% CL and 95.4% CL based on joint analysis of *SNe + BAO*. In Fig. the words ep, bt and gm denote ε, β and γ parameters, respectively.

4.6 Evolution of the model

In this section, we discuss the evolution of the different cosmological quantities using the best-fit values of free parameters obtained from different observational data set. Figure 4.5 shows the evolution of the scale factor for different values of model parameters using observational data. It shows that the model starts expanding with accelerated rate at early time. The dots denote the transition point where the universe transits from deceleration to acceleration phase. We have also plotted the trajectories for other different values of parameters. The first bottom curve gives the trajectory without matter creation ($\beta = 0$, $\gamma = 0$) in general relativity ($\varepsilon = 0$) which clearly shows the expansion in decelerated rate.

From (4.3.10), we have

$$\frac{d\dot{a}}{da} = \frac{H_0}{(\varepsilon + 3(1-\beta))}\left[3\gamma + \frac{(\varepsilon + 3(1-\beta-\gamma))(2-\varepsilon-3(1-\beta))}{2}\, a^{-\frac{\varepsilon+3(1-\beta)}{2}}\right]. \tag{4.6.1}$$

Putting $d\dot{a}/a = 0$ in (4.6.1) to get the value of scale factor at transition, which is given by

$$a_{tr} = \left[\frac{(\varepsilon + 3(1-\beta-\gamma))(\varepsilon + 3(1-\beta) - 2)}{6\gamma}\right]^{\frac{2}{\varepsilon+3(1-\beta)}}, \tag{4.6.2}$$

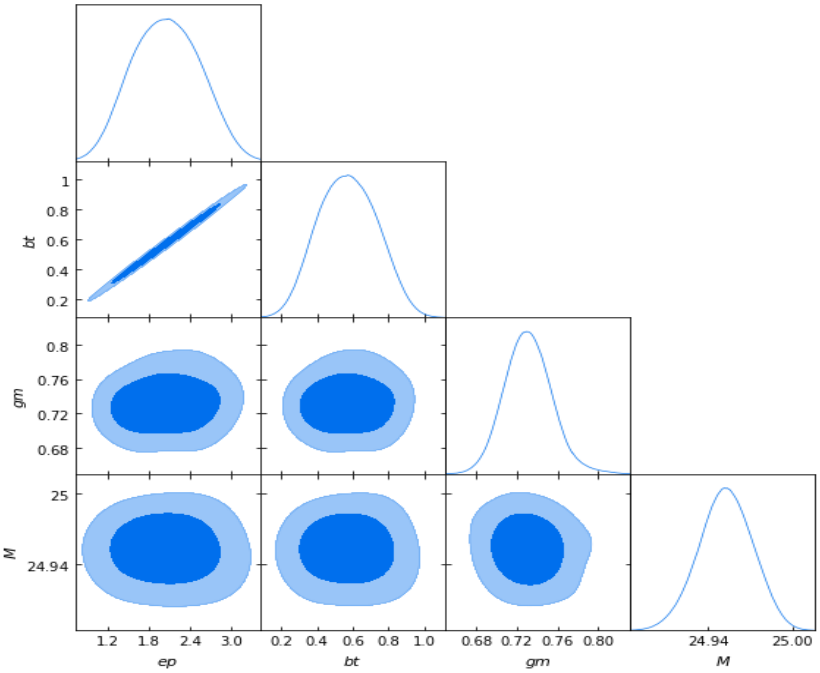

Figure 4.4: The likelihood contours at 68.3% CL and 95.4% CL based on joint analysis of *SNe* + *OHD* + *BAO*. In Fig. the words *ep*, *bt* and *gm* denote ε, β and γ parameters, respectively.

Table 4.1: The best-fit results of model parameters obtained from the analysis with different combinations of the data sets.

Dataset	ε	β	γ	M	χ^2_{min}
SNe	$1.898^{+0.633}_{-0.535}$	$0.667^{+0.210}_{-0.240}$	$0.645^{+0.218}_{-0.240}$	$24.941^{+0.020}_{-0.022}$	18.427
SNe +OHD	$2.142^{+0.593}_{-0.698}$	$0.512^{+0.205}_{-0.224}$	$0.840^{+0.066}_{-0.079}$	$24.945^{+0.018}_{-0.020}$	28.223
SNe +BAO	$1.915^{+0.665}_{-0.651}$	$0.448^{+0.225}_{-0.199}$	$0.813^{+0.072}_{-0.059}$	$24.932^{+0.021}_{-0.020}$	17.497
SNe +OHD+BAO	$2.141^{+0.596}_{-0.672}$	$0.597^{+0.200}_{-0.215}$	$0.731^{+0.021}_{-0.020}$	$24.951^{+0.017}_{-0.018}$	30.671

where the subscript "tr" denotes the transition. The values of a_{tr} are listed in Table 4.2 for different values of model parameters. In the expression (4.3.8), If we assume $\varepsilon + 3(1-\beta) = 3\gamma$, we obtain the de Sitter universe $a(t) = e^{H_0(t-t_0)}$ as shown in Fig. 4.5 (solid black line). In this case the model predicts an eternal accelerated expansion. For $0 < \varepsilon + 3(1-\beta) < 3\gamma$, the model expanding forever (see, brown curve) and for $\varepsilon + 3(1-\beta) > 3\gamma$, we find that model begin with a Big-Bang followed by an eternal expansion.

Using the best fitted values of parameters listed in Table 4.1 into (4.3.22) the variation of q with z is shown in Fig.4.6. We have found that the evolution corresponding the best estimates from all observational data are identical. The deceleration parameter starts from negative redshift, $z = -1$ and takes the trajectory from negative to positive. The model transits from decelerated to accelerated epoch at around $z_{tr} \sim 0.8$ with

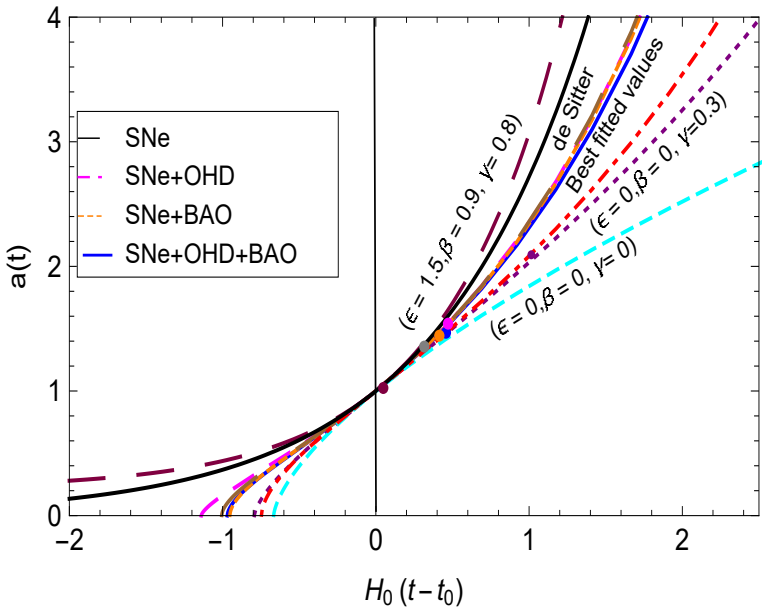

Figure 4.5: The scale function as a function of time for different values of model parameters ε, β and γ. The dots show the transition point.

$SNe+OHD$ and $SNe+OHD+BAO$, whereas SNe and $SNe+BAO$ predict the transition at around $z\sim 1.818$ and $z\sim 1.005$, respectively which are significantly higher and hint a strong deviation from other two. The transition redshift z_{tr}, at which q enters the negative region and the present-day value of q_0 are given in Table 4.2. The present-day negative value $-1<q_0<0$ with each observational data shows that the model behaves quintessence like.

The effective equation of state parameter, w_{eff} as defined in equation (2.6.1), is calculated as

$$w_{eff}=-1+\frac{1}{3}\frac{(\varepsilon+3(1-\beta-\gamma))(1+z)^{\frac{(\varepsilon+3(1-\beta))}{2}}}{h} \tag{4.6.3}$$

Table 4.2: The transition scale factor and redshift, and current values of $q(z)$ and $w_{eff}(z)$ using best-fit results of model parameters.

Data	a_{tr}	z_{tr}	q_0	$w_{eff}(z)$
SNe	0.3548	1.8180	−0.779	−0.679
SNe +OHD	0.5551	0.8013	−0.457	−0.638
SNe +BAO	0.4986	1.005	−0.434	−0.662
SNe +OHD+BAO	0.5398	0.8522	−0.422	−0.614

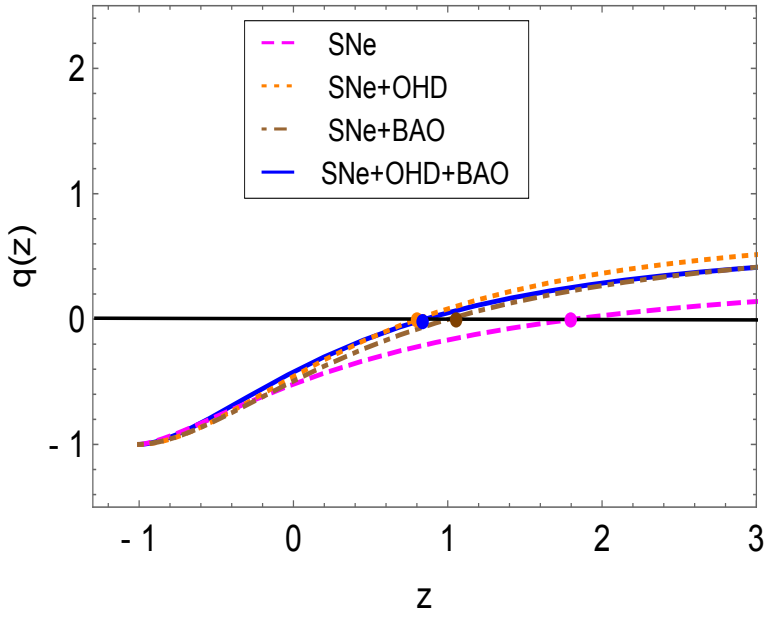

Figure 4.6: The evolution of the deceleration parameter $q(z)$ vs redshift z for the best estimated values of parameters. The dot denotes the value of z_{tr} at which q(z)=0 as mentioned in Table 4.2.

As $z \to -1$, $(a \to \infty)$, we get $w_{eff} \to -1$, which can also be observed from Fig. 4.7. It means that the model tends to ΛCDM in future time. The matter creation model is free from big-rip singularity as EoS does not cross the phantom divide line $w \leq -1$.

The current value $(h = 1)$ of w_{eff} is found to be

$$w_{eff}(z=0) = -1 + \frac{\varepsilon + 3(1-\beta-\gamma)}{3}. \tag{4.6.4}$$

The present value of w_{eff} are listed in Table 4.2 for different observational datasets which are higher than that predicted by the joint analysis of $WMAP + BAO + H_0 + SNe$ data which is around -0.93 [14].

In Fig 4.8, we see the Hubble evolution of our model and compare ΛCDM model with the error bar plots of Hubble dataset in the range $z \in (0,2)$. At the low redshifts, the curves coincide, while their evolution with increasing z differ appreciably in case of SNe and $SNe + BAO$. However, a good fit may be obtained using joint statistical analysis of $SNe+OHD$ and $SNe + OHD + BAO$.

It is to be noted that the present age of the universe for a flat CDM model dominated by matter ($\Omega_{m0} = 1$, $t_0 = 2/(3H_0)$) gives $t_0 \approx 8 - 10\ Gyr$, i.e., this model suffers the age problem. However, for ΛCDM model, it easily satisfies the constraint $t_0 > 11 - 12\ Gyr$. A plot of the age of the universe with redshift for the best fit values of model parameters is shown in fig. 4.9. The ages of the universe corresponding to $SNe + OHD$ and

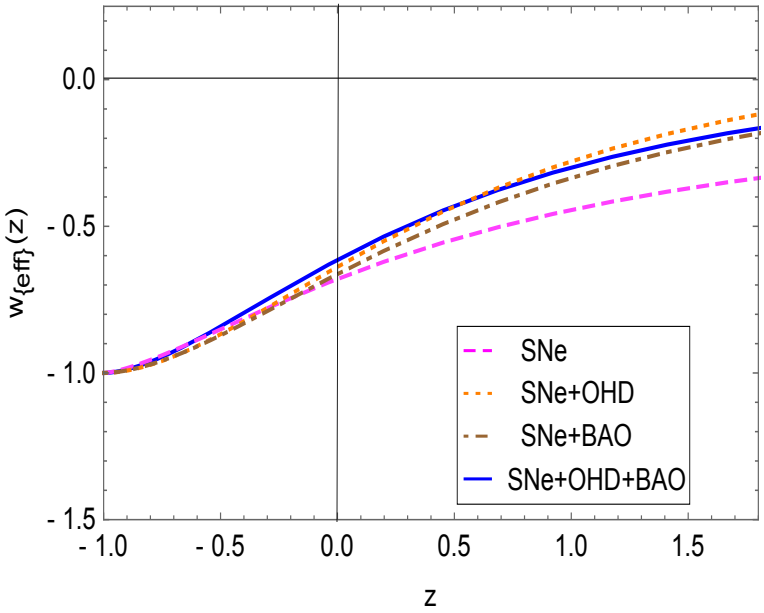

Figure 4.7: Plot of effective equation of state parameter w_{eff} versus redshift z for best fitted parameters.

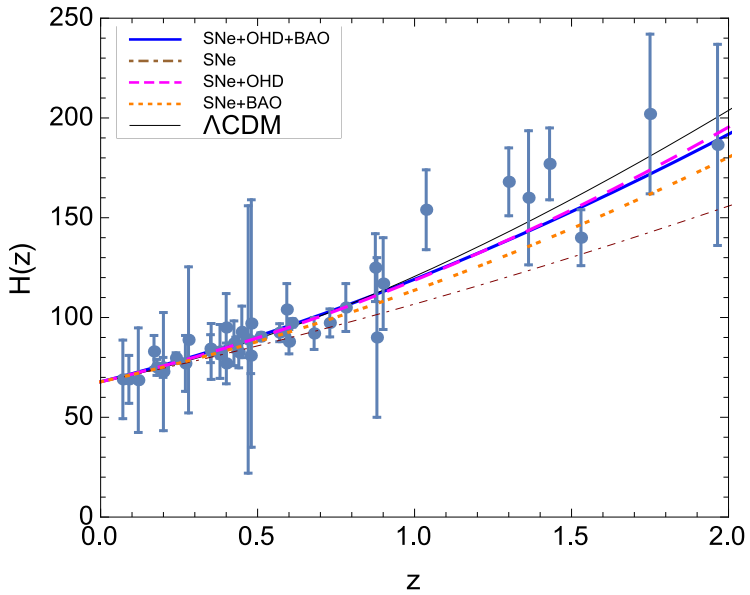

Figure 4.8: The Hubble function in terms of the redshift for ΛCDM model and the fitted model with error bar plots from Hubble data.

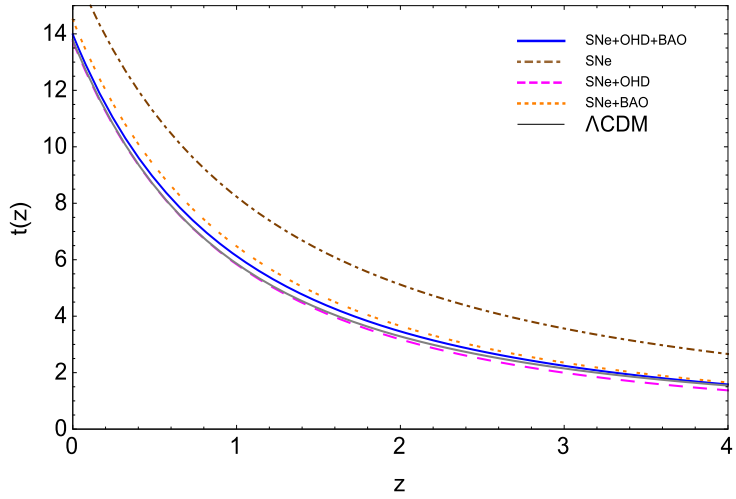

Figure 4.9: The age of universe for best fitted values and ΛCDM model in the units of Gyr(gega-year) with redshift.

$SNe+OHD+BAO$ are found to be 13.9 Gyr. So, the age predicted by the present model is agreeing with the age deduced from ΛCDM model which is around 13.799 ± 0.021 Gyr.

4.7 Diagnostic parameters

Let us compare our model with ΛCDM model by calculating the diagnostic parameters. The statefinder parameters are given by

$$\begin{aligned} r &= \frac{(2-(\varepsilon+3(1-\beta)))\,(2-2(\varepsilon+3(1-\beta)))}{4}+\frac{9\gamma}{4}(2-(\varepsilon+3(1-\beta)))\,e^{-\frac{3\gamma H_0}{2}(t-t_0)} \\ &\times\left[1+\frac{\varepsilon+3(1-\beta)}{3\gamma}\left(e^{\frac{3\gamma H_0}{2}(t-t_0)}-1\right)\right]+\frac{9\gamma^2}{4}e^{-3\gamma H_0(t-t_0)}\left[1+\frac{\varepsilon+3(1-\beta)}{3\gamma}\left(e^{\frac{3\gamma H_0}{2}(t-t_0)}-1\right)\right]^2 \end{aligned} \tag{4.7.1}$$

$$s=\frac{(r-1)}{3\left[-\frac{3}{2}+\left(\frac{3\gamma-3(1-\beta)-\varepsilon}{2}\right)e^{-\frac{3\gamma}{2}H_0(t-t_0)}\right]} \tag{4.7.2}$$

We observe that as $(t-t_0)\to\infty$, $\{r,s\}\to\{\frac{(3\beta-\varepsilon-1)(3\beta-\varepsilon-2)}{2},\frac{2(1-r)}{9}\}$, which deviates from the ΛCDM model. However, it corresponds to the ΛCDM model for $\varepsilon=0$ and $\beta=0$. The $\{r,s\}$ plane trajectory of the model for best estimated values of parameters by $SNe+OHD+BAO$ is shown in Fig. 4.10. The plot lies in the region $r<1$, $s>0$, which is the behavior of any quintessence model. The $\{r,q\}$ trajectory of the model is shown in Fig. 4.11. Our model tends to the standard model like ΛCDM and

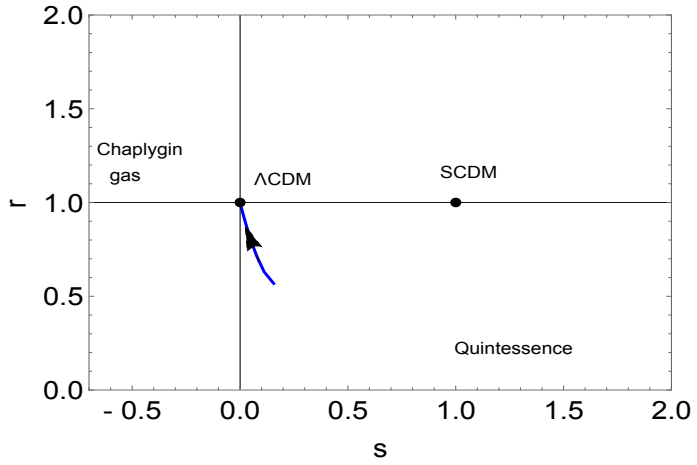

Figure 4.10: The trajectory of $\{r,s\}$ in $s-r$ plane corresponds to best fitted parameters obtained from joint analysis of $SNe+OHD+BAO$. The arrow shows the direction of the evolution of the trajectory.

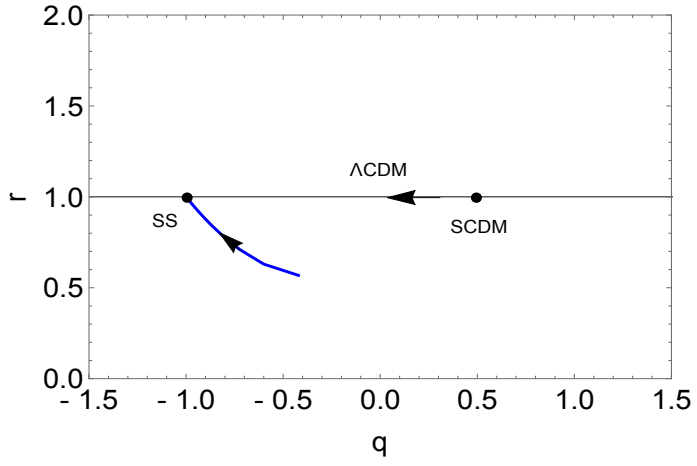

Figure 4.11: The trajectory of $\{r,q\}$ in $q-r$ plane for the best fitted parameters obtained from joint analysis of $SNe+OHD+BAO$. The arrow shows the direction of the evolution of the trajectory.

quintessence model ($Q-model$) in late time.

4.8 Thermodynamic Analysis

In this section, we discuss the validity of generalized second law (GSL) of thermodynamic in the present model dominated by matter creation. It is to be noted that according to the thermodynamic the entropy of isolated systems can never diminishes. We explore the calculations of total entropy, S for matter creation model. We assume that the apparent horizon is related to temperature and entropy analogous to associated with black hole event horizon [289]. So, according to GSL, the total entropy S must include the entropy of all sources. During the evolution of the universe the rate of the entropy change of the fluid within the universe and that of the horizon must always be greater than or equal to zero. As we are studying only the recent and future times, the total entropy is equal to the sum of the contribution of entropy to matter, S_m and apparent horizon, S_h, i.e., $S = S_m + S_h$, where $S_h = \frac{\kappa_B A}{4l_{Pl}^2}$ is the entropy of apparent horizon and S_m is entropy of pressureless matter. A and l_{Pl} are the area of the horizon and Planck's length, respectively, and κ_B is the Boltzman constant. The area of the apparent horizon is given by $A = 4\pi r_h^2$, where $r_h = \frac{1}{\sqrt{(H^2+ka^{-2})}}$. As we are restricting our analysis to spatially flat model $(k=0)$, this assumption yields $r_h = H^{-1}$. Therefore, the horizon entropy reads as

$$S_h = \frac{\kappa_B \pi}{l_{Pl}^2 H^2}. \tag{4.8.1}$$

Using Eq.(4.3.7), the first derivative of Eq. (4.8.1) gives

$$\dot{S_h} = \frac{\kappa_B \pi H_0}{l_{Pl}^2} \frac{H_0}{H^2} \left(\varepsilon + 3(1-\beta-\gamma)\right) a^{-\frac{\varepsilon+3(1-\beta)}{2}}. \tag{4.8.2}$$

It is observed from the above equation that $\dot{S_h} \geq 0$ for $0 < \beta + \gamma \leq 1$. The matter entropy inside the dynamical apparent horizon is described by Gibb's relation [290]

$$T dS_m = d(\rho V) + p\, dV, \tag{4.8.3}$$

where $V = \frac{4\pi}{3} r_h^3$ is the spatial volume enclosed by the horizon and T is the temperature of fluid and we assume that the temperature T is equal to the temperature at horizon

T_h, where $T_h = 1/2\pi r_h$ [94].
Using (4.3.4), the above equation gives

$$\dot{S_m} = \frac{8\pi^2 H_0 \rho}{H^4}\left[\frac{(3\gamma-(\varepsilon+3(1-\beta)))}{2}a^{-\frac{\varepsilon+3(1-\beta)}{2}}+\varepsilon H\right], \tag{4.8.4}$$

As H and ρ are positive, the positivity of $\dot{S_m}$ is ensured whenever $\varepsilon+3(1-\beta)<3\gamma$. Adding (4.8.2) and (4.8.4), we get $\dot{S_h}+\dot{S_m}\geq 0$ provided $0<(\beta+\gamma)<1$ and $\varepsilon+3(1-\beta)<3\gamma$. This means that GSL is always valid with these constraints.

4.9 Conclusion

In this chapter we have studied a matter-dominated model with 'adiabatic' matter creation in Brans-Dicke theory with matter creation rate $\Gamma = 3\gamma H_0 + 3\beta H$ to explain the late-time accelerated expansion of the universe. We have demonstrated how matter creation works well with the expanding universe. In order to constrain the model parameters, statistical analysis using cosmic observations data from SNe, OHD and BAO have been performed. Further, in order to reduce the number of the free variables, we select to use the present value of the Hubble function, i.e., $H_0 = 67.8\ Km\ s^{-1}Mpc^{-1}$. The results are given in Table 4.1 and 4.2. In figures 4.1-4.4, we have plotted the contour maps obtained from dataset. According to the $MCMC$ analysis, it is found that the best fitting values of model parameters from SNe and $SNe+BAO$ are little different than those obtained from $SNe+OHD$ and $SNe+OHD+BAO$. The later best fit values are compatible with the ΛCDM model.

Using the best fit values, we plot the evolutions of scale factor, deceleration parameter and effective equation of state parameter. From Fig. 4.5, it has been found that the model starts from Big-Bang followed by decelerated expansion at early times and with a transition to an accelerated epoch at later time corresponding to the defined constraints. In some other constraints, the model predicts an eternally expanding universe beginning with a Big-Bang in the past followed by decelerated expansion and a smooth transition to an accelerated expansion. Table 4.2 gives the transition point a_{tr} from best fitted values obtained from different dataset.

We have also discussed the evolution of the deceleration parameter q and effective EoS w_{eff}. From Fig.4.6, it is observed that there is a transition from decelerated phase to accelerated phase. The present day value of q_0 and transition redshift are found from each observational data. In general, $q\to -1$ as $a\to\infty$ which corresponds

to de Sitter model of the universe. We have also plotted the trajectories for w_{eff} for best fitted values of parameters in Fig 4.7. In each case the model does not cross the phantom-divide line. Irrespective of the values of parameters, $w_{eff} \to -1$ as $z \to -1$.

The Hubble function of the model with error bar fits in to the ΛCDM model for best fitted values obtained from $SNe + OHD$ and $SNe + OHD + BAO$ (see, Fig. 4.8). The age of the universe obtained from $SNe + OHD$ and $SNe + OHD + BAO$ for best fitting values predict the same as ΛCDM model. However, it is comparatively higher than those obtained from SNe and $SNe + BAO$ as shown in Fig 4.9.

We have discussed the statefinder diagnostic for the model. In Fig.4.10, we have plotted the trajectory of $\{r,s\}$ in $s-r$ plane. The trajectory is different from the ΛCDM model. The model shows the behavior of quintessence like. However, as $a \to \infty$, the statefinder parameter $\{r,s\} \to \{1,0\}$, corresponds to the ΛCDM point.

We have analysed the validity of GSL in the present model and found that the GSL of thermodynamic is valid with apparent horizon as the boundary for $0 < (\beta + \gamma) < 1$ and $\varepsilon + 3(1-\beta) < 3\gamma$.

In summary, this chapter keeps itself in the domain of cosmology, more especially in the accelerating cosmology which is a certain plight to explain the evolution of the universe.

****

Chapter 5

Holographic dark energy model with matter creation in Brans-Dicke theory

---

In this chapter [1]*, the adiabatic matter creation for a spatially homogeneous and isotropic flat FLRW universe is discussed in holographic dark energy (HDE) in the context of BD theory. Since the HDE density is considered as a dynamical cosmological constant, it is natural to study it in a dynamical frame of BD theory. The models are constrained with the latest observational data from SNe, measurements of OHD and BAO/CMB data. Using the MCMC method, we obtain the best fit values of the parameters for different models. It is found that the HDE model without matter creation does not achieve transition phase when the Hubble horizon is taken as an IR cut-off. However, it achieves the phase transition from decelerated phase to accelerated phase with same IR cut-off with the inclusion of gravitationally induced matter creation. Using AIC and BIC, and geometrical diagnostic parameters, we compare the models with* Λ*CDM model and discuss the viability of the model. A detailed thermodynamic analysis is also carried out.*

---

[1]This chapter is based on a published research paper "Constraints on holographic dark energy model with matter creation in Brans-Dicke theory and thermodynamic analysis, *Physics of the Dark Universe* **33**, 100869 (2021)".

5.1 Introduction

Many theoretical approaches have been carried out to investigate the recent cosmic acceleration. In general relativistic cosmology, the presence of negative pressure is the key ingredient for the accelerating universe. The negative pressure occurs naturally in many different contexts when the physical systems depart from thermodynamic equilibrium. One such example is the matter creation induced by the time-varying gravitational field in an expanding universe [170, 171, 173, 291, 292].

On the other hand, there is another concept in which the DE is assumed a dynamically evolving component. In fact, several dynamical models of DE have been proposed and studied in detail. One of such dynamical models is the holographic dark energy (HDE) model in which HDE density depends on the choice of IR cut-off. In a paper, Xu et al. [293] have studied HDE model with Hubble horizon as an IR cut-off in BD theory and found that there is no accelerated expansion of the universe. However, an accelerated expansion is obtained once the event horizon is considered as an IR cut-off.

The BD theory is the most natural choice as the scalar tensor generalization of general relativity which was formulated in order to incorporate the Mach's Principle. In this chapter, we consider HDE model with matter creation in a more dynamical framework, i.e., in BD cosmology. It is to be noted that the HDE density belongs to a dynamical cosmological constant, therefore, we need a dynamical frame to accommodate it instead of Einstein gravity. Thus, the study of HDE model in the framework of BD theory is well motivated. A number of authors [249, 294–298] have studied HDE models with different IR cut-offs in the framework of BD theory to explain the recent acceleration and to alleviate the cosmic coincidence problem. Xu and Li [293] have constrained the HDE model in BD theory by cosmic observational data.

The purpose of this paper is to study a cosmological model of late acceleration in BD theory with the assumption that the pressureless dark matter with matter creation and HDE conserve separately. Instead of assuming the other IR cut-off, we include matter creation mechanism in HDE model with the same Hubble horizon as an IR cut-off with the possibility that this model would be consistent with the current observations and show the phase transition. We consider four different HDE models with and without matter creation. We discuss the evolution and dynamics of the model by constraining the model parameters through combined observational data of type Ia

SNe, OHD and combined data of BAO and CMB. It is found that the HDE model with matter creation shows phase transition from decelerated phase to accelerated phase. The model behaves quintessence like and approaches to ΛCDM model in late times.

The chapter is organized as follows. In section 5.2, we present the field equations of HDE model with Hubble horizon as an IR cut-off in BD theory when adiabatic matter creation is allowed. Section 5.3 is devoted to the analytical solution of the different HDE models with and without matter creation. Section 5.4 studies the constraints on cosmological model by using data of Type Ia SNe, OHD and BAO/CMB data. In section 5.5, we present the result of the best-fit values of different model parameters to discuss the evolution of the universe. Section 5.6 discusses the geometrical diagnostic parameters to distinguish HDE models with ΛCDM model. We present the thermodynamic analysis of the model based on generalized second law of thermodynamics in section 5.7. Finally, we summarize our findings in section 5.8.

5.2 HDE Model with matter creation in BD theory

We assume the background as a spatially homogenous and isotropic flat FLRW space-time as defined in (1.3.8). The BD field equations from the action (1.10.2) with respect to flat FLRW metric $g_{\mu\nu}$ (1.3.8) and the BD scalar field ϕ are

$$R_{\mu\nu} - \frac{1}{2} g_{\mu\nu} R = \frac{8\pi}{\phi} T_{\mu\nu} + 8\pi T^{BD}_{\mu\nu}, \tag{5.2.1}$$

and

$$\nabla_\alpha \nabla^\alpha = \frac{8\pi}{(2\omega+3)} T^\lambda{}_\lambda = 0, \tag{5.2.2}$$

where $T_{\mu\nu}$ is the energy-momentum tensor for perfect fluid and $T^{BD}_{\mu\nu}$ is the energy-momentum tensor of BD scalar field. We assume that the universe contains the dark matter and HDE in which a process of dark matter creation from gravitational field takes place. Therefore, the energy-momentum tensor $T_{\mu\nu}$ is the sum of matter fluid including creation and HDE, and adopts the perfect fluid form as

$$T_{\mu\nu} = (\rho_t + p_t) u_\mu u_\nu + p_t g_{\mu\nu}, \tag{5.2.3}$$

where ρ_t is the sum of energy density of matter and HDE, i.e., $\rho_t = \rho_m + \rho_h$, and p_t is the sum of pressures due to perfect fluid, matter creation and HDE i.e., $p_t =$

$p_m + p_c + p_h$. The energy-momentum tensor for BD scalar field $T^{BD}_{\mu\nu}$ is defined by

$$T^{BD}_{\mu\nu} = \frac{1}{8\pi}\left[\frac{\omega}{\phi^2}\left(\nabla_\mu\phi\nabla_\nu\phi - \frac{1}{2}g_{\mu\nu}\nabla_\varepsilon\phi\nabla^\varepsilon\phi\right) + \frac{1}{\phi}\left(\nabla_\mu\nabla_\nu\phi - g_{\mu\nu}\nabla_\varepsilon\nabla^\varepsilon\phi\right)\right]. \tag{5.2.4}$$

The gravitational field equations for a universe dominated by pressureless dark matter (DM) and HDE in which a process of DM creation from the gravitational field, governed by (5.2.1), yield

$$3H^2 + 3H\frac{\dot{\phi}}{\phi} - \frac{\omega}{2}\frac{\dot{\phi}^2}{\phi^2} = \frac{8\pi}{\phi}\rho_t, \tag{5.2.5}$$

$$2\dot{H} + 3H^2 + \frac{\ddot{\phi}}{\phi} + 2H\frac{\dot{\phi}}{\phi} + \frac{\omega}{2}\frac{\dot{\phi}^2}{\phi^2} = -\frac{8\pi}{\phi}p_t. \tag{5.2.6}$$

The dynamical equation for the scalar field is given by

$$\frac{\ddot{\phi}}{\phi} + 3H\frac{\dot{\phi}}{\phi} = \frac{8\pi}{(2\omega+3)\phi}(\rho_t - 3p_t), \tag{5.2.7}$$

Ignoring the inhomogeneities arising from the (linear) field perturbations, the BD field can be treated as a perfect fluid $T^{BD}_{\mu\nu} = (\rho_{BD} + p_{BD})u_\mu u_\nu + p_{BD}g_{\mu\nu}$ with energy and pressure are respectively given by

$$\rho_{BD} = \frac{1}{8\pi G}\left[\frac{\omega}{2}\left(\frac{\dot{\phi}}{\phi}\right)^2 - 3H\frac{\dot{\phi}}{\phi}\right], \tag{5.2.8}$$

$$p_{BD} = \frac{1}{8\pi G}\left[\frac{\omega}{2}\left(\frac{\dot{\phi}}{\phi}\right)^2 + 2H\frac{\dot{\phi}}{\phi} + \frac{\ddot{\phi}}{\phi}\right]. \tag{5.2.9}$$

Finally, the geometric Bianchi identity in equation (5.2.1), which play a role of consistency relation, leads to

$$\nabla_\nu\left(R^{\mu\nu} - \frac{1}{2}g^{\mu\nu}R\right) = 0 = \nabla_\nu\left(\frac{8\pi}{\phi}T^{\mu\nu} + 8\pi T^{\mu\nu}_{BD}\right). \tag{5.2.10}$$

In this chapter, we study the model dominated by pressureless dark matter $(p_m = 0)$ in the presence of matter creation and HDE in BD theory. Further, we assume that dark components - the pressureless dark matter with matter creation and the HDE - do not interact with each other. Therefore, the energy conservation equation for each conserves separately. It means that $T^{\mu\nu}$ obeys the usual conservation law, $T^{\mu\nu}_{;\nu} = 0$, which take the forms

$$\dot{\rho_m} + 3H(\rho_m + p_c) = 0, \tag{5.2.11}$$

and

$$\dot{\rho_h} + 3H\left(\rho_h + p_h\right) = 0. \tag{5.2.12}$$

One interesting thing about working in Jordan frame is that the conservation equation holds for matter and BD scalar field separately, i.e., equations of motion of matter do not enter into the BD scalar field. Therefore, from (5.2.10), we are left

$$\left(\nabla_\nu\{\frac{8\pi}{\phi}\}T^{\mu\nu} + \nabla_\nu\{8\pi T^{\mu\nu}_{BD}\}\right) = 0, \tag{5.2.13}$$

which gives

$$\dot{\rho}_{BD} + 3H\left(\rho_{BD} + p_{BD}\right) = \left(\frac{\dot{\phi}}{\phi^2}\right)\rho_t, \tag{5.2.14}$$

which can be treated as an additional conservation law [116, 299].

It can be checked that the covariant conservation laws (5.2.11), (5.2.12) and (5.2.14) can also be obtained upon lengthy but straight forward computation by combining equations (5.2.5)-(5.2.7) which are identical to that of general relativity. Although the calculation is more involved than in general relativity, the final result turns out to be the same. Thus, we shall use (5.2.11), (5.2.12) and (5.2.5) to obtain the solution of the model and finally we use (5.2.14) to get the consistency condition, which will be used to constraint the model parameters.

The general analytical solutions to the system (5.2.5)-(5.2.7) are not known. However, physical sense guides us into searching for possible solutions in which the BD scalar field ϕ evolves very slowly. We assume that BD scalar field can be described as a power-law of the scale factor, namely $\phi = \phi_0\, a^\varepsilon$ as taken in the previous chapter. With this power-law assumption, the Friedmann equation (5.2.5) can be rewritten as

$$\left(1 + \varepsilon - \frac{\omega}{6}\varepsilon^2\right)H^2 = \frac{8\pi}{3\phi}(\rho_m + \rho_h). \tag{5.2.15}$$

We have discussed that there are various choices of IR cut-off for the cosmological length scale available in literature. The Hubble horizon, which is given by $\rho_h = 3b^2(8\pi G L^2)^{-1}$, where $L = H^{-1}$ is the IR cut-off, is the simplest choice of IR cut-off but this IR cut-off does not describe the cosmic acceleration [62]. In the framework of BD theory, the scalar field ϕ plays the role of Newton's constant ($\phi \sim 1/G$). Therefore, the modify HDE in BD theory is given by [299]

$$\rho_h = \frac{3b^2}{8\pi}\phi H^2 \tag{5.2.16}$$

Now, using this form of ρ_h with (5.2.11) and (5.2.12), the evolution equation (5.2.15) for cold dark matter can be written as

$$\dot{H}+\left(\frac{3+\varepsilon}{2}+\frac{9b^2w_h}{6+6\varepsilon-\omega\varepsilon^2}\right)H^2=\frac{(6+6\varepsilon-\omega\varepsilon^2-6b^2)}{2(6+6\varepsilon-\omega\varepsilon^2)}\,\Gamma H, \tag{5.2.17}$$

where $w_h=p_h/\rho_h$ is the equation of state (EoS) parameter of HDE. In what follows, we shall solve the above equation for different choices of particle creation rate Γ and perform the observational constraints on the model parameters.

5.3 Solution of HDE model

Now, one can observe from (5.2.17) that the dynamics of the universe can only be observed if the matter creation rate Γ is known. In what follows, we present different models depending on the choices of the matter creation rate Γ.

5.3.1 Solution with $\Gamma=0$

Let us first find the solution of HDE model with Hubble horizon as an IR cut-off without matter creation (hereafter *HDE 1*). Taking $\Gamma=0$, Eq. (5.2.17) reduces to

$$\dot{H}+\left(\frac{3+\varepsilon}{2}+\frac{9b^2w_h}{6+6\varepsilon-\omega\varepsilon^2}\right)H^2=0. \tag{5.3.1}$$

The solution of (5.3.1) is given by

$$H=H_0\left(\frac{a}{a_0}\right)^{-\left(\frac{3+\varepsilon}{2}+\frac{9b^2w_h}{6+6\varepsilon-\omega\varepsilon^2}\right)}, \tag{5.3.2}$$

The solution of the scale factor, normalized to unity at present epoch, in terms of cosmic time t can be obtained as

$$a=\left[1+\left(\frac{3+\varepsilon}{2}+\frac{9b^2w_h}{6+6\varepsilon-\omega\varepsilon^2}\right)H_0\,(t-t_0)\right]^{\frac{1}{\left(\frac{3+\varepsilon}{2}+\frac{9b^2w_h}{6+6\varepsilon-\omega\varepsilon^2}\right)}}. \tag{5.3.3}$$

The deceleration parameter is given by

$$q=\left(\frac{3+\varepsilon}{2}+\frac{9b^2w_h}{6+6\varepsilon-\omega\varepsilon^2}\right)-1. \tag{5.3.4}$$

Using (5.3.2) and (2.6.1), the effective EoS parameter is calculated as

$$w_{eff} = -1 + \frac{2}{3}\left(\frac{3+\varepsilon}{2} + \frac{9b^2 w_h}{6+6\varepsilon-\omega\varepsilon^2}\right). \tag{5.3.5}$$

From (5.3.3), (5.3.4) and (5.3.5), we observe that the expansion of the model is of power-law form, and the deceleration parameter and effective EoS parameter are constant. Therefore, the HDE model with Hubble horizon as an IR cut-off in BD theory does not show the phase transition. The HDE model will decelerate or accelerate through out the evolution depending on the value of parameters. Thus, the HDE model with Hubble horizon as an IR cut-off in BD theory is ruled out to fit the observational data. In Refs. [62, 63, 300], the authors have also found such solutions. Many authors [69, 77, 97, 301] proposed different IR cut-off like particle horizon, event horizon, Ricci scalar, etc., to discuss the accelerating universe. However, it is to be noted that the Hubble horizon is a natural choice of cosmological length scale. Therefore, instead of considering any other IR cut-off or interaction between the fluids as did by many authors, we restrict ourselves to Hubble horizon as an IR cut-off but in the presence of matter creation to realize an accelerated expansion of the universe.

5.3.2 Solution with $\Gamma \neq 0$

The purpose of review of the power-law solution of HDE model in previous section is to present our motivation to work with matter creation. In this subsection, let us study the evolution equation (5.2.17) of HDE model with matter creation. We assume the functional form of matter creation rate of a more general form [181,182,302](hereafter, *HDE 2*)

$$\Gamma = 3\gamma H_0 + 3\beta H, \tag{5.3.6}$$

where the parameters γ and β lie on the interval [0, 1]. Inserting (5.3.6) into (5.2.17), one finds

$$H' + \frac{k_1}{a}H = \frac{3\gamma(6+6\varepsilon-\omega\varepsilon^2-6b^2)}{2(6+6\varepsilon-\omega\varepsilon^2)}\frac{H_0}{a}, \tag{5.3.7}$$

where $k_1 = \frac{(\varepsilon+3(1-\beta))(6+6\varepsilon-\omega\varepsilon^2)+18(w_h+\beta)b^2}{2(6+6\varepsilon-\omega\varepsilon^2)}$ and a prime denotes derivative with respect to the scale factor a. The solution of (5.3.7) in terms of redshift z reads

$$H = H_0\left[\frac{3\gamma(6+6\varepsilon-\omega\varepsilon^2-6b^2)}{2(6+6\varepsilon-\omega\varepsilon^2)k_1} + \left(1-\frac{3\gamma(6+6\varepsilon-\omega\varepsilon^2-6b^2)}{2(6+6\varepsilon-\omega\varepsilon^2)k_1}\right)(1+z)^{k_1}\right]. \tag{5.3.8}$$

Using $H = \dot{a}/a$ and $1+z = a^{-1}$, integration of the above expression, in normalized unit of the scale factor at present time, gives

$$a = \left[1 + \frac{2(6+6\varepsilon-\omega\varepsilon^2)k_1}{3\gamma(6+6\varepsilon-\omega\varepsilon^2-6b^2)}\left(e^{\frac{3\gamma(6+6\varepsilon-\omega\varepsilon^2-6b^2)}{2(6+6\varepsilon-\omega\varepsilon^2)}H_0(t-t_0)} - 1\right)\right]^{1/k_1}. \tag{5.3.9}$$

We observe that as $(t-t_0)\to 0$, $a \to [1+k_1H_0(t-t_0)]^{1/k_1}$, which shows the power-law expansion in early time. As $(t-t_0)\to\infty$, the scale factor tends to $a \to e^{\frac{3\gamma(6+6\varepsilon-\omega\varepsilon^2-6b^2)}{2(6+6\varepsilon-\omega\varepsilon^2)}H_0(t-t_0)}$, which corresponds to the expansion like de Sitter. Thus, the model has early deceleration phase followed by an acceleration phase in the later stage of the evolution.

The cosmic time $t(a)$ in terms of the scale factor is given by

$$t(a)-t_0 = \frac{2(6+6\varepsilon-\omega\varepsilon^2)H_0^{-1}}{3\gamma(6+6\varepsilon-\omega\varepsilon^2-6b^2)} ln\left(1+\frac{3\gamma(6+6\varepsilon-\omega\varepsilon^2-6b^2)}{2(6+6\varepsilon-\omega\varepsilon^2)k_1}(a^{k_1}-1)\right) \tag{5.3.10}$$

Thus, the cosmic time t_{BB} when the Big-Bang $a(t_{BB})=0$ happens, is given by

$$t_{BB} = t_0 + \frac{2(6+6\varepsilon-\omega\varepsilon^2)H_0^{-1}}{3\gamma(6+6\varepsilon-\omega\varepsilon^2-6b^2)} ln\left(1-\frac{3\gamma(6+6\varepsilon-\omega\varepsilon^2-6b^2)}{2(6+6\varepsilon-\omega\varepsilon^2)k_1}\right) \tag{5.3.11}$$

The age of the universe, i.e., the elapsed time between the time t_{BB} until the present time t_0, is given by

$$|t_0-t_{BB}| = \left|\frac{2(6+6\varepsilon-\omega\varepsilon^2)H_0^{-1}}{3\gamma(6+6\varepsilon-\omega\varepsilon^2-6b^2)} ln\left(1-\frac{3\gamma(6+6\varepsilon-\omega\varepsilon^2-6b^2)}{2(6+6\varepsilon-\omega\varepsilon^2)k_1}\right)\right|. \tag{5.3.12}$$

Using (5.3.8) into (1.7.11), the deceleration parameter in terms of redshift is given by

$$q(z) = -1 + \frac{1}{2(6+6\varepsilon-\omega\varepsilon^2)} \frac{\left(2(6+6\varepsilon-\omega\varepsilon^2)k_1 - 3\gamma(6+6\varepsilon-\omega\varepsilon^2-6b^2)\right)(1+z)^{k_1}}{\frac{3\gamma(6+6\varepsilon-\omega\varepsilon^2-6b^2)}{2(6+6\varepsilon-\omega\varepsilon^2)k_1} + \left(1-\frac{3\gamma(6+6\varepsilon-\omega\varepsilon^2-6b^2)}{2(6+6\varepsilon-\omega\varepsilon^2)k_1}\right)(1+z)^{k_1}}. \tag{5.3.13}$$

Thus, the parameter q is time-dependent, which means that the transition of the universe from deceleration to late-time acceleration is possible. One can obtain transition redshift by taking $q=0$ in Eq. (5.3.13), which implies that

$$z_{tr} = -1 + \left[\frac{3\gamma(6+6\varepsilon-\omega\varepsilon^2-6b^2)}{(k_1-1)\{2(6+6\varepsilon-\omega\varepsilon^2)k_1 - 3\gamma(6+6\varepsilon-\omega\varepsilon^2-6b^2)\}}\right]^{\frac{1}{k_1}}. \tag{5.3.14}$$

The present value of q at $z=0$ is obtained as

$$q_0 = \frac{2(6+6\varepsilon-\omega\varepsilon^2)(k_1-1)-3\gamma(6+6\varepsilon-\omega\varepsilon^2-6b^2)}{2(6+6\varepsilon-\omega\varepsilon^2)}. \tag{5.3.15}$$

Thus, the transition from decelerated to accelerated phase occurs at present for $2(6+6\varepsilon-\omega\varepsilon^2)(k_1-1)=3\gamma(6+6\varepsilon-\omega\varepsilon^2-6b^2)$. At this value, the transition scale factor $a_{tr}=1$ which is the value of scale factor to be assume at present. For $2(6+6\varepsilon-\omega\varepsilon^2)(k_1-1)>3\gamma(6+6\varepsilon-\omega\varepsilon^2-6b^2)$, we have decelerated universe in the present time and for $2(6+6\varepsilon-\omega\varepsilon^2)(k_1-1)<3\gamma(6+6\varepsilon-\omega\varepsilon^2-6b^2)$, we have an accelerated one today.

For this model, we get the effective EoS, given by

$$w_{eff} = -1+\frac{H_0}{3H}\frac{[(3+\varepsilon-3\gamma)(6+6\varepsilon-\omega\varepsilon^2)+18(w_h+\gamma)b^2](1+z)^{k_1}}{(6+6\varepsilon-\omega\varepsilon^2)}. \tag{5.3.16}$$

The present effective EoS parameter when $H=H_0$, is given by

$$w_{eff}(z=0) = -1+\frac{1}{3}\frac{(3+\varepsilon-3\gamma)(6+6\varepsilon-\omega\varepsilon^2)+18(w_h+\gamma)b^2]}{(6+6\varepsilon-\omega\varepsilon^2)}. \tag{5.3.17}$$

The condition of EoS parameter, $w_{eff}<-1/3$ for acceleration of the present universe can be obtained as

$$3w_{eff}(z=0)+1 = (1+\varepsilon-3\gamma)(6+6\varepsilon-\omega\varepsilon^2)+18(w_h+\gamma)b^2<0. \tag{5.3.18}$$

Now, it is interesting to discuss in what sense this HDE model with matter creation behaves like an irreversible process. Let us consider the entropy behavior of the model. In adiabatic matter creation the specific entropy (per particle) $\sigma=S/N$, where S and N are, respectively, the entropy of the dominant component and the corresponding number of particles, remains constant, i.e., $\dot{\sigma}=0$. This implies that $\frac{\dot{S}}{S}=\frac{\dot{N}}{N}$. Since $N=na^3$, it follows from (1.11.7) and (5.3.6) that N increases as $N=N_0\,a^{3\beta}\,e^{3\gamma H_0(t-t_0)}$, where a is obtained in Eq. (5.3.9). The corresponding S can be obtained as $S=S_0\,a^{3\beta}\,e^{3\gamma H_0(t-t_0)}$.

Using (5.2.8), (5.2.9) and (5.2.15), one can check that the consistency condition (5.2.14) can be written as

$$2(\omega\varepsilon-3)\dot{H}+(\omega\varepsilon^2+6\omega\varepsilon-12)H^2=0 \tag{5.3.19}$$

Putting (5.3.8) in (5.3.19), we obtain

$$2(\omega\varepsilon-3)(X-k_1)a^{-k_1}+(\omega\varepsilon^2+6\omega\varepsilon-12)\left[\frac{X}{k_1}+\left(1-\frac{X}{k_1}\right)a^{-k_1}\right]=0, \tag{5.3.20}$$

where $X=\frac{3\gamma(6+6\varepsilon-\omega\varepsilon^2-6b^2)}{2(6+6\varepsilon-\omega\varepsilon^2)}$. The above equation can not be always satisfied. So, we assume this equation is satisfied nowadays, i.e., when $a=a_0=1$, which gives a relation between the constants as

$$2(\omega\varepsilon-3)(X-k_1)+(\omega\varepsilon^2+6\omega\varepsilon-12)=0. \tag{5.3.21}$$

5.4 Observational data and method

In this section, we consider most recent following observational data sets to constrain free parameters of our models (*HDE 1* and *HDE 2*):

- **SNe(Pantheon data):** We use the latest compilation of SNe (Pantheon sample), consisting 40 binned data points in the redshift range $0.014\leq z\leq 1.62$ or 1048 data points in the redshift range of $z\in[0.014,2.3]$ from SNLS, SDSS, Pan-STARRS1, HST survey [211].

- **OHD:** We use Hubble data $H(z)$ to study the cosmic expansion history which includes 36 measurements in which 31 measurements are determined from the cosmic chronometric technique (CC) [215].

- **Local Hubble constant:** In addition, we take the recently measured local Hubble constant H_0 as $H_0=73.5\pm1.4\ km\,s^{-1}Mpc^{-1}$ by SH0ES as mentioned in [241].

In order to constrain the model parameters with the above datasets we perform a Bayesian MCMC method. In our calculation, we have minimized the chi-square for two combinations of data set, which we believe are helpful for better fit values. The first one is labeled $DS1$ and contains chi-square function as $\chi^2_{DS1}=\chi^2_{Pan}+\chi^2_{CC}+H_0$ and the second one, $DS2$ as $\chi^2_{DS2}=\chi^2_{Pan}+\chi^2_{CC}$ where the minimised χ^2 for each dataset is mentioned in section 1.14.

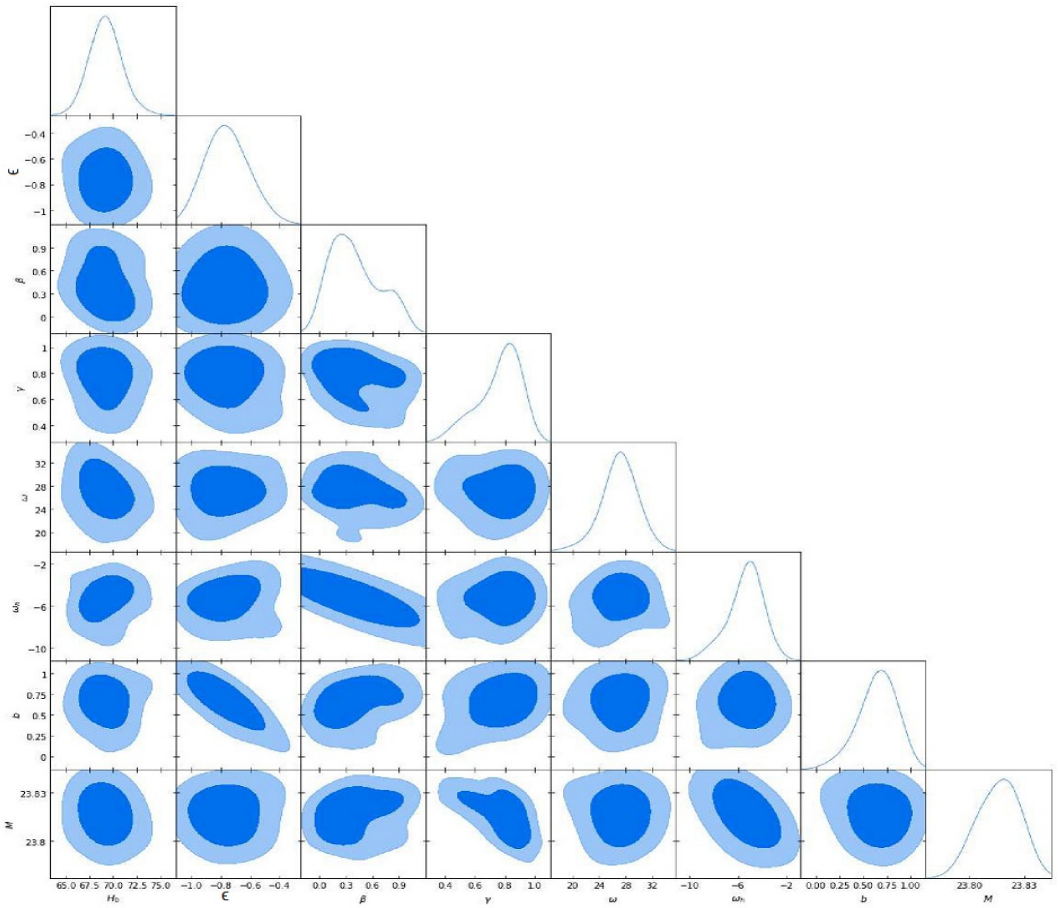

Figure 5.1: The contour map of HDE2 model using DS1 data set with marginalized probability for the parameters

5.5 Results and discussion

In this section we present and discuss our results obtained in Bayesian analysis. Table 5.1 presents the mean fitting values obtained for HDE1, HDE2 and ΛCDM models using two data sets, DS1 and DS2. The reported uncertainties correspond to 1σ confidence level (CL). In our study, keeping due consideration of $(5.3.21)$, we choose $-1 < \varepsilon < 1$, $0 < \beta < 1$, $0 < \gamma < 1$, $\omega > 0$, $-20 < \omega_h < 0$ and $0 < b < 1$. The contour maps of space parameters of HDE2 model for DS1 and DS2 data sets with $1\sigma(68.3\%)$ and $2\sigma(95.4\%)$ confidence level are shown in Figs. 5.1 and 5.2.

Using best-fit values, we find the matter density Ω_m and dark energy density Ω_l parameters for the HDE2 and ΛCDM models with DS1 and DS2 data sets which are listed in Table 5.1. The data set DS1 for HDE2 model yields the present density parameters $\Omega_m = 0.279^{+0.032}_{-0.077}$ and $\Omega_l = 0.720^{0.077}_{-0.032}$ where as these are $\Omega_m = 0.255^{+0.1487}_{-0.1245}$ and $\Omega_l = 0.745^{0.124}_{-0.148}$ with DS2 data set. It is observed that Ω_m is less and Ω_l is more than ΛCDM model for these two data sets.

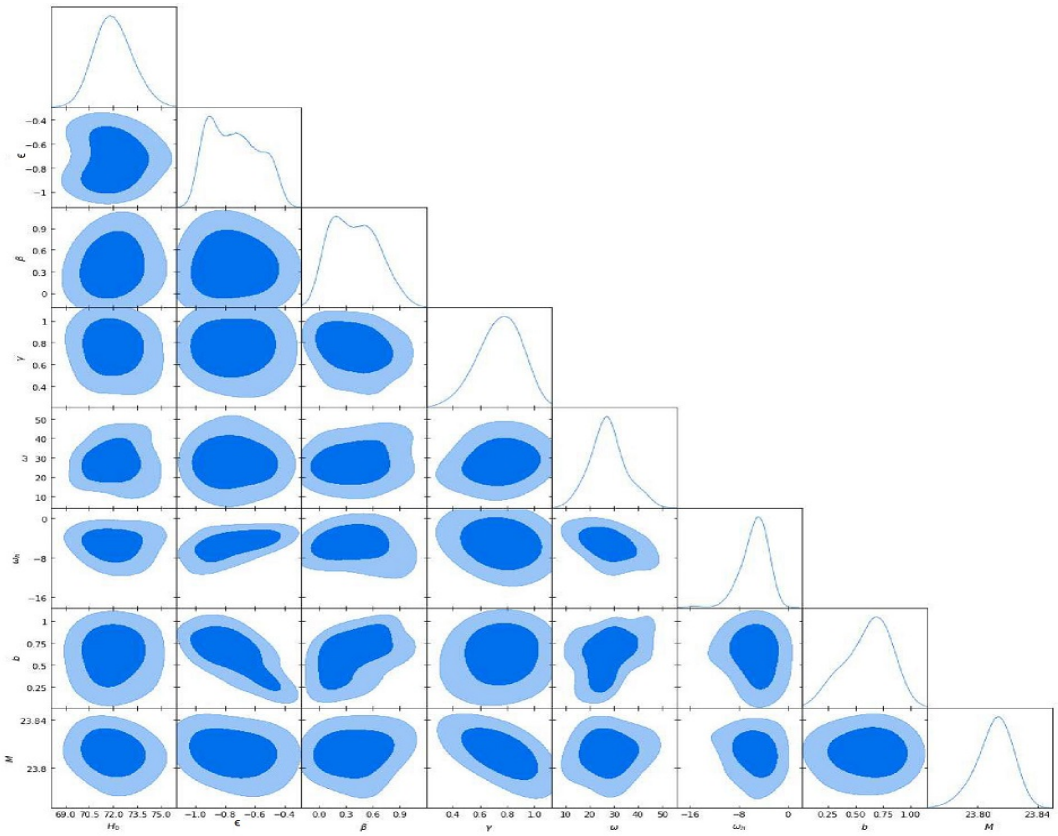

Figure 5.2: The contour map of HDE2 model using DS2 data set with marginalized probability for the parameters

In comparison with ΛCDM, we see that HDE1 and HDE2 models push the value of H_0 towards a smaller direction for DS1 and DS2. The H_0 tension between HDE models and local measurement value $73.5 \pm 1.4\ km\ s^{-1}Mpc^{-1}$ are mentioned in Table 5.1. We also notice the similar tension between ΛCDM model and local measurement value of the Hubble constant. Also, the value of the Hubble constant obtained from DS2 is close to the local value $H_0 = 69.8 \pm 0.8\ km\ s^{-1}Mpc^{-1}$ based on a calibration of the Tip of Red Giant Branch (TRGB) [303].

In what follows, we reconstruct the cosmological parameters, such as scale factor, deceleration parameter, effective equation of state parameter for both HDE models using best fit value obtained from two data sets, DS1 and DS2.

We calculate the corresponding deceleration- acceleration transition scale factor (redshift), the present value of deceleration parameter q_0 and effective EoS parameter $w_{eff}(z = 0)$, and the present age of the universe t_0 for HDE1 and HDE2 models using DS1 and DS2 data sets which are listed in Table 5.2.

The evolutions of the scale factor of HDE1 and HDE2 models with the cosmic time are shown in Fig. 5.3. It is observed that the scale factor of HDE 1 model, for data sets DS1 and DS2, evolve from finite past big-bang singularity and expand with accel-

Table 5.1: The best fit values for the considered models (HDE 1, HDE 2 and ΛCDM) using two datasets DS1, i.e., $SNe(Pan)+CC+H_0$ and DS2, i.e., $SNe(Pan)+CC$.

	DS1			DS2		
Parameter	HDE1	HDE2	ΛCDM	HDE1	HDE2	ΛCDM
H_0	$71.903^{+1.360}_{-1.114}$	$71.926^{+1.222}_{-1.057}$	$72.525^{+1.274}_{-1.305}$	$68.964^{+2.645}_{-1.888}$	$68.957^{+1.540}_{-1.511}$	$69.030^{+2.196}_{-2.591}$
ε	$0.032^{+0.397}_{-0.277}$	$-0.746^{+0.226}_{-0.189}$	–	$0.041^{+0.363}_{-0.316}$	$-0.763^{+0.137}_{-0.168}$	–
β	–	$0.380^{+0.266}_{-0.288}$	–	–	$0.347^{+0.460}_{-0.257}$	–
γ	–	$0.758^{+0.163}_{-0.167}$	–	–	$0.805^{+0.105}_{-0.207}$	–
ω	$12.967^{+12.398}_{-8.459}$	$27.495^{+7.058}_{-6.700}$	–	$13.212^{+6.218}_{-6.409}$	$27.136^{+2.537}_{-2.359}$	–
w_h	$-4.501^{+1.906}_{-2.547}$	$-5.153^{+1.804}_{-2.330}$	–	$-4.124^{+2.131}_{-3.346}$	$-5.101^{+1.057}_{-1.601}$	–
b	$0.345^{+0.153}_{-0.124}$	$0.648^{+0.171}_{-0.303}$	–	$0.333^{+0.183}_{-0.104}$	$0.667^{+0.204}_{-0.221}$	–
Ω_m	–	$0.279^{+0.032}_{-0.077}$	$0.284^{+0.021}_{-0.023}$	–	$0.255^{+0.1487}_{-0.1245}$	$0.300^{+0.032}_{-0.022}$
Ω_l	–	$0.720^{0.077}_{-0.032}$	$0.676^{+0.023}_{-0.018}$	–	$0.745^{0.124}_{-0.148}$	$0.697^{+0.041}_{-0.034}$

Table 5.2: Summary of the computed values of a_{tr}, z_{tr}, q_0, $w_{eff}(z=0)$ and t_0 coming from best fit results of HDE model with and without matter creation obtained from DS1 and DS2 data sets

	DS1		DS2	
Model	HDE1	HDE2	HDE1	HDE2
a_{tr}	–	$0.557^{+0.201}_{-0.310}$	–	$0.549^{+0.047}_{-0.161}$
z_{tr}	–	$0.794^{+0.476}_{-1.09}$	–	$0.821^{+0.172}_{-2.402}$
q_0	$-0.264^{+0.456}_{-0.504}$	$-0.478^{+0.046}_{-0.103}$	$-0.140^{+0.066}_{-0.415}$	$-0.509^{+0.023}_{-0.185}$
$w_{eff}(z=0)$	$-0.509^{+0.304}_{-0.336}$	$-0.402^{+0.033}_{-0.023}$	$-0.427^{+0.44}_{-0.277}$	$-0.461^{+0.063}_{-0.029}$
t_0	$15.782^{+0.745}_{-0.406}Gyr$	$13.67^{+0.558}_{-0.406}Gyr$	$14.6018^{+0.676}_{-0.506}Gyr$	$13.75^{+0.721}_{-0.036}Gyr$

erated rate through out the evolution. Therefore, HDE1 model does not show phase transition. However, in case of HDE 2 model for DS1 and DS2, the scale factors start to evolve from finite past with decelerated rate and take the transition to accelerated phase at $a_{tr}=0.557^{+0.201}_{-0.310}$ ($z_{tr}=0.794^{+0.476}_{-1.099}$) and $a_{tr}=0.549^{+0.047}_{-0.161}$ ($z_{tr}=0.821^{+0.172}_{-2.402}$) respectively.

In Fig. 5.4, we plot the trajectory of deceleration parameter with redshift for HDE1 and HDE2 models with their respective best-fit values obtained from DS1 and DS2. The HDE 1 has negative constant value of $q=-0.264^{+0.456}_{-0.504}$ and $q=-0.140^{+0.066}_{-0.415}$ through out the evolution for both DS1 and DS2, respectively. Hence, this model expands with accelerated rate through out the evolution. In HDE2 model, q shows a transition from decelerated phase (positive value of q) to accelerated phase (negative value of q) at transition redshifts $z_{tr}=0.794^{+0.476}_{-1.099}$ and $z_{tr}=0.821^{+0.172}_{-2.402}$, for DS1 and DS2, respectively. The corresponding current values of q are $q_0=-0.478^{+0.046}_{-0.103}$ and $q_0=-0.509^{+0.023}_{-0.185}$, respectively. It is to be noted that the latest observations indicate that $q_0\simeq-0.63\pm0.12$ [304, 305]. It is observed that $q\to-1$ in late time evolution of

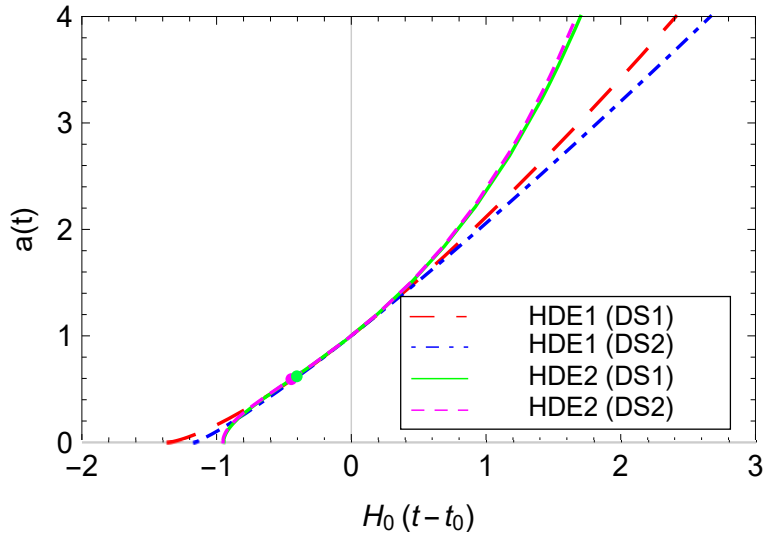

Figure 5.3: The evolution of the scale factor for the best-fit value of the free parameters of HDE models using DS1 and DS2 data sets. A dot denotes the transition point where the transition from decelerated phase to accelerated phase occurs.

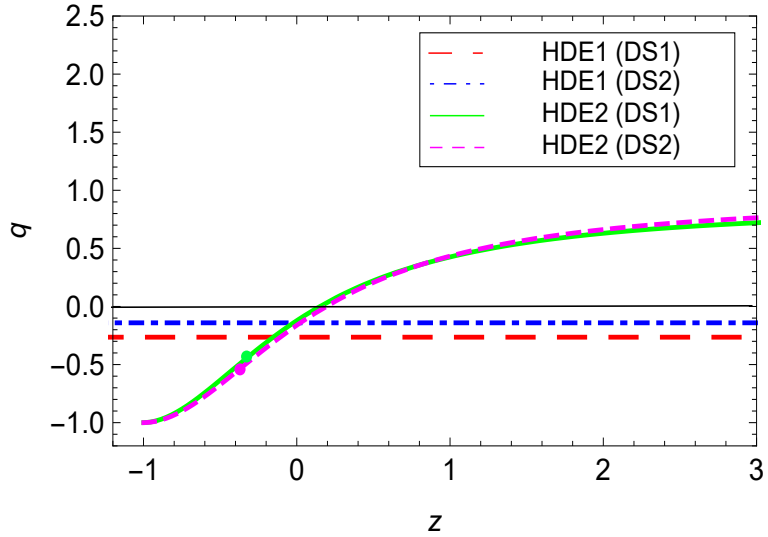

Figure 5.4: The deceleration parameter versus redshift for best fit values of HDE model for DS1 and DS2 data sets. A dot denotes the current value of q (hence, q_0)

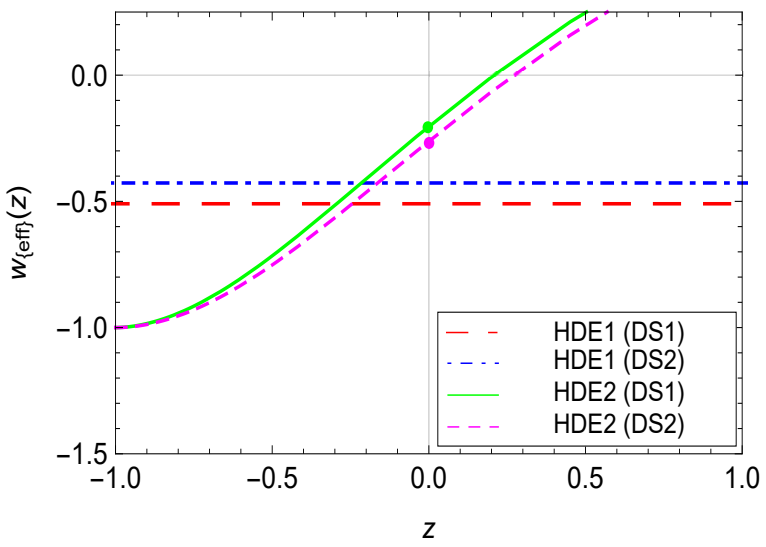

Figure 5.5: The effective EoS parameter as a function of redshift for best fit values of HDE1 and HDE2 models using DS1 and DS2 data sets. A dot denotes the present value of w_{eff}.

the universe with both the data sets.

The evolution of effective EoS parameter w_{eff} with redshift z is plotted in Fig.5.5 for different models with their respective best fit values. The present values of ω_{eff} for HDE 1 and HDE 2 models are listed in Table 5.2. In HDE 1 model, w_{eff} is negative constant values, $w_{eff} = -0.509^{+0.304}_{-0.336}$ and $w_{eff} = -0.427^{+0.44}_{-0.277}$ for DS1 and DS2, respectively, which are less than $w_{eff} = -(1/3)$ showing the accelerated phase. The respective present values of w_{eff} for HDE2 at $z = 0$ are $w_{eff}(z = 0) = -0.402^{+0.033}_{-0.023}$ and $w_{eff}(z = 0) = -0.461^{+0.063}_{-0.029}$. These values are relatively higher than the values predicted by the joint analysis of $WMAP + BAO + H_0 + SNe$ data which is approx $-0.93^{+0.13}_{-0.13}$ [14]. The data obtained in [14] is consistent with a flat universe dominated by a cosmological constant. In late time, w_{eff} of these two models approaches to -1 leading to Einstein-de-Sitter behavior. It has been observed that these models do not cross the phantom-divide line $w_{eff} = -1$.

Figure 5.6 plots the evolution of Hubble function versus redshift with the error bar of Hubble dataset in the range $z \in (0,4)$ and compare HDE 1 and HDE 2 models with the ΛCDM model. It can be observed that for both the combination of data sets, HDE 1 do not fit with the error bar of Hubble data set at higher redshift. However, HDE 2 gives the best fit with ΛCDM model through out the evolution for both DS1 and DS2. The trajectories of these models pass through most of the data set of error bar of Hubble parameter.

In HDE 1, the current age of the universe are found to be $15.78^{+0.745}_{-0.406}$ Gyr and $14.60^{+0.676}_{-0.506}$ Gyr with DS1 and DS2, respectively, which are higher than the age predict-

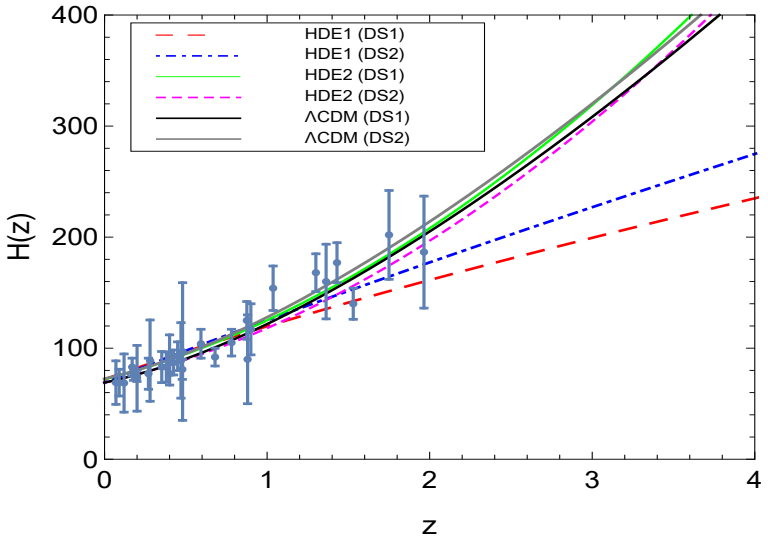

Figure 5.6: The Hubble function as a function of the redshift z for the best fit values of HDE1 and HDE2 models. The observational 31 $H(z)$ data points are shown with error bars (grey colour). The variation of the Hubble function in the standard ΛCDM model is also represented as the Grey and black solid curves for DS1 and DS2 respectively.

ed by ΛCDM model($13.978^{+0.234}_{-0.140}$ Gyr for DS1 and $13.889^{+0.24}_{-0.103}$ Gyr for DS2) . However, in HDE 2, the current age of universe is calculated as $13.67^{+0.558}_{-0.406}$ Gyr and $13.75^{+0.721}_{-0.036}$ Gyr, for DS1 and DS2 respectively, which are agreeing with the age deduced from ΛCDM model.

The reduced χ^2, denoted by χ^2_{red}, is defined as $\chi^2_{red} = \chi^2_{min}/(N-d)$, where N and d are respectively the total number of data points used in the model and the number of free parameters of model, and their values are $N = 1080$ for DS1 (or 1079 for DS2) and $d = 3$ for ΛCDM, $d = 5$ for HDE1, $d = 7$ for HDE 2 models. The values of χ^2 and χ^2_{red} of ΛCDM and HDE models are given in Table 5.3. The HDE 1 and HDE 2 models have the values $\chi^2_{red} < 1$ for both the data sets DS1 and DS2. Thus, HDE 1 and HDE 2 are in good agreement with the observational data.

We shall now use Akaike information criterion (AIC) and Bayesian information cri-

Table 5.3: Summary of χ^2, χ^2_{red}, *AIC* and *BIC* values and their differences from the reference model of Λ*CDM* obtained from DS1 and DS2 data sets

	DS1			DS2		
Model	HDE1	HDE2	Λ*CDM*	HDE1	HDE2	Λ*CDM*
χ^2	50.45	30.19	27.67	64.88	28.31	27.43
χ^2_{red}	0.046	0.028	0.025	0.060	0.026	0.025
AIC	60.45	44.19	33.67	74.88	42.31	33.43
BIC	85.35	79.07	48.61	99.78	77.19	48.37
Δ*AIC*	26.78	10.52	0	41.45	8.88	0
Δ*BIC*	36.74	30.46	0	51.41	28.82	0

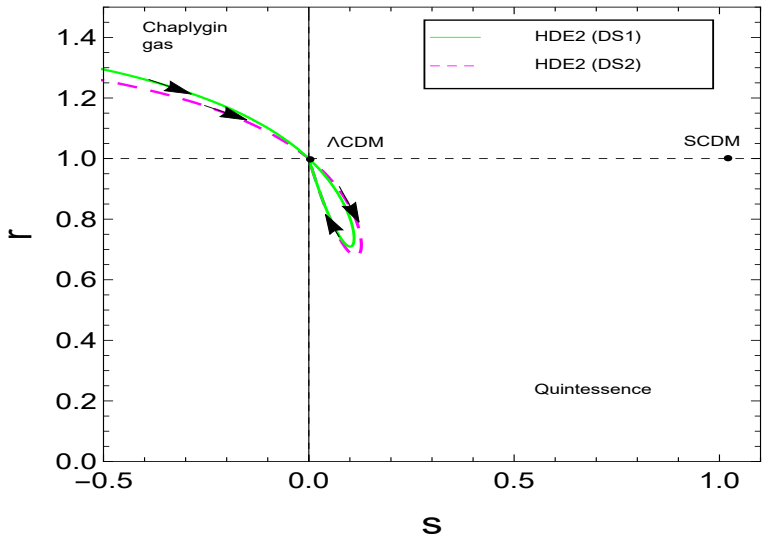

Figure 5.7: The trajectory of $\{r,s\}$ in $s-r$ plane corresponds to best fitted parameters of HDE 2 model for DS1 and DS2. The arrow shows the direction of the evolution of the trajectory

terion (BIC) as model selection criteria.We present the calculation results of AIC and BIC, and relative value between different models, ΔAIC and ΔBIC in Table 5.3. Since ΛCDM model is an important reference model for the study of DE models, we also include its results in Table 5.3.

It is observed from Table 5.3 that HDE 1 model is not supported over ΛCDM taking into account DS1 and DS2 data. However, HDE 2 is much better, though they are still less accurate than the ΛCDM model. Also, it has been found that the concordance ΛCDM model remains the best one to explain current data. Therefore, the HDE models are punished due to the large number of parameters, thus is not favoured by the Information criterion from a model selection point of view. On the other hand, the HDE models give good fit to the data from reduced chi-square point of view because it does not contain the information of the complexity as Information criterion have.

5.6 Diagnostic parameters

In this section, we discuss the geometric view of HDE model with matter creation through statefinder and *Om* parameters.

5.6.1 Statefinder parameter

The expressions for r and s can be obtained by using (5.3.8) and (5.3.13) into (1.12.1). It is observed that as $a \to \infty$, $\{r,s\} \to \{1,0\}$ which coincide with the ΛCDM model.

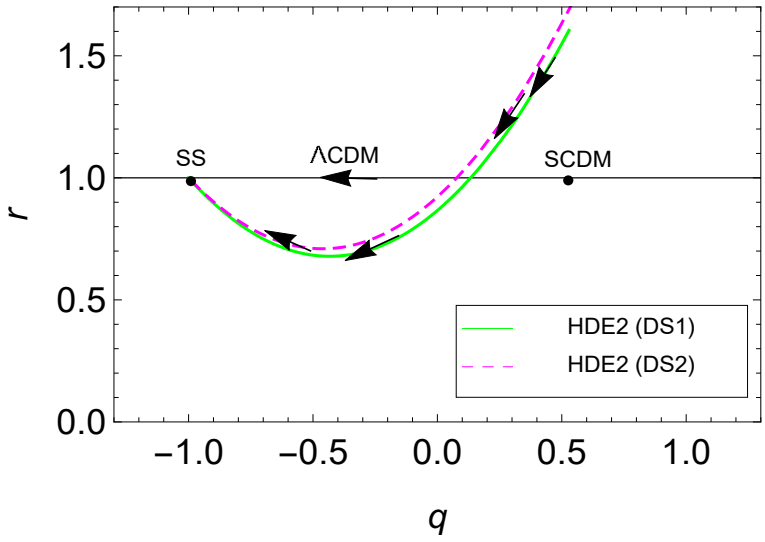

Figure 5.8: The trajectory of $\{r,q\}$ in $q-r$ plane for the best fitted parameters of HDE 2 model for DS1 and DS2. The arrow shows the direction of the evolution of the trajectory

The $s-r$ plane trajectory of the HDE 2 models for their best fit values of parameters obtained by observational data sets are shown in Fig. 5.7. The direction of evolution of trajectory is shown by the arrows. The trajectories of both the models start from the Chaplygin gas region $(r>1, s<0)$ at early time and in intermediate time pass through quintessence region $(r<1, s>0)$ and then ultimately reach to ΛCDM in late time. The present position of the universe corresponds to $\{r_0,s_0\}=\{0.680,0.108\}$ and $\{r_0,s_0\}=\{0.711,0.095\}$ for HDE 2 model for DS1 and DS2, respectively, which are different from the ΛCDM model. Thus, our HDE model with matter creation is well discriminated from the ΛCDM model.

We have also plotted the $\{r,q\}$ trajectory of HDE 2 model for DS1 and DS2 as shown in Fig. 5.8. The trajectories show that both the models approach to SS model as the standard model like ΛCDM in late time [200].

5.6.2 *Om(z)* parameter

Another diagnostic approach to distinguish different dark energy models is by evaluating the *Om*. Using (5.3.8) into (1.12.2), we can write the expression of *Om(z)* for HDE 2 as

$$Om(z)=\frac{\left[-1+\left(\frac{3\gamma(6+6\varepsilon-\omega\varepsilon^2-6b^2)}{2(6+6\varepsilon-\omega\varepsilon^2)k_1}+(1-\frac{3\gamma(6+6\varepsilon-\omega\varepsilon^2-6b^2)}{2(6+6\varepsilon-\omega\varepsilon^2)k_1})(1+z)^{k_1}\right)^2\right]}{(1+z)^3-1}, \qquad (5.6.1)$$

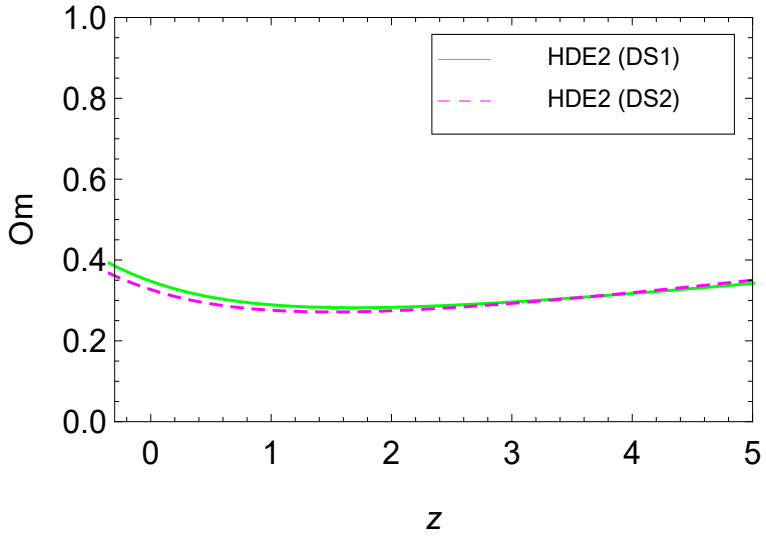

Figure 5.9: The trajectory of *Om(z)* for the best fit value of parameters of HDE 2 model for DS1 and DS2

Figure 5.9 shows the evolution of *Om(z)* with respect to the redshift z for HDE 2 model for DS1 and DS2, corresponding to different best-fit values of model parameters. The negative slope of each trajectory shows that the model behaves like quintessence.

5.7 Thermodynamics analysis

This section provides the thermodynamics analysis of the models presented in the previous sections. The validity of a cosmological model is tested from its thermodynamical behavior. Many authors [302, 306–312] have studied the relation between gravity and thermodynamics. In Ref. [289], it has been demonstrated that cosmological apparent horizons are also endowed with thermodynamic properties. It can relate temperature and entropy to the apparent horizon like to the black hole event horizon.

Macroscopic systems tend towards a thermodynamical equilibrium where, according to the generalized second law (GSL) of thermodynamic, the total entropy $S = S_{hor} + S_m + S_h$ of an isolated system never decreases, i.e., $\dot{S}_{hor} + \dot{S}_m + \dot{S}_h \geq 0$. Here, S_{hor} is the entropy of the apparent horizon, S_m and S_h are the entropy of dark matter and HDE, respectively enclosed by the horizon. The entropy of apparent horizon is defined as $S_{hor} = \kappa_B A/4l_{Pl}^2$ [313], where κ_B is the Boltzmann's constant, $A = 4\pi r_{hor}^2$ is the horizon area in which $r_{hor} = H^{-1}$ is the horizon radius for flat FLRW universe and $l_{Pl} = 1/\sqrt{8\pi}M_{Pl}$ is the Planck's length.

Using (5.3.8), we obtain

$$\dot{S_{hor}} = -\frac{2\pi\kappa_B}{l_{pl}^2}\frac{\dot{H}}{H^3} = \frac{2\pi\kappa_B H_0}{l_{pl}^2 H^2}\frac{a^{-k_1}}{2(6+6\varepsilon-\omega\varepsilon^2)}\times$$
$$[(3(1-\beta-\gamma)+\varepsilon)(6+6\varepsilon-\omega\varepsilon^2)+18b^2(w_h+\beta+\gamma)]. \tag{5.7.1}$$

Now, we need to study the entropy of fluids S_f (dark matter and HDE), which arises from Gibb's equation [314] for the fluid

$$TdS_f = d(\rho V)+pdV = Vd\rho+\rho dV+pdV, \tag{5.7.2}$$

where $V = 4\pi r_h^3/3$ is the spatial volume enclosed by the horizon and T is the fluid temperature.

The "gravity- thermodynamics" conjecture says that the temperature and the entropy of horizon can be interpreted by the corresponding quantities of black-hole thermodynamics, but with the apparent horizon in place of the black-hole one. According to this conjecture, the universe background geometry becomes FLRW once the equilibrium establishes. At this position, all the fluids in the universe acquire the same temperature T [93], which is moreover equal to the temperature of the horizon T_{hor} [315], otherwise the energy flow would deform the geometry of flat FLRW [290]. However, this happens when the universe fluids and the horizon will have interacted for a long time in late time. In general, two systems must interact for some length of time before they can attain thermal equilibrium. The assumption of equilibrium is widely accepted in the GSL literature [290, 316, 317]. We can see that this choice is also backed by the holographic principle [58–60]. Therefore, we follow this assumption keeping in mind that the results hold at late times of the evolution of the universe. Thus, under the thermal equilibrium condition between the fluids and horizon, we have $T = T_{hor}$, where $T_{hor} = 1/2\pi r_{hor} = H/2\pi$, which is equal to the Hawking temperature of the horizon. Using (5.3.8), the above equation for HDE gives

$$\dot{S_h} = \frac{24\pi^2\rho_h(1+w_h)H_0}{H^4}\Big[\frac{a^{-k_1}}{2(6+6\varepsilon-\omega\varepsilon^2)}\Big\{(3(1-\beta-\gamma)+\varepsilon)(6+6\varepsilon-\omega\varepsilon^2)$$
$$+18b^2(w_h+\beta+\gamma)\Big\}-\frac{H}{H_0}\Big] \tag{5.7.3}$$

From (5.7.2), the change of entropy for pressureless dark matter is given by

$$\dot{S_m} = \frac{24\pi^2\rho_m H_0}{3H^4}\Big[3\gamma + \frac{a^{-k_1}}{2(6+6\varepsilon-\omega\varepsilon^2)}\Big\{(3(1-\beta-\gamma)+\varepsilon)(6+6\varepsilon-\omega\varepsilon^2) + 18b^2(w_h+\beta+\gamma)\Big\} - (1-\beta)\frac{H}{H_0}\Big] \tag{5.7.4}$$

From (5.7.1), (5.7.3) and (5.7.4), it is observed that $\dot{S_{hor}}$, $\dot{S_h}$ and $\dot{S_h}$ would be positive for $0 < (\beta+\gamma) < 1$ and $(6+6\varepsilon-\omega\varepsilon^2) > 0$ in an expanding universe. Thus, the total change in entropy is always positive with this best fit value. This indicates that the GSL of thermodynamics is satisfied for HDE model with Hubble horizon as IR cut-off in the presence of matter creation in BD theory.

5.8 Conclusion

In this chapter, we have carried out a study on matter creation dominated HDE model with Hubble horizon as an IR cut-off in BD theory. We have studied two different HDE models with $\Gamma = 0$ and $\Gamma = 3\gamma H_0 + 3\beta H$, respectively. We have presented the exact solution for these HDE models using a power-law relation between the BD scalar field and the scale factor. It can be observed that the HDE model gives the constant deceleration parameter in the absence of matter creation ($\Gamma = 0$). However, the HDE model, with suitable choice of Γ gives the time-dependent deceleration parameter, which describes the phase transition from decelerated phase to accelerated phase.

We have constrained the model parameters by using two latest data sets DS1: $SNe(Pantheon) + CC + H_0$ and DS2: $SNe(Pantheon) + CC$. The best fit values of parameters for both HDE models have been given in Table 5.1. We have presented a comparative study of these models by studying the evolution of cosmological parameters through plotting the graphs using the best fit parameters. We summarise the main results as follows.

It has been found that the HDE 1 ($\Gamma = 0$) model with Hubble horizon as an IR cut-off is not able to describe the transition of the universe. In this model, the scale factor varies as power-law form, and q and w_{eff} are constant. These show that the model may decelerate or accelerate through out the evolution depending upon the conditions applied. Using best fit values obtained from DS1 and DS2 in the analytical solutions, we have obtained $q = -0.264^{+0.456}_{-0.504}$ and $q = -0.140^{+0.066}_{-0.415}$, respectively where as the respective effective EoS are $w_{eff} = -0.509^{+0.304}_{-0.336}$ and $w_{eff} = -0.427^{+0.44}_{-0.277}$. These

observations show that this model expands with accelerated rate for both the combination of data sets. The evolution of the Hubble functions of this model is far from evolution of ΛCDM model and Hubble data points. The age of the universe are found to be $15.78^{+0.745}_{-0.406}$ Gyr and $14.601^{+0.676}_{-0.506}$ Gyr, respectively which are very high from the predicted value. The respective reduced χ^2 are 0.046 and 0.06 which are less than $\chi^2_{red} = 0.025$ and $\chi^2_{red} = 0.025$ of ΛCDM model, respectively. We have also studied the model selection criterion for this model and have found the values ΔAIC=26.78 and ΔBIC=36.74 from DS1, and ΔAIC=41.45 and ΔBIC=51.41 from DS2. Thus, we do not have support for the HDE1 model over ΛCDM. The statefinder parameters $\{r,s\}$ of this model for both data sets are found to be constant,i.e., $\{r,s\} = \{-0.101, 0.572\}$ and $\{r,s\} = \{-0.124, 0.490\}$, respectively, which show the quintessence behavior.

To consider the phase transition we have introduced matter creation in HDE model with the same IR cut-off in BD theory. We have assumed the functional form of matter creation rate as $\Gamma = 3\gamma H_0 + 3\beta H$. The best fit values of HDE 2 model obtained from data sets DS1 and DS2 have been given in Table 5.1. Using best fit values, we have plotted the trajectory of various cosmological parameters and have discussed the evolution accordingly. We have observed that the both the models describe a universe having Big-bang at finite past, then entering an early stage of decelerated expansion followed by acceleration in the later stage of the evolution as shown in Fig. 5.3. The transitions from the decelerated to accelerated expansion in HDE 2 model occur at $a_{tr} = 0.557^{+0.201}_{-0.310}$ (or $z_{tr} = 0.794^{+0.476}_{-1.099}$) and $a_{tr} = 0.549^{+0.047}_{-0.161}$ (or $z_{tr} = 0.821^{+0.172}_{-2.402}$), respectively which are higher than the ΛCDM value ($z_{tr} = 0.66$). We have found a time-dependent deceleration parameter, which shows that q transits from positive to negative values corresponds to the transition from deceleration to acceleration in the expansion of the universe (Fig. 5.4). From the observational results, the present values of q for HDE 2 using DS1 and DS2 are $q_0 = -0.478^{+0.046}_{-0.103}$ and $q_0 = -0.509^{+0.023}_{-0.185}$, respectively, which are higher than the current observational value $q_0 = -0.64 \pm 0.03$ [148].

The evolutions of effective EoS parameter of both the data sets of HDE2 model are shown in Fig. 5.5. It has been observed that as $z \to -1$ ($a \to \infty$), $w_{eff} \to -1$ in future, which corresponds to the de Sitter universe. Since it does not cross the phantom divide line, both the model is free from Big-rip singularity. Using the best fit values obtained from DS1 and DS2, the present values of effective EoS for HDE2 model are found to be $w_{eff}(z=0) = -0.402^{+0.033}_{-0.023}$ and $w_{eff}(z=0) = -0.461^{+0.063}_{-0.029}$, respectively, which are higher than the current value $-0.93^{+0.13}_{-0.13}$ [14]. The evolutions of Hubble

functions is shown in Fig. 5.6. The ages of universe for this model with data sets DS1 and DS2 have been found as $t_0 \sim 13.67$ Gyr and $t_0 \sim 13.75$ Gyr, respectively which are in very good agreement with the age predicted by ΛCDM model ~ 13.97 Gyr and ~ 13.88 Gyr, respectively.

We have calculated the χ^2_{red} of ΛCDM and HDE models using the best fit values (See, Table 5.3). It has been found that the χ^2_{red} of these two models are very close to ΛCDM model. We have also studied the AIC and BIC to test the stability of the models. It has been found that the concordance ΛCDM model remains the best one to explain current data. The HDE model with matter creation are punished by AIC and BIC mainly because of large number of parameters and thus is not favoured by the current joint data set from a model selection point of view. It is to be noted that AIC and BIC strongly penalize the models when they have large number of free parameters. However, the HDE models with matter creation give good fit to the data from reduced chi-square point of view as it does not contain the information of the complexity.

We have studied the geometrical diagnostic, like statefinder parameters and *Om* to compare the HDE 2 model with other existing DE models, like ΛCDM model. We have found that as $a \to \infty$ ($z \to -1$), $\{r,s\}$ and $\{r,q\}$ tend to $\{1,0\}$ and $\{1,-1\}$, respectively, which are in good agreement with ΛCDM model. Using best fit values from DS1 and DS2, the current values of $\{r,s\}$ for this model are $\{r_0,s_0\} = \{0.680,0.108\}$ and $\{r_0,s_0\} = \{0.711,0.095\}$, respectively, which show deviation from the ΛCDM model, and thus, the models are well discriminated from ΛCDM model. The evolution of *Om* shows that the model behaves like quintessence. Using AIC and BIC with data obtained from both the combination of data sets, we compare the HDE model with ΛCDM model. It has been found that the model has less evidence in favour.

In the last section we have studied the thermodynamics of generalized second law in the present HDE2 model. It has been found that the generalized second law of thermodynamics is valid with apparent horizon as the boundary.

We therefore conclude that the present HDE model with suitable form of matter creation is capable of producing acceleration of the universe in BD theory with Hubble horizon as an IR cut-off.

****

Chapter 6

Evolution of holographic dark energy model with matter creation

---

In this chapter [1], we study the holographic dark energy (HDE) with adiabatic matter creation process to explain the present-day accelerated expansion of the universe. The HDE model with Hubble horizon as an IR cut-off with matter creation is solved with a more generalized form of particle creation rate. The statistical analysis of model has been done using the three different combinations of latest datasets. Various cosmological and geometric parameters have been plotted for the best fit values of model parameters to check the viability of our model. The HDE model, with IR cut-off as Hubble horizon does not show the phase transition. While the induction of matter creation to the same model shows the recent transition from a decelerating to an accelerated phase. The outcomes show that the model with matter creation is compatible with the data sets used.

---

[1]This chapter is based on a published research paper "Evolution of holographic dark energy model with adiabatic matter creation, *Modern Physics Letters A* **37**, No. 24, 2250161 (2022)".

6.1 Introduction

The late-time era observed by various astronomical observations is known as 'dark energy'(DE) era which is so far a mystery in modern cosmology. In this regard, the most successful model is the standard ΛCDM model. However, this model suffers some theoretical problems like fine-tuning [16,318] and cosmic coincidence [20,319], and observational problems such as the unprecedented precision in the evaluation of basic cosmological parameters.

As discussed in chapter 5, one interesting way for describing the DE arises from holographic principle [58–60], which is based on the quantum gravity theory. But the holographic dark energy models suffer with the possibilities of IR cut-offs. We have discussed the results of HDE model with IR cut-off as Hubble Horizon in previous chapters. As the source of HDE is still a mystery, some more forms of IR cut-off such as Granda -Oliveros [80], Ricci scalar [97], etc., have been studied to explain the evolution of the universe.

It is worthwhile to note that in the context of relativistic cosmology, an accelerating regime of the universe can be obtained in the presence of negative pressure. Many authors have explained the late time acceleration of universe has been explained through the matter creation cosmology which provides us a viable alternative to the ΛCDM model. The dynamics of matter creation is generally described by the matter creation rate, Γ. In this chapter we consider the matter creation rate by taking a combination of H, H^2 and its derivatives. In a recent paper [186], the authors have proposed a class of $\Gamma(H_0, H, \dot{H})$ in general relativity which successfully describes the quintessence behavior of the universe.

The aim of this chapter is to extend the work carried out in Ref. [186] in a more dynamical framework, i.e., in HDE framework. As discussed earlier, the HDE models suffer with the proper choice of IR cut off. Hsu [62] tried to exhibit the current expansion of Universe by choosing the IR cut-off as Hubble horizon on HDE model but he could not do so. In this chapter, keeping the same Hubble horizon as an IR cut-off, we induce matter creation in holographic dark energy model, with the possibility that this model with proper choice of matter creation rate as proposed in Ref. [186], would be consistent with the current observations. We examine the evolution of the HDE model with matter creation by constraining the parameter space using the joined observational data of Type Ia supernovae(Pantheon), Hubble data, combine data of baryon

acoustic oscillations/ cosmic microwave background and local Hubble constant.

The content of the chapter is as follows: Section 6.2 presents HDE model with adiabatic matter creation and derives it's basic evolution equations. In Section 6.3, with the appropriate choice of matter creation rate, we solve the evolution equations to get the various cosmological parameters. In Section 6.4, we present the observational data to constraint the main parameters of HDE model by using joint likelihood statistical analysis. Section 6.5 presents the results and discussion on various cosmological parameters. In Section 6.6, geometric and cosmographic analyses of the HDE model are carried out to compare the model with ΛCDM model. In Section 6.7, we draw our conclusions.

6.2 HDE model with matter creation

Let us assume a homogeneous and isotropic flat Friedmann-Lemaître-Robertson-Walker (FLRW) universe described by the line element (1.3.8). We assume that the universe contains HDE and pressureless dark matter (excluding baryonic matter). The Einstein's Field Equations (EFEs) are given by

$$R_{\mu\nu} - \frac{1}{2}R\, g_{\mu\nu} = T_{\mu\nu}, \tag{6.2.1}$$

where $T_{\mu\nu}$ is the total energy-momentum tensor of the cosmic fluid. The other symbols have their usual meaning. We assume that the universe contains HDE and pressureless dark matter (excluding baryonic matter). In open thermodynamical systems where the irreversible matter creation/ decay occurs, we include the matter creation mechanism in the energy-momentum tensor phenomenologically and define it as [170, 171]

$$T_{\mu\nu} = (\rho + \bar{P})u_\mu u_\nu + \bar{P}\, g_{\mu\nu}, \tag{6.2.2}$$

where $\rho = \rho_m + \rho_h$ represents total energy density and $\bar{P}$ is the effective pressure which is the sum of pressures of HDE fluid and matter creation, i.e., $\bar{P} = p_h + p_c$. Here, ρ_m and ρ_h are the energy densities of dark matter and HDE respectively, while p_h and p_c are the corresponding pressures due to HDE and matter creation.

In the framework of FLRW metric (1.3.8), the basic field equations of (6.2.1) in case of matter-dominated epoch ($p_m = 0$), are as follows

$$3H^2 = \rho = \rho_m + \rho_h, \tag{6.2.3}$$

and

$$\dot{\rho_m} + \dot{\rho_h} + 3H(\rho_m + \rho_h + p_h + p_c) = 0, \tag{6.2.4}$$

where p_c is the particle creation pressure.

The particle flux vector N^μ defined as $N^\mu = nu^\mu$, which obeys the general balance equation $\nabla_\mu N^\mu = \Gamma$. Here Γ is the matter creation rate, u^μ is the particle four-velocity and $n = N/V$ is the particle number density. The quantity Γ has a special meaning. A positive Γ represents a particle source and a negative Γ indicates to a particle sink. Using FLRW metric and comoving observer, $u^\mu = \delta^\mu_i$, in which $u^\mu u_\mu = -1$, we transform the balance equation into

$$\dot{n} + 3nH = n\Gamma, \tag{6.2.5}$$

where the comoving volume is $V = a^3$. We know that the particles and entropy are created during the adiabatic matter creation process but the entropy per particle does not change. In this scenario, the second law of thermodynamics with equation(1.11.7), leads to the emergence of a negative pressure which is related to the creation rate as [181, 182, 186]

$$p_c = -\frac{\rho_m}{3H}\Gamma. \tag{6.2.6}$$

where Γ is the particle creation rate.

We suppose that the two fluids (HDE and dark matter) considered in this chapter do not interact to each other. It means that the energy conservation equation (6.2.4) conserves separately for these two fluids, which are given by

$$\dot{\rho_m} + 3H\left(1 - \frac{\Gamma}{3H}\right)\rho_m = 0, \tag{6.2.7}$$

$$\dot{\rho_h} + 3(\rho_h + p_h)H = 0. \tag{6.2.8}$$

As we know that the HDE model depends on the choices of IR cut-off L such as particle horizon, Hubble horizon, event horizon, Granda-Oliveros cut-off, Ricci scalar, etc. It is also noticeable that the HDE model with Hubble horizon does not explain the present scenario of the universe [62, 63]. To alleviate this problem, we propose the HDE model with matter creation with same Hubble horizon as an IR cut-off, i.e., assuming the infra-red cut-off as the inverse of Hubble scale ($L = H^{-1}$). In this case,

the HDE energy density is given by

$$\rho_h = 3b^2H^2. \tag{6.2.9}$$

Using the usual equation of state for HDE, $p_h = w_h\rho_h$, where w_h is the equation of state parameter (EoS) of HDE, and (6.2.9), a combined evolution equation from Eqs. (6.2.3), (6.2.7) and (6.2.8) for Hubble function is obtained as

$$\dot{H} + \frac{3}{2}\left[(1-b^2)\left(1-\frac{\Gamma}{3H}\right) + (1+w_h)b^2\right]H^2 = 0. \tag{6.2.10}$$

It is clear that by considering a particular functional form of Γ as a function of H, it may be developed the dynamics of the universe. The adiabatic creation models with $\Gamma \propto H$ are always decelerating or accelerating depending on the proportionality constant. Such type of model does not show a transition redshift from decelerating to an accelerating phase as needed by observations. In order to overcome such difficulty, some constant term was added [181]. In this work, we assume Γ as a linear combination of these three terms: first term being constant, second term is proportional to Hubble parameter (expansion ratio or velocity) and the third term takes the acceleration [186], that is,

$$\Gamma = 3\left(\gamma H_0 + \beta H + \alpha\frac{\ddot{a}}{\dot{a}}\right) = 3\left[\gamma H_0 + \beta H + \alpha\left(\frac{\dot{H}}{H} + H\right)\right] \tag{6.2.11}$$

where γ, β and α are dimensionless parameters which are defined in the interval $[0,1]$ and H_0 is the current value of Hubble parameter. The constant 3 has been considered for calculation purpose. The reason behind for assuming the above mentioned form of matter creation rate is that the rate of transfer of gravitationally induced matter creation is related to the velocity and acceleration of the expansion of the universe. Hence, keeping in mind this thermodynamical behaviour of matter creation and the dynamical behavior of HDE, we explore the HDE model with the above generalized matter creation rate (6.2.11) in describing the current observed expansion of universe. As we shall see that this scenario is compatible to show the transition redshift from decelerating to accelerating regime.

6.3 Cosmological solutions

In this section, we will solve equation(6.2.10) for the matter creation rate defined in Eq.(6.2.11). Using (6.2.11), the dynamical equation (6.2.10) becomes

$$H' + 3k\frac{H}{a} = \frac{3\gamma(1-b^2)H_0}{[2-3(1-b^2)\alpha]a} \tag{6.3.1}$$

where $k = \frac{3\left((1-\beta-\alpha)+(\beta+\alpha+w_h)b^2\right)}{2-3(1-b^2)\alpha}$ and a prime indicates the derivative with respect to lna. On solving (6.3.1), we get the Hubble parameter as

$$H = H_0\left[\frac{3\gamma(1-b^2)}{k[2-3\alpha(1-b^2)]} + \left(1 - \frac{3\gamma(1-b^2)}{k[2-3\alpha(1-b^2)]}\right)a^{-k}\right] \tag{6.3.2}$$

We can see that if $b = 0$, i.e., without HDE, the solution (6.3.2) reduces to the solution obtained in paper [186]. Further, by putting $\alpha = 0$, it reduces to the solution of [276] and by setting $\beta = 0$ and $\alpha = 0$, the solution reduces to [187]. Also, one can find the solution of matter-dominated epoch $H = H_0 a^{-3/2}$ by setting all the parameters equal to zero.

We can further solve (6.3.2) to get scale factor as

$$a(t) = \left[1 + \frac{(2-3(1-b^2)\alpha)k}{3\gamma(1-b^2)}\{e^{\frac{3\gamma(1-b^2)H_0}{2-3(1-b^2)\alpha}(t-t_0)} - 1\}\right]^{1/k}. \tag{6.3.3}$$

From the above equation, it can be observed that the scale factor varies as a power-law $a(t) \propto [1+kH_0(t-t_0)]^{1/k}$ in early time where as it varies as an exponential form $a(t) \propto e^{\frac{(1-b^2)\gamma}{k(2-3(1-b^2)\alpha)}H_0(t-t_0)}$ in late epoch, which describes the de Sitter universe. Thus, holographic dark energy model with matter creation describes the phase transition from decelerated epoch to accelerated epoch.

Now, using, $a = (1+z)^{-1}$, Eq. (6.3.2) in terms of redshift z can be rewritten as

$$H(z) = H_0\left[\frac{3\gamma(1-b^2)}{k(2-3\alpha(1-b^2))} + \left(1 - \frac{3\gamma(1-b^2)}{k(2-3\alpha(1-b^2))}\right)(1+z)^k\right] \tag{6.3.4}$$

Next, We know that a cosmological parameter is required to describe the phase transition from of universe. In this context, the first cosmological parameter is the deceleration parameter, which measures the cosmic acceleration of Universe, This parameter plays a vital role in describing the transition phase and it is straightforward

to calculate this parameter from (1.7.11) and (6.3.4) for our present model, which takes the form

$$q(z) = -1 + \frac{k - \frac{3\gamma(1-b^2)}{2-3(1-b^2)\alpha}}{1 + \frac{3\gamma(1-b^2)}{(2-3(1-b^2)\alpha)k}\{(1+z)^{-k} - 1\}}. \tag{6.3.5}$$

The transition redshift z_{tr}, which is defined at $q = 0$, is given by

$$z_{tr} = -1 + \left[\frac{3\gamma(1-b^2)}{3\gamma(1-b^2) + k(1 - 3\gamma - 3\beta + 3\gamma b^2 + 3\beta b^2 + 3w_h b^2)}\right]^{1/k} \tag{6.3.6}$$

It is noted that if $\gamma = 0$, there will be no phase transition. The present value of q at $z = 0$ is

$$q_0 = \frac{\left(1 - 3\gamma - 3\beta + 3\gamma b^2 + 3\beta b^2 + 3b^2 w_h\right)}{(2 - 3(1-b^2)\alpha)}. \tag{6.3.7}$$

The second cosmological parameter is the equation of state (EoS) parameter. It describes the evolution of universe filled with matter. The effective EoS w_{eff} for this model is given by

$$w_{eff} = -1 + \frac{2}{3}\left[\frac{k - \frac{3\gamma(1-b^2)}{2-3(1-b^2)\alpha}}{1 + \frac{3\gamma(1-b^2)}{(2-3(1-b^2)\alpha)k}\{(1+z)^{-k} - 1\}}\right]. \tag{6.3.8}$$

The present value of w_{eff} is calculated as

$$w_{eff}(z=0) = -1 + \frac{2}{3}\left(k - \frac{3\gamma(1-b^2)}{2-3(1-b^2)\alpha}\right). \tag{6.3.9}$$

In the next section, we constrain the model parameters coming from the background tests and discuss the evolution of the universe.

6.4 Observational Data

In this section, we estimate the model parameters of Eq.(6.3.2) through statistical analysis using the latest observational data obtained from Type Ia SNe (Pantheon data), Hubble parameter $H(z)$ (CC + galaxy distribution) observation, combined data of baryon acoustic oscillations/cosmic microwave background and latest local H_0 by SH0ES. The brief outlines of these datasets are given as

- **SNe(Pantheon data):** We use the latest compilation of SNe (Pantheon sample), consisting 1048 data points from SNLS, SDSS, Pan-STARRS1, HST survey in

the redshift range of $0.014 \leq z \leq 2.3$ [211].

- **Hz(CC + Galaxy distribution):** We use Hubble data $H(z)$ to study the cosmic expansion history which includes 36 measurements in which 31 measurements are determined from the cosmic chronometric technique (CC) [215], 3 correlated measurements from the radial BAO signal in the galaxy distribution [216], and 2 measurements determined from the BAO signal in Lyman forest distribution alone [217, 218].

- **BAO:** BAO are excellent geometrical probes. We include the sample of BAO distances measurements from from SDSS(R) [236], the 6dF Galaxy survey [237], BOSS CMASS [229] and three parallel measurements from WiggleZ survey [238].

- **Local Hubble constant:** We also take the recently measured local Hubble constant H_0 as $H_0 = 73.5 \pm 1.4\ km\ s^{-1} Mpc^{-1}$ by SH0ES as mentioned in [241].

6.4.1 Estimation of parameters

Now, using MCMC method in EMCEE library [209], we constrain our model parameters. In particular, we consider prior constraints $0 < \gamma < 1$, $0 < \beta < 1$ and $0 < \alpha < 1$. Since $supernovae$, $H(z)$, BAO and H_0 are effectively independent measurements, we can take the different joint analysis by simply adding together the χ^2 functions. Here, the most probable values of the model free parameters are estimated correspond to the minimal χ^2_{total} values of the three different combined datasets, namely DS1: $\chi^2_{DS1} = \chi^2_{pan} + \chi^2_{H(z)36} + \chi^2_{BAO} + \chi^2_{H_0}$, DS2: $\chi^2_{DS2} = \chi^2_{pan} + \chi^2_{H(z)36} + \chi^2_{H_0}$ and DS3: $\chi^2_{DS3} = \chi^2_{pan} + \chi^2_{H(z)36} + \chi^2_{BAO}$, where the minimised χ^2 for each dataset is mentioned in section 1.14. The best fit ranges of free parameters are presented in Table 6.1 and the $1\sigma(68.3\%)$ and $2\sigma(95.4\%)$ likelihood contours using DS1, DS2 and DS3 data sets are represented in Figs. 6.1-6.3 .

The chi-square, χ^2 from DS1, DS2 and DS3 are 52.93, 34.01 and 50.88, respectively. The reduced chi-squared χ^2_{red} statistics are very useful for model comparison and error estimation in cosmology. It is defined as $\chi^2_{red} = \chi^2_{min}/(N_{tot} - n_{fit})$, where N_{tot} represents total number of data points used and n_{fit} is the number of free parameters. The value $N_{tot} - n_{fit}$ is said to be degree of freedom (dof). If we fit our model to data

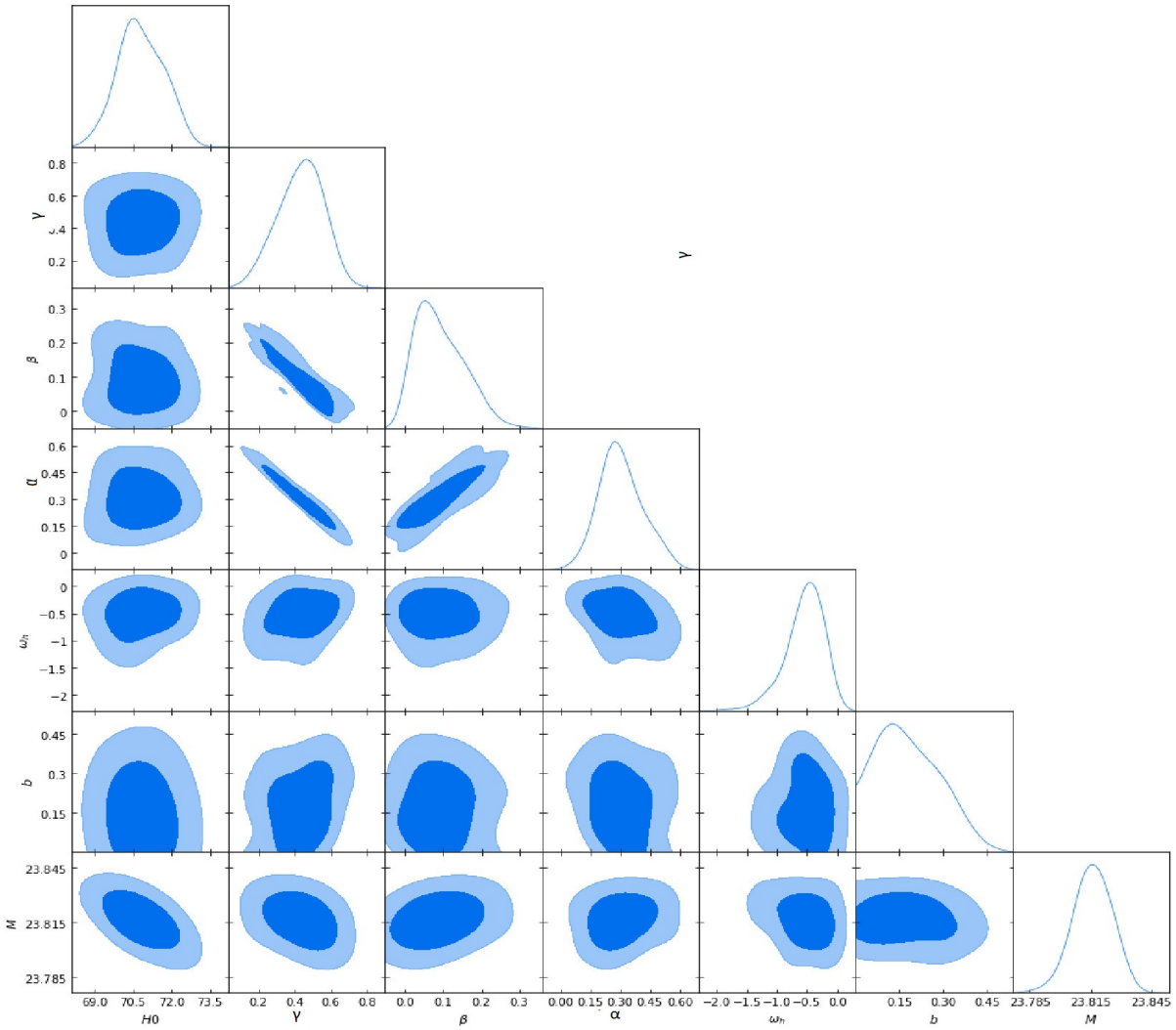

Figure 6.1: 68.3% and 95.4% confidence level contours and posterior distributions from MCMC analysis of data set $DS1 : pan, H(z), BAO$ and H_0.

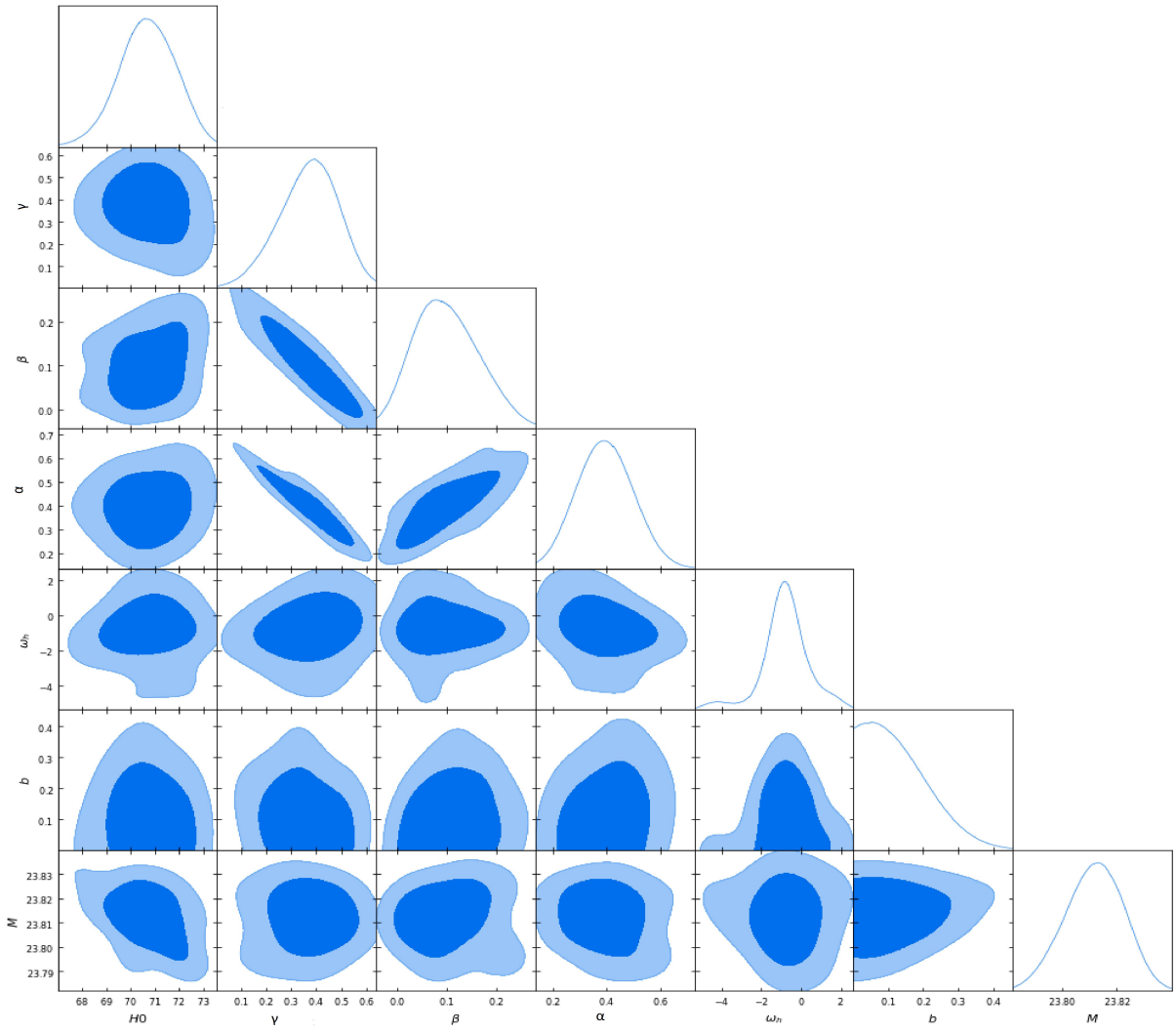

Figure 6.2: 68.3% and 95.4% confidence level contours and posterior distributions from M-CMC analysis of data set $DS2 : pan, H(z)$ and H_0.

Table 6.1: The best fit values of model parameters obtained through different combination of datasets.

Parameters	$DS1$	$DS2$	$DS3$
H_0	$71.001^{+0.882}_{-1.253}$	$71.017^{+1.070}_{-0.892}$	$68.713^{+1.424}_{-1.379}$
α	$0.418^{+0.077}_{-0.143}$	$0.408^{+0.105}_{-0.120}$	$0.412^{+0.085}_{-0.056}$
β	$0.068^{+0.089}_{-0.047}$	$0.076^{+0.096}_{-0.046}$	$0.075^{+0.085}_{-0.056}$
γ	$0.324^{+0.126}_{-0.066}$	$0.327^{+0.088}_{-0.136}$	$0.318^{+0.142}_{-0.078}$
w_h	$-0.543^{+0.222}_{-0.312}$	$-0.564^{+0.277}_{-0.200}$	$-0.586^{+0.256}_{-0.229}$
b	$0.127^{+0.107}_{-0.095}$	$0.121^{+0.161}_{-0.191}$	$0.129^{+0.118}_{-0.138}$

and obtained $\chi^2_{red} < 1$ and closer to 1, it is considered a best fit where as $\chi^2_{red} > 1$ is considered as a bad fit. In our observation, we have included 40 data of SNe Pantheon, 36 data of H(z), 6 data of BAO and 1 data of H_0. Therefore, we have $N_{tot} = 83$, $n_{fit} = 6$ for DS1, $N_{tot} = 77$, $n_{fit} = 6$ for DS2 and $N_{tot} = 82$, $n_{fit} = 6$ for DS3 data sets. In this way, we get χ^2_{red} as 0.687, 0.479 and 0.669 with data sets DS1, DS2 and DS3, respectively, which are less than unity. These show that our matter created induced HDE model is well fitted with each data set.

The present values H_0 of Hubble parameter from DS1, DS2 and DS3 data sets are extracted as $71.001^{+0.882}_{-1.253}$ $Km\,sec^{-1}\,Mpc^{-1}$, $71.017^{+1.070}_{-0.892}$ $Km\,sec^{-1}\,Mpc^{-1}$ and $68.713^{+1.424}_{-1.379}$ $Km\,sec^{-1}\,Mpc^{-1}$, respectively. The constraints on H_0 are slightly high as compared to some latest observations. The constraints from DS1 and DS2 show a slight variation from the observational value of WMAP sky survey value $71.9^{+2.6}_{-2.7}$ $Km\,sec^{-1}\,Mpc^{-1}$ [320] where as the constraint from DS3 shows a slight variation from Planck 2018 observation $67.4^{+0.5}_{-0.5}$ $Km\,sec^{-1}\,Mpc^{-1}$ [281].

6.5 Dynamics of Cosmological parameters

The dynamics of universe can be discussed through the graphs of different cosmological parameters with respect to redshift by using best fit values obtained through statistical analysis of our model. In what follows, we discuss the dynamics of three parameters, namely deceleration parameter, EoS parameter and Hubble parameter.

The evolutions of deceleration parameter for all three combinations of data sets are shown in Fig. 6.4. The transition redshift z_{tr} and present value of deceler-

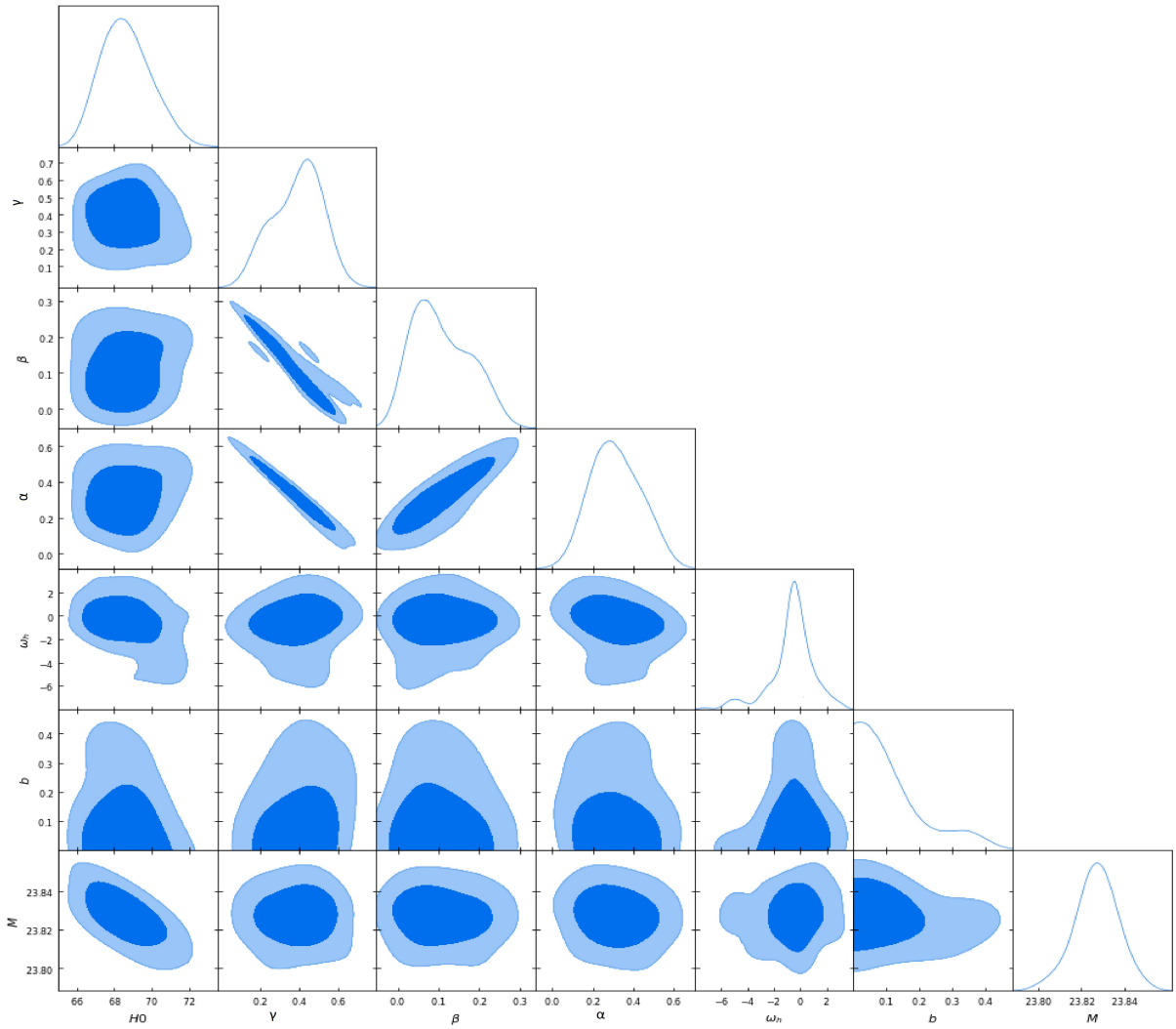

Figure 6.3: 68.3% and 95.4% confidence level contours and posterior distributions from MCMC analysis of data set $DS3 : pan, H(z)36$ and BAO.

Table 6.2: The values of z_{tr}, q_0, $w_{\text{eff}}(z=0)$ and t_0 (Gyr) using different combinations of data sets.

Values	DS1	DS2	DS3
z_{tr}	$0.827^{+0.312}_{-0.424}$	$0.843^{+0.500}_{-0.701}$	$0.862^{+0.100}_{-0.201}$
q_0	$-0.441^{+0.053}_{-0.045}$	$-0.440^{+0.061}_{-0.047}$	$-0.438^{+0.043}_{-0.036}$
$w_{\text{eff}}(z=0)$	$-0.621^{+1.7}_{-1.6}$	$-0.627^{+1.9}_{-1.4}$	$-0.625^{+1.9}_{-1.5}$

ation parameter q_0 are calculated for the best fit values of our model parameters and their values are listed in Table 6.2. In all the three combinations of data set, the HDE model shows the phase transition which take place at transition redshift $z_{tr} = 0.827^{+0.312}_{-0.424}$, $z_{tr} = 0.843^{+0.500}_{-0.701}$ and $z_{tr} = 0.862^{+0.100}_{-0.201}$ for DS1, DS2 and DS3, respectively. We observe that z_{tr} with these data sets are slightly higher than ΛCDM model $(z_{tr} = 0.662 \pm 0.014)$ which shows that the transition takes place earlier than ΛCDM model. The present values of q obtained from $DS1$, $DS2$ and $DS3$ data sets are $q_0 \approx -0.441$, $q_0 \approx -0.440$ and $q_0 \approx -0.438$ which show good agreement with the ΛCDM model with $q_0 \approx -0.59$ [281, 321].

The evolutions of effective EoS parameter with respect to redshift z, for all three combinations of data sets are shown in Fig. 6.5 and the respective present values are mentioned in Table 6.2. Figure 6.5 shows that for all three combinations DS1, DS2 and DS3, $w_{eff} \to -1$ in the late time which implies that our model converges to a de sitter universe in late time. Note that EoS parameter for each dataset is $w < -1$ i.e., it does not cross the phantom divide line which shows that our derived model is free from big-rip singularity. As $w > -1$, our HDE model is of quintessence type. The present values of w_{eff} for DS1, DS2 and DS3 are ≈ -0.621 , ≈ -0.627 and ≈ -0.625, respectively.

Figure 6.6 plots the evolution of Hubble function with respect to redshift along with the error bar of Hubble data set in the range $z \in (0,4)$ and presents a comparison with the standard ΛCDM model. Here, for ΛCDM model, the parameters are estimated from the Planck spacecraft data [281]. The trajectories of the model for all the data sets DS1, DS2 and DS3 coincide with the most of the data set of error bar of Hubble parameter, which shows that our HDE model with matter creation is in good agreement with ΛCDM model. In this cosmological scenario, the current ages of the universe are found to be $t_0 \approx 14.2\,Gyr$, $t_0 \approx 14.1\,Gyr$ and $t_0 \approx 14.2\,Gyr$, respectively. The ages obtained are very much compatible with that obtained from the CMB anisotropic

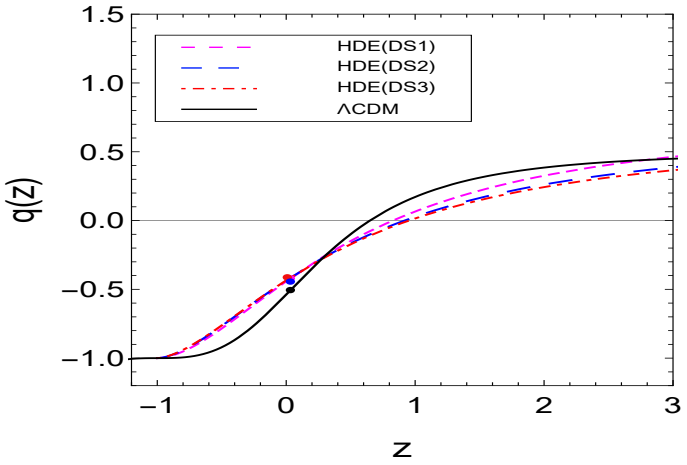

Figure 6.4: Plot of the deceleration parameter q versus redshift z for best-fit values of model parameters obtained from DS1, DS2 and DS3 data sets. We plot the corresponding q for ΛCDM to compare the phenological model. A dot on the trajectory represents the present value q_0.

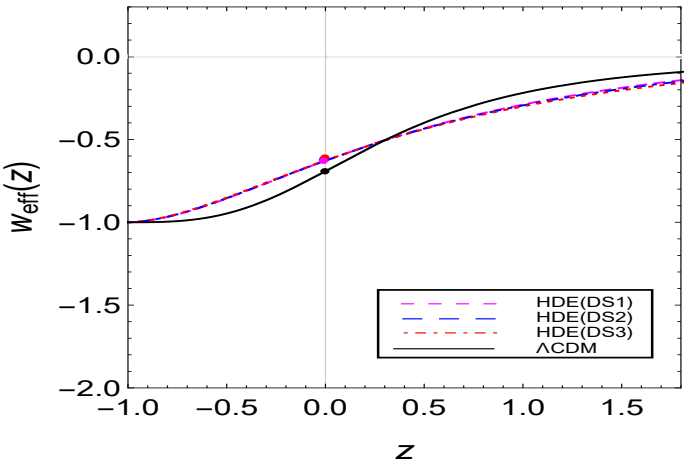

Figure 6.5: Plot of effective EoS parameter w_{eff} versus redshift z for best-fit values of parameters obtained from DS1, DS2 and DS3 data sets. We plot the corresponding w_{eff} for ΛCDM (solid curve) in order to compare the phenological model. A dot on the trajectory shows the current $w_{\text{eff}}(z=0)$.

data, $t_0 \approx 14.03\ Gyr$ [322]. However, these values are relatively higher than the ΛCDM obtained from joint data of WMAP, BAO and SNe, $t_0 \approx 13.7$ [320].

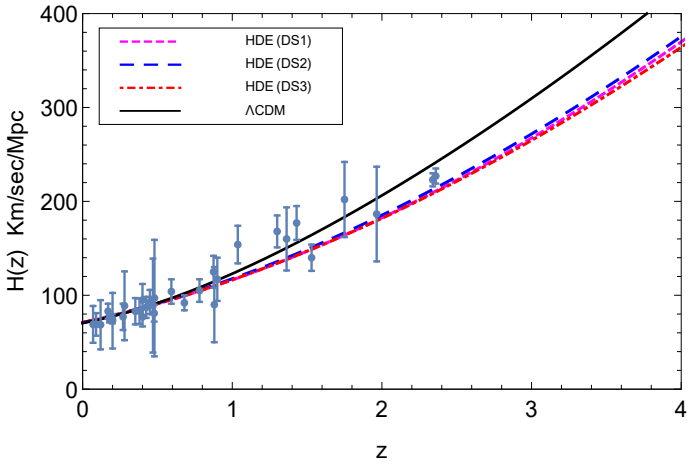

Figure 6.6: The Hubble function with respect to redshift for our derived HDE model from DS1, DS2 and DS3 data sets. The solid curve relates to the ΛCDM model. The $H_{obs}(z)$ data are also plotted with their error bars.

6.6 Geometric and Cosmographic Analyses

As χ^2 statistics is good at finding the best-fit values of parameters. Using the χ^2 statistic we can compare our derived dark energy model with the most compatible and accepted model of the universe. The ineffectiveness of this method arises for models with more number of parameters as χ^2_{min} lowers down in such cases, hence it is not well advised to use χ^2_{min} with likelihood contours or best-fit parameters to compare dark energy models always.

In this respect, we have a model-independent technique to compare various DE models by studying their cosmographical features. In this section, we will study various geometric and cosmographic parameters which are used to distinguish many DE models. Firstly, we discuss geometrical analysis of our model. Using (6.3.3), for our derived holographic dark energy model with matter creation, r and s are obtained as

$$r = 1 + \frac{k(k+1)\left(1-\frac{3\gamma(1-b^2)}{k(2-3(1-b^2)\alpha)}\right)a^{-(k+2)}}{H_0{}^2\left\{\frac{3\gamma(1-b^2)}{k(2-3(1-b^2)\alpha)}+(1-\frac{3\gamma(1-b^2)}{k(2-3(1-b^2)\alpha)})\right\}^3} - \frac{3\left(k-\frac{3(1-b^2)\gamma}{2-3(1-b^2)\alpha}\right)}{1+\frac{3(-1+a^k)(1-b^2)\gamma}{k(2-3(1-b^2)\alpha)}} \tag{6.6.1}$$

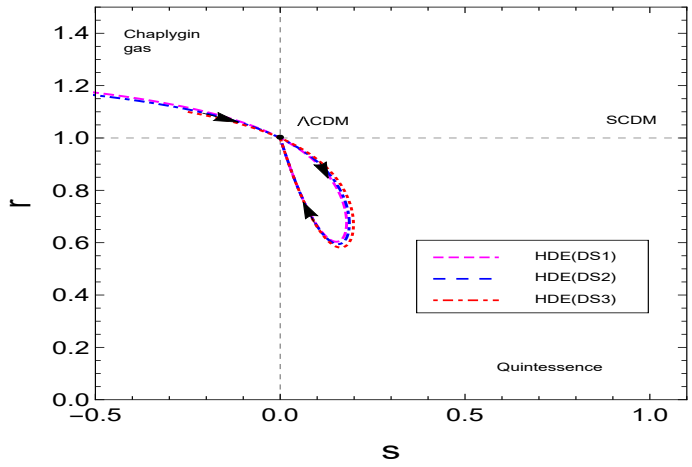

Figure 6.7: The evolutions of $\{r,s\}$ in $s-r$ plane corresponding to best fit values of model parameters obtained from data sets DS1, DS2 and DS3. The direction of the evolution are shown by the arrows on each trajectory.

$$s=\frac{\frac{k(k+1)\left(1-\frac{3\gamma(1-b^2)}{k(2-3(1-b^2)\alpha}\right)a^{-(k+2)}}{H_0{}^2\left\{\frac{3\gamma(1-b^2)}{k(2-3(1-b^2)\alpha)}+(1-\frac{3\gamma(1-b^2)}{k(2-3(1-b^2)\alpha)})\right\}^3}-\frac{3\left(k-\frac{3(1-b^2)\gamma}{2-3(1-b^2)\alpha}\right)}{1+\frac{3(-1+a^k)(1-b^2)\gamma}{k(2-3(1-b^2)\alpha)}}}{3\left(\frac{-3}{2}+\frac{k-\frac{3\gamma(1-b^2)}{2-3(1-b^2)\alpha}}{1+\frac{3\gamma(1-b^2)}{(2-3(1-b^2)\alpha)k}\{a^k-1\}}\right)} \tag{6.6.2}$$

We plot the $\{r,s\}$ and $\{r,q\}$ evolutions of the trajectory in $s-r$ and $q-r$ planes for the best fit values of model parameters obtained by observational data sets DS1, DS2 and DS3 which are shown in Figs. 6.7 and 6.8, respectively. It can be observed that the all the trajectory of $\{r,s\}$ begin from chaplygin gas type DE ($r>1$, and $s<0$) [323] in early times and go to the quintessence region ($r<1$ and $s>0$) [198,199] in intermediate phase, and finally approach to ΛCDM model ($r=1$ and $s=0$) in late time. The present values $\{r_0,s_0\}$ parameters are $\{0.627,0.120\}$, $\{0.615,0.126\}$ and $\{0.608,0.128\}$ corresponding to DS1, DS2 and DS3, respectively. From equations (6.6.1) and (6.6.2), we can also observe analytically that at the asymptotic limit $a\to\infty$, $\{r,s\}\to\{1,0\}$ which shows that the present model will tend to ΛCDM in late time evolution.

In Fig. 6.8, the evolutions of the trajectory corresponding to data sets $DS1$, $DS2$ and $DS3$ show that the model starts from decelerated phase in early time and after transition to accelerated phase, the model with each data sets approach to de Sitter model.

Apart from the above mentioned two geometric parameters, the comparing of models can also be extracted by cosmography. We obtain the cosmographic parameter (CP) usually referred to as $jerk\ (j)$, $snap\ (\mathbf{s})$, $lerk\ (l)$ and m parameters for our model using (1.2) As $jerk$, $snap$, $lerk$ and m parameters involve third, fourth, fifth and sixth derivative of scale factor $a(t)$, they help in measuring more accurate rate of cosmic

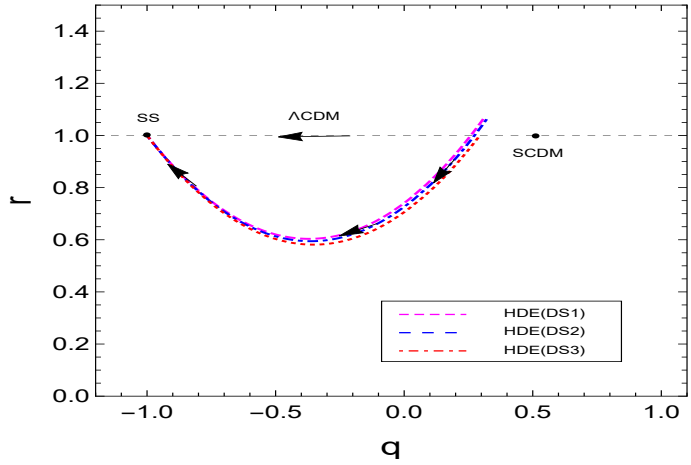

Figure 6.8: The evolutions of $\{r,q\}$ in $q-r$ plane corresponding to best fit values of model parameters for data sets DS1, DS2 and DS3. The direction of the evolution are shown by the arrows on each trajectory.

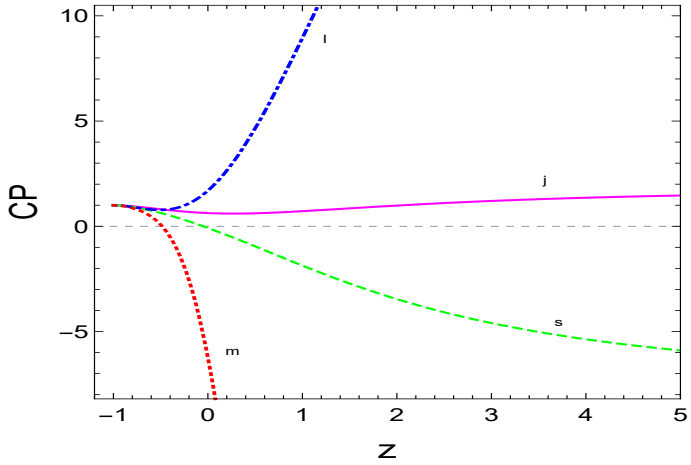

Figure 6.9: Plot of the cosmographic parameters j, $\mathbf{s}$, l and m with redshift z for best fit values of model parameters using $DS1$.

expansion. As per the current observations about the evolution of universe it can be concluded that the jerk of the universe is one [324]. These CP are important, for instance, when one attempts at comparing the ΛCDM model with any alternative DE such as HDE. In Fig. 6.9, we plot the trajectory of the CP for HDE model with matter creation, using data set DS1. We can find almost similar trajectories of CP using data sets DS2 and DS3. The present values of $jerk$, $snap$, $lerk$ and m parameters, using data set DS1, DS2 and DS3 are $(j_0 = 0.627, \mathbf{s}_0 = -0.077, l_0 = 1.692, m_0 = -6.238)$, $(j_0 = 0.615, \mathbf{s}_0 = -0.113, l_0 = 1.74, m_0 = -6.623)$ and $(j_0 = 0.608, \mathbf{s}_0 = -0.077, l_0 = 1.692, m_0 = -6.238)$, respectively. It is observed that the parameters j and l have similar evolution where as $\mathbf{s}$ and m show an equivalent evolution.

We find that j, $\mathbf{s}$, l and $m \to 1$ as $z \to -1$, i.e., in late time evolution, all CP approach to the values of CP of standard ΛCDM model. It can also be seen through

the graph that $jerk$ and $lerk$ parameters are positive throughout the cosmic evolution, which implies that the universe has gone under a phase transition from deceleration to acceleration. The jerk parameter informs about inflection points in the expansion history of the Universe. However, there is no such physical significance of $snap$ and m parameters but being important part of the Taylor series of the Hubble parameter in cosmography, they give us more precision in the preferred model. Figure 6.9 shows that $snap$ and m transit from initial negative values to later positive ones.

6.7 Conclusion

As mentioned, with Hubble horizon as an IR cut-off the HDE model can not explain the phase transition (see, Appendix A). So, in order to overcome this drawback we have presented the HDE model using same IR cut-off but with gravitationally induced matter creation mechanism to show the possible transition phase of the universe. In solving the field equations, our motive is to find one correct form of particle creation rate which can describe the current observable expansion of universe. But, an accurate functional form of Γ is still unknown. Therefore, in general, different phenomenological forms of Γ have been proposed in literature to fit the corresponding model parameters with the latest observational data.

In this chapter, we have assumed the most general phenomenological form of Γ in terms of H and $\dot{H}$ and investigated the evolution equation by using three different latest observational data sets: DS1 (SNe Pantheon, $H(z)(36)$, BAO and local H_0 by SH0ES), DS2: (SNe Pantheon, $H(z)$ and local H_0) and DS3: (SNe Pantheon, H(Z) and BAO) to observe how the HDE model with matter creation depicts the present scenario of the universe. It should be emphasized that Bayesian joint analysis cannot automatically show inconsistencies between the datasets. However, for the purpose of investigating whether our model can relieve the tension or not, we still combine the joint local H_0 measurement with SNe, H(z) and BAO to perform the joint analysis.

It is noted that in papers [186, 187], different data sets of SNe (JLA), observational Hubble data (OHD) and BAO have been taken as background observation. We found that the HDE model with matter creation predicts the phase transition from decelerating epoch to accelerating epoch at transitional redshift $z_{tr} \sim 0.83$. Further, we have discussed two model independent tests, namely, the statefinder and the cosmographic parameters to measure the divergence of our model from the best described model

of universe i.e., ΛCDM.

We have plotted the trajectories of different cosmological parameters with respect to redshift to observe the evolution of the model. We know that the current observational data favours an EoS for DE greater than -1. The present values q_0 and $\omega_{eff}(z=0)$ for HDE model are very much compatible with the present value of these parameters of ΛCDM model. The evolutions of these parameters almost match with the evolution of the ΛCDM from the data sets of DS1, DS2 and DS3. We find that the evolution of the universe commences from higher redshift, from a decelerating phase to lower redshift, i.e. to accelerating phase. In late time, the HDE model with matter creation tends to standard ΛCDM model. The present values of effective EoS parameter are relatively higher than the one anticipated by the joint analysis of WMAP, BAO, H_0 and SNe [14]. The age of universe with each data set is found to be slightly higher than that of ΛCDM model.

We have calculated the chi-squared minimum and reduced chi-squared for the model using DS1, DS2 and DS3 data sets. We have observed that the χ^2_{red} is less than unity with all the combinations implying that the model shows the good support to ΛCDM model. We have also discussed the statefinder parameters and have plotted the trajectories of {r, s} in $s-r$ plane and {r, q} in $q-r$ plane using best fit values of model parameters for all three combination of data sets. It can be noticed that each trajectory starts from chaplygin gas region in early times, enters into quintessence region in medieval time and finally approaches to ΛCDM in late times.

In conclusion, we have discussed the overall dynamics of HDE model with matter creation using a more general form of matter creation rate along with the Hubble horizon as an IR cut-off. This dynamical HDE model provides a transition phase from decelerating to accelerating phase of the cosmic expansion. The analytical and numerical analysis show that the HDE model with inclusion of matter creation provides a good fitting to the cosmological parameters at all redshifts and it mimics the global dynamics of the standard ΛCDM model.

****

Chapter 7

Conclusion and Future Scope

7.1 Conclusion

In relativistic cosmology, the current accelerating expansion of the universe is obtained by assuming the existence of a dark energy component in addition to cold dark matter. Dark energy (DE) is an exotic fluid endowed with negative pressure which violates the strong energy condition. The negative pressure occurs naturally in many different context when the physical systems depart from thermodynamic equilibrium states.

In this connection, the bulk viscosity and the process of cosmological matter creation at the expense of the gravitational field can phenomenologically be described by a negative pressure. It has been observed since long ago that bulk viscosity in cosmology can produce an accelerated expansion. It may be assumed that the expansion process is a collection of states out of thermal equilibrium which gives the existence of bulk viscosity. The explicit form of bulk viscosity is still unknown, therefore, its form has to be assumed a priori or obtained from a known or proposed physical mechanism. We have chosen the first option to discuss the effect of bulk viscosity, but we can explore the section option in future works. It has been found that bulk viscous cosmology explains the present accelerating universe.

The matter creation process in cosmology at the expenses of gravitational field can phenomenologically be described by a negative pressure. Earlier, the consequences of matter creation was studied macroscopically mainly as a byproduct of bulk viscosity near the Planck era. However, the first self-consistent macroscopic formulation of matter creation was put forward by Prigogine and coworkers [170, 171] through co-

variant formulation. It has also been shown that matter creation can effectively be discussed in the realm of relativistic non-equilibrium thermodynamics. The process of bulk viscosity and matter creation has been investigated in literature by many authors to discuss the early and late-time evolution of the universe.

It is to be noted that matter creation is an irreversible process which is completely different from bulk viscosity mechanism [172].

In the thesis, we have studied the effects of bulk viscosity and matter creation on various cosmological models. In chapter 2, we have checked if bulk viscosity can be a possible candidate of DE to explain the expansion of universe. We have explored a bulk viscous matter dominated model with constant bulk viscous coefficient $\zeta = \zeta_0$ in the framework of BD theory. We have identified three possible conditions for bulk viscous coefficient, $0 \leq \bar{\zeta}_0 < (3-n)$, $\bar{\zeta}_0 = (3-n)$ and $\bar{\zeta}_0 > (3-n)$. Depending on these conditions, we have analyzed the different possible evolutions predicted by the viscous model. We have observed that the viscous model predicts a universe with a Big-bang in the past and then transition from decelerating epoch to an accelerating epoch in late times for the values of $\bar{\zeta}_0$ in the range $0 < \bar{\zeta}_0 \leq (3-n)$. For $\bar{\zeta}_0 = (3-n)$, the model corresponds to the de Sitter and it always predicts accelerated expansion for $\bar{\zeta}_0 > (3-n)$. We have found that the transition from decelerated phase to accelerated one occurs in future in $0 < \bar{\zeta} < (1-n)$. When $\bar{\zeta}_0 = (1-n)$, the transition from decelerated to accelerated epoch takes place today. The transition between the deceleration-acceleration epoch takes place in past in $(1-n) < \bar{\zeta}_0 \leq (3-n)$. In limiting case, when $\bar{\zeta}_0$ approaches to $(3-n)$, the transition takes place very close to Big-bang. We have constrained the model parameters through the MCMC method on the latest observational data to discuss various cosmological parameters and then compared using the tools taken from information criterion.

In chapter 3, we have extended the work to explore the effect of bulk viscosity in HDE model. We have discussed a viscous HDE model with Granda-Oliveros as an infra red cutoff in the framework of FLRW space-time to show the current observable expansion of universe. We have obtained the solutions of the field equations by assuming the parameterized form of $\zeta = \zeta_0 + \zeta_1 H + \zeta_2 \left(\frac{\dot{H}}{H} + H\right)$. We have constrained the space parameters of model using the two combinations of latest observational datasets to find the best fit values of model parameters which are used to depict the universe which matches the current observable universe. Using statefinder and cosmographic parameters it has been found that our model starts from a region of Chaplygin gas

model and tends to ΛCDM model in future i.e. ,model explains the late time evolution of universe.

Further, chapter 4 deals with the adiabatic matter creation process in Brans-Dicke theory with matter creation rate as $\Gamma = 3\gamma H_0 + 3\beta H$ with the motivation of considering it as an alternative choice to explain the recent accelerating phase of the universe. The model is studied statistically using the available astronomical data. We have discussed the evolution of model using the deceleration parameter, equation of state parameter and statefinder diagnostic parameters. Under certain conditions the generalized second law of thermodynamics remained valid for the model.

In chapter 5, we have extended the work of chapter 4 and explored the effect of matter creation in the HDE model in the framework of Brans Dicke theory to observe the current accelerated phase. We have analysed the model without ($\Gamma = 0$) and with ($\Gamma = 3\gamma H_0 + 3\beta H$) particle creation. We have constrained the model parameters using two different combinations of latest available datsets. Using best-fitted model parameters, we have analysed the evolution of various cosmological parameters. Diagnostic analysis of model has been done to distinguish the model with matter creation from model without matter creation and other standard dark energy models. The result shows that the HDE model with Hubble horizon as an Infra red cutoff does not show the phase transition while the same model with matter creation shows the phase transition.

Chapter 6 explores the matter-dominated model with matter creation in the FLRW model to show the current accelerated expansion of universe. We have proposed a generalized form of matter creation rate, $\Gamma = 3\left[\gamma H_0 + \beta H + \alpha\left(\frac{\dot{H}}{H} + H\right)\right]$. We have performed the statistical analysis to find the best-fit values of model parameters using the MCMC technique on a different combination of publicly available data sets. Exact solutions of deceleration parameter and effective equation of state parameter have been found and their evolution for the best-fit values of model parameters has been discussed. Phase transition from deceleration to recent acceleration has been shown through their trajectories. The model has been distinguished from other existing dark energy models using two geometrical diagnostics: statefinder parameter and cosmographic parameters.

7.2 Future Scope

We know that the cosmological model is a mathematical representation of the universe. We try to formulate a model which must be consistent with what is already known about the universe. To define the physical processes governing the model, we must know the types of material within the universe and its evolution equations. There are the cosmological parameters whose values can be obtained from the observations. There are some dynamical frame where we can model the physical laws. In this thesis, we have obtained few new results by analyzing bulk viscous and matter creation cosmology in the framework of GTR and BD theory to explain the current observable universe.

The BD theory which is a simple extension of GR where Newton's constant is assumed as a time varying scalar field. It is one of the scalar-tensor theories that has been studied by many authors. The BD gravity theory introduces an additional scalar field ϕ besides the metric tensor $g_{\mu\nu}$ of spacetime and is considered a viable alternative to GR, one which respects Mach's principle. The effective gravitational constant G is proportional to the inverse of the scalar field. We have used the power-law form of BD scalar field to show the late-time evolution of universe. The study of structure formation and perturbation theory with this form of BD scalar field will be interesting.

It has been found that the HDE model is also a dynamical model which explains the present-day accelerated expansion of the universe. Various choices of IR cut-offs in HDE models have been proposed. We have considered Hubble Horizon as an IR cut-off, i.e. $L = H^{-1}$ and HDE density proposed by Granda-Oliveros as $\rho_h = 3(n_1 H^2 + n_2 \dot{H})$ in different viscous and matter creation cosmological models in GTR and BD theory. In the forthcoming papers it could be interesting to study the viscous and particle creation cosmology with other different cut-offs available in literature in GTR, BD theory or in other modified theories of gravity.

We have assumed various particular and appropriate choices of bulk viscous coefficient ζ and particle creation rate Γ. It has been found out that the choice of bulk viscous coefficient and particle creation rate led to sudden change in the evolution of universe from decelerated phase to accelerated phase. Since the nature of bulk viscous coefficient and matter creation are still unknown, therefore, the other choices for these coefficients may be assumed to study the late time evolution of universe.

We have analysed all proposed cosmological models statistically using the various combinations of available datsets. We have various other available datasets like gamma-ray bursts, which we have not used in our thesis and may be used in the forthcoming papers. As in today's data driven era, new observational data may provide the better results for the cosmological models in understanding the problems faced by the standard ΛCDM model. Thus, present thesis put forward the theoretical and observational understanding of cosmological models which provides further to study the evolution of universe with recent available observational data.

****

Bibliography

[1] A. Einstein; *The foundation of the general theory of relativity*, Ann. Phys. **49**, 769 (1916); Sitz. Preuss. Akad. Wiss. Phys. **1**, 142 (4) (1917); Ann. Phys. **69**, 436 (1922).

[2] A. Friedmann; *Über die Krümmung des Raumes*, Zeitschriftfür Physik **10**, 377 (1922).

[3] H.P. Robertson; *Kinematics and world-structure*, Astrophys. J. **82**, 284 (1935).

[4] A.G. Walker; *On Milne's theory of world structure*, Proceedings of the London Mathematical Society **42**, 90 (1936).

[5] G. Lemaître; *A homogenous universe of constant mass and increasing radius accounting for the radial velocity of extra-galactic nebulae*, Annales de la Société Scientifique de Bruxelles **47**, 49 (1927).

[6] E.P. Hubble; *A relation between distance and radial velocity among extra-galactic nebulae*, Proc. Nat. Acad. Sci. USA **15**, 168 (1929).

[7] A.G. Riess et al.; *Observational evidence from supernovae for an accelerating universe and a cosmological constant (Supernova Search Team Collaboration)*, Astron. J. **116**, 1009 (1998); [arXiv:astro-ph/9805201].

[8] S. Perlmutter et al.; *Measurements of Omega and Lambda from 42 high redshift supernovae (The Supernova Cosmology Project)*, Astrophys. J. **517**, 565 (1999); [arXiv:astro-ph/9812133].

[9] G. Hinshaw et al.; *Nine-Year Wilkinson Microwave Anisotropy Probe (WMAP) observations: Cosmological parameter results*, Astrophys. J. Suppl. **208**, 19 (2013); [arXiv:astro-ph/1212.5226].

[10] C.L. Bennett et al.; *Nine-Year Wilkinson Microwave Anisotropy Probe (WMAP) Observations: Final maps and results (WMAP Collaboration)*, Astrophys. J. Suppl. **208**, 20 (2013); [arXiv:astro-ph/1212.5225].

[11] L. Anderson et al.; *The clustering of galaxies in the SDSS-III Baryon Oscillation spectroscopic survey: Baryon Acoustic Oscillations in the data release 9 spectroscopic galaxy sample*, Mon. Not. Roy. Astron. Soc. **427**, 3435 (2013); [arXiv:astro-ph/1203.6594].

[12] P.A.R. Ade et al.; *Planck 2013 results. I. Overview of products and scientific results (Planck Collaboration)*, Astron. Astrophys. **571**, A1 (2014); [arXiv:astro-ph/1303.5062].

[13] P.A.R. Ade et al.; *Planck 2015 results*, Astron. Astrophys. **594**, A13 (2016).

[14] E. Komatsu et al.; *WMAP Collaboration, Seven-year Wilkinson Microwave Anisotropy Probe (WMAP) observations: Cosmological interpretation*, Astrophys. J. Suppl. **192**, 18 (2011).

[15] A.G. Sanchez et al.; *The clustering of galaxies in the SDSS-III Baryon Oscillation spectroscopic survey: cosmological implications of the large-scale two-point correlation function*, Mon. Not. Roy. Astron. Soc. **425**, 415 (2012).

[16] S. Weinberg; *The cosmological constant problem*, Rev. Mod. Phys. **61**, 1 (1989).

[17] V. Sahni, A.A. Starobinsky; *The case for a positive cosmological Λ-term*, Int. J. Mod. Phys. D **9**, 373 (2000); [arXiv:astro-ph/9904398].

[18] T. Padmanabhan; *Cosmological constant: The weight of the vacuum*, Phys. Rept. **380**, 235 (2003); [arXiv:hep-th/0212290].

[19] H.E.S. Velten et al.; *Aspects of the cosmological "coincidence problem“*, Eur. Phys. J. C **74**, 3160 (2014).

[20] E.J. Copeland, M. Sami, S. Tsujikawa; *Dynamics of dark energy*, Int. J. Mod. Phys. D **15**, 1753 (2006); [arXiv:hep-th/0603057].

[21] J. Sola; *Cosmological constant and vacuum energy: old and new ideas*, J. Phys.: Conf. Ser. **453**, 012015 (2013);

[22] I. Zlatev, L.M. Wang, P.J. Steinhardt; *Quintessence, cosmic coincidence, and the cosmological constant*, Phys. Rev. Lett. **82**, 896 (1999); [arXiv:astro-ph/9807002].

[23] P.J. Steinhardt, L.M. Wang, I. Zlatev; *Cosmological tracking solutions*, Phys. Rev. D **59**, 123504 (1999); [arXiv:astro-ph/9812313].

[24] T. Chiba; *Quintessence, the gravitational constant, and gravity*, Phys. Rev. D **60**, 083508 (1999); [arXiv:gr-qc/9903094].

[25] L. Wang, R.R. Caldwell, J.P. Ostriker, P.J. Steinhardt; *Cosmic concordance and quintessence*, Astrophys J. **530**, 17 (2000); [arXiv:astro-ph/9901388].

[26] T. Chiba, T. Okabe and M. Yamaguchi; *Kinetically driven quintessence*, Phys. Rev. D **62**, 023511 (2000).

[27] L. Amendola; *Coupled quintessence*, Phys. Rev. D **62**, 043511 (2000).

[28] W. Zimdahl, D. Pavón, L.P. Chimento; *Interacting quintessence*, Phys. Lett. B **521**, 133 (2001).

[29] S. Capozziello; *Dark energy exponential potential models as curvature quintessence*, Class. Quantum Grav. **23**, 1205 (2006).

[30] Y. Zhang, Y.X. Gui; *Quasinormal modes of gravitational perturbation around a Schwarzschild black hole surrounded by quintessence*, Class. Quantum Grav. **23**, 6141 (2006).

[31] J. Martin; *Quintessence: a mini-review*, Mod. Phys. Lett. A **23**, 1252 (2008); [arXiv:astro-ph/0803.4076].

[32] R. Ratra, P.J. Peebles; *Cosmological consequences of a rolling homogeneous scalar field*, Phys. Rev. D **37**, 3406 (1988).

[33] E.J. Copeland, A.R. Liddle, D. Wands; *Exponential potentials, scaling solutions and inflation*, Ann. N. Y. Acad. Sci. **688**, 647 (1993).

[34] J.D. Barrow, P. Saich; *Scalar field cosmologies*, Class. Quantum Grav. **10**, 279 (1993).

[35] J.W. Lee, I.G. Koh; *Galactic halos as boson stars*, Phys. Rev. D **53**, 2236 (1996); [arXiv:hep-ph/9507385].

[36] R.R. Caldwell, R. Dave, P.J. Steinherdt; *Cosmological imprint of an energy component with general equation of state*, Phys. Rev. Lett. **80**, 1582 (1998).

[37] J.M.F. Maia and J.A.S. Lima; *Scalar field description of decaying-? cosmologies*, Phys. Rev.D **65**, 083513 (2002).

[38] V. Sahni; *Dark matter and dark energy*, Lect. Notes Phys. **653**, 141 (2004); [arXiv:astro-ph/0403324].

[39] V. Sahni, A. Starobinsky; *Reconstructing dark energy*, Int. J. Mod. Phys. D **15**, 2105 (2006); [arXiv:astro-ph/0610026].

[40] S. Lee, G.C. Liu and K.W. Ng; *Constraints on the coupled quintessence from cosmic microwave background anisotropy and matter power spectrum*, Phys. Rev. D **73**, 083516 (2006).

[41] R.R. Caldwell; *A Phantom Menace? Cosmological consequences of a dark energy component with super-negative equation of state*, Phys. Lett. B **545**, 23 (2002); [arXiv:astro-ph/9908168].

[42] V. Faraoni; *Superquintessence*, Int. J. Mod. Phys. D **11**, 471 (2002).

[43] R.R. Caldwell, M. Kamionkowski and N.N. Weinberg; *Phantom energy: Dark energy with w<-1 causes a cosmic doomsday*, Phys. Rev. Lett. **91**, 071301 (2003).

[44] R.R. Caldwell, M. Kamionkowski, N.N. Weinberg; *Phantom energy and cosmic doomsday*, Phys. Rev. Lett. **91**, 071301 (2003); [arXiv:astro-ph/0302506].

[45] E. Elizalde, S. Nojiri, S.D. Odintsov; *Late-time cosmology in (phantom) scalar-tensor theory: dark energy and the cosmic speed-up*, Phys. Rev. D **70**, 043539 (2004); [arXiv:hep-th/0405034].

[46] M. Sami, A. Toporensky; *Phantom field and the fate of universe*, Mod. Phys. Lett. A **19**, 1509 (2004); [arXiv:gr-qc/0312009].

[47] A. Vikman; *Can dark energy evolve to the phantom?*, Phys. Rev. D **71**, 023515 (2005).

[48] Z.K. Guo, Y.S. Piao, X.M. Zhang, Y.Z. Zhang; *Cosmological evolution of a quintom model of dark energy*, Phys. Lett. B **608**, 177 (2005); [arXiv: astro-ph/0410654].

[49] Z.K. Guo, Y.S. Piao, X.M. Zhang, Y.Z. Zhang; *Cosmological evolution of a quintom model of dark energy*, Phys. Lett. B **608**, 177 (2005).

[50] G.B. Zhao; *Perturbations of the quintom models of dark energy and the effects on observations*, Phys. Rev. D **72**, 123515 (2005).

[51] T. Padmanabhan; *Accelerated expansion of the universe driven by tachyonic matter*, Phys. Rev. D **66**, 021301 (2002); [arXiv:hep-th/0204150].

[52] G.W. Gibbons; *Cosmological evolution of the rolling tachyon*, Phys. Lett. B **537**, 1 (2002); [arXiv:hep-th/0204008].

[53] T. Chiba, T. Okabe, M. Yamaguchi; *Kinetically driven quintessence*, Phys. Rev. D **62**, 023511 (2000); [arXiv:astro-ph/9912463].

[54] C. Armendariz-Picon, V.F. Mukhanov, P.J. Steinhardt; *Essentials of k-essence*, Phys. Rev. D **63**, 103510 (2001); [arXiv:astro-ph/0006373].

[55] R.J. Scherrer; *Purely kinetic k essence as unified dark matter*, Phy. Rev. Lett. **93**, 011301 (2004).

[56] A. Kamenshchik, U. Moschella, V. Pasquier; *An alternative to quintessence*, Phys. Lett. B **511**, 265 (2001); [arXiv:gr-qc/0103004].

[57] M.C. Bento, O. Bertolami, A.A. Sen; *Generalized Chaplygin gas, accelerated expansion and dark energy-matter unification*, Phys. Rev. D **66**, 043507 (2002); [arXiv:gr-qc/0202064].

[58] G.'t Hooft; *Dimensional reduction in quantum gravity*, (1993); [arXiv:gr-qc/9310026].

[59] L. Susskind; *The world as a hologram*, J. Math. Phys. **36**, 6377 (1995).

[60] R. Bousso; *The holographic principle for general backgrounds*, Class. Quantum Grav. **17**, 997 (2000).

[61] A.G. Cohen, D.B. Kaplan, A.E. Nelson; *Effective field theory, black holes, and the cosmological constant*, Phys. Rev. Lett. **82**, 4971 (1999).

[62] S.D. Hsu; *Entropy bounds and dark energy*, Phys. Lett. B **594** (2004) 13.

[63] M. Li; *A model of holographic dark energy*, Phys. Lett. B **603**, 1 (2004).

[64] J. Zhang, X. Zhang, H. Liu; *Holographic dark energy in a cyclic universe*, Eur. Phys. J. C **52**, 693 (2007).

[65] F. Canfora, G. Vilasi; *The Holographic Principle and the Early Universe*, Phys. Lett. B **625**, 171 (2005).

[66] Q.G. Huang, M. Li; *The holographic dark energy in a non-flat universe*, J. Cosmol. Astropart. Phys. **08**, 013 (2004).

[67] Q.G. Huang, M. Li; *Anthropic principle favours the holographic dark energy*, J. Cosmol. Astropart. Phys. **03**, 001 (2005).

[68] K. Ke, M. Li; *Cardy-Verlinde formula and holographic dark energy*, Phys. Lett. B **606**, 173 (2005).

[69] X. Zhang; *Statefinder diagnostic for holographic dark energy model*, Int. J. Mod. Phys. D **14**, 1597 (2005).

[70] B. Wang, Y. Gong, E. Abdalla; *Transition of the dark energy equation of state in an interacting holographic dark energy model*, Phys. Lett. B **624**, 141 (2005).

[71] H. Kim, H.W. Lee, Y.S. Myung; *Equation of state for an interacting holographic dark energy model*, Phys. Lett. B **632**, 605 (2006).

[72] B. Hu, Y. Ling; *Interacting dark energy, holographic principle, and coincidence problem*, Phys. Rev. D **73**, 123510 (2006).

[73] E.N. Saridakis; *Restoring holographic dark energy in brane cosmology*, Phys. Lett. B **660**, 138 (2008).

[74] Y.S. Myung; *Holographic principle and dark energy*, Phys. Lett. B **610**, 18 (2005).

[75] Y.S. Myung; *Instability of holographic dark energy models*, Phys. Lett. B **652**, 223 (2007).

[76] Y.S. Myung, M.G. Seo; *Origin of holographic dark energy models*, Phys. Lett. B **671**, 435 (2009).

[77] M. Li, X.D. Li, S. Wang, X. Zhang; *Holographic dark energy models: A comparison from the latest observational data*, J. Cosmol. Astropart. Phys. **06**, 036 (2009).

[78] H. Wei, S.N. Zhang; *Age problem in the holographic dark energy model*, Phys. Rev. D **76**, 063003 (2007); [arXiv:0707.2129].

[79] D. Pavón, W. Zimdahl; *Holographic dark energy and cosmic coincidence*, Phys. Lett. B **628**, 206 (2005).

[80] L.N. Granda, A. Oliveros; *Infrared cut-off proposal for the holographic density*, Phys. Lett. B **669**, 275 (2008).

[81] L.N. Granda, A. Oliveros; *New infrared cut-off for the holographic scalar fields models of dark energy*, Phys. Lett. B **671**, 199 (2009).

[82] K. Karami, J. Fehri; *Holographic dark energy in a non-flat universe with Granda-Oliveros cut-off*, Int. J. Theor. Phys. **49**, 1118 (2010).

[83] F. Yu, et al.; *A more general interacting model of holographic dark energy*, Phys. Lett. B **688**, 263 (2010).

[84] Y. Wang, L. Xu; *Current observational constraints to the holographic dark energy model with a new infrared cut-off via the Markov chain Monte Carlo method*, Phys. Rev. D **81**, 083523 (2010).

[85] M. Malekjani, A. Khodam-Mohammadi and N. Nazari-pooya; *Cosmological evolution and statefinder diagnostic for new holographic dark energy model in non flat universe*, Astrophys. Space Sci. **332**, 515 (2011).

[86] A. Oliveros and M.A. Acero; *New holographic dark energy model with non-linear interaction* , Astrophys. Space Sci. **357**, 12 (2015).

[87] M. Abdollahi Zadeh, A. Sheykhi and H. Moradpour; *Holographic dark energy with the sign-changeable interaction term*, Int. J. Mod. Phys. D **26**, 1750080 (2017).

[88] A. Akhlagi, M. Malekjani, S. Basilakos and H. Haghi; *Model selection and constraints from holographic dark energy scenarios*, Mon. Not. Roy. Astron. Soc. **477**, 3659 (2018).

[89] M. Srivastava, C.P. Singh; *New holographic dark energy model with constant bulk viscosity in modified $f(R,T)$ gravity theory*, Astrophys. Space Sci. **363**, 117 (2018).

[90] C.P. Singh, M. Srivastava; *Viscous cosmology in new holographic dark energy model and the cosmic acceleration* , Eur. Phys. J. C **78** 190 (2018).

[91] S. Nojiri, S.D. Odintsov; *Unifying phantom inflation with late-time acceleration: scalar phantom non-phantom transition model and generalized holographic dark energy*, Gen. Relativ. Gravit. **38**, 1285 (2006).

[92] M.R. Setare; *Holographic tachyon model of dark energy*, Phys. Lett. B **653**, 116 (2007).

[93] M.R. Setare; *Interacting holographic generalized Chaplygin gas model*, Phys. Lett. B **654**, 1 (2007).

[94] R.G. Cai; *A dark energy model characterized by the age of the universe*, Phys. Lett. B **657**, 228 (2007).

[95] E.N. Saridakis; *Holographic dark energy in braneworld models with a Gauss-Bonnet term in the bulk. Interacting behavior and the* $w = -1$ *crossing*, Phys. Lett. B **661**, 335 (2008).

[96] H. Wei, R.G. Cai; *A new model of agegraphic dark energy*, Phys. Lett. B **660**, 113 (2008).

[97] C. Gao, F. Wu, X. Chen, Y.G. Shen; *Holographic dark energy model from Ricci scalar curvature*, Phys. Rev. D **79**, 043511 (2009).

[98] C.P. Singh, P. Kumar; *Holographic dark energy in Brans-Dicke theory with logarithmic form of scalar field*, Int. J. Theor. Phys. **56**, 3297 (2017).

[99] P. Kumar, C.P. Singh; *New agegraphic dark energy model in Brans-Dicke theory with logarithmic form of scalar field*, Astrophys. Space Sci. **362**, 52 (2017).

[100] X. Zhang, F.Q. Wu; *Constraints on holographic dark energy from type Ia supernova observations*, Phys. Rev. D **72**, 043524 (2005).

[101] C. Feng et al.; *Testing the viability of the interacting holographic dark energy model by using combined observational constraints*, J. Cosmol. Astropart. Phys. **09**, 005 (2007).

[102] O. Luongo; *A thermodynamic approach to holographic dark energy*, Adv. High Energy Phys. **2017**, 1424503 (2017).

[103] M. Malekjani et al.; *Can holographic dark energy models fit the observational data?*, Phys. Rev. D **98**, 063533 (2018).

[104] A.S. Eddington; *The mathematical theory of relativity*, Cambridge University Press, (1923).

[105] H. Weyl; *A new extension of Relativity Theory (In German)*, Ann. Phys. **59**, 101 (1919); Surveys High Energy Phys. **5**, 237 (1986); Ann. Phys. **364**, 101 (1919).

[106] T. Kaluza; *Zum Unitätsproblem der Physik*, Sitz. Preuss. Akad. Wiss. Phys. Math. **K1**, 966 (1921); T. Appelquist, A. Chodos and P.G.O. Freund; *Modern Kaluza-Klein theories*, Addison-Wesley, (1987).

[107] O. Klein; *Quantentheorie und fünfdimensionale Relativitätstheorie*, Zeits. Phys. **37**, 895 (1926); Nature **118**, 516 (1926); T. Appelquist, A. Chodos and P.G.O. Freund; *Modern Kaluza-Klein theories*, Addison-Wesley, (1987).

[108] E. Witten; *String theory dynamics in various dimensions*, Nucl. Phys. B **443**, 85 (1995); [arXiv:hep-th/9503124].

[109] K. Becker, M. Becker, J.H. Schwarz; *String theory and M-theory: A modern introduction*, Cambridge University Press, ISBN: 978-0-512-86069-7 (2007).

[110] P.G. Bergmann; *Unified field theory with fifteen variables*, Ann. Math **49**, 225 (1948).

[111] G.W. Horndeshe; *Second order scalar tensor field equations in a four-dimensional space*, Int. J. Theor. Phys. **10**, 363 (1974).

[112] C. Brans, R.H. Dicke; *Mach's principle and a relativistic theory of gravitation*, Phys. Rev. **124**, 925 (1961).

[113] E. Mach; *Mechanics in their development*, Leipzig, (1883).

[114] P. A. M. Dirac; *The cosmological constants*, Nature **139**, 323 (1937).

[115] B. Bertotti, L. Iess, P. Tortora; *A test of general relativity using radio links with the Cassini spacecraft*, Nature **425**, 374 (2003).

[116] H. Kim; *Brans-Dicke theory as a unified model for dark matter-dark energy*, Mon. Not. R. Astron. Soc. Lett. **364**, 813 (2005).

[117] C. Mathiazhagen, V.B. Johri; *An infationary universe in Brans-Dicke theory: A hopeful sign of theoretical estimation of the gravitational constant*, Class. Quantum Grav. **1**, L29 (1984).

[118] D. La, P.J. Steinhardt; *Extended infationary cosmology*, Phys. Rev. Lett. **62**, 376 (1989).

[119] A.D. Linde; *Extended chaotic inflation and spatial variations of the gravitational constant*, Phys. Lett. B **238**, 160 (1990).

[120] N. Banerjee, A. Beesham; *Brans-Dicke cosmology with causal viscous fluid*, Aust. J. Phys. **49**, 899 (1996).

[121] S. Ram, C.P. Singh; *Early cosmological models with bulk viscosity in Brans-Dicke theory*, Astrophys. Space Sci. **254**, 143 (1997).

[122] S. Ram, C.P. Singh; *Early universe in Brans-Dicke cosmology*, Nuovo Cim. B **114**, 245 (1999).

[123] A.R. Liddle, A. Mazumdar, J.D. Barrow; *The radiation-matter transition in Jordan-Brans-Dicke theory*, Phys. Rev. D **58**, 027302 (1998).

[124] S. de Campo, R. Herrera, P. Labrãna; *Emergent universe in a Jordan-Brans-Dicke theory*, J. Cosmol. Aastropart. Phys. **030**, 0711 (2007); [arXiv:gr-qc/0711.1559]

[125] C.P. Singh; *FRW models with particle creation in Brans-Dicke theory*, Astrophys. Space Sci. **338**, 411 (2012).

[126] M. Campanelli, C.O. Lousto; *Are black holes in Brans-Dicke theory precisely the same as in general relativity?*, Int. J. Mod. Phys. D **02**, 451 (1993).

[127] G. Kang; *Black hole area in Brans-Dicke theory*, Phys. Rev. D **54**, 7483 (1996).

[128] T. Tamaki, T. Torii, K. Maeda; *Non-abelian black holes in Brans-Dicke theory*, Phys. Rev. D **57**, 4870 (1998).

[129] H. Kim; *New black hole solutions in Brans-Dicke theory of gravity*, Phys. Rev. D **60**, 024001 (1999).

[130] H. Maeda, G. Giribet; *Lifshitz black holes in Brans-Dicke theory*, J. High Energy Phys. **11**, 015 (2011); [arXiv: gr-qc/1105.1331].

[131] O. Bertolami, P.J. Martins; *Nonminimal coupling and quintessence*, Phys. Rev. D **61**, 064007 (2000).

[132] M. K. Mak, T. Harko; *Brans-Dicke cosmology with a scalar field potential*, Europhys. Lett. **60**, 155 (2002).

[133] T. Clifton, J.D. Barrow; *Decaying gravity*, Phys. Rev. D **73**, 104022 (2006).

[134] C. Eckart ; *The thermodynamics of irreversible processes. III. Relativistic Theory of the Simple Fluid* Phys. Rev. **58**, 919 (1940).

[135] W. Israel, J. Stewart; *Transient relativistic thermodynamics and kinetic theory*, Ann. Phys. **118**, 341 (1979).

[136] R. Maartens; *Dissipative cosmology*, Class. Quantum Phys. **12**, 1455 (1995).

[137] B. Saha; *Bianchi type universe with viscous fluid*, Mod. Phys. Lett. A **20**, 2127 (2005).

[138] B. Saha, V. Rikhvitsky; *Bianchi type I universe with viscous fluid and a Λ term: A qualitative analysis*, Physica D **219**, 168 (2006).

[139] B. Saha, V. Rikhvitsky; *Anisotropic cosmological models with spinor field and viscous fluid in presence of a Λ term: qualitative solutions*, J. Phys. A: Math. Theor. **40**, 14011 (2007).

[140] M. Zeyauddin, B. Saha; *Bianchi type V bulk viscous cosmological models with particle creation in General Relativity*, Eur. Phys. J. P **129**, 177 (2014).

[141] G.L. Murphy; *Big-Bang model without singularities*, Phys. Rev. D **8**, 4231 (1973).

[142] M.K. Mak, T. Harko; *Full causal bulk-viscous cosmological models*, J. Math. Phys. **39**, 5458 (1998).

[143] S. Nojiri, S.D. Odintsov; *Inhomogeneous equation of state of the universe: Phantom era, future singularity, and crossing the phantom barrier*, Phys. Rev. D **72**, 023003 (2005).

[144] M. Cataldo, N. Cruz, S. Lepe; *Viscous dark energy and phantom evolution*, Phys. Lett. B **619**, 5 (2005).

[145] S. Capozziello et al.; *Observational constraints on dark energy with generalized equations of state*, Phys. Rev. D **73**, 043512 (2006).

[146] N. Cruz, S. Lepe, F. Peña; *Dissipative generalized Chaplygin gas as phantom dark energy*, Phys. Lett. B **646**, 177 (2007).

[147] J. Ren, X.H. Meng; *Cosmological model with viscosity media (dark fluid) described by an effective equation of state*, Phys. Lett. B **633**, 1 (2006).

[148] M.G. Hu, X.H. Meng; *Bulk viscous cosmology: Statefinder and entropy*, Phys. Lett. B **635**, 186 (2006).

[149] X.H. Meng, J. Ren, M.G. Hu; *Friedmann cosmology with a generalized equation of state and bulk viscosity*, Commun. Theor. Phys. **47**, 379 (2007).

[150] C.P. Singh, S. Kumar, A. Pradhan; *Early viscous universe with variable gravitational and cosmological constants*, Class. Quantum Grav. **24**, 455 (2007).

[151] C.P. Singh; *Bulk viscous cosmology in early universe*, Pramana J. Phys. **71**, 33 (2008).

[152] C.J. Feng, X.Z. Li; *Viscous Ricci dark energy*, Phys. Lett. B **680**, 355 (2009).

[153] L. Sebastiani; *Dark viscous fluid coupled with dark matter and future singularity*, Eur. Phys. J. C **69**, 547 (2010).

[154] M.R. Setare, A. Sheykhi; *Viscous dark energy and generalized second law of thermodynamics*, Int. J. Mod. Phys. D **19**, 1205 (2010).

[155] I. Brevik; *Viscosity in modified gravity*, Entropy **14**, 2302 (2012).

[156] J.S. Gagnon, J. Lesgourgues; *Dark goo: Bulk viscosity as an alternative to dark energy*, J. Cosmol. Astropart. Phys. **09**, 026 (2011); [arXiv:astro-ph/1107.1503v2].

[157] C.P. Singh; *Viscous FRW models with particle creation in early universe*, Mod. Phys. Lett. A **27**, 1250070 (2012).

[158] Y.D. Xu, Z.G. Huang, X.H. Zhai; *Generalized chaplygin gas model with or without viscosity in the $w-w'$ plane*, Astrophys. Space Sci. **337**, 493 (2012).

[159] C.P. Singh, P. Kumar; *Friedmann model with viscous cosmology in modified $f(R,T)$ gravity theory*, Eur. Phys. J. C **74**, 3070 (2014).

[160] M. Zeyauddin, B. Saha; *Bianchi type V bulk viscous cosmological models with particle creation in general relativity.*, Eur. Phys. J. Plus **129**, 177 (2014).

[161] P. Kumar, C.P. Singh; *Viscous cosmology with matter creation in modified $f(R,T)$ gravity*, Astrophys. Space Sci. **357**, 120 (2015).

[162] I. Brevik, V.V. Obukhov, A.V. Timoshkin; *Cosmological models coupled with dark matter in a dissipative universe* , Astrophys. Space Sci. **359**, 11 (2015).

[163] I. Brevik, V.V. Obukhov, A.V. Timoshkin; *Dark Energy coupled with dark matter in viscous fluid cosmology*, Astrophys. Space Sci. **355**, 399 (2015).

[164] I. Brevik et al.; *Viscous cosmology for early- and late-Time Universe*, Int. J. Mod. Phys. D **26**, 1730024 (2017).

[165] I. Brevik, A.N. Makarenko, A.V. Timoshkin; *Viscous accelerating universe with nonlinear and logarithmic equation of state fluid*, Int. J. Geom. Meth. Mod. Phys. **16**, 1950150 (2019).

[166] C.P. Singh, A. Kumar; *Observational constraints on viscous Ricci dark energy model*, Astrophys. Space Sci. **364**, 94 (2019).

[167] I. Brevik, A.V. Timoshkin; *Viscous fluid holographic bounce*, Int. J. Geom. Meth. Mod. Phys. **17**, 2050023 (2020).

[168] I. Brevik, B.D. Normann; *Remarks on cosmological bulk viscosity in different epochs*, Symmetry **12**, 1085 (2020).

[169] I. Brevik, A.V. Timoshkin; *Rip brane cosmology from a viscous holographic dark fluid*, Int. J. Geom. Meth. Mod. Phys. **17**, 2050087 (2020).

[170] I. Prigogine et al.; *Thermodynamics of cosmological matter creation*, Proc. Natl. Acad. Sci. USA **85**, 7428 (1988).

[171] I. Prigogine et al.; *Thermodynamics and cosmology*, Gen. Relativ. Gravit. **21**, 8 (1989).

[172] J.A.S. Lima, A.S.M. Germano; *On the equivalence of bulk viscosity and matter creation*, Phys. Lett. A **170**, 373 (1992).

[173] M.O. Calv$\tilde{a}$o, J.A.S. Lima, I. Waga; *On the thermodynamics of matter creation in cosmology*, Phys. Lett. A **162**, 223 (1992).

[174] J.A.S. Lima, A.S.M Germano, L.R.W. Abramo; *FRW-type cosmologies with adiabatic matter creation*, Phys. Rev. D **53**, 4287 (1996).

[175] E. Gunzig, R. Maartens, A.V. Nesteruk; *Inflationary cosmology and thermodynamics*, Class. Quantum Grav. **15**, 923 (1998).

[176] J.S. Alcaniz, J.A.S. Lima; *Closed and open FRW cosmologies with matter creation: kinematic tests*, Astron. Astrophys. **349**, 729 (1999).

[177] T. Harko, F.S.N. Lobo, J.P. Mimoso, D. Pavon; *Gravitational induced particle production through a non-minimal curvature-matter coupling*, Eur. Phys. J. C **75**, 386 (2015).

[178] T. Harko, F.S.N. Lobo, J.P. Mimoso, D. Pavon; *Irreversible matter creation processes through a non-minimal curvature matter coupling*, The Fourteenth Marcel Grossmann Meeting, 1204 (2017); [arXiv:1508.03069].

[179] W. Zimdahl, D.J. Schwarz, A.B. Balakin, D. Pav$\acute{o}$n; *Cosmic antifriction and accelerated expansion*, Phys. Rev. D **64**, 063501 (2001).

[180] Y. Qiang, T.J. Zhang, Z.L. Yi; *Constraint on cosmological model with matter creation using complementary astronomical observations*, Astrophys. Space Sci. **311**, 407 (2007).

[181] J.A.S. Lima, F.E. Silva, R.C. Santos; *Accelerating cold dark matter cosmology ($\Omega_\Lambda = 0$)*, Class. Quantum Grav. **25**, 205006 (2008).

[182] G. Steigman, R.C. Santos, J.A.S. Lima; *An accelerating cosmology without dark energy*, J. Cosmol. Astropart. Phys. **06**, 033 (2009); [arXiv:astro-ph/0812.3912].

[183] J.A.S. Lima, J.F. Jesus, F.A. Oliveira, *CDM accelerating cosmology as an alternative to LCDM model*, J. Cosmol. Astropart. Phys. **11**, 027 (2010); [arXiv:astro-ph/0911.5727]

[184] V.H. C$\acute{a}$rdenas; *Dark energy, matter creation and curvature*, Eur. Phys. J. C **72**, 2149 (2012).

[185] T. Harko, F.S.N. Lobo; *Irreversible thermodynamic description of interacting dark energy-dark matter cosmological models*, Phys. Rev. D **87**, 044018 (2013).

[186] C.P. Singh, A. Kumar; *Quintessence behavior via matter creation cosmology*, Eur. Phys. J. C **80**, 106 (2020).

[187] A. Kumar, C.P. Singh; *Observational constraints on holographic dark energy-model with matter creation*, Astrophys. Space Sci. **365**, 84 (2020).

[188] J.D. Barrow; *String-driven inflationary and deflationary cosmological models*, Nucl. Phys. B **310**, 743 (1988).

[189] T. Padmanabhan, S.M. Chitre; *Viscous universes*, Phys. Lett. A **120**, 433 (1987).

[190] J. Triginer, D. Pavón; *Particle production in a viscous cosmological fluid*, Gen. Relativ. Gravit. **26**, 513 (1994).

[191] I. Brevik, G. Stokkan; *Viscosity and matter creation in the early universe*, Astrophys. Space Sci. **239**, 89 (1996).

[192] C.P. Singh, A. Beesham; *Early universe cosmology with particle creation: Kinematics tests*, Astrophys. Space Sci. **336**, 469 (2011).

[193] C.P. Singh; *Viscous FRW models with particle creation in early universe*, Mod. Phys. Lett. A **27**, 1250070 (2012).

[194] J. de Haro, S. Pan; *Gravitationally induced adiabatic particle production: From big bang to de Sitter*, Class. Quant. Grav. **33**, 165007 (2016).

[195] S. Pan, S. Chakraborty; *Will there be future deceleration? A study of particle creation mechanism in nonequilibrium thermodynamics*, Adv. High Energy Phys. **201**, 654025 (2015).

[196] L.R.W. Abramo, J.A.S. Lima; *Inflationary models driven by adiabatic matter creation*, Class. Quantum Grav. **13**, 2953 (1996).

[197] S. Pan, J. de Haro, A. Paliathanasis, R.J. Slagter; *Evolution and dynamics of a matter creation model*, Mon. Not. Roy. Astron. Soc. **460**, 1445 (2016).

[198] V. Sahni, T.D. Saini, A.A. Starobinsky, U. Alam; *Statefinder-A new geometrical diagnostic of dark energy*, J. Exp. Theor. Phys. **77**, 201 (2003).

[199] U. Alam, V. Sahni, T.D. Saini, A.A. Starobinsky; *Exploring the expanding universe and dark energy using the statefinder diagnostic*, Mon. Not. R. Astron. Soc. **344**, 1057 (2003).

[200] V. Sahni, A. Shafieloo, A.A. Starobinsky; *Two new diagnostics of dark energy*, Phys. Rev. D **78**, 103502 (2008).

[201] M.L. Tong, Y. Zhang; *Cosmic age, statefinder, and Om diagnostics in the decaying vacuum cosmology*, Phys. Rev. D **80**, 023503 (2009).

[202] J.B. Lu, L.X. Xu; *Geometrical diagnostic for the generalised chaplygin gas model*, Int. J. Mod. Phys. D **18**, 1741 (2009).

[203] Z.G. Huang, H.Q. Lu, K. Zhang; *Om diagnostic for dilaton dark energy*, Astrophys. Space Sci. **331**, 331 (2011).

[204] M. Visser; *Jerk, snap, and the cosmological equation of state*, Class. Quant. Grav. **21**, 2603 (2004).

[205] M. Visser; *Cosmography: Cosmology without the Einstein equations*, Gen. Relativ. Gravit. **37**, 1541 (2005).

[206] H. Akaike; *A new look at the statistical model identification*, IEEE Transactions on Automatic Control **19**, 716 (1974).

[207] G. Schwarz; *Estimating the dimension of a model*, Ann. Statist. **6**, 461 (1978).

[208] A.R. Liddle; *Information criteria for astrophysical model selection*, Mon. Not. R. Astron. Soc. **377**, L74 (2007).

[209] D. Foreman-Mackey, D. Hogg, D. Lang, J. Goodman; *emcee: The MCMC Hammer*, Publications of the Astronomical Society of the Pacific **125**, 306 (2012).

[210] M. Betoule et al.; *Improved cosmological constraints from a joint analysis of the SDSS-II and SNLS supernova samples*, Astron. Astrophys. **568**, A22 (2014).

[211] D.M. Scolnic et al.; *The complete light-curve sample of spectroscopically confirmed SNe Ia from Pan-STARRS1 and cosmological constraints from the combined Pantheon sample*, Astrophys. J. **859**, 101 (2018).

[212] A. Conley et al.; *Supernova constraints and systematic uncertainties from the first three years of the supernova legacy survey*, Astrophys. J. Suppl. Ser. **192**, 1 (2011).

[213] R. Jimenez, A. Loeb; *Constraining cosmological parameters based on relative galaxy ages*, Astrophys. J. **573**, 37 (2002).

[214] S.L. Cao et al.; *Testing backreaction effects with observational Hubble parameter data*, Eur. Phys. J. C **78**, 170 (2018).

[215] M. Moresco et al.; *Improved constraints on the expansion rate of the universe up to $z \sim 1.1$ from the spectroscopic evolution of cosmic chronometers*, J. Cosmol. Astropart. Phys. **08**, 006 (2012).

[216] S. Alam et al.; *The clustering of galaxies in the completed SDSS-III Baryon Oscillation Spectroscopic Survey: cosmological analysis of the DR12 galaxy sample*, Mon. Not. R. Astron. Soc. **470**, 2617 (2017).

[217] T. Delubac et al.; *Baryon acoustic oscillations in the Lyα forest of BOSS DR11 quasars*, Astron. Astrophys. **574**, A59 (2015).

[218] A. Font-Ribera et al.; *Quasar-Lyman α forest cross-correlation from BOSS DR11: Baryon Acoustic Oscillations*, J. Cosmol. Astropart. Phys. **05**, 027 (2014).

[219] G.S. Sharov, V.O. Vasiliev; *How predictions of cosmological models depend on Hubble parameter data sets*, Math. Model. geom. **6**(1), 1 (2018); [arXiv:1807.07323v1].

[220] J. Simon, L. Verde, R. Jimenez; *Constraints on the redshift dependence of the dark energy potential*, Phys. Rev. D **71**, 123001 (2005).

[221] E. Gaztaaga et al.; *Clustering of luminous red galaxies IV : Baryon acoustic peak in the line-of-sight direction and a direct measurement of H(z)*, Mon. Not. R. Astron. Soc. **399**, 1663 (2009).

[222] D. Stern et al.; *Cosmic chronometers: constraining the equation of state of dark energy. I: H(z) measurements*, J. Cosmol. Astropart. Phys. **02**, 008 (2010).

[223] C. Blake et al.; *The WiggleZ Dark Energy Survey: joint measurements of the expansion and growth history at z < 1*, Mon. Not. R. Astron. Soc. **425**,405 (2012).

[224] C.H. Chuang, Y. Wang; *Modelling the anisotropic two-point galaxy correlation function on small scales and single-probe measurements of H(z), DA(z) and f(z)s8(z) from the Sloan Digital Sky Survey DR7 luminous red galaxies*, Mon. Not. R. Astron. Soc. **435**,255 (2013).

[225] N.G. Busca et al.; *Baryon Acoustic Oscillations in the Lya forest of BOSS quasars*, Astron. Astrophys. **552**, A96 (2013).

[226] C.H. Chuang et al.; *The clustering of galaxies in the SDSS-III Baryon Oscillation spectroscopic survey: single-probe measurements and the strong power of*

f(z)Sigma(8)(z) on constraining dark energy, Mon. Not. R. Astron. Soc. **433**,3559 (2013).

[227] C. Zhang et al.; *Four new observational H(z) data from luminous red galaxies in the Sloan Digital Sky Survey data release seven*, Res. Astron. Astrophys. **14**, 1221 (2014).

[228] A. Oka et al.; *Simultaneous constraints on the growth of structure and cosmic expansion from the multipole power spectra of the SDSS DR7 LRG sample*, Mon. Not. R. Astron. Soc. **439**, 2515 (2014).

[229] L. Anderson et al.; *The clustering of galaxies in the SDSS-III Baryon Oscillation spectroscopic survey: Baryon Acoustic Oscillations in the data releases 10 and 11 galaxy samples*, Mon. Not. R. Astron. Soc. **441**,24 (2014).

[230] M. Moresco; *Raising the bar: new constraints on the Hubble parameter with cosmic chronometers at z* $\approx$ *2*, Mon. Not. R. Astron. Soc. Lett. **450**,L16 (2015).

[231] M. Moresco et al.; *A 6% measurement of the Hubble parameter at z 0.45: direct evidence of the epoch of cosmic re-acceleration*, J. Cosmol. Astropart. Phys. **05**, 014 (2016).

[232] A.L. Ratsimbazafy et al.; *Age-dating luminous red galaxies observed with the Southern African Large Telescope*, Mon. Not. R. Astron. Soc. **467**, 3239 (2017).

[233] J.E. Bautista et al.; *Measurement of Baryon Acoustic Oscillation correlations at z?=?2.3 with SDSS DR12 Lya-Forests*, Astron. Astrophys. **603**, A12 (2017).

[234] Y. Wang et al.; *The clustering of galaxies in the completed SDSS-III Baryon Oscillation spectroscopic survey: tomographic BAO analysis of DR12 combined sample in configuration space*, Mon. Not. R. Astron. Soc. **469**, 3762 (2017).

[235] M.V. dos Santos, R.R.R. Reis, I. Waga; *Constraining the cosmic deceleration-acceleration transition with type Ia supernova, BAO/CMB and H(z) data*, J. Cosmol. Astropart. Phys. **02**, 066 (2016).

[236] N. Padmanabhan et al.; *A 2 per cent distance to* $z = 0.35$ *by reconstructing Baryon Acoustic Oscillations-I. Methods and application to the Sloan Digital Sky survey*, Mon. Not. Roy. Astron. Soc. **427**, 2132 (2012).

[237] F. Beutler et al.; *The 6dF Galaxy survey: Baryon Acoustic Oscillations and the local Hubble constant*, Mon. Not. Roy. Astron. Soc. **416**, 3017 (2011).

[238] C. Blake et al.; *The WiggleZ Dark Energy Survey: joint measurements of the expansion and growth history at* $z < 1$, Mon. Not. Roy. Astron. Soc. **425**, 405 (2012).

[239] R. Narayan and M. Bartelmann; “Lectures on gravitational lensing." arXiv astro-ph/9606001 (1996).

[240] M. H. Amante, et al. *Testing dark energy models with a new sample of strong-lensing systems*, Mon. Not. Roy. Astron. Soc. **498**, 6013 (2020); [arxiv: 1906.04107].

[241] M. J. Reid, D. W. Pesce and A. G. Riess; *An improved distance to NGC 4258 and its implications for the Hubble constant*, Astrophys. J. **886 (2)**, L27 (2019).

[242] A. Tawfik, T. Harko; *Quark-hadron phase transitions in the viscous early universe*, Phys. Rev. D: **85**, 084032 (2012).

[243] L. O. Pimentel; *Exact self-creation cosmological solutions*, Astrophys. Space Sci.: **116**, 395 (1985).

[244] J.C. Fabris, S.V.B. Goncalves, R. de Sa Ribeiro; *Bulk viscosity driving the acceleration of the Universe*, Gen. Rel. Grav. **38**, 495 (2006).

[245] A. Avelino, U. Nucamendi; *Can a matter-dominated model with constant bulk viscosity drive the acceleraterd expansion of the universe?*, J. Cosmol. Astropart. Phys. **04**, 006 (2009).

[246] A. Avelino, U. Nucamendi; *Constraining a bulk viscous matter-dominated cosmological model using SNe Ia, CMB and LSS*, AIP Conf.Proc.: **1026**, 300 (2008a).

[247] A. Avelino, U. Nucamendi; *Constraining a matter-dominated cosmological model with bulk viscosity proportional to the Hubble parameter*, AIP Conf.Proc. **1083**, 1 (2008b).

[248] W.A. Hiscock, L. Lindblom; *Generic instabilities in first-order dissipative relativistic fluid theories*, Phys. Rev. **31**, (1985) 725.

[249] N. Banerjee, D. Pavon; *Holographic dark energy in Brans-Dicke theory*, Phys. Lett. B: **647**, 447 (2007).

[250] A. Sheykhi; *Thermodynamics of interacting holographic dark energy with the apparent horizon as an IR cut-off*, Class. Quantum Grav. **27**, 025007 (2010).

[251] J. Solàă Peracaula, *BransŰDicke gravity: From Higgs physics to (dynamical) dark energy*, Int. J. Mod. Phys. D **27** 1847029 (2018).

[252] J. de Cruz Pérez, J. Solà Peracaula, *BransŰDicke cosmology mimicking running vacuum*, Mod. Phys. Lett. A **33** 1850228 (2018).

[253] C.M. Will; *The confrontation between general relativity and experiment*, Living Rev. Relativ.: **9**, 3 (2006).

[254] F.Q. Wu, X. Chen; *Cosmic microwave background with Brans-Dicke gravity II : Constraints with the WMAP and SDSS data*, Phys. Rev. D: **82**, 083003 (2010).

[255] M. Tegmark et al.; *Cosmological constraints from the SDSS luminous red galaxies*, Phys. Rev. D **74**, 123507 (2006).

[256] G. Hinshaw et al.; *Five-Year Wilkinson Microwave Anisotropy Probe (WMAP) observations: Data processing, Sky maps, and basic results*, Astrophys. J. Suppl. **180**, 225 (2009).

[257] U. Alam, V. Sahni, A.A. Starobinsky; *The case for dynamical dark energy revisited*, J. Cosmol. Astropart. Phys. **08**, 0406 (2004).

[258] P. Praseetha, T.K. Mathew; *Interacting modified holographic ricci dark energy model and statefinder diagnosis in flat universe*, Int. J. Mod. Phys. D **23**, 1450024 (2014).

[259] A.G. Riess, et al.; *New Hubble space telescope discoveries of type Ia supernovae at $z > 1$: narrowing constraints on the early behavior of dark energy*, Astrophys. J. **659**, 98 (2007).

[260] D.N. Spergel, et al.; *Wilkinson microwave anisotropy probe (WMAP) three year results: implications for cosmology*, Astrophys. J. Suppl. **170**, 377 (2007).

[261] R. Kessler, et al.; *First-year Sloan Digital Sky Survey-II supernova results: Hubble diagram and cosmological parameters*, Astrophys. J. Suppl. **185**, 32 (2009).

[262] T.M.C. Abbott, et al.; *First cosmology results using type Ia supernovae from the dark energy survey: constraints on cosmological parameters*, Astrophys. J. **872**, L30 (2019).

[263] D. Brout; *First cosmology results using Type Ia supernovae from the dark energy survey: analysis, systematic uncertainties and validation*, Astrophys. J. **874**, 150 (2019).

[264] M. Koussour, H. Filali, S.H. Shekh, M. Bennai; *Holographic dark energy in Gauss-Bonnet gravity with Granda-Oliveros cut-off*, Nucl. Phys. B **978**, 115738 (2022).

[265] A. Oliveros, M.A. Sabogal, Mario A. Acero; *Barrow holographic dark energy with Granda-Oliveros cut-off*, Eur. Phys. J. P **137**, 783 (2022); arXiv:2203.14464.

[266] Ø. Grøn; *Viscous inflationary universe models*, Astrophys. Space Sci. **173**, 191 (1990).

[267] I. Brevik, S.D. Odintsov; *Cardy-Verlinde entropy formula in viscous cosmology*, Phys. Rev. D **65**, 067302 (2002).

[268] I. Brevik, O. Gorbunova; *Dark energy and viscous cosmology*, Gen. Relativ. Gravit. **37**, 2039 (2005).

[269] B. Li, J.D. Barrow; *Does bulk viscosity create a viable unified dark matter model?*, Phys. Rev. D **79**, 103521 (2009) .

[270] X.H. Meng, X. Dou; *Singularities and entropy in bulk viscosity dark energy model*, Commun. Theor. Phys. **52**, 377 (2009).

[271] A. Avelino, U. Nucamendi; *Exploring a matter-dominated model with bulk viscosity to drive the accelerated expansion of the Universe*, J. Cosmol. Astropart. Phys. **08**, 009 (2010).

[272] Y.D. Xu, Z.G. Huang, X.H. Zhai; *Generalized Chaplygin gas model with or without viscosity in the w-w' plane*, Astrophys. Space Sci. **337**, 493 (2012).

[273] I. Brevik, E. Elizalde, S.D. Odintsov, A.V. Timoshkin; *Inflationary universe in terms of a van der Waals viscous fluid*, Int. J. Geom. meth. Mod. Phys. **14**, 1750185 (2017).

[274] I. Brevik, Ø. Grøn, J. de Haro, S. D. Odintsov, E. N. Saridakis; *Viscous cosmology for early- and late-time universe*, Int. J. Mod. Phys. D **26**, 1730024 (2017).

[275] S.D. Odintsov, V.K. Oikonomou, A.V. Timoshkin, E.N. Saridakis and R. Myrzakulov; *Cosmological fluids with logarithmic equation of state*, Ann. of Phys. **398**, 238 (2018).

[276] C.P. Singh, S. Kaur; *Probing bulk viscous matter dominated model in Brans-Dicke Theory*, Astrophys. Space Sci. **365**, 2 (2020)

[277] J. Ren, X.-H. Meng; *Dark viscous fluid described by a unified equation of state in cosmology*, Int. J. Mod. Phys.D **16**, 1341 (2007).

[278] A. Avelino et al.; *Bulk Viscous Matter-dominated universes: Asymptotic properties*, J. Cosmol. Astropart. Phys. **08**, 012 (2013).

[279] A. Sasidharan, T.K. Mathew; *Bulk viscous matter and recent acceleration of the universe*, Eur. Phys. J. C **75**, 348 (2015).

[280] A. Sasidharan, T. K. Mathew; *Phase space analysis of bulk viscous matter dominated universe*, J. High Energy Phys. **06**, 138 (2016).

[281] Planck Collaboration, N. Aghanim et. al.; *Planck 2018 results: VI. Cosmological parameters*, Astron. Astroophys. **641**, A6 (2020); [arXiv:1807.06209].

[282] A. A. Mamon; *Constraints on a generalized deceleration parameter from cosmic chronometers*, Mod. Phys. Lett. A **33**, 1850056 (2018).

[283] S. Capozziello, R.D. Agostine and O. Luongo; *High-redshift cosmography: auxiliary variables versus Padé polynomials*, Mon. Not. Roy. Astron. Soc. **494**, 2576 (2020).

[284] S. Basilakos and J.A.S. Lima; *Constraints on cold dark matter accelerating cosmologies and cluster formation*, Phys. Rev.D **82**, 023504 (2010).

[285] J.A.S. Lima, J.F. Jesus and F.A. Oliveira; *CDM accelerating cosmology as an alternative to LCDM model* , J. Cosmol. Astropart. Phys. **11**, 027 (2010).

[286] J.A.S. Lima, L.L. Gracf, D. Pavón and S. Basilakos; *Cosmic acceleration without dark energy: background tests and thermodynamic analysis*, J. Cosmol. Astropart. Phys. **10**, 042 (2014).

[287] S. Chakraborty, S. Pan and S. Saha; *A third alternative to explain recent observations: Future deceleration*, Phys. Lett. B **738**, 424 (2014).

[288] R.C. Nunes, D. Pavón; *Phantom behavior via cosmological creation of particles*, Phys. Rev.D **91**, 063526 (2015)

[289] R.G. Cai, L.M. Cao, Y.P. Hu; *Hawking radiation of apparent horizon in a FRW universe*, Class. Quantum Grav. **26**, 155018 (2009); [arXiv:0809.1554].

[290] G. Izquierdo, D. Pavón; *The generalized second law in phantom dominated universes in the presence of black holes*, Phys. Lett. B **639**, 1 (2006).

[291] L. Parker, *Quantized fields and particle creation in expanding universes. II*, Phys. Rev. D **3**, 346 (1971)

[292] I. Prigogine, J. Geheniau; *Entropy, matter, and cosmology*, Proc. Natl. Acad. Sci. **83**, 6245 (1986)

[293] L. Xu, W. Li and J. Lu; *Holographic dark energy in Brans-Dicke theory*, Eur. Phys. J. C **60**, 135 (2009).

[294] X.L. Liu, X. Zhang; *New Agegraphic Dark Energy in Brans-Dicke Theory*, Commun. Theor. Phys. **52**, 761 (2009).

[295] A. Sheykhi; *Interacting holographic dark energy in Brans-Dicke theory*, Phys. Lett.B **681**, 205 (2009).

[296] A. Sheykhi; *Interacting new agegraphic dark energy in non-flat Brans-Dicke cosmology*, Phys. Rev.D **81**, 023525 (2010).

[297] F. Felegary, F. Darabi, M.R. Setare; *Interacting holographic dark energy model in Brans-Dicke cosmology and coincidence problem*, Int. J. Mod. Phys. D **27**, 1850017 (2018).

[298] M. Srivastava, C.P. Singh; *Cosmological evolution of non-interacting and interacting holographic dark energy model in Brans-Dicke theory*, Int. J. Geom. Meth. Mod. Phys. **15**, 1850124 (2018).

[299] H. Kim, H.W. Lee, Y.S. Myung; *Role of the Brans-Dicke scalar in the holographic description of dark energy*, Phys. Lett. B **628**, 11 (2005).

[300] S. Basilakos, J. Solà; *Entropic-force dark energy reconsidered*, Phys. Rev.D **90**, 023008 (2014) [arXiv:1402.6594].

[301] B. Chen, M. Li, Y. Wang; *Inflation with holographic dark energy*, Nucl. Phys. B **774**, 256 (2007).

[302] L.A. Salo, J. de Haro; *Cosmological solutions in spatially curved universes with adiabatic particle production*, Class. Quantum Grav. **34**, 065001 (2017).

[303] W.I. Freeman, et al.; *The Carnegie-Chicago Hubble Program. VIII. An independent determination of the Hubble constant based on the Tip of the Red Giant Branch*; Astrophys. J. **882**, 34 (2019).

[304] N. Aghanim, et al.; *Planck intermediate results-XLVI. Reduction of large-scale systematic effects in HFI polarization maps and estimation of the reionization optical depth*, Astron. Astrophys. **596**, A107 (2016).

[305] R. Adam, et al.; *Planck intermediate results-XLVII. Planck constraints on reionization history*, Astron. Astrophys. **596**, A108 (2016).

[306] S. Pan, B.K. Pal and S. Pramanik; *Gravitationally influenced particle creation models and late-time cosmic acceleration*, Int. J. Geom. Methods Mod. Phys. **15**, 1850042 (2018).

[307] J.D. Bekenstein; *Black holes and entropy*, Phys. Rev. D **7**, 2333 (1973).

[308] J.D. Bekenstein; *Generalized second law of thermodynamics in black-hole physics*, Phys. Rev.D **9**, 3292 (1974).

[309] S. Hawking; *Particle creation by black holes*, Commun. math. Phys. **43**, 199 (1975).

[310] G.W. Gibbons and S.W. Hawking; *Cosmological event horizons, thermodynamics, and particle creation*, Phys. Rev.D **15**, 2738 (1977).

[311] T. Jacobson; *Thermodynamics of spacetime: The Einstein equation of state*, Phys. Rev. Lett. **75**, 1260 (1995).

[312] T. Padmanabhan; *Gravity and the thermodynamics of horizons*, Phys. Rep. **406**, 49 (2005).

[313] D. Bak, S.J. Rey; *Cosmic holography+*, Class. Quantum Grav. **17**, L83 (2000).

[314] G. Izquierdo, D. Pavón; *Dark energy and the generalized second law*, Phys. Lett. B **633**, 420 (2006).

[315] M. Akbar, R.G. Cai; *Thermodynamic behavior of the Friedmann equation at the apparent horizon of the FRW universe*, Phys. Rev. D **75**, 084003 (2007).

[316] T. Padmanabhan; *Thermodynamical aspects of gravity: New insights*, Rept. Prog. Phys. **73**, 046901 (2010).

[317] M. Jamil, E.N. Saridakis, M.R. Setare; *The generalized second law of thermodynamics in Horava-Lifshitz cosmology*, J. Cosmol. Astropart. Phys. **10**, 032 (2010).

[318] S.M. Carroll; *The cosmological constant*, Living Rev. Rel. **4**, 1 (2001); [astro-ph/0004075].

[319] N. Dalal et al.; *Testing the cosmic coincidence problem and the nature of dark energy*, Phys. Rev. Lett. **87**, 141302 (2001); [astro-ph/0105317].

[320] E. Komatsu et al.; *Five-Year Wilkinson Microwave Anisotropy Probe Observations: Cosmological Interpretation*, Astrophys. J. Suppl. Ser. **180**, 330 (2009).

[321] L. Herrera-Zamorano, A. Hernández-Almada, M. García-Aspeitia; *Constraints and cosmography of ΛCDM in presence of viscosity*, Eur. Phys. J. C **80**, 637 (2020).

[322] L. Knox, N. Christensen, C. Skordis; *The age of the universe and the cosmological constant determined from cosmic microwave background anisotropy measurements*, Astrophys. J. **563**, L95 (2001).

[323] Y.-B. Wu, S. Li, M.-H. Fu and J. He; *A modified Chaplygin gas model with interaction*, Gen. Relativ. Grav. **39**, 653 (2007).

[324] M. Dunajski, G. Gibbons; *Cosmic jerk, snap and beyond*, Class. Quantum Grav. **25**, 235012 (2008).

****

List of Publications

1. C.P. Singh and **Simran Kaur**; *Probing Bulk Viscous matter-Dominated model in Brans-Dicke Theory*, Astrophysics and Space Science **365**, 2 (2020). **Impact Factor (1.909)**

2. **Simran Kaur** and C.P. Singh; *Viscous cosmology in holographic dark energy with Granda-Oliveros cut-off*, Communications in Theoretical Physics, **Accepted** (2022). **Impact Factor (2.877)**

3. C.P. Singh and **Simran Kaur**; *Matter creation cosmology in Brans-Dicke theory: observational tests and thermodynamic analysis*, Physical Review D **100**, 084057 (2019). **Impact Factor (5.407)**

4. **Simran Kaur** and C.P. Singh; *Constraints on holographic dark energy model with matter creation in Brans-Dicke theory and thermodynamic analysis*, Physics of the Dark Universe **33**, 100869 (2021). **Impact Factor (5.09)**

5. **Simran Kaur** and C.P. Singh; *Evolution of holographic dark energy model with adiabatic matter creation*, Modern Physics Letter A **37**, No. 24, 2250161 (2022). **Impact Factor (1.594)**

****

Conferences attended and Paper presented

1. Presented a research paper titled *'A study on Holographic Dark Energy Model with adiabatic matter creation'* in Asia Pacific School and Workshop on Gravitation and Cosmology, Taiwan (March 2022).

2. Presented a research paper titled *'Holographic Dark Energy Model with Matter Creation in Brans-Dicke Theory'* in 26th International Conference of International Academy of Physical Sciences held at S.L.I.E.T. Longowal (December 2020).

3. Presented a research paper titled *'Probing bulk viscous matter dominated model in Brans-Dicke theory'* in International Conference on Differential Geometry and Relativity held at Deen Dayal Upadhyaya Gorakhpur University (November 2019).

4. Received the award of 'Young Relativist' for presenting a paper entitled *'Matter dominated model with bulk viscosity and particle creation'* at International Conference on Gravitation, Cosmology and Mathematical Physics in 2019 held at GLA University, Mathura (April, 2019).

5. Presented a paper entitled *'Friedmann Cosmology with matter creation: An alternative to explain the cosmic expansion'* in 30th IAGRG (Indian Association of General Relativity and Gravitation) meet held at BITS- Pilani Hyderabad (January, 2019).

Gmail

Simran Kaur <skjuneja.maths@gmail.com>

Communications in Theoretical Physics - Decision on Manuscript ID CTP-220789.R1

Bolin Wang <onbehalfof@manuscriptcentral.com> Mon, Nov 28, 2022 at 3:50 PM
Reply-To: wangbl@itp.ac.cn
To: skjuneja.maths@gmail.com
Cc: ctp@itp.ac.cn

28-Nov-2022

Dear Ms. Kaur,

It is a pleasure to inform you of the acceptance of your manuscript entitled "Viscous cosmology in holographic dark energy with Granda-Oliveros cut-off" in its current form for publication in Communications in Theoretical Physics. The comments of the reviewer(s) who reviewed your manuscript are included at the foot of this letter.

We will send to you one hard copy of the journal and 15 offprints of your article. Please send by E-mail your name and air mail address to ctp@itp.ac.cn. Your E-mail should include the Manuscript ID number. Chinese authors please send your name and address in Chinese.
我们将寄送一本纸质期刊和15份您文章的抽印本给您。请国内作者将您的中文姓名和中文地址发送到 ctp@itp.ac.cn。
发送邮件时请标明稿件编号。
Thank you for your fine contribution. On behalf of the Editors of Communications in Theoretical Physics, we look forward to your continued contributions to the Journal.

Sincerely,
Dr. Bolin Wang
Managing Editor
Editorial Office, Communications in Theoretical Physics
wangbl@itp.ac.cn